

MODELING URBAN GROWTH IN THE ATLANTA, GEORGIA METROPOLITAN AREA
USING REMOTE SENSING AND GIS

by

ZHIYONG HU

This study examines the dynamics of human-induced land use/cover changes, especially urban growth, in Atlanta, Georgia metropolitan area. Land use/cover changes of Atlanta between 1987 and 1997 were observed from LANDSAT TM satellite images and linked with the biophysical and socio-economic data using image processing, spatial analysis and modeling integrated in the framework of a geographic information system(GIS). Normalized Vegetation Difference Index (NDVI) differencing and temporal logic were employed to improve the accuracy of land use/cover change detection. A Markov chain model was used to conduct a ‘what-if’ analysis to predict the quantity distributions and spatial patterns of the future land use/cover based on the 1987-1997 land use/cover transition probabilities. In addition, a logistic regression model was used to identify the factors governing the process of urban growth and to predict the most probable sites of the growth. This study found that from 1987 to 1997 the most intense land use/cover change in Atlanta was deforestation for urban development. During the ten years, high-density urban area increased 12.94% from 876.78km² to 990.27 km²; low-density urban area increased 42.57% from 2468.62 km² to 3519.56 km²; and forest decreased 10.62% from 9217.04 km² to 8238.28 km². The Markov chain simulation revealed that urban use will continue to grow at the expense of forest. The proportion of urban area was 20.93% in 1987, and it will be 35.45% in 2020. Forest will decrease from 57.67% in 1987 to 43.64% in 2020. Urban growth will occur in the rural and urban-fringe areas, taking on a fragmented pattern. It was found from the logistic regression model that urban growth tends to occur around existing urban areas and close to major roads (road influenced growth), while some new urban clusters located at a distance from the existing urban areas can also form(diffusive growth). Whereas the logistic regression model can incorporate human dimensions, the Markov chain model is more temporally dynamic. Recommendations were made for further exploration of a more realistic land use/cover change model that can deal with space, time, and people simultaneously.

INDEX WORDS: Land use, Land cover, Urban growth, GIS, Remote sensing, Temporal logic, NDVI, Markov chain, Logistic regression

MODELING URBAN GROWTH IN THE ATLANTA, GEORGIA METROPOLITAN AREA
USING REMOTE SENSING AND GIS

by

ZHIYONG HU

B.S., Northeast University, China, 1992

M.S., Northeast University, China, 1995

A Dissertation Submitted to the Graduate Faculty of the University of Georgia in Partial
Fulfillment of the Requirements for the Degree

DOCTOR OF PHILOSOPHY

ATHENS, GEORGIA

2004

© 2004

Zhiyong Hu

All Rights Reserved

MODELING URBAN GROWTH IN THE ATLANTA, GEORGIA METROPOLITAN AREA
USING REMOTE SENSING AND GIS

by

ZHIYONG HU

Major Professor: Chor-Pang Lo

Committee: Thomas W. Hodler
Xiaobai Yao
Lynn E. Usery
Hamid R. Arabnia

Electronic Version Approved:

Maureen Grasso
Dean of the Graduate School
The University of Georgia
August 2004

DEDICATION

To Ronghui, my loving wife, thank you for allowing me to spend more time on this venture than with you. You will never know how much I appreciated the many times you assumed my responsibilities at home and with family.

To my parents and mother-in-law, thank you for your encouragement and for always letting me know how proud you were of my accomplishments.

And, to my lovely daughter, Lucy, and son, James. Your smile has brought me happiness.

ACKNOWLEDGEMENTS

I would like to express my sincere appreciation to my major advisor, Chor-Pang Lo. Without Dr. Lo's guidance, support, and encouragement, there were times that this dissertation may have never materialized. He can be credited for much of my personal development, and showed much patience in the pursuit of my research goals. His faith in my ability to complete this endeavor was what sustained me. He opened the doors for me to visualize myself as a researcher and educator with great potential for an academic career. I would also like to thank my advisory committee members, Thomas Hodler, Lynn Userly, Hamid Arabnia, and Xiaobai Yao. Their academic advice and guidance are greatly appreciated. Thanks are extended to Emily Duggar and Audrey Hawkins, who have provided helps in many ways. I also thank Bo Xu for her help.

TABLE OF CONTENTS

	Page
LIST OF TABLES.....	ix
LIST OF FIGURES	xi
CHAPTER	
1 INTRODUCTION	1
Research background	1
Study area	8
Research objectives	17
Dissertation structure	19
2 LITERATURE REVIEW	20
Introduction	20
Basic concepts and theories on urban land use/cover system and its modeling	20
Land use/cover change detection methods	29
Land use change models	34
Summary	56
3 MAPPING THE 1987-1997 LAND USE/COVER CHANGE IN ATLANTA FROM LANDSAT TM IMAGES: A NEW APPROACH TO ACCURACY IMPROVEMENT.....	58
Introduction	58
Satellite data	60

Co-registration of multi-date images	63
Computer-assisted land use/cover classification	67
Principal components analysis and change vector analysis	69
Errors in computer-assisted land use/cover classification from Landsat TM images	77
Correction of classification errors caused by cloud shadows.....	84
Error propagation in post-classification comparison.....	87
Using NDVI differencing and temporal logic to improve land use/cover classification accuracy	90
Post-classification comparison for land use/cover change detection	107
Discussions and conclusions	112
4 MARKOV CHAIN ANALYSIS OF LAND USE AND LAND COVER CHANGE.....	117
Introduction	117
Markov chain model	118
Formulation of a Markov chain model of land use/cover change	120
Testing for the Markov property	124
Prediction of land use/cover proportions	125
Prediction of future urban spatial patterns	129
Discussions and conclusions.....	130
5 LOGISTIC REGRESSION MODELING OF URBANIZATION PROBABILITY.....	134
Introduction	134

Spatial data handling and integration	134
Statement of model	144
Multi-scale modeling and fractal analysis	153
Testing logistic regression residual for spatial autocorrelation	163
Correcting for spatial autocorrelation	168
Refining the model at the resolution of 225 meters	170
Testing for the significance of the model	173
Assessment of goodness of fit	179
Model interpretation	184
Prediction and validation	188
Prediction of spatial patterns of urban distribution.....	194
Conclusions	196
6 SUMMARY AND CONCLUSIONS	199
REFERENCES	205

LIST OF TABLES

	Page
Table 2.1: Summary of human drivers reflected in land use/cover change model variables.....	37
Table 3.1: Characteristics of the satellite images.	61
Table 3.2: PCA eigenvalues and percentage of variance explained by each component.....	71
Table 3.3: Factor loadings of each principal component with each band.....	72
Table 3.4: Accuracy assessment of the 1997 land use/cover map produced from Landsat TM image.....	79
Table 3.5: Parameters for the calculation of at-satellite spectral reflectance.....	94
Table 3.6: Interpretation of NDVI difference classes.....	102
Table 3.7: Using NDVI differencing and temporal logic to enhance land use/cover classifications.....	105
Table 3.8: Quantitative information of land use/cover change.....	109
Table 4.1: and use/cover transition probability matrix, 1987-1997.....	124
Table 4.2: Land use/cover proportions (%) from 1987 to 2020.....	127
Table 4.3: Simulated transition probability matrix, 1997-2020.....	129
Table 5.1: Original data for logistic regression modeling.....	136
Table 5.2: List of variables in the logistic regression model.....	146
Table 5.3: The coding of the design variables for land use/cover, coded at six levels.....	146
Table 5.4: Effect of multi-resolution modeling.....	156
Table 5.5: Number of steps for calculation of fractal dimensions of predicted probability	

surfaces using triangular prism surface area method.....161

LIST OF FIGURES

	Page
Figure 1.1: Urban growth indicated by night-time light brightness increase from 1992 for the Conterminous USA.....	2
Figure 1.2: Percentage change in population and urbanized land in the United States, 1982-1997, by census region.....	3
Figure 1.3: Urban and rural populations of more developed regions and less developed regions.....	4
Figure 1.4: Study Area: Thirteen-county metropolitan region of Atlanta, Georgia.....	9
Figure 1.5: Major activity Centers in Atlanta region in 1994,1995 and 1996.....	16
Figure 2.1: Models of urban structure.....	25
Figure 2.2: A Framework for Reviewing Land Use Change Models.....	35
Figure 3.1: Landsat TM images.....	62
Figure 3.2: Image subset to the area of interest.....	62
Figure 3.3: Accurate georeference (RMSE < 0.5 pixel) does not guarantee co-registration of multi-date images for land use/cover change detection.....	65
Figure 3.4: Examination of pixel shift of the 1997 Landsat TM image relative to the 1987 image.....	66
Figure 3.5: Pixel shift corrected by offsetting coordinates of the 1997 image: both images become co-registered.....	66
Figure 3.6: Principal components 1, 2 and 7 from PCA of Landsat 1997 TM image.....	73

Figure 3.7: Principal components 1, 2,3 composite image displayed in red, green, and blue color combination.....	75
Figure 3.8: Change vector defined on the principal components 1 and 2 measurement space....	75
Figure 3.9: Land use/cover change magnitude and direction from change vector analysis.....	76
Figure 3.10: Change vector magnitude vs. direction and the type of land use/cover change.....	78
Figure 3.11: Major classification errors in the initial land use/cover classifications.....	81
Figure 3.12: Spectral signature curves developed from some AOIs on the 1987 Landsat TM image.....	82
Figure 3.13: Spectral confusions between land use/cover classes indicated by the overlaps in digital numbers (pixel values) of band 1, 1987 Landsat TM.....	83
Figure 3.14: Cloud and cloud shadow (shown in white) distribution in the 1987 image or the 1997 image.....	86
Figure 3.15: Landsat images for the both dates, Lake Lanier area.....	86
Figure 3.16: The initial classification of the 1997 image and correct classification.....	86
Figure 3.17: Error propagation in the boolean AND operation in land use/cover change detection.....	89
Figure 3.18: NDVI Images for the year 1987 and 1997.....	96
Figure 3.19: NDVI difference image for the whole study area.....	98
Figure 3.20: NDVI difference image, northeast of Atlanta.....	99
Figure 3.21: NDVI 1987-1997 difference classification map.....	101
Figure 3.22: Results of the use of temporal logic and NDVI differencing approach to improve the accuracy of land use/cover classification.....	106
Figure 3.23: Final improved land use/cover maps for years 1987 and 1997.....	108

Figure 3.24: Land use/cover changes from 1987 to 1997.....	109
Figure 3.25: Land use/cover change from 1987 to 1997 for four major land use/cover types...111	
Figure 3.26: Urban growth from 1987 to 1997.....	113
Figure 4.1: A segment of Markov chain representing land use/cover change in the study area.....	122
Figure 4.2: Quantitative land use/cover change trends.....	128
Figure 4.3: Historical and Markov chain model predicted urban patterns, 1987-2020.....	131
Figure 5.1: Atlanta metropolitan transportation network showing DOT road type 1 (interstate and state highways), 1990.....	137
Figure 5.2: Census block groups, 1990, Atlanta metropolitan area.....	138
Figure 5.3: Sliver polygons in the census shape file.....	141
Figure 5.4: Basic steps of pycnophylactic interpolation.....	142
Figure 5.5: Surface of population density (<i>person/km²</i>), Atlanta, Georgia based on the 1990 census data at the level of census block groups obtained using pycnophylactic interpolation method.....	143
Figure 5.6: Variables in the logistic regression model, represented by raster layers.....	147
Figure 5.7: Effect of multi-resolution data aggregation on the percentage of urban growth area.....	157
Figure 5.8: Effect of resolution on logistic regression model pseudo R square.....	157
Figure 5.9: Effect of resolution on logistic regression model validation index relative operating characteristic (ROC).....	158
Figure 5.10: Coordinate structure for triangular prism method.....	161
Figure 5.11: R-square values against resolutions.....	162

Figure 5.12: Lumped fractal dimension of logistic regression model predicted probability surface plotted against resolution.....	162
Figure 5.13: King’s case in determining spatial autocorrelation.....	165
Figure 5.14: Urbanization probability maps of Atlanta, Georgia.....	190
Figure 5.15: ROC curve.....	194
Figure 5.16: Spatial patterns of urban area in the Atlanta region, 1987-2020.....	195
Figure 5.17: Spatial order of urban growth.....	197

CHAPTER ONE

INTRODUCTION

1.0 Research background

The last century has seen the unprecedented concentration of humans into urban area around the globe, creating an extensive urban landscape. In the United States, urban growth rates show no signs of slowing. Cities have changed from small, isolated population centers to large, interconnected metropolitan regions. Based on a study using Defense Meteorological Satellite Program Operational Linescan System (DMSP-OLS) nighttime images, Gallo *et al.* (2004) found that the night-time light increase can be associated with urbanization (Figure 1.1). It was found that over 13% of the land area within the conterminous USA exhibited greater night-time light emitted in 2000 compared to 1992/1993. Most of the night-time light brightness increases between 1992/1993 and 2000 were located near urban areas. Over the past 50 years, one of the dominant geographical trends in the United States has been suburbanization. In 1950, the share of metropolitan area residents who lived in central cities was 57 percent of the nation, but by 1990, had fallen to 37 percent (Mieskowski and Milles 1993). Most metropolitan areas in the United States are adding urbanized land at a much faster rate than they are adding population (Fulton *et al.* 2001) (Figure 1.2). People are increasingly choosing to live in low-density, vehicle-dependent suburban areas. For all the American urban areas, population grew by 92.3 percent while land area increased by 245.2 percent between 1950 and 1990 (Mieskowski and



Figure 1.1 Urban growth indicated by night-time light brightness increase from 1992 for the Conterminous USA. The image was derived from the Defense Meteorological Satellite Program-Operational Linescan System (DMSP-OLS) nighttime images. Yellow areas are brightness values greater than 0; red indicates grid cells where 2000 brightness values were greater than 1992 values. Images obtained from the same sensor have also been used to detect urban morphology and land use for China (Lo 2002).

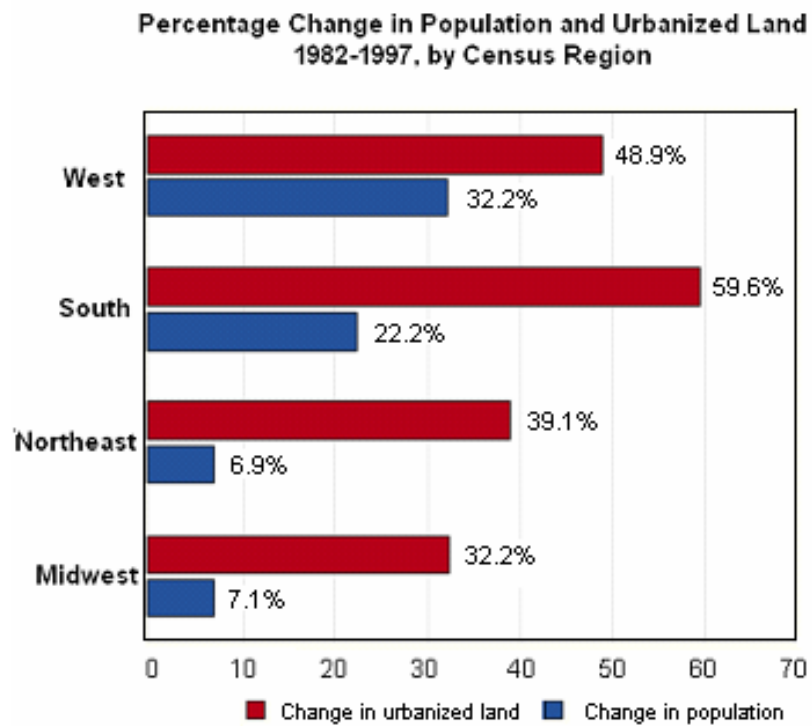


Figure 1.2 Percentage change in population and urbanized land in the United States, 1982-1997, By census region (Source: Fulton *et al.* 2001).

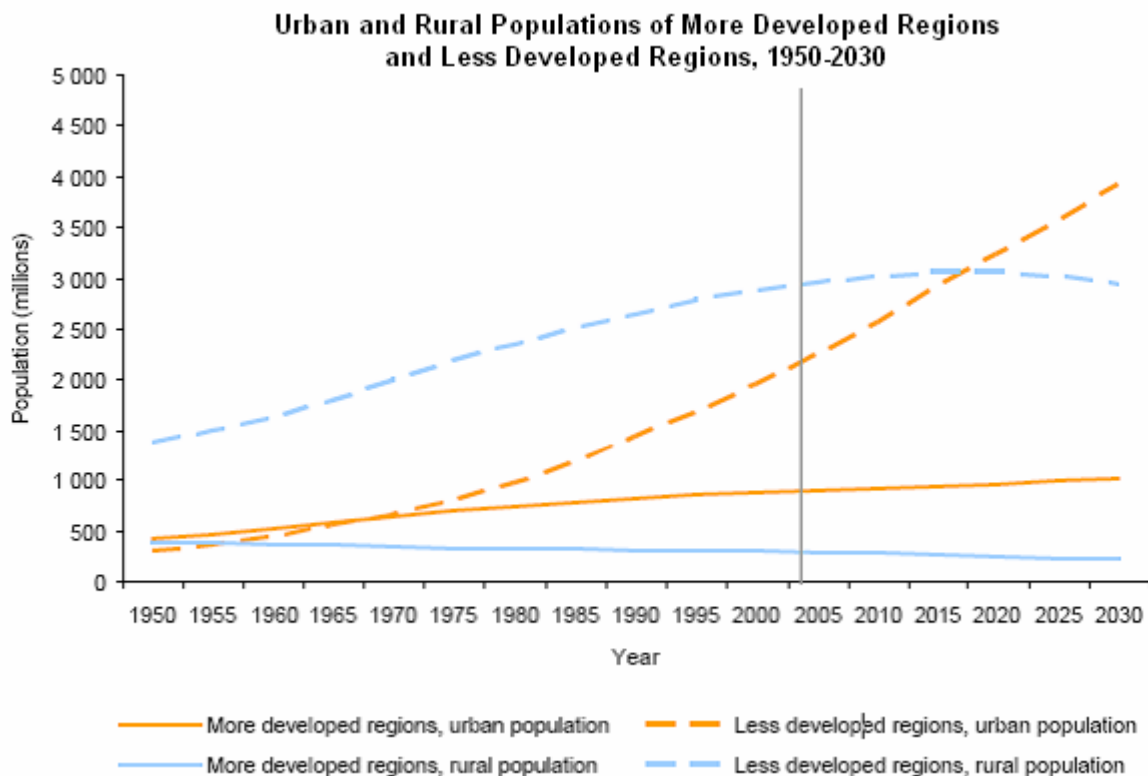


Figure 1.3 Urban and rural populations of more developed regions and less developed regions, 1950-2030. (Source: United Nations Department of Economic and Social Affairs/Population Division 11 *World Urbanization Prospects: The 2003 Revision*).

Milles 1993). The trend of rapid urbanization is now global, with urban population in developing regions growing faster than developed regions (United Nations report 2003) (Figure 1.3).

Urban growth and the concentration of people in urban areas are creating environmental and societal problems world-wide. Urban development has consumed large extents of farmland and green space. Pollutants discharged from urban areas lower the quality of air and water.

Urban growth is stressing ecological systems and leading to the decline in the extent and connectivity of wildlife habitats. Urbanization can warm the regional climate. Many metropolitan areas are facing problems of traffic congestion. Unchecked urban sprawl has brought about many societal problems, such as, increasing spatial segregation of races and disparity of incomes, increasing spatial mismatch between low-income residents and jobs, the spatial disintegration of labor markets, and increasing threats from natural hazards as urban structure becomes more dispersed and internally complex (Knox 1993).

With the recognition of the impact of urban growth on the environment and society, the study of urban growth has gained interests among social and environmental scientists. Urbanization and urban growth has long been studied by social scientists with a focus on economic transformation, population and migration, and societal problems. Although the studies from the perspective of social science can reveal the socioeconomic process behind the urban growth, these studies are not able to show explicit spatial details since they are often conducted using survey data or data collected on enumeration data. Recently, urban growth research has attracted the attention of environmental scientists in the broader context of land use/cover change study. In their perspective, urbanization is just one form of human-induced land use/cover changes. Land use/cover change is increasingly recognized as being an important driver of global and regional environmental change. Patterns of landscape modifications are the results of complex interactions between physical, biological and social forces (Turner 1987).

Of critical importance in human-induced land use/cover change study is linking the observed changes in land use/cover to the socioeconomic and biophysical driving forces. To understand and predict change processes, one needs to monitor and characterize spatial patterns of land use/cover change. Land use/cover change models have been used by geographers and

environmental scientists to reveal and understand the spatio-temporal dynamics of land use/cover changes, to forecast future land use/cover extent and spatial pattern, and to evaluate the impact of land use/cover changes. There are various kinds of land use/cover change models. Basically, a land use/cover change model can fall into two categories: statistical models or simulation models. To best represent the land use/cover system and predict the future, a land use/cover change model must take spatial, temporal and human dimensions into account. However, few models can deal with the three dimensions simultaneously. It is a necessity to find innovative modeling methods or apply different models in a study to cover the full dimensions of the processes behind the land use/cover changes.

Land use/cover change models intended to link land use/cover changes to socioeconomic and environmental conditions rely on socioeconomic data and historical temporal observation of the changes. Assessment and monitoring of urbanization and other land transformations are exceptionally difficult at the regional and global scales (Masek *et al.* 2000), if only field observation data of land use/cover change can be obtained. However, field studies are generally not sufficient to quantify and analyze spatiotemporal patterns of land use/cover changes at an aggregated level in a spatially explicit and timely way (Liverman *et al.* 1998). Remote sensing images have offered considerable promise for monitoring land use/cover change. Remote sensing has emerged as the most useful data source for quantitatively and spatially measuring land use/cover changes. The dynamics of change processes can be investigated using a temporal series of remote sensing data. While census data provide a statistical view of demographics and economics, the actual spatial patterns of urban landscape can only be efficiently observed by remote sensing. The frequent revisiting observations by remote sensing updates our view of urban landscape, manifesting time series of urban growth, recording the variability of urban

development in space and time, thus permitting a rigorous comparison with economic and demographic data (Masek *et al.* 2002). Thus, historical land use/cover change data obtained from remote sensing integrated with socioeconomic data are often used as inputs to land use/cover change models.

The reliability of the results of land use/cover change modeling is not only affected by the selected modeling method, but is also highly dependent on the accuracy of land use/cover change mapping from remote sensing and the quality of socioeconomic data. Computer-assisted production of spatially-detailed and thematically-accurate land use/cover maps from satellite images is still a challenge for the remote sensing and photogrammetry research community. How to improve the accuracies of land use/cover classification maps for land use/cover change detection has been a topic heavily investigated in remote sensing and photogrammetry (Aplin and Atkinson 2004; Congalton 1991, 1996, 2002). Land use/cover change detection using data obtained from the classification of remotely sensed images using a single conventional classification method often cannot achieve the best accuracy. It is necessary to explore innovative methods or combine existing land use/cover classification methods to improve the accuracy. To be integrated with remote sensing data in a monolithic modeling environment, socioeconomic data need to be pixelized. Proximate variables are often derived from socioeconomic and biophysical data. Integrating remotely sensed, socioeconomic, and derived data for proximate variables relies on a common framework. Geographic information systems (GIS) can offer an integrative environment for spatial analysis and modeling using heterogeneous socioeconomic and environmental data.

1. 1 Study area

The Atlanta, Georgia metropolitan region is the study area for this dissertation. The region is defined here to include 13 urban counties: Cherokee, Cobb, Fulton, Gwinnett, Dekalb, Rockdale, Clayton, Fayette, Douglas, Henry, Coweta , Forsyth, and Paulding (Figure 1.4). The first ten counties form the planning area of the Atlanta Regional Commission (ARC).

1.1.1 Urban growth in Atlanta: an overview

In the last half of the 20th century, Atlanta, Georgia has risen as the premier commercial, industrial, and transportation urban area of the southeastern United States. The rapid growth of the Atlanta area, particularly within the last 25 years, has made Atlanta one of the fastest growing metropolitan areas in the United States. The population of the Atlanta metropolitan area increased 27% between 1970 and 1980, 33% between 1980-1990, and 39% between 1990-2000 (Research Atlanta, Inc. 1993; US Census Bureau 2000). Concomitant with this high rate of population growth has been an explosive growth in retail, industrial, commercial, and transportation services within the Atlanta region. This has resulted in tremendous land cover change within the metropolitan region, wherein urbanization has consumed vast acreages of forested and agricultural land adjacent to the city proper and has pushed the rural/urban fringe farther and farther away from the original Atlanta urban core. An enormous transition of land from forest and agriculture to urban land uses has occurred in the Atlanta area in the last 25 years. Between 1982 and 1997, Atlanta had the largest absolute (but not the percentage) increase in urbanized land of any metropolitan area in the nation—approximately 571,000 acres, which

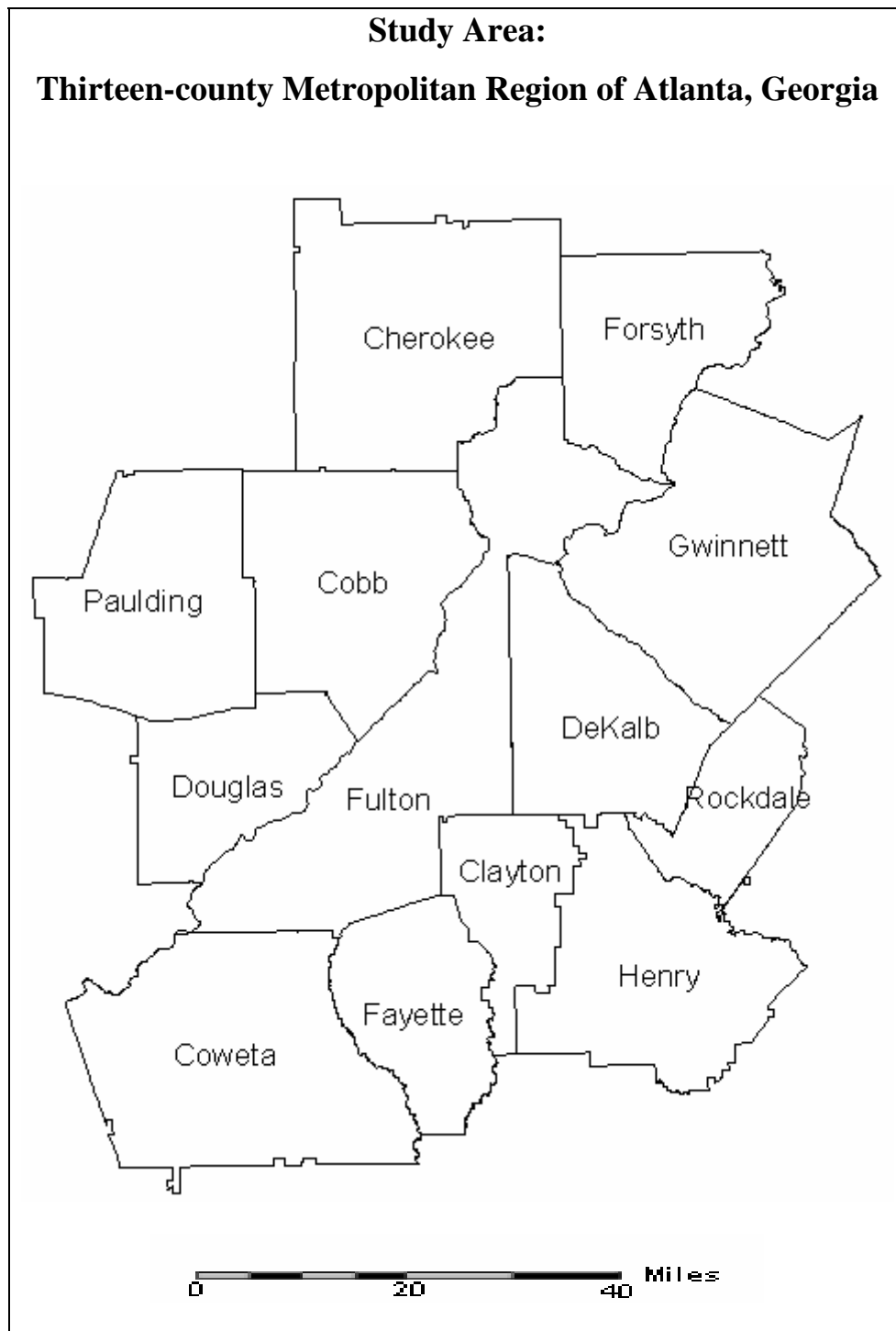


Figure 1.4 Study Area: Thirteen-county metropolitan region of Atlanta, Georgia.

was far ahead of New York, Dallas, Los Angeles, and Houston, which ranked second through fifth nationally (Fulton *et al.* 2001).

Atlanta's urban growth is characteristic of low-density development with the urban growth rate being much greater than the population rate. In 1982, Atlanta had a metropolitan population of approximately 2.2 million persons using 701,000 acres of urbanized land — an overall metropolitan density of 3.20 persons per urbanized acre. In 1997, Atlanta had a metropolitan population of 3.6 million people and 1.27 million acres of urbanized land — a metropolitan density of 2.84 persons per urbanized acre (Fulton *et al.* 2001). The Atlanta region's growth partly conforms to the national trends towards low-density development, automobile dependence, decentralized labor markets, and the shift of population towards suburbs rather than cities or rural areas.

1.1.2 Unbalanced growth in Atlanta

There has been an unbalanced and polarizing growth in Atlanta: a dividing line exists between the north and the south, strongly corresponding with the long-standing residential racial segregation patterns. This unbalanced growth has many dimensions: separation by class and race, poverty, job and housing growth, and transportation patterns (BICUMP 2000).

(1) Population

Explosive population growth is occurring in the northern and outer suburbs of the Atlanta region (BICUMP 2000), with almost 70 percent of the growth from 1990 to 1998 occurring north of the region. Southside areas gained about 170,000 people from 1990 to 1998. The population growth in southern counties has occurred entirely in exurban bedroom communities.

(2) Poverty

The distribution of poverty in the Atlanta region is also uneven. The poor tend to live in the southern parts (south Dekalb, south Fulton, Clayton, Douglas counties), while the northside (Gwinnett, Cherokee) has a low poverty rate and almost no areas of concentrated poverty.

Concentrated poverty "... pushes away businesses and middle-class families, further undermining those neighborhoods and fueling sprawl ..." (BICUMP 2000, 10). The serious financial burdens serving the poor in those areas has imposed tax rate increases on middle-class taxpayers and firms, hence a "white flight" from those areas to the suburb. Higher income families live in the region's northern and far southern areas.

(3) Race

Race segregation is also observed from the census statistics. According to the 1998 data, the Atlanta region's overall population was 72 percent white. North of Interstate 20 highway, the proportion of white was over 80%. In the far southern suburban communities, at least 85% of the population was white. Fulton and Dekalb counties were home to 74% of the region's non-white population. In 1999, almost one-third of the region's non-white population lived in the city of Atlanta. In some places, particularly the city of Atlanta, the racial divide corresponds to great income disparities. In the region, the racial divide and income divide are often related, but not identical. The region is becoming increasingly diverse in races. The Atlanta region has become home to a growing population of Hispanics and Asians during the 1980s and 1990s. Different races have different cultural identities, and location preferences. Repelling or attracting effects exist among races. According to a survey conducted by Research Atlanta (Geller *et al.* 1995), 90 percent of whites surveyed in metropolitan Atlanta expressed a willingness to move into an area

with one black household. As the number of black households increased to eight, however, the percentage of whites willing to move into such a neighborhood decreased to 26 percent.

(4) Employment

Unbalanced growth of employment also has fueled the urban sprawl. Most new jobs and high-paying jobs are on the north side of the region, in north Fulton, north Dekalb, Gwinnett, and Cobb Counties. Of 348,000 new jobs added to the Atlanta region between 1990 and 1997, almost three-fourths of this job growth had occurred in the northern part of the region (ARC 1997). Many of the areas of greatest job increases are outside Atlanta's I-285 perimeter highway. The city of Atlanta is slipping overall in its share of jobs despite flourishing commercial areas in the north of the city, such as Buckhead, Midtown and Lenox. There is little or no job growth in the majority non-white neighborhoods. The declined shares of jobs in central cities and slow-growing suburbs reflect three forces that work behind the job growth as observed in other regions (BICUMP 2000): (1) certain service- and retail- sector jobs are increasing in the suburbs in order to serve a growing suburban population; (2) businesses without a primarily residential customer base choose to locate in the suburbs because other, similar firms are there; and (3) employers choose wealthier suburban locations "pulled" by the residential suburbanization and "pushed" by high taxes, regulatory constraints, and public service inefficiencies in the city and aging suburbs.

(5) Housing

The spatial distribution of affordable housing is one of the important factors shaping metropolitan growth patterns. Although some government policies or laws encourage fair housing, such as Federal Fair Housing Act, Atlanta Metro Fair Housing, Discrimination Complaint Activity, racial gaps in housing conditions still exist – many blacks, minorities, and

the poor are “locked out of the American dream”(Torres *et al.* 2000). Many middle-class families cannot afford to live in the city of Atlanta’s residential areas or in job-rich parts of the suburbs. Developments sprawl into the exurban fringe because many families cannot afford the near northside houses and avoid the southside (BICUMP 2000). This partly explains why the residential area of the Atlanta region is growing at such a fast pace.

(6) Transportation

Transportation plays an important role in shaping urban development. Many simulation models include distance to roads or “road-gravity” (Clarke and Hoppen 1997) as exogenous variables. The bulk of the Atlanta region’s infrastructure funds have been spent on highways, particularly in the northern part of the region (ARC 1997). Today many of the largest job centers in the region are not served by public transit. Transportation patterns play into the north-south divide in the Atlanta Region.

1.1.3 Polycentric structure of metropolitan Atlanta

Like other American metropolises, the massive suburbanization of economic activities since the 1960s contributed significantly to the spatial restructuring of the business landscape of the Metropolitan Atlanta, resulting in the clustering of high-order activities in new metropolitan-level urban centers — ‘suburban downtowns’ (Hartshorn and Muller 1989). The emergence of these large multifunctional complexes in the outer suburban city rendered obsolete the three classic models of urban structure — the concentric zone, sector, and multiple nuclei models, but conformed to the urban realms model.

Hartshorn and Muller (1989) proposed a four-stage model of suburban economic-spatial development. These stages are: (1) bedroom community (pre-1960), dominated by high rates of

city-to-suburb migration with dependency on the central business district (CBD); (2) independence (1960-1970), characterized by the transformation of suburbs from a dependence status to independency with the arrival of regional shopping centers and industrial and office parks; (3) catalytic growth (1970-1980), characterized by the agglomeration and clustering processes in the forms of corridors (suburban freeway, retail-strip, and high-technology corridors) and various types of clusters (rings of office buildings, diversified office center, large-scale mixed-use center, old town center and suburban specialty center); and (4) high-rise/high-technology stage (1980- present) when high-rise buildings surpassed the CBD in office activity, distinctive labor markets emerged, and the high-technology corridor matured.

The four-stage growth model is applicable to the evolution of suburban business landscapes in metropolitan Atlanta with small variations only in the timing of a particular stage as demonstrated by two of metropolitan Atlanta's suburban downtowns, which ranked among the largest in the United States: the Cumberland/Galleria suburban downtown (adjacent to the interchange of I-285 and I-75 in Cobb County) and the Perimeter Center/Georgia-400 (adjacent to the interchange of I-285 and GA-400 in Dekalb County) suburban downtown. The other two downtowns present in the area are the traditional CBD in downtown Atlanta, and Buckhead /Lenox, referred to as a new downtown in the study by Hartshorn and Muller (1989) (Fujü and Hartshorn 1995).

The polycentric structure can also be seen from the examination of employment data. According to Fujü and Hartshorn (1995) in 1990, the total number of workers in the four Atlanta downtowns, including the CBD, was 295,000, or 21% of the workers in Atlanta region. The largest suburban downtown, Perimeter center/GA-400, had 85,469 employees, close to the number of employment in the CBD (97,701). Forty-three percent of finance, insurance, and real

estate (FIRE) employment in the Atlanta region was concentrated in these four downtowns, with 15% in Perimeter Center/GA-400 and 11% in the CBD. These figures suggest that even for FIRE employment, which is the most concentrated of the three types of employment (FIRE, retail and services), over one-half occurred outside the major downtown areas. Fujü and Hartshorn(1995) also found that corporate office locations occur both in the CBD and in other downtowns.

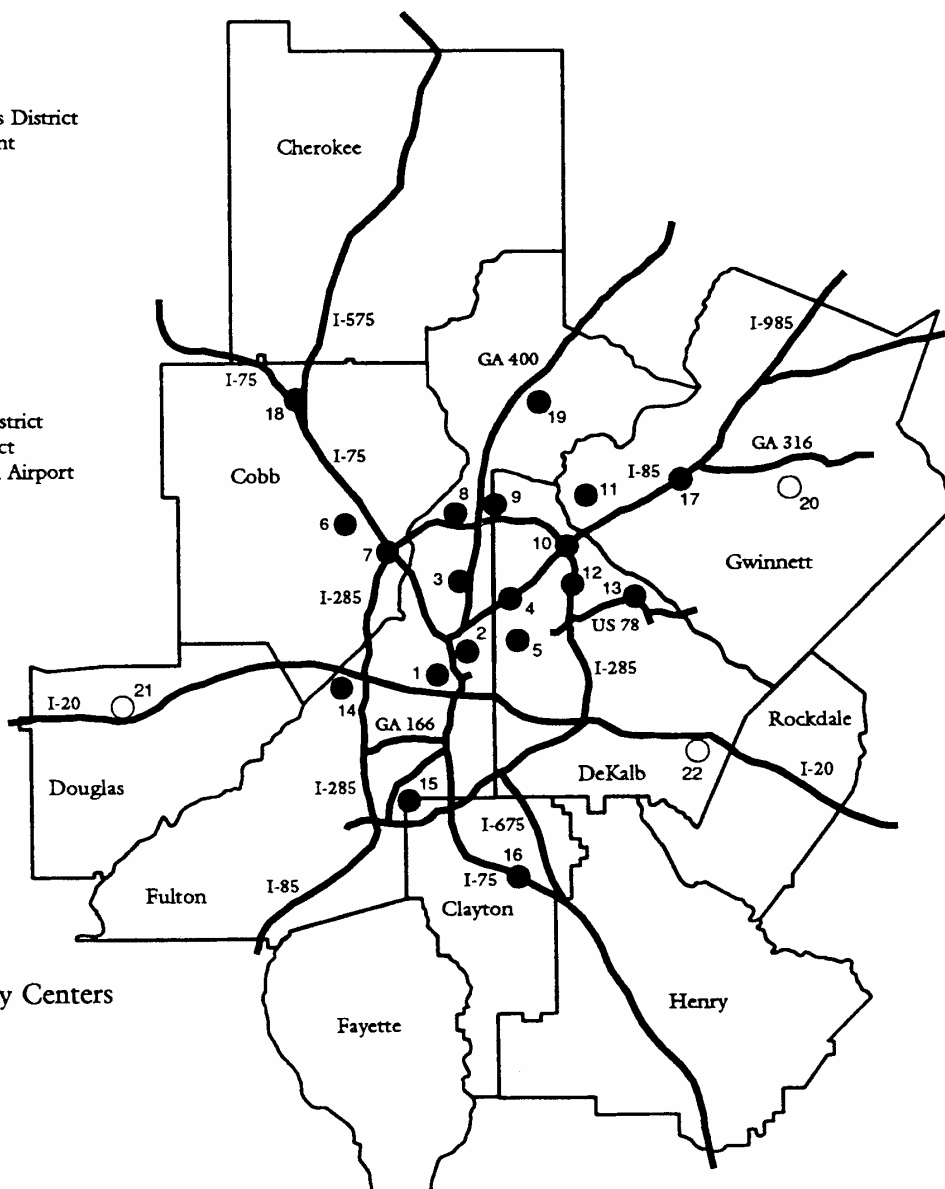
The decentralization continues with astonishing rapidity today. Major suburban downtowns have developed at the intersections of the major freeways. The ARC counted 22 existing or emerging major activity centers in metro Atlanta in 1994, 1995 and 1996 (Figure 1.5) (ARC 1994, 1995, 1996), 23 in 1997 with the addition of the new Mall of Georgia, and 24 in 2001 with the emergence of Sugarloaf Mills, nearly all north of I-20 and many north of the I-285 beltway (ARC 1997, 2001).

1.1.4 Impacts of urban growth in Atlanta

The continuous urban sprawl has many negative effects. Sprawl affects the quality of life, and intensifies economic and racial polarizations. The unchecked growth has caused traffic congestion, environment endangerment and spatial mismatch of job locations and living places. Atlanta has serious air pollution, especially caused by ground-level ozone. Atlanta ranks eighth in the year 2003's 20 most polluted metropolitan areas in the US (MSN news, April 30, 2003). The extensive system of natural waterways within the region such as the Chattahoochee River, has been endangered. Large quantities of green space have been converted to development, which has dramatically increased the urban heat island effect around Atlanta as found by the

● Activity Centers

1. Atlanta Central Business District
2. Midtown/Pershing Point
3. Buckhead
4. N.Druid Hills/I-85
5. Emory/CDC
6. Lockheed/Dobbins
7. Cumberland/Galleria
8. Sandy Springs
9. Perimeter Center
10. Doraville/I-85
11. Peachtree Corners
12. Northlake
13. Mountain Industrial District
14. Fulton Industrial District
15. Hartsfield International Airport
16. Southlake
17. Gwinnett Place
18. Town Center at Cobb



○ Emerging Activity Centers

19. North Point
20. Lawrenceville
21. Douglasville
22. StoneCrest

— Interstates and Major Highways

Figure 1.5 Major activity Centers in Atlanta region in 1994,1995 and 1996.

(Source: Atlanta Regional Commission).

Project ATLANTA (Atlanta Land-use Analysis: Temperature and Air-quality) project funded by NASA (Quattrochi and Luvall 1999). Low-density settlement increases the cost of maintaining roads, streets, sewers, water, storm drains, and schools. The Atlanta people's recent anxieties about sprawl and traffic congestion have resulted in their greater demand for information on the area's growth trends and for responses to some of the negative consequences of the region's growth, so that planning can do something about the urban sprawl.

1.2 Research objectives

This dissertation research is to model the land use/cover changes, especially urban growth, in the Atlanta, Georgia metropolitan area through linking the land use/cover change observed from satellite image data with the biophysical and socioeconomic data using spatial analysis and modeling supported by GIS. Specific objectives of this study are:

(1) To develop an accurate and effective method that takes advantage of computer automation abilities to characterize quantitatively and spatially, based on historical remotely sensed data, the process of land use and land cover change;

(2) To conduct a 'what-if' analysis to predict the quantity of distributions and spatial patterns of the future land use/cover based on land use/cover change transition probabilities revealed in the historical data analysis using a stochastic dynamic model; and

(3) To identify and improve our understanding of the socioeconomic and biophysical factors that have governed the urban growth and to find the most probable sites of urban growth using a statistical model.

This study will contribute to the remote sensing and GIS literature in three aspects:

(1) In the technology and science aspect, this study will demonstrate that the integration of GIS with remote sensing, image processing, spatial analysis, and spatial modeling can be used to explore the complex dynamics of human-induced land use/cover changes. It will show that the suite of geospatial techniques has gone beyond their role as a tool for data collection, inventory, and handling toward a disciplinary paradigm — geographical information science, which enables information mining from the data, as well as modeling and prediction of the complex human-land interaction system.

(2) In the theoretic aspect in the context of land use/cover change, particularly, urban growth, this dissertation research will advance our knowledge of spatio-temporal dynamics and human dimensions in the process of land use/cover change, provide insights on and understanding of the processes behind the changes of urban landscape patterns.

(3) In the application aspect, the results from the characterization and modeling of the land use/cover changes, especially the urban growth, using remotely sensed images and socioeconomic data, are useful for the guiding of decision making in the management of the land resources in the region. The model results can further be used to analyze the impacts of urban growth on the environment. The research findings will supply the general public with the information of their concerns about urban sprawl, and challenge the urban planning decision-makers to think broadly and critically about solutions necessary to reduce sprawl, create “smart growth” and improve life in the region. It is also expected that the methodology used to monitor and model the land use/cover change processes in this region clearly identified as a land use/cover change ‘hot-spot’, if tested to be valid, could be applied to other regions experiencing a similar urbanization process.

1.3 Dissertation structure

This dissertation is organized into six chapters. Chapter One introduces the research background, states study objectives and significance, and gives an introduction of the study area. Chapter Two reviews literature on urban morphology models, land use/cover change detection methods, and land use/cover change models. Chapter Three presents a new approach to improve the accuracy of land use/cover change detection from Landsat TM data using principal components analysis, change vector analysis, temporal logic, and a Normalized Difference Vegetation Index (NDVI) difference map. Chapter Four uses Markov chain model to characterize temporal and spatial changes in land use/cover and predicts the quantities and spatial patterns of land use/cover in the near future. Chapter Five uses a logistic regression model to establish the relationship between urban growth and the driving forces of the change using historical land use maps derived from remote sensing and demographic, biophysical and econometric data. An urbanization probability map is produced to show the spatial patterns of the most probable sites for future urban growth. Chapter Six provides a summary and conclusions of this dissertation research.

CHAPTER TWO

LITERATURE REVIEW

2.0 Introduction

This chapter gives a review of the theory and methodology that are relevant to the subject of this dissertation study. The chapter first gives a review of literature of the basic concepts and theories on urban land use/cover system, then a methodology review on land use/cover change detection methods and land use/cover modeling.

2.1 Basic concepts and theories on urban land use/cover system and its modeling

An urban land use system is dominated by human activities with complex spatiotemporal dynamics. Modeling such a system needs to be grounded in various scientific concepts and theories. The whole process of the dissertation study, from the selection of an appropriate land use model, identification of variables, to explanation of modeling results, was implicitly or explicitly guided by theoretical considerations. These concepts and theories include some philosophical, geographical, and methodological thoughts on space-time-being system, urban econometrics, urban morphology models, temporal and scalar dynamics, and the theory of complex systems.

2.1.1 Space, time, and humans in a land use system

2.1.1.2 Space

Space, time, and human being are three formative dimensions of human existence. Space is not only a social production; its organization also shapes the social relations with a feedback mechanism. When we construct an urban land use model, we must take social factors that shape the urban spatial patterns into account. Land use models should contain a feedback mechanism so that the effect of the change of spatial pattern on social factors could be considered.

Marxism links the spatial and environmental with the social and economic. With its notion of the social production of nature and space, Marxism links both human and physical geographies to society and creates a single understanding by combining the two traditions of geography: physical geography and human geography (Soja 1989). These two geographies are linked through conceptions of space and time. Spatial entities exist both in physical and human geography. Both geographies are sciences about complex spatio-temporal systems in which time and space must be thought together. What does this mean to urban land use modeling? It means that a spatio-temporally dynamic model is ideal to approach the real problems with urban sprawl.

2.1.1.2 Time

Geographers incorporate time into their explanations, which seek to recover some temporal relationships among phenomena over a longer period. These temporal relationships are the only way of referring to historical conditions that shed light on the current situations under thinking and investigation. The only way to develop objective measures of time is in terms of some processes. In a process, laws govern the mechanism and direct the trajectory of a dynamic

system. Geographical dynamic modeling seeks to simulate the process, such as Markov chain modeling of land-use change and cellular automata (CA) modeling of urban growth.

There are four major types of temporal explanations in geography: narrative, reference to time and stage, hypothesized process, and reference to actual process (Harvey 1969). In explanation by hypothesized process, a particular process is assumed to exist, and, given that process, an artificial time scale is produced to locate events and hence explain them. The hypothesized processes are thought of as deterministic. In explanation by reference to actual process, the actual process is based on empirical evidence.

Structuralist and realist philosophies argue that explanation for observed patterns cannot be discovered through analysis of the patterns themselves, but only by the development of theories of the underlying processes that generate the conditions with which human agents can create those patterns. Marxism is foremost within this group, which argues that the processes are themselves changing, and can be altered by concerted political actions, so that no laws of spatial organization are possible (Soja 1989; Curry 1996). The observed urban spatial pattern cannot be explained by the pattern itself. It must seek social, economical and environmental explanations.

2.1.1.3 Systems approach and mathematical modeling

A system is a series of linked elements interacting to form an operational whole. The study of systems allows dynamic processes to be incorporated within geographical analysis (Livingstone 1992). Social systems are open or at most quasi-closed systems producing regularities that are only approximate and spatially and temporally restricted. Accurate and reliable explanatory prediction for open systems are impossible. The predictive methods dealing with open systems are neither non-explanatory nor fully explanatory, but a compromise taking the form of an

empirical model in which some of the main processes are summarily represented by variables is possible. Whether systems of interest are closed or open has a strong bearing upon the use of mathematical models. Theoretical models posit the existence of a hypothetical closed system (Hilts 1973). Statistical processes are often said to be probabilistic and involve chance or random elements. One of the weaknesses of statistics is that there often exists dependency between independent variables.

2.1.2 Urban econometrics

To develop a spatially explicit land use/cover model, one needs to understand the economic process at work, i.e., the human behavioral component that underlies land use change (Irwin and Geoghegan 2001). For example, the Von Thünen model relates intensity and type of land use to transportation costs and land rent (Von Thünen 1966). The model involves a homogeneous plain within which exists an isolated city. Land-use patterns around this city are a function of travel cost to the city. Land uses producing goods with a relatively high transportation cost would be produced close to the city, and land uses producing more durable goods with lower transportation costs would be produced farther from the city. This arrangement results in a series of different land use zones around the city. A Von Thünen-like model can be used to guide the identification of determinants of land use and land cover change. Bid-rent theory suggests different functions will bid differently for land in various parts of the city (Alonso 1964). It suggests that the more accessible the site of land, the higher its value. The relationship between development factors and urban structure is conceptualized by bid-rent theory in urban econometrics (Wu 2002). The main determinant of land use change, according to mono-centric bid-rent theory, is the distance to the city center. This is an elegant but too simplified deduction.

With the rapid development of modern transportation, telecommunications, computer and networking technologies, and under the situation of globalization of economy, using the distance to a single city-center as a main determinant of urban land use is not appropriate. Travel cost is no longer determined only by distance; longer distance transportation may not cost more than shorter distance. Urban development does not necessarily take on a monocentric form. The actual land development is subject to many biophysical, socioeconomic and policy factors.

2.1.3 Models of urban structure

Both urban econometric factors and social forces help shape the spatial structure of cities. Cities are spatially organized to perform their functions as a place of commerce and a place to live (de Blij 1993). There are four well-known models of urban structure (Figure 2.1).

(1) Concentric zone model (Figure 2.1(a))

Burgess (1925) proposed the concentric zone model based on his observations of Chicago during the early years of the 20th century. He recognized five concentric zones. The innermost zone is the CBD (region 1), containing shops, offices, banks, government buildings, and hotels. Surrounding the CBD is a transitional area, a zone of residential deterioration, also marked by the encroachment of business and light manufacturing. Region 3 is the zone of workingmen's homes, a ring of closely built but adequate residences of the urban blue-collar labor force. The next zone (region 4) consists of middle-class residences, and out-central-city/inner suburban areas, characterized by greater affluence and spaciousness. Region 5 is the commuters' zone where residents commute to the CBD to work. An important feature of this model is the positive correlation of socioeconomic status of households with distance from the CBD — more affluent households were observed to live at

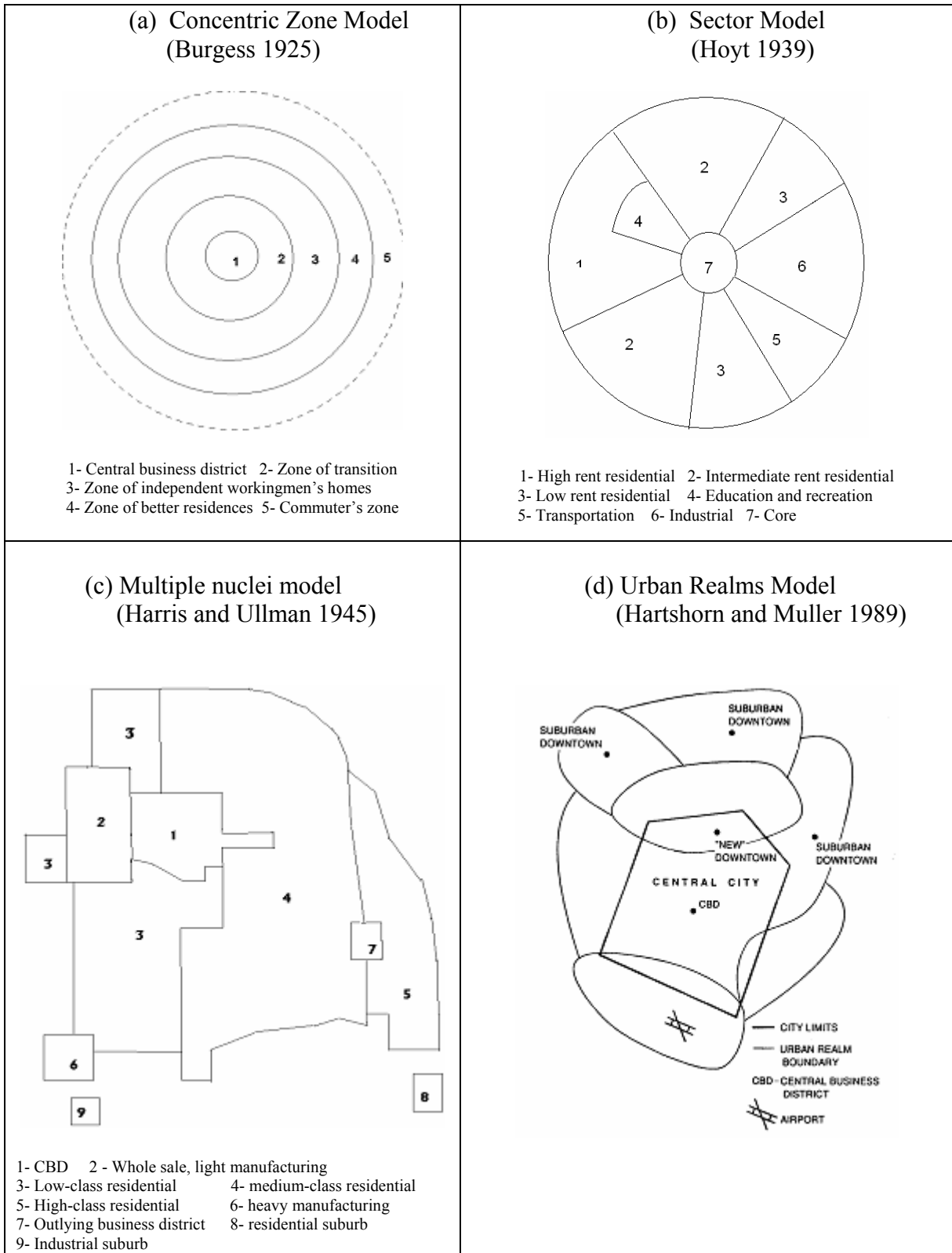


Figure 2.1 Models of urban structure.

greater distances from the central city. Burgess described the changing spatial patterns of residential areas as a process of “invasion” and “succession”. As the city grows and develops over time, the CBD would exert pressure on the zone immediately surrounding it (the zone of transition) and invade nearby residential neighborhoods causing them to expand outward. The process was thought to continue with each successive neighborhood moving further from the CBD.

(2) Sector model (Figure 2.1(b))

Hoyt (1939) proposed the sector model of urban structure. Hoyt modified the concentric zone model to account for the influence of major transportation routes. Recognizing that transportation routes represent lines of greater access, Hoyt theorized that cities would tend to grow in wedge-shaped patterns, or sectors, radiating from the CBD (core) and centering on major transportation routes. Higher levels of access translate to higher land values. Thus, many commercial functions would remain in the CBD, but manufacturing activity would develop in a wedge surrounding transportation routes. Residential land use patterns also would grow in wedge-shaped patterns with a sector of lower-income households bordering the manufacturing/warehousing sector and sectors of middle- and higher-income households located away from the industrial sites. Major intercity transport lines may be converged so closely together that a transportation sector can be recognized. A major university and several schools can also form a discrete sector.

(3) Multiple nuclei model (Figure 2.1(c))

Harris and Ullman (1945) proposed the multiple nuclei model in which a metropolis was seen as consisting of discrete functional areas, each forming around their own separate nuclei. The model suggests that an urban area may grow and develop from not just around one

functional focus, but several. While Harris and Ullman (1945) still saw the CBD as the major center of commerce, they suggested that specialized cells of activity would develop according to specific requirements of certain activities, different rent-paying abilities, and the tendency for some kinds of economic activity to cluster together. At the center of their model is the CBD, with light manufacturing and wholesaling located along transportation routes. Heavy industry was thought to locate near the outer edge of the city, perhaps surrounded by lower-income households, and suburbs of commuters and smaller service centers would occupy the urban periphery.

(4) Urban realms model (Figure 2.1(d))

The urban realms model was originally developed to reflect the situation in the 1950s in the San Francisco Bay Area (Vance 1964). A key element of the urban realm model is the emergence of large centers of diversified economic activities in the suburbs, which represents the transition from the single-centered to the polycentric city. Hartshorn and Muller (1989) called these suburban centers 'suburban downtowns' in the case of Atlanta. The suburban downtowns are self-sufficient and independent of the central city. Suburban downtowns provide specialized goods and services for a particular realm. At the regional level, the entire metropolis becomes reorganized into a set of independent urban realms.

2.1.4 Scale dynamics

Scale is the spatial, temporal, quantitative, or analytic dimension used by scientists to measure and study objects and processes (Gibson *et al.* 2000). All scales have extent and resolution. For each process important to land use and land cover change, a range of scales may be defined over which it has a significant influence on the land use pattern (Meentemeyer 1989). Processes and

relationships change both with the spatial (temporal) resolution and extent at which they are observed. Some social and ecological processes may be associated with a particular scale, while other processes might occur across multiple scales. Ecological and social processes may not operate at the same scale and linkages may have to be developed to connect across scales (Agarwal *et al.* 2001).

2.1.5 Temporal dynamics

The process of land use change is dynamic. “Change” itself is a temporal concept. Land use has a temporal dimension which is of great importance for land use modeling. The changes are nonlinear. We cannot simply interpolate or extrapolate a spatial pattern linearly from a time series of satellite images. Non-linear behavior asks for dynamic modeling with relatively short time steps.

Path-dependency of system evolution should be considered. The present land use spatial pattern cannot be simply explained as the equilibrium result of the present set of driving forces. When considering path-dependency, we are actually incorporating temporal interactions, a counterpart of spatial interactions. Path-dependency means that a system’s current state and trajectory of change depend on its history, not on current values of driving forces alone. A path-dependent system may exhibit several properties that must be considered in land use/cover change assessments (Arthur 1989): varying predictability; non-ergodicity (historical events are not averaged away, and small perturbations may significantly influence long-run development); progressive inflexibility (the system is ultimately insensitive to perturbations); and potential inefficiency (the outcome is not optimal for society).

2.1.6 Theory of complex systems

A land use system in a rapid sub-urbanization region is a complex system, in which human and land interact dynamically. Several important sources of complexity influence land use decisions, for example, spatial heterogeneity, spatial interdependencies, scale dependencies. A complex system consists of a large number of intelligent, adaptive agents (Battern 2001). To be more realistic, models representing such a system should consider theories of system complexity.

The main idea in complexity theory is emergence. An emergent phenomenon is defined as the collective behavior which does not seem to have any clear explanation in terms of its microscopic parts that look chaotic individually. In emergent systems, a small number of rules, applied at a local level and among many agents are capable of generating surprising complexity and often ordered patterns in aggregate form (Torrens 2001). Large-scale regularities or order emerge purely from the micro-dynamics without the direction of a centralized executive.

Sometimes, this order takes the form of self-similarity at different scales. Segregation and self-similarity are familiar examples of emergence. Interactions among agents take on nonlinear character. Actions of parts constituting a complex system do not sum to the activity of the whole. In urban land use systems, macroscopic and regional spatial patterns can be understood to operate from local-scale interactive dynamics. Cities show several of the signature characteristics of complexity, including fractal dimensionality and self-similarity across scales, self-organization, and emergence (Batty and Longley 1994; Allen 1997; Portugali *et al.* 1997).

2.2 Land use/cover change detection methods

Land use/cover change detection provides a fundamental input for planning management and environment studies, such as landscape dynamics or natural risks and impacts (Sommer *et al.*

1998). Digital change detection based on satellite images is a process of identifying differences in the state of an object or phenomena by observing it at different times. The basic premise in using remote sensing data for change detection is that changes in land use/cover must result in changes in radiance values, and changes in radiance due to land use/cover change must be large with respect to radiance changes caused by other factors, such as the differences in atmospheric conditions, sun angle, and soil moisture (Singh 1989). Several authors have reviewed and/or compared remote sensing change detection techniques in general (Singh 1989) and in particular (Coppin and Bauer 1996; Macleod and Congalton 1998; Mas 1999). The major land use/cover classification methods are post-classification comparison, image differencing, change vector analysis, image ratioing, classification of multi-date image date sets, and principal components analysis.

In the *post-classification comparison* change detection method, two dates of images are classified independently and registered. The corresponding pixels are compared. A frequency matrix is generated to cross-tabulate the specific 'from-to' nature of the changes between the two dates. A change map is created to label the specific nature. This method is intuitive and direct in that it outputs the specific nature of changes. Also this method bypasses the problem of radiometric normalization since the two dates images are independently classified (Singh 1989). However, the classification errors are compounded in the pixel-by-pixel comparison process, resulting in low accuracy of the change detection. For example, in an urban landscape, post-classification land use/cover change detection could result in the disappearance of urban areas, although this is usually impossible.

In the *image differencing* method, registered images of two dates are subtracted to produce a residual image which represents the change between the two dates. Pixels of no

radiance change are distributed around the mean, while pixels of radiance change are distributed at the tails of the distribution(Singh 1986).

Change vector analysis is a change detection procedure that is a conceptual extension of image differencing. A two dimensional coordinate space is defined by two spectral variables (e.g., the digital numbers from two bands, or derived data values, such as vegetation index). A vector for each pixel can be plotted by connecting the time t1 data point to the time t2 data point. The magnitude of the vector can be used to determine areas of change using a threshold, and the direction of the vector indicates the nature of change (Malila 1980; Michalek *et al.* 1993).

Image ratioing for change detection computes the ratio of the images from two dates of imaging. Ratios for areas of no change tend toward 1 and areas of change will have higher or lower ratio values (Howarth and Wickware 1981). One of the advantages of the image ratioing method is that it tends to normalize the data for changes in terms of sun angle and shadows. Both image ratioing and image differencing methods need analysts to define a meaningful threshold value to differentiate change from no-change.

In change detection by *classification of multi-date image date sets*, a single classification is performed on a combined data set for the two dates of interest using either supervised or unsupervised clustering approaches (Weismiller *et al.* 1977; Singh 1986). The success of this method depends on the extent to which “change classes” are significantly different spectrally from the “no-change” classes.

Principal components analysis is often used to analyze multi-date image composites for change detection (Richardson and Milne 1983; Fung and LeDrew 1987). In this approach, two images are registered to form a new multi-band image containing all bands from each date. Several of the uncorrelated principal components computed from the composite dataset can often

be related to areas of change. One disadvantage to this process is that it is often difficult to interpret and identify the specific nature of the changes involved.

The various land use/change detection approaches explained above were grouped into two basic categories of approaches for change detection (Singh 1989). The first category is *map-to-map comparison*, which is comparative analysis of independently produced classifications from different dates. The post-classification comparison method belongs to this category. The second category is *simultaneous analysis of multi-temporal data*, including image differencing, change vector analysis, image ratioing, classification of multi-date image date sets, and principal components analysis.

The first category *map-to-map comparison* has several sources of uncertainty. Aspinall and Hill (1997) emphasize two of them: (1) misregistration of the polygon boundaries (location inaccuracy) in the different classifications creates border pixels with false or negative changes. In vector format, misregistration can generate slivers; and (2) problems derived from classification errors result in false positive changes being recorded when no change has taken place because a polygon in one or both of the two maps is misclassified, or false negative changes, when no change is identified although a change has taken place.

Some problems with the second category *simultaneous analysis of multi-temporal data* are (Serra *et al.* 2003): (1) most of these procedures provide little information about the specific nature of land use/cover change; (2) the threshold techniques used to differentiate change from no-change is not usually clear; and (3) mis-registration between images continues to be a problem, and it is not properly considered in the quantification of the land use/cover change detection.

When multi-sensor images are used, some problems appear for both categories of land use/cover change detection methods (Serra *et al.* 2003): (1) the classifications differ because some features are not detected in the coarser resolution images which do appear in the finer resolution images; (2) overlaying for land use/cover change analysis is complicated by different pixel size and grid origin, resulting in misregistration; and (3) the number of bands, their wavelengths (spectral information), and sensitivity of the sensors are different.

Recently, some new methods of land use/cover change detection have appeared. One of them is *cross-correlation analysis* (CCA). CCA is a change detection method measuring the differences between an existing land use/cover image and a recent single date multispectral image (Koeln and Bissonnette 2000). CCA works by using the class boundaries from land use/cover image to derive an expected class average spectral response. This information is used to derive a *Z*-statistic for each pixel falling within a given land use/cover type. The *Z*-statistic describes how close a pixel's response is to the expected spectral response of its corresponding class value in the land cover image. Pixels that have undergone change between the time t_1 land use/cover image and the time t_2 multi-spectral image will produce high *Z*-statistics values while those that have not changes will produce low *Z*-statistic values. The advantage of this technique is that it eliminates the problems associated with radiometric and phenological variations between multi-date images. The limitation of this method is that it can only detect a single type of change by setting a user-defined threshold of the *Z*-statistics values.

2.3 Land use change models

2.3.1 Uses of land use models

Models are used for prediction, explanation and discovery of the unknown through heuristic learning (Gross and Strand 2000). Land use change modeling, especially if done in a spatially-explicit, dynamic, integrated and multiple-scale manner, is an important technique for the projection of alternative pathways into the future and for conducting experiments that test our understanding of key processes in land use changes (Veldcamp and Lambin 2001). Land use models are used to support causal and consequential analyses of land use dynamics and to inform land use planning and policy making through their scenario analysis ability. Land use change models should represent part of the complexity of land use systems. They offer the possibility to test the sensibility of land use patterns to changes in selected driving forces.

2.3.2 A three-dimensional framework to review land use models

Land use is determined by the interaction in space and time of biophysical factors and human factors (such as population, technology, economic conditions, etc.) (Veldcamp and Fresco 1996). How to deal with space, time and human dimensions in the modeling of the complex land use systems is what land use modelers should consider. Agarwal *et al.* (2001) proposed a three-dimensional framework to review land use models. The three critical dimensions are *space, time, and human decision-making* (Figure 2.2). Each axis of the three-dimensional framework represents the degree of the complexity with which a model can deal. Based on this framework, Agarwal *et al.* (2001) examined a summary of 250 relevant citations and developed a bibliography of 136 papers from which 19 representative land-use models were reviewed. In the 19 models, 10 modeling methods were identified: Markov, logistic function, regression,

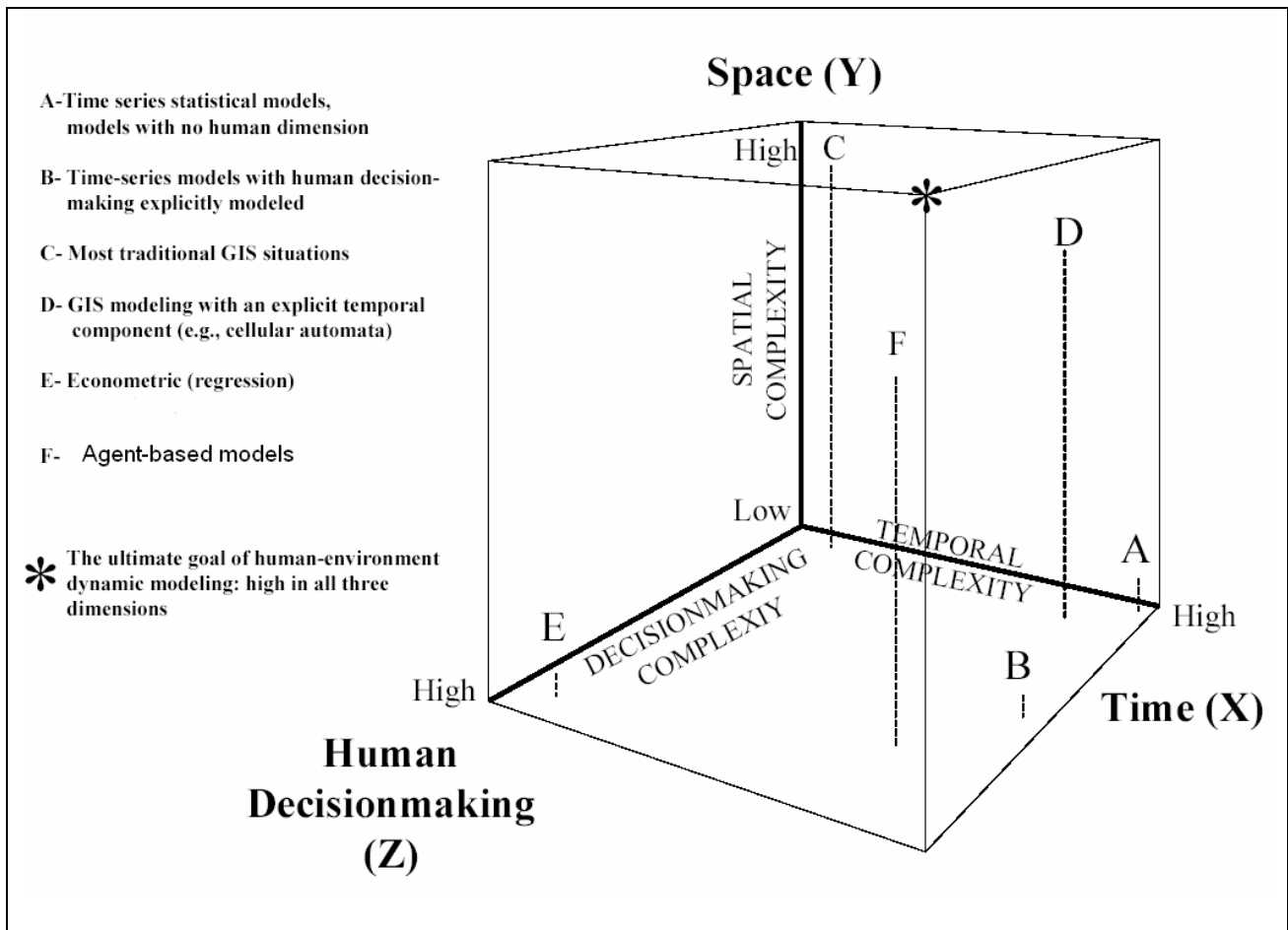


Figure 2.2 A Framework for Reviewing Land Use Change Models. (Source: Agarwal *et al.* 2001).

econometric, dynamic systems, linear planning, nonlinear mathematical planning, mechanistic GIS, cellular automata (CA), and agent-based models. They also provided a list of variables regarding social drivers of land use/cover change summarized from the models that have been reviewed (Table 2.1). These variables are related to demography, technology, economy, political and social institutions, information and its flow, and culturally determined attitudes, beliefs, and behavior. They propose that there is a need for land use models to be able to include the relative effects of different social drivers on land use change in the context of space, time, and human decision-making.

2.3.3 Classifications of land use models

Researchers have reviewed and categorized land use models from different points of view. Parks (1990) classified economic land use models into three categories. *Inventory/descriptive* models do not employ explicit economic theory. *Engineering/optimization* models solve for the landscape patterns that best achieve quantifiable goals and meet constraints. Multiple criteria evaluation (MCE) models fall into this category. *Statistical/econometric* models of land use describe relationships between changes in landscape and various economic, social, policy, or environmental variables.

Irwin and Geoghegan (2001) classify land use models into *spatially explicit non-economic models* and *economic models* by examining if a model uses economic theory to guide the model development. Spatially explicit non-economic models use an *ad hoc* approach to identify physical variables that represent the outcomes of economic and social processes, e.g., the location of roads and urban centers, without any underlying economic theory to guide the choice of variables. This group of models includes simulation (e.g., Cellular Automata model),

Table 2.1 Summary of human drivers reflected in land use/cover change model variables

(Source: Agarwal *et al.* 2001)

Human Drivers or Social Patterns and Preferences	Model Variables
	Population Size
	Population Growth
	Population Density
	Returns to Land Use (costs and prices)
	Job Growth
	Costs of Conversion
	Rent
Collective Rule Making	Zoning
	Tenure
Infrastructure/Accessibility	Relative Geographic Position to Infrastructure: Distance from Road
	Distance from Town/Market
	Distance from Village/Settlement
	Presence of Irrigation
	Generalized Access variable
	Village Size
	Silviculture
	Agriculture
	Technology Level
	Affluence
	Human Attitudes and Values
	Food Security
	Age

empirical, and hybrid models that include estimated parameters with simulation. Economic models attempt to fit the spatial process of land use change by developing an underlying structural model that seeks to explain the human behavior generating these patterns. Economic models include non-spatially explicit economic models (such as traditional microeconomic models, regional economic models), and spatially explicit economic models.

Baker(1989) gives a taxonomy of landscape change models based on the criteria of the level of aggregation and the use of continuous or discrete mathematics. Landscape models are classified as whole landscape, distributional landscape, or spatial landscape models.

Distributional models are divided into differential equation (time as continuous, including continuous state space and discrete space models), and difference equation (time as discrete, including Markov chain, semi-Markov chain, and projection models).

2.3.4 Issues in land use modeling

Several issues are of great importance in land use modeling. These include: the level of analysis, scalar dynamics, drivers of land use change, spatial interactions and neighborhood effects, temporal dynamics, and level of integration (Verburg 2004). No single modeling method has the ability to deal with all these issues. The choice of an appropriate model or a combination of models must seek a trade-off balance, subject to data availability, theoretical assumptions and research objectives. In the following sections, the ability of the different land use models to deal with these important issues inherent in land use modeling will be examined.

2.3.4.1 Level of analysis

Land use modeling has been an active research area both in social sciences and environmental science. Social scientists and environmental scientists conduct research on a different level of observation and analysis. In the social sciences, land use modeling employs a micro-level individual behavior approach. On the other hand, environmental scientists model land use on the macro-scale; their models are spatially explicated through the integration of remote sensing and GIS, as well as the use of macro-properties of social organization in order to identify social factors connected to the macro-scale patterns.

Two approaches have been used to model land use from the *micro-level perspective*:

(1) *Agent-based models* (ABM, also known as individual based model). ABMs include three basic components: *agents*, *environment* (a two-dimensional space in the context of land use change modeling), and a set of behavioral rules. Just a few simple micro-level local rules can produce richly complex outcomes. The best known ABM development tool for use in the social sciences that can be adapted for ecological and land use simulation is the Swarm software package developed by the Santa Fe Institute. Most current multi-agent models are only able to simulate very simplified, artificial landscapes. Using the Swarm development tool, Rand *et al.* (2003) present and evaluate an agent-based model of land use change at the rural-urban fringe for an artificial city represented by a grid of 301 by 301 cells with each cell having two exogenous characteristics: a natural beauty score (an index describing how beautiful the natural environment of a location is) and the presence or absence of an initial service center. Two kinds of agents are modeled: residents and service centers. Agents behave according to their location preferences, finally producing a residential spatial pattern. Efforts are currently underway to build operational multi-agent models for realistic land use change simulations. One challenge in

this area is to obtain sufficient data at the individual, household or land parcel level to develop a well-parameterized and validated model of decision-making. There exist several obstructions to an agent based model's successful use in operational urban geographic simulation, particularly with regard to the capacity of these methodologies to handle top-down dynamics in urban systems (Torrens 2001). In urban contexts there are several systems and mechanisms that operate in this manner, including constraints such as planning restrictions.

(2) *Based on the micro-economic theory*, as reviewed by Irwin and Geoghegan (2001).

An individual landowner makes his/her land use decisions with the objective of expecting maximum returns or utility. The choice of explanatory variables is guided by economic theory. Problems arise when these models are used at a higher aggregation level as often needed because at a higher level, individuals cannot be discerned and aggregated data derived from individuals do not sum individuals linearly.

Macro-level analyses are based either on macro-economic theory or the systems approach. For example, the IIASA-LUC (Land Use Change project by International Institute for Applied Systems Analysis) model developed for China by Fischer and Sun (2001) establishes an integrated assessment of the spatial and inter-temporal interactions among various socioeconomic and biophysical forces that drive land use and land cover change. This model is based on recent advances in applied general equilibrium modeling in macro economics. Other land use models are based on macro spatial structure of land use, such as the CLUE-CR (Conversion of Land Use and its Effects – Costa Rica) model (Veldcamp and Fresco 1996) and GEOMOD2 (Pontius *et al.* 2001).

Traditional urban (simulation) models (spatial interaction or gravity) are macro-level models. The minimum of resolution analysis is an aggregate-level enumeration district (ED)

(e.g., a census tract, a traffic analysis zone (TAZ)). Their assumptions portray cities as operating from the top down. Models are often illustrated as flow diagrams that begin with a regional scale and filter to TAZ-level components. The shortcomings of this centralized approach are: a poor treatment of dynamics, weak attention to micro-scale detailed phenomena, limited usability, reduced flexibility (difficulty in scaling and lack of modularity), and lack of realism (due to the ‘reductionist’ view of urban systems) (Torrens 2001).

In urban system modeling, often a single level of analysis is not sufficient to explore the urban dynamics. An approach that is based purely on micro-level modeling or purely on macro-models is weaker than a combined approach. There is a need for developing hybrid models that contain mechanisms for linking macrostructure to micro-behavior. Torrens (2001) presents a framework for developing a hybrid model for urban geographic simulation. Macro-scale dynamics that operate from the top-down are handled by traditional land-use and transport models, while micro-scale dynamics that work from the bottom-up are delegated to agent-based models and cellular automata. The two methodologies are fused in a modular fashion using a system of feedback mechanisms.

2.3.4.2 Scalar dynamics

The issue of scale is related to the level of analysis, which has been discussed above. To address the issues of scalar dynamics, interpreting, merging, analyzing the data, and analyzing the effects of multiple spatial, temporal, and hierarchical scales are often needed in land use change modeling.

To date, most land use models are based on one scale or level exclusively. In these models, the resolution of analysis is determined by the measurement technique or data quality

instead of the processes specified. Of the 19 models reviewed by Agarwal *et al.* (2001), 11 are raster-based, most of which have spatial resolutions of 30 to 80m, mirroring the pixel size of remote sensing data, and have spatial extents at or less than the area covered by one Landsat scene (185km×185km). Dynamic cellular automaton model calibration is very computation intensive, and as a result coarser resolutions are used. For example, Clarke and Hoppen (1997) applied a self-modifying cellular automaton model to the analysis of historical urbanization in the San Francisco Bay area based on a 300m resolution.

Although most existing models only take a single scale of analysis into account, some models implement multiple scales. These models implement a multi-scale procedure either in the quantification of the driving variables or in the structure of the model.

(1) *Multiple-scale quantification of the driving variables*

Different driving forces operate at different scales. Models should explicitly take into account of the scale dependency of the quantitative relation between land use and its driving forces. There have been three different approaches to quantifying the multi-scale relations between land-use and driving forces. The first is to use *varying resolution* raster layers representing driving variables; at each individual resolution the relations between land use and driving forces are statistically determined (Walsh *et al.* 2001; Kok and Veldcamp 2001; Kok *et al.* 2001). The second is to use *varying extent* data sets to derive the relationship between land use change and the determining factors (Kok and Veldcamp 2001). The third approach uses multi-level statistics (Goldstein 1995). It has been found recently that the multi-level statistical technique for the analysis of hierarchically structured data could also be used to analyze land use, taking different driving forces at different levels of analysis into account. Polsky and Easterling

(2001) applied this technique to the analysis of the land use structure in the Great Plains of the U.S..

(2) Hierarchical model structure

A number of land use change models take the form of a hierarchical structure, thus taking scalar dynamics into account. For example, the total amount of change is determined for the study area as a whole using a model at the top of the hierarchy and allocated to individual grid-cells by adapting a threshold value of a probability surface generated by a model at the lower part of the hierarchy. The underlying rationale for this method is the demand-driven nature of land use change. In the CLUE-CR model (Veldcamp and Fresco 1996), a top-down allocation procedure links a national scale for demand calculations with two spatially explicit lower-level scales to take driving forces at different scales into account.

2.3.4.3 Drivers of land use change

A prerequisite to the development of realistic models of land use change is the identification of the most important drivers of change (Veldcamp and Lambin 2001). Traditionally, modelers only focus on biophysical attributes (e.g., altitude of terrain, slope, or soil type). However, land use change is human-induced, and as a result the incorporation of data on a wide range of socioeconomic drivers of change is required. Land use policies also often determine the land conversion. However, incorporation of social, political and economic factors is often hampered by a lack of spatially explicit data and by methodological difficulties in linking social and biophysical data. Biophysical data used are often extracted from satellite remote sensing data in raster format. Socioeconomic data are often collected by censuses or surveys. For the biophysical data, the observation unit is cells (pixels); but for the socioeconomic data, the observation unit is

artificial enumeration districts (ED) (e.g., census tracts) or sampling points. To link people with pixels, socioeconomic data need to be disaggregated to cells upon which modeling is based.

Another related issue is how best to represent these drivers that cannot be measured directly in a model. Proxy variables are often used, for example, distance to a road or a town as a proxy of travel cost.

For land use modeling, two aspects regarding drivers of land use change are of importance and should be considered in the modeling. One is the selection of drivers (explanatory variables); the other is how to quantify the relations between land use and driving forces.

Selection of drivers is dependent on the simplification made and the theoretical and behavioral assumptions used in modeling land use system. In most economic approaches to land use modeling, optimization of utility is the assumed behavior, leading to bid-rent models. In its simplest form, the monocentric model, the location of a land parcel relative to a central city or the business district is the major determinant of the parcel rent (Irwin and Geoghegan 2001).

There are three approaches to *quantification of relations* between land use and driving forces:

(1) *Process-based models*. These models base relations between land use and driving forces directly on the processes involved in the land use conversion, using theories and physical laws. Process-based models have sound theoretical basis and can be used for hypothesis formulation and identification of variables that should be incorporated into a statistical model (Veldcamp and Lambin 2001). Examples are economic models based on economic input-output analysis (Fischer and Sun 2001). In an integrative land use change analysis, this method is often

not very successful due to the difficulty of quantifying socioeconomic factors without the use of empirical data.

(2) *Empirical estimation models*. Many econometric (Geoghegan *et al.* 1997) and non-econometric models (Veldcamp and Fresco 1996; Pontius and Schneider 2001; Pontius *et al.* 2001; Serneels and Lambin 2001) use statistical techniques, mainly regression, to quantify the defined models based on the historic data of land use change. Most of these approaches describe historic land use conversions as a function of the changes in driving forces and location characteristics. Empirical statistical models are easier to implement, and allow for hypotheses testing given limitations in data availability. Empirical models often rely on the implicit assumption that land-use change processes are stationary (the rate of change keeps constant at different time periods) (Veldcamp and Lambin 2001). In many cases, these models fit the spatial process and land use change outcome reasonably well (Irwin and Geoghegan 2001). However, they are less successful at explaining the human behavior that leads to the spatial process or the outcome of land use change because the unit of analysis is either an individual pixel or an enumeration district (ED), rather than the individual decision-maker. Empirical models often result in a relatively low degree of explanation due to the relatively short time-period of analysis, variability over this time period and a relatively small sample size, thus inducing uncertainty with respect to the causality of the supposed relations. Little consideration has been given to temporal dynamics in these models, most likely due to the lack of data on driving forces, which can bias estimation results.

There are two empirical modeling techniques suitable for each of the two kinds of unit of analysis discussed above (either an enumeration district or a pixel). At the level of aggregated enumeration districts, *traditional multivariate analysis*, especially multiple linear regression

techniques, are generally used to identify explicitly the proximate causes of land cover changes. Since the unit of analysis is coarse (e.g., census tract), this method is not spatially explicit enough to portray the spatial pattern of land use change. They are unable to deal with spatial variability in the processes of land use change. In most regions, there is a high geographic variability in land cover types, biophysical and socioeconomic drivers of land use changes, or institutions (including policies). This spatial heterogeneity leads to variability in the causes and processes of land use changes.

Multinomial logit models are often used to empirically and spatially explicitly quantify the relationship between land use change and driving forces at the level of a pixel. Discrete choice modeling (DCM), sometimes called qualitative choice modeling, is an exciting new statistical technique sweeping the world of market research (Train 2003). Discrete choice theory was developed in parallel by economists and cognitive psychologists. DCM looks at choices that customers make between products (or services). By identifying patterns in these choices, DCM models how different consumers respond to a marketplace filled with competing products. DCM allows marketers to examine the market-share impact of product configuration, service bundling, pricing and promotion on different classes of customers. Discrete choice theory suggests that the specific form is dependent upon the statistical distribution of an error item and that in the context of a discrete choice it should be in the form of the binomial logit model or multinomial logit model.

Land development can be modeled through a discrete choice framework. In land use models based on discrete choice theory, there are alternative discrete states of land use for a particular land parcel. Land development is considered as a process of particular land users choosing particular land uses. In a binomial logit model, the choices are dichotomous: there are

two states of choice, e.g., urban versus non-urban use. In a multinomial logit model, there are more than two choices, such as commercial, residential, forest, agriculture/pasture and bare land. Multinomial logit models have also been used at an observation unit other than a pixel, such as a land parcel. For example, McMillen and McDonald (1989) uses an empirical multinomial logit model to predict land use in an urban fringe area of Chicago. The observation units are 382 land lots. However, the model is not fully spatially explicit.

Landis and Zhang (1998) model development and redevelopment in an urban setting using a spatially explicit and disaggregate discrete choice approach. The observation unit is a 1-hectare cell. The choice of explanatory variables includes initial site use, variables to capture demand pressures, distance/accessibility measures, costs of development, returns to alternative uses, and non-conforming uses.

Schneider and Pontius (2001) empirically model deforestation in the watershed of the Ipswich River in Massachusetts of the US (404 square kilometers, 30m cell size) using a multinomial logit model, including elevation, slope and distance to residential area as explanatory variables. While the model generates probability maps, the quantity of change is calibrated using regression or simple extrapolation of historical data. The model does not have complicated dynamics.

Geoghegan *et al.* (2001) model tropical deforestation for an area of 1600 square kilometers in southern Yucatan peninsular region using a binomial logit model. The unit of observation is the Landsat TM pixel (28.5m by 28.5m). The probability of deforestation in a specific pixel is estimated as a function of explanatory variables: environmental factors, distance, socioeconomic census data and spatial indices of the land uses surrounding a pixel capturing the effect of landscape diversity or fragmentation on land cover. The model deals with the census

data in an aggregate way: a single average value for each socioeconomic variable is assigned for all pixels within each census unit.

Serneels and Lambin (2001) use a binomial logit model to analyze the proximate causes of land use change in Narok, Kenya. The limitations of the model are: the spatial model developed allows us to predict *where* land-cover conversions are most likely to take place in the near future, but does not address the question "*when* are land-cover conversions likely to take place?" A dynamic model that considers the driving forces of change needs to be developed.

To overcome the shortcomings that empirical stochastic models lack temporal dynamics, empirical models are combined with CA models to take advantage of their dynamic nature. Wu (2002) develops a stochastic CA model for urban growth in Tianhe district, Guangzhou, China (30-meter cell, 546 rows by 629 columns), which derives its initial (global) probability of simulation from observed sequential land use data using a binomial logit model. This initial probability is updated dynamically through local rules based on the strength of neighborhood development.

(3) *Rule-based models* such as CA and agent-based models. These models demonstrate how complex structure arises internally from the interactions among individual cells. While these models are instructive and offer a practical approach to understanding of how interactions among individual agents “aggregate up” over space to determine regional patterns of land use (Irwin and Geoghegan 2001), the theoretical basis for the specification of rules is poor. When the number of data layers (variables) increases, the definition of the rule becomes more difficult. As a result, most CA models cannot incorporate enough socioeconomic variables in the estimation models. The model developed by Clarke and Hoppen (1997) is not capable of linking external parameters (such as an economic growth rate) to the self-modification of the CA rules. Rule-based models

reveal, but do not always explain, the inherent dynamics (Battern 2001). Conclusions about their explanatory power could be misleading and should not be overstated.

2.3.4.4 Spatial interactions and neighborhood effects

Land use patterns often exhibit spatial dependence. This can be partly explained by the spatial interactions among land use types. Urban expansion often occurs next to the existing urban area, especially when scale economy development plays a role in shaping urban forms; in this case, attracting effects (e.g., central city, road, public services) among developed parcels result in a clustered pattern. Repelling effects often result in a fragmented pattern found in many US urban-fringe areas of residential development.

The models most suitable to incorporate the spatial interaction effect are cellular automata models and agent-based models, in which the interaction is often explored and specified as behavioral rules applied to a Von Neumann (with four direct neighboring cells) or Moore (with 3×3 or 5×5 surrounding cells) neighborhood.

Econometric land use change models are also increasingly paying attention to neighborhood interactions, often by a simple measure of neighborhood composition, e.g., the area or percentage of a land use type under investigation in a neighborhood is included in the explanatory variables (Geoghegan *et al.* 1997; Irwin and Bockstael 2002). Irwin and Bockstael (2002) estimate the transition probabilities as a function of exogenous variables and an interaction term that captures the effect of neighboring land use conversions. The negative interaction results in the evolution of a more fragmented land use pattern.

Another way of taking the neighborhood effect into account is to apply a *spatial filter* to an empirically derived change probability map. Schneider and Pontius (2001) account for the

spatial dependence explicitly in the suitability maps by using a spatial filter with a kernel size of 35 acres, which is the average size of the patches deforested. Thus, the suitability value of each cell is changed to a weighted average of the value of itself and the values of the cells in the surrounding 35 acres.

2.3.4.5 Temporal dynamics

Current GISs are good at dealing with static geographic data layers; they still lack the ability to explicitly handle the temporal dimension. A realistic dynamic GIS-supported land use model has yet to be developed. Considerations on temporal dynamics are often omitted from spatially empirical models estimating land use/cover change using remotely sensed data, most likely due to data constraints, which can bias the estimation results (Irwin and Geoghegan 2001).

A number of land use models take temporal dynamics into account. Spatially dynamic simulation models are most suitable for handling temporal dynamics. The economic land allocation model of the Patuxent landscape (Irwin and Geoghegan 2001) explicitly considers the temporal dimension such that the location of change in one year influences the probability of change in the subsequent year. The land conversion is determined by an optimal timing decision in which a land owner seeks to maximize expected returns from the conversion by choosing the optimal time. CLUE-CR model (Veldcamp and Fresco 1996) is fully integrated with a dynamic systems model to compute both the quantity and location of land change.

However, many models do not account for temporal dynamics. While GEOMOD2 model (Pontius *et al.* 2001) is dynamic in that it determines candidates for forest disturbance by recomputing which grid cells neighbor a disturbed cell, drivers do not change rapidly over time. The model uses one set of relatively stable biophysical variables for all model runs and does not

incorporate dynamic social-demographic factors, such as population density, hence the non-dynamic application of the model. Traditional urban simulation models, such as spatial interaction or gravity models, use cross-sectional or longitudinal data as proxies for dynamics; dynamics are not explicit and not in a more realistic manner (Torrens 2001).

Due to the lack of data in a short-interval series, explanatory variables in empirical models are often assigned static values for a longer period, rather than updated dynamically. These models simply project land use trend by extrapolation and regression (Schneider and Pontius 2001; Serneels and Lambin 2001; Geoghegan *et al.* 2001). This type of model is not suitable for scenario analysis, because they are only valid within the temporal range of land use change on which they are based.

2.3.4.6 Level of integration

Land use systems are groups of interacting, interdependent parts linked together by exchanges of energy, matter and information. Land-use change models are often used to assess the impact of land use change on biophysical processes, e.g. climate change, land degradation, ecosystem stability and diversity. The biophysical response to changes in land-cover themselves feedback on drivers of land-use, calling for a dynamic, endogenous coupling between models of land use change and biophysical models to achieve integration of the different sub-systems. This research area is just emerging (Veldcamp and Lambin 2001).

Two approaches for integration can be distinguished: *loose coupling* of sub-systems and *tight coupling* in a holistic way. In loose coupling, interactions among subsystems and feedbacks are ignored. Relationships among subsystems are only simple one-direction input-output. Most often, land use modeling is done using a loose coupling. In a tightly coupled modeling

environment, sub-modules interact with each other; more variables are endogenous to the system; causes and consequences are not explicitly distinguished; and the system is integrative. An example of a fully integrated model is the IIASA-LUC model (Fischer and Sun 2001). Another example is the Patuxent Landscape Model (Geoghegan *at al.* 1997) in which the economic module dealing with land use change and the ecological module simulating hydrological and ecological processes are linked so that the output of economic module (land use patterns) is used as input for the ecological module whereas the output of the ecological module are used as the input of the economic module, allowing for feedbacks within the system.

2.3.5 Land use model validation methods

Model validation is the overall process of comparing the model and its behavior to the real system and its behavior. A model is valid to the extent that it adequately represents the system being modeled, i.e., the model is able to correctly answer the questions it was designed to answer (Casti 1997).

An important insight from contemporary philosophy of science is that the relations between a model of a given type and its practical use are diverse (Gross and Strand 2000). *Predictive models* aim at a quantitative or qualitative prediction of future states of a specific real system; *explanatory models* seek to elucidate the essential mechanisms or processes; and *heuristic models* are used to invent and discover unknown properties of a system through a learning process.

Validation in the classical *logical empiricism philosophy* would require verification of a one-to-one correspondence between the model output and the real world, but today many scientists and philosophers would argue that a model can also be useful when such a strict

procedure cannot be completed. An explanatory or heuristic model may help to clarify assumptions and inferences in the decision-making process. Under some circumstances it may be rational to take a chance and believe in a particular predictive model, even if it cannot be properly validated.

Popper's philosophy of science has been seen to show that complete verification is impossible and that we can approach the truth only negatively, by falsification and elimination of error (Popper 1959). Casti (1997) argues that perfect fidelity of a model is neither sufficient nor necessary for its successful use. Validation is not an either/or proposition – no model is ever totally representative of the system under study (Banks *et al.* 2000).

A possible criticism of model validation is that the model has been validated only for the one data set used; that is the model has been “fit” to one data set. One way to alleviate this criticism is to collect a new set of system data (or to reserve a portion of the original system data) to be used at the final stage of validation (Banks *et al.* 2000).

Comparison of the model to reality is carried out using a variety of tests – some subjective and others objective. Which validation method to use depends on particular modeling and analysis objectives. In the context of urban land use modeling, sometimes, though rarely, the detailed location of a particular urban area at a micro level is of concern, while at other times the goal is to explain or predict macro patterns that are used for general planning.

When we validate land use models, the first thing we often do is to visually compare the predicted map with the actual. Visual comparison is intuitive and direct, and is also facilitated by geographic linking and zooming functions of remote sensing and GIS software. However, one cannot compare all pixels by naked eye one by one due to a large quantity of pixels. This method

only gives a first impression, and it is only qualitative in nature. Quantitative and objective measurements are needed.

A *contingency table* is often generated by visual inspection of randomly distributed number of points, and indices of agreement are calculated. Any index of agreement that is based on a contingency table has a weakness: a contingency table is a summary containing no information of location. Other indices that share this weakness are percent correct, any chi-square based statistic such as *phi*, and any kappa-based statistic such as *kappa*. When the spatial pattern of distribution of errors is needed, these measures are not appropriate.

Landscape spatial pattern indices - such as core area, edge density, and connectivity - have long been used by ecologists to characterize certain ecological functions. For example, in an urban ecological system, nearest neighbor metrics and evenness indices reflect spatial concentration of land area and can be used to measure clustering of similar land uses resulting from agglomeration economies, or spatial dispersal of land uses due to monopolistic competition. Irwin and Bockstael (2002) use *nearest neighbor spatial statistics* to validate a spatial simulation model predicting patterns of land use change in an urbanizing area, in which the transition probabilities are estimated as functions of a variety of exogenous variables and an interaction term that captures the effect of neighboring land use conversions. Clarke and Gaydos (1998) used four statistical measures to evaluate the model performance. These include a series of R-squared fits between actual and predicted development and between urban edges, and a modified Lee-Sallee shape index.

Besides spatial pattern indices, there are other methodologies of model validation suitable for different uses. Serneels and Lambin (2001) validate a land use change model by *graph analysis*. The model's output is a probability map. A graph showing predicted probability of

change versus percentage of pixels that have actually been converted was generated. The percentage is an indicator of model validity: the higher is the percentage, the more valid is the model.

Turner *et al.* (1989) developed a *multiple-resolution fitting* method to validate spatial simulation models. This is a *cell-by-cell* comparison method. But the cell size is variable from the finest resolution (a pixel) to the whole image. The goodness of fit is calculated on a weighted average basis. This method can be used if accurate simulated location is important.

What has been discussed so far is all about the validation of maps predicted from land use change models. It is easy to be confused with accuracy assessment of land use maps produced from the classification of remotely sensed images although some approaches to evaluating land use change models are drawn from image classification evaluation, such as the statistical methods based on contingency tables. However, there have been more recent studies which acknowledged that generalized methodologies developed to assess the accuracy of classified images may not be appropriate for maps of land use change (Congalton & Macleod 1994), especially when, on the change map, change is relatively rare and is also to be concentrated in relatively few areas, such as a small amount of urban sprawl in the urban fringe. Under these circumstances, for maps of land cover changes, one is confronted with the general statistical problem of sampling for a rare event. To overcome this problem, Lowell (2001) developed a methodology, based on areal rather than point samples to validate land use change maps.

The concept of predictability in information theory implies the reduction in uncertainty about one variable from knowledge of another. The application of this concept in spatial phenomena measures the reduction in uncertainty about the state of a particular pixel obtained

from other knowledge about the pattern. In the urban context, Turner *et al.* (1989) used spatial predictability to measure two spatial patterns to see if they match.

Recently the *Relative Operating Characteristic (ROC)* method was brought to the field of land use change modeling to measure the relationship between simulated change and real change (Pontius 2000). ROC curves were developed in the 1950's as a by-product of research into making sense of radio signals contaminated by noise. Pontius and Schneider (2001) explain how to use the ROC technique to examine how well a suitability map portrays the likely locations of a category of new development. Schneider and Pontius (2001) apply the ROC method to compare several modeling techniques. ROC method is an excellent method to evaluate the validity of a model that predicts the occurrence of an event by comparing a suitability image depicting the probability of that event occurring and a binary image showing where that class actually exists.

2.4 Summary

An urban land use system is dominated by human activities with complex spatiotemporal dynamics. The prerequisite for knowing, representing and predicting such a system is scientific conceptualization of space and time and systematic approach. Human modifications of urban landscapes are a process of reshaping the structure of urban space over time. To reveal the process behind human-induced land use/cover changes, the only way is to characterize and recover the temporal relationship between urban spatial patterns over a period in the past.

Historical remotely sensed data can be used to reveal the temporal changes of urban landscapes using various land use/cover change detection methods. Once the land use/cover change process is characterized and recovered, it is possible to represent the system using a collection of land use/cover modeling techniques that take into account of the dynamic interactions among space, time, and humans. Further, the model, if it is valid, can be used to for prediction. The following

chapters will show that the breadth of study will be relevant to many different fields covering theory, methodology and techniques, such as philosophy, geographic thoughts, urban economics, urban morphology theories, theory of complexity, mapping land use/cover using remote sensing, land use/cover change detection, spatial analysis and modeling of land use/cover changes in a GIS environment.

CHAPTER THREE

MAPPING THE 1987-1997 LAND USE/COVER CHANGE IN ATLANTA FROM LANDSAT TM IMAGES: A NEW APPROACH TO ACCURACY IMPROVEMENT

3.0 Introduction

Satellite remote sensing has offered considerable promise for characterizing landscape patterns at different spatial scales and for monitoring landscape dynamics by detecting changes of landscape patterns. Remote sensing has the advantages of large area coverage, repeated viewing capability and ease of integration with GIS. When the environment in a large metropolitan area experiencing rapid suburbanization needs to be monitored constantly, the use of remote sensing has demonstrated more advantages than the traditional field surveying. In such areas, human-induced land use/cover changes can be substantial but are difficult to grasp when they occur incrementally. Mapping from a time series of satellite data has successfully revealed the dynamics of urban land characteristics for large metropolitan areas (Lo and Shipman 1990; Lo 1998; Masek *et al.* 2000). The spatial databases derived from remote sensing provide a strong visual portrayal of urban growth patterns, and convey how the progress of modern urbanization has caused profound changes to the landscape, which in turn have affected the environment, the micro-climate and the quality of human life (Lo and Faber, 1997; Lo *et al.*, 1997; Weng 2001; Yang and Lo 2002).

This chapter will explain the detection of land use/cover change from 1987 to 1997 in the Atlanta region using Landsat TM images. The land use/cover statistics and spatial patterns of the

past land use/cover changes provide the data input to the modeling and prediction of future land use/cover patterns to be explained in Chapters 4 and 5.

Various approaches have been developed to detect land use/cover change from remote sensing, such as, post-classification comparison, classification of multi-temporal composite data sets, principal component analysis, temporal image differencing, temporal image ratioing, and change vector analysis (Lillesand and Kiffer 1999). In this study, the choice of a land use/cover change detection method depends on whether the output information from the detection meets the data requirements of the two modeling approaches of this dissertation, the Markov chain model and the logistic regression model, in terms of content and accuracy. The requirements are accurate land use/cover classification maps, a change/no-change matrix, and an accurate historical urban growth map.

Existing studies have shown that change vector analysis can detect the nature of land use/cover change (MacLeod & Congalton 1998; Mas 1999). This study first uses change vector analysis to detect land use/cover change. The change vector analysis is based on the measurement space defined by the principal components of the Landsat Images. Interpretation of the magnitude and direction of the change vectors has shown that in the complex landscape such as the rapidly changing urban environment of Atlanta, different land use/cover transformations can manifest similar magnitude and direction of spectral change, while different magnitude and direction of change may indicate same kind of land use/cover change. Specific 'from-to' nature of land use/cover change and a change/no-change matrix cannot be derived from change vector analysis. Only the post-classification comparison method can effectively detect the specific 'from-to' nature of land use/cover changes and generate a change/no-change matrix. However, post-classification comparison change detection compounds the classification errors in the land

use/cover maps compared. Thus, to improve the change detection accuracy, the accuracy of land use/cover classifications must be improved.

This study demonstrates the use of an NDVI differencing method combined with temporal logic to improve the accuracy of land use/cover maps. This combination method is not the same as the conventional NDVI differencing method (Masek *et al.* 2000), which can only differentiate change and no-change by trial and error of a single artificially assigned threshold value. In this study, the NDVI difference map is classified and interpreted to indicate different types of land use/cover change, and temporal logic is used to take advantage of the temporal information latent in the relationships between vegetation cover changes and land use/cover changes. Last, post-comparison of the accuracy-enhanced land use/cover maps is conducted to detect land use/cover change. Quantitative land use/cover change information will be obtained and spatial patterns of changes will be displayed as land use/cover change maps.

3.1 Satellite data

Two Landsat TM images were used for land use/cover change detection. One image was acquired on June 29, 1987, and the other was obtained on July 29, 1997, for a time span of 10 years. The technical parameters are shown in Table 3.1. Since the study area spans two rows in the Worldwide Reference System (WRS) used for the cataloging and referencing of images transmitted from the Landsat sensors, the two images have been center-shifted so that the entire area is covered within one whole scene. The two satellite images are shown in Figure 3.1. A rectangle area of interest (AOI) bounding the 13-county study area was created to subset the two images (Figure 3.2). Both images were re-sampled to a spatial resolution of 25 meters.

Table 3.1 Characteristics of the satellite images

Date	29 June 1987	29 July 1997
Landsat No.	5	
Sensor	Thematic Mapper (TM)	
Nominal Spatial resolution(m)	30	
Quantization	Byte (8 bits)	
Resampling	NN	
Sun elevation (°)	61.84	61.00
Sun azimuth (°)	103.71	106.00
Center-shift	The center of the north scene has been shifted 50%	
Scene coverage	Approximately 185×185km ²	
Georeference system	Projection: UTM Zone: 16 Earth ellipsoid: GRS 1980 Horizontal datum: NAD83	
Band designations	Band #	Wavelength (micrometers)
	Band 1	0.45-0.52
	Band 2	0.52-0.60
	Band 3	0.63-0.69
	Band 4	0.76-0.90
	Band 5	1.55-1.75
	Band 6	10.40-12.50
	Band 7	2.08-2.35

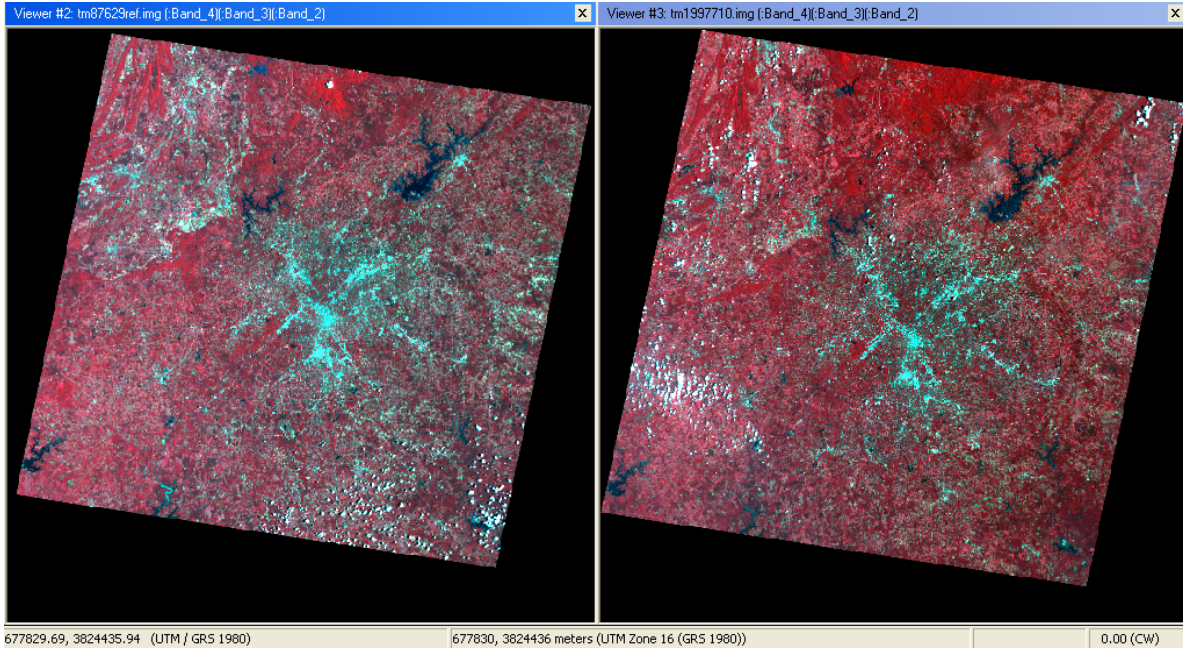
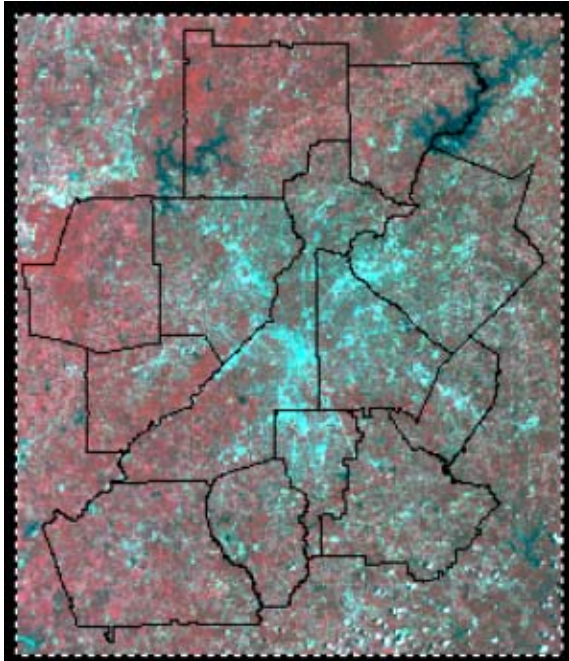


Figure 3.1 Landsat TM images (Left: June 29, 1987; Right: July 29, 1970).



Spatial extent of Area of interest (AOI):

Upper Left X: 679950 m
 Upper Left Y: 3811525 m
 Lower Right X: 796525 m
 Lower Right Y: 3674350 m

Figure 3.2 Image subset to the area of interest.

Remotely sensed data used for urban applications in urban environments characterized by highly heterogeneous surfaces must meet certain conditions in terms of temporal, spatial, spectral, and radiometric characteristics (Lo 1986). When remote sensing images are applied to land use/cover change detection, those requirements are especially important. The ideal conditions for change detection are the use of data acquired by the same or similar sensor and recorded using the same spatial resolution, viewing geometry, spectral bands, radiometric resolution, season and time of day (Lillesand and Kiefer 1999). The satellite data of the years 1987 and 1997 were acquired using the same sensor with the same spatial, spectral, and radiometric resolutions (Table 3.1). Both images were acquired in leaf-on season with a difference of 31 days, thus it does not strictly meet the anniversary date requirement. The sun-synchronous orbit of Landsat 5 TM ensures repeatable sun illumination conditions during the specific seasons. Repeatable illumination conditions are desirable when comparing annual changes in land cover (Lillesand and Kiefer 1999).

3.2 Co-registration of multi-date images

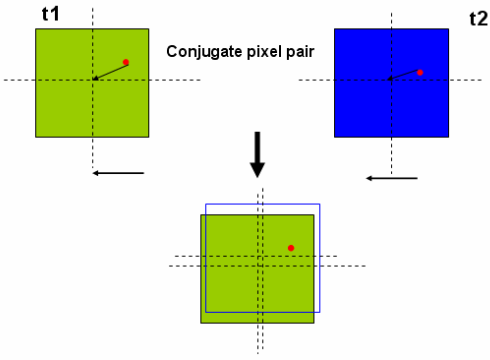
Whatever land use/cover change detection methods are used, the final discrimination of the change relies on the comparison of the pixel pairs (or conjugate pixels) that represent the same ground location. Accurate spatial co-registration of the multi-temporal images is a requirement for reliable land use/cover change detection. Land cover change may be overestimated due to positional errors. False land use/cover change detected from a 20-class Landsat classification could reach more than 33% due to mis-registration (Verbyla 2000).

If two images are used for land use/cover change detection, a root mean square error (RMSE) of less than 0.5 pixel for each image with reference to true ground locations does not

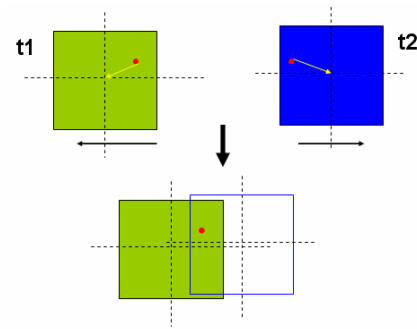
necessarily guarantee the accurate co-registration of the two images. This can be demonstrated in Figure 3.3. In Figure 3.3(a), the pixel shifts less than 0.5 pixel relative to its true location represented by a red point in the same direction both in the first date image and in the second date image. In this case, they are co-registered and change detection can be conducted on the two pixels. In Figure 3.3(b), although the pixel shifts less than 0.5 pixel relative to its true location on both dates, which certainly meets geometric rectification accuracy requirement, the directions of the displacement are opposite. This would result in a less than 50% overlap if the two pixels overlay with each other for change detection. The negative impact of the shift in the opposite directions is that the left-neighboring pixel under consideration will be compared with the pixel of interest on the first date image (Figure 3.3(c)). This would cause overestimation of the change.

The 1997 Landsat TM image supplied by Space Imaging EOSAT had already been georeferenced to the UTM coordinate system (Zone 16 North), NAD 1983 horizontal datum, and GRS 1980 ellipsoid. The 1987 image supplied by USGS EROS Data Center was registered with the 1997 image using the 1997 image as a reference.

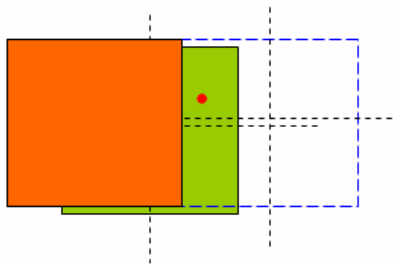
It was found that after the registration, the two Landsat TM images were still not accurately co-registered as revealed by examining the conjugate pixels on the two images. Visually finding conjugate pixels on the Landsat TM images with resampled 25m spatial resolution is not easy task due to the mixed pixel problem. Only large buildings with distinct boundaries on both images can be used to find the conjugate pixels. Most land features, either natural or artificial, have fuzzy boundaries. A few large commercial buildings with distinct boundaries have been found and their conjugate corners are compared using the geographic linking function of ERDAS Imagine software. Figure 3.4 (a) shows a building in the northwest Atlanta area displayed in the 1987 (left) and 1997 (right) images. If the two images are



(a) Pixel shifts relative to the true location in the same direction: images are co-registered accurately.

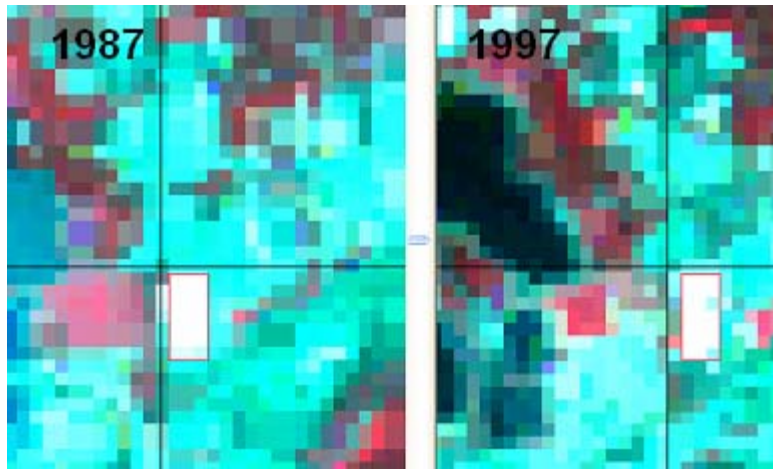


(b) Pixel shifts relative to the true location in the opposite direction: images are not coregistered.

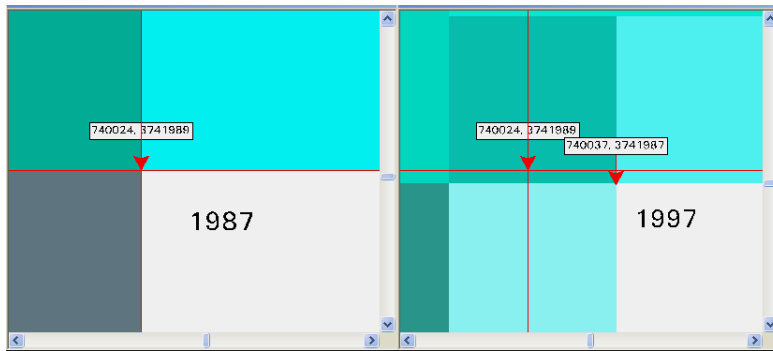


(c) The negative impact of mis-registration on change detection: the left neighboring pixel of the second date is compared to the pixel under consideration on the first date image.

Figure 3.3 Accurate georeference (RMSE < 0.5 pixel) does not guarantee co-registration of multi-date images for land use/cover change detection.



(a) A large building used to examine the pixel shift.



(b) Pixel shift of the NW corner of the building.

Figure 3.4 Examination of pixel shift of the 1997 Landsat TM image relative to the 1987 image.

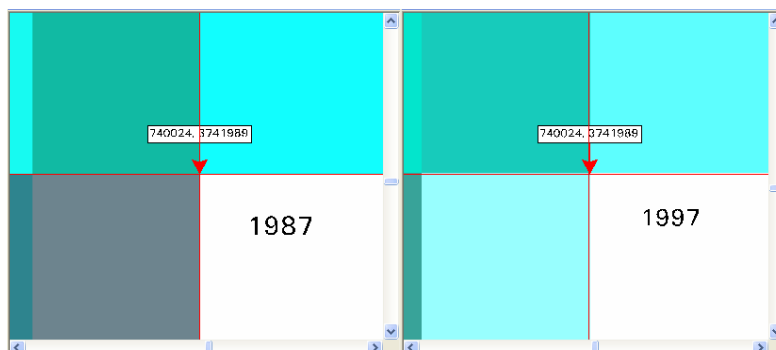


Figure 3.5 Pixel shift corrected by offsetting coordinates of the 1997 image: both images become co-registered.

accurately registered to each other, the building's corners should coincide. Closer examination of the two images by zooming into the building area has shown that the 1997 image has shifted 13 meters eastward and 2 meters to the south (Figure 3.4(b)). Since the shift of 13 meters exceeds half a pixel width (12.5 meters), conjugate pixels will not be spatially matched for change detection.

The problem of pixel shift was also examined on the four corner areas and the central part of the study area. It was found that the pixel shift is uniform within the whole study area — the 1997 image has shifted 13 meters eastward and 2 meters southward relative to the 1987 image, thus suggesting a systematic error. The uniformity of the shift makes it easy to correct. The shift was simply corrected by offsetting the coordinates of the 1997 image by subtracting 13 meters from the X coordinates and adding 2 meters to Y coordinates. This operation has resulted in the 1997 image being exactly co-registered with the 1987 image (Figure 3.5), setting a base for reliable pixel comparison for change vector analysis (Section 3.4), NDVI differencing (Section 3.8), and post-classification comparison for land use/cover change detection (Section 3.9).

3.3 Computer-assisted land use/cover classification

The land use/cover classification was based on Anderson's land use/cover classification scheme (Anderson *et al.* 1979) with modifications to adapt to computer-assisted land use/cover mapping. A total of six classes of land use/cover will be mapped: (1) high-density urban, (2) low-density urban, (3) bare land, (4) cropland or grassland, (5) forest, and (6) water. Detailed explanations of the classification scheme are shown in Table 3.1. The classification scheme is one of the most important factors affecting the attribute accuracy of image classification. Generally, the larger the number of categories in a classification scheme, the more precisely the data can be presented,

Table 3.1 Land use/cover classification scheme

Codes	Land use/cover classes	Description
1	High-density urban	Central business districts, multi-family dwellings, commercial and industrial facilities, high impervious surface areas of institutional facilities, large transportation facilities, e.g. airports, multilane interstate/state highways
2	Low-density urban	Single family residential areas, urban recreational areas, cemeteries, playing fields, campus-like institutions, parks, schools, local roads
3	Bare land	Areas with sparse vegetation (less than 20%), forest clear-cut, fallowed cropland, quarries, strip mines, rock outcrop, sand beach along rivers and lakes
4	Cropland or grassland	Row crop agriculture, orchards, vineyards, horticultural businesses, pastures, non-tilted grasses, golf courses
5	Forest	Evergreen forest, deciduous forest, and mixed forest
6	Water	Rivers, streams, lakes, and reservoirs

but the more difficult it is to achieve high classification accuracy (Lo and Yeung 2002).

Classification scheme design can also influence land use/cover modeling results.

The original land use/cover maps employed in this study were classified by Yang (2000) using the unsupervised Iterative Self-Organizing Data Analysis (ISODATA) classification method. The ISODATA clustering method makes use of the minimum spectral distance formula to form clusters. It begins with either arbitrary cluster means or means of an existing signature set, and each time the clustering repeats, the means of these clusters are shifted. The new cluster means are used for the next iteration. The ISODATA utility repeats the clustering of the image until either a maximum number of iterations has been performed, or a maximum percentage of unchanged pixels has been reached between two iterations (Jensen 1996). ISODATA is a conventional multi-spectral classification technique performing class assignments based only on the spectral signatures of a classification unit without referring to contextual information.

3.4 Principal components analysis and change vector analysis

Change vector analysis is one of the land use/cover change detection methods. It is a change detection procedure that is a conceptual extension of image differencing (Lillesand and Kiefer 1999). A certain number of spectral variables define a multi-dimensional coordinate space. Each pixel on the satellite images acquired at dates 1 and 2 can be located at a point for each date in the coordinate space by its spectral variable values. The vector connecting the two points indicates both the magnitude and direction of spectral change between these two dates. The magnitude of the change vector is the Euclidean distance between these two points, indicating the intensity of the land use/cover change. The decision that a change has occurred is made if the magnitude of the computed spectral change vector exceeds a specified threshold criterion (Singh 1989). The direction of the change vector indicates the nature of change, for example forest clear-cut or re-growth. In this section, principal components obtained from a PCA which accounts for most of the variance in the original Landsat TM images will be used as spectral variables to define the coordinate space for change vector analysis. In multi-temporal studies, the principal components for two or more dates are often compared as in image differencing (Singh 1989).

The technique of PCA can be used to reduce information redundancy in multi-band remote sensing images. It allows redundant data to be compacted into fewer bands to achieve the reduced dimensionality of the data. The bands of PCA data are non-correlated and independent, and are more interpretable than the source data (Jensen 1996). PCA reduces data by deriving a new set of orthogonal data axes for the dataset which represents the maximum variance along the

first component axis, the next largest variance along the second component axis, and the least variance along the last axis.

To determine the principal components, the covariance matrix, Cov , of the original TM images is calculated. From the covariance matrix, a diagonal matrix E , whose non-diagonal elements are equal to zero and diagonal elements are eigenvalues λ_p ($p=1,2,\dots,n$, where n is the number of components in the original image), is derived using the following equation :

$$|Cov - \lambda_p I| = 0 \quad (3-1)$$

where I is the identity matrix. Eigenvalue λ_p is the variance of the p^{th} principal component.

The eigenvector matrix EV , whose elements are a_{kp} ($k=1$ to n bands, $p=1$ to n components), is computed such that (Jensen 1996):

$$EV \times Cov \times EV^T = E \quad (3-2)$$

where EV^T is the transpose of the eigenvector matrix, EV .

The percent of total variance explained by each of the principal components, $\%p$, can be computed from eigenvalues as follows (Jensen 1996):

$$\%p = \frac{\lambda_p}{\sum_{p=1}^n \lambda_p} \times 100 \quad (3-3)$$

By computing the correlation of each band k with each component p , it is possible to determine how each band “loads” or is associated with each principal component. The equation is (Jensen 1996) :

$$R_{kp} = \frac{a_{kp} \times \sqrt{\lambda_p}}{\sqrt{Var_k}} \quad (3-4)$$

where R_{kp} is the element in a $n \times n$ matrix filled with factor loadings representing the association of band k with component p , and Var_k is the variance of band k in the covariance matrix Cov .

The principal component images are computed according to the following formula (Jensen 1996):

$$newBV_{i,j,p} = \sum_{k=1}^n a_{kp} BV_{i,j,k} \quad (3-5)$$

where $BV_{i,j,k}$ is brightness value in band k for the pixel at row i and column j .

Principal components analysis was conducted using ERDAS Imagine. Table 3.2 shows the eigenvalues, the percentage of variance explained by each component, and the cumulative percentage of variance explained of the two Landsat images in the study. The first two principal components explain 91.48% of the total variance of the 1987 image, and 89.52% of the total variance of the 1997 image. Therefore a majority of the scene information is found in the first two principal components. This is typically the case with TM data as the first and second principal components contain a majority of the total radiance and vegetation greenness information (Jensen 1996).

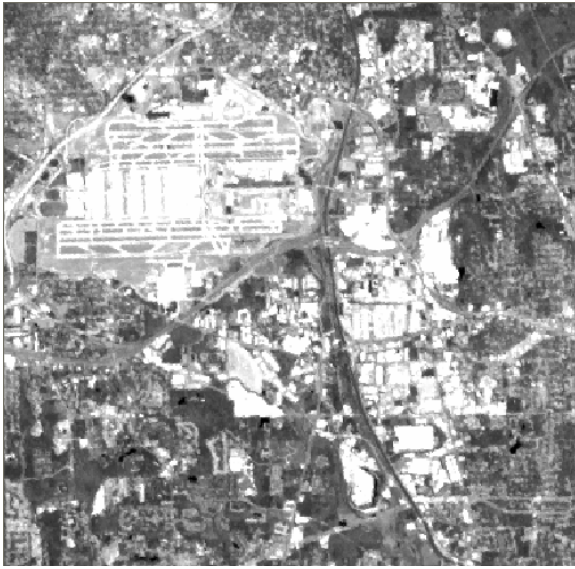
Table 3.2 PCA eigenvalues and percentage of variance explained by each component

Principal component #	1987			1997		
	Eigenvalue	%	Cumulative	Eigenvalue	%	Cumulative
1	1575.67	69.36	69.36	1067.39	67.65	67.65
2	502.53	22.12	91.48	345.02	21.87	89.52
3	135.42	5.96	97.44	112.34	7.12	96.64
4	21.62	0.95	98.40	26.12	1.66	98.30
5	18.93	0.83	99.23	13.81	0.88	99.17
6	13.67	0.60	99.83	10.91	0.69	99.87
7	3.85	0.17	100.00	2.12	0.13	100.00
Total	2271.69	100.00		1577.71	100.00	

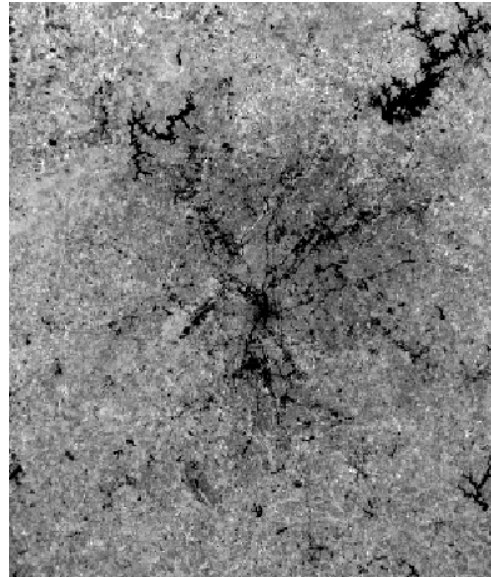
Table 3.3 Factor loadings of each principal component with each band
(Significant factor loadings are shown in bold type)

	Band #	Principal component #						
		1	2	3	4	5	6	7
TM 1987	1	0.74	-0.42	-0.46	0.18	-0.17	-0.05	-0.03
	2	0.83	-0.34	-0.40	0.03	0.07	0.01	0.19
	3	0.84	-0.41	-0.30	-0.06	0.16	0.06	-0.05
	4	0.40	0.89	-0.21	-0.03	-0.01	0.00	0.00
	5	0.97	0.08	0.21	0.06	0.02	0.01	0.00
	6	0.56	-0.35	0.05	-0.14	-0.39	0.62	0.02
	7	0.94	-0.24	0.04	-0.19	-0.09	-0.08	0.00
TM 1997	1	0.72	-0.42	-0.52	0.07	-0.12	-0.13	-0.02
	2	0.82	-0.35	-0.42	-0.01	0.00	0.10	0.16
	3	0.83	-0.42	-0.30	-0.06	0.06	0.18	-0.05
	4	0.42	0.88	-0.21	-0.06	0.01	0.00	0.00
	5	0.97	0.07	0.21	0.06	-0.04	0.01	0.00
	6	0.57	-0.37	0.31	-0.74	-0.28	-0.02	0.00
	7	0.93	-0.26	0.07	-0.10	0.19	-0.11	0.00

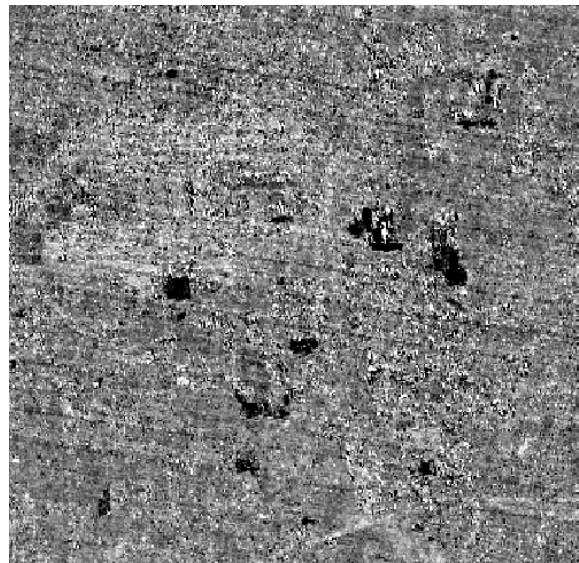
Table 3.3 shows the factor loading of each principal component with each band. Factor loading values for both image demonstrate the same pattern. The correlations of principal component 1 with all the bands except band 4 (NIR band) are high. The first principal component contains information from almost all the bands and explains the maximum amount of variation in the seven-dimensional space defined by the seven Thematic Mapper bands. The image (Figure 3.6(a)) produced from principal component 1 data covering the area of Atlanta Hartsfield International Airport resembles an actual aerial photograph. In fact, this is the normal character of the first component of Landsat TM images, in that it broadly simulates standard black and white photography and it contains most of the pertinent information inherent to a scene (Jensen 1996). The second component has high loadings only in the near-infrared (NIR) band



(a) Principal component 1.



(b) Principal component 2.



(c) Principal component 7 image.

Figure 3.6 Principal components 1, 2 and 7 from PCA of Landsat 1997 TM image. (a) and (c) shows the Atlanta Hartsfield International Airport area; (b) shows the whole study area.

(band 4). This suggests that this component is an NIR reflectance band (Figure 3.6(b)) with water being dark and vegetation being bright. Component 3 is weakly related to MIR band with a factor loading value of 0.21. The remaining components provide very little information. For example the last component (Figure 3.6(c)) is noise only.

Figure 3.7 shows color composite images of the years 1987 and 1997 displaying the first three principal components in red, green and blue color combination. High-density urban and cloud show red color. Areas in purple are residential. Forest clear-cuts are in magenta. Cropland or grassland look yellow. Forests take on their natural green color. Water body and cloud shadow are blue. The patterns of urban area, especially commercial, industrial, and transportation, are easy to perceive.

Since the first two principal components contain a majority of information, it is logical and reasonable to use them for change vector analysis. Plotting the principal component 2 value against the principal component 1 value of a pixel for the year 1987, a data point was obtained. The data point for the year 1997 for the same pixel was also plotted (Figure 3.8). The vector pointing from the 1987 data point to the 1997 point is expected to indicate the intensity and nature of land use/cover change. Change vector analysis on the first two principal components produces a magnitude image and a direction image. Figure 3.9 shows the detailed images in the Mall of Georgia area. It is more intuitive to identify land conversion from the direction image than from the magnitude image. In the direction image, white tone indicates deforestation for commercial, residential and transportation development; the majority of the area on the image is grey, indicating no change of land use/cover. The magnitude image looks more heterogeneous and hard to interpret. However, it is still obvious that brighter tone indicates commercial urban development. The dark tone is for the forest area with moisture variation between the two years.

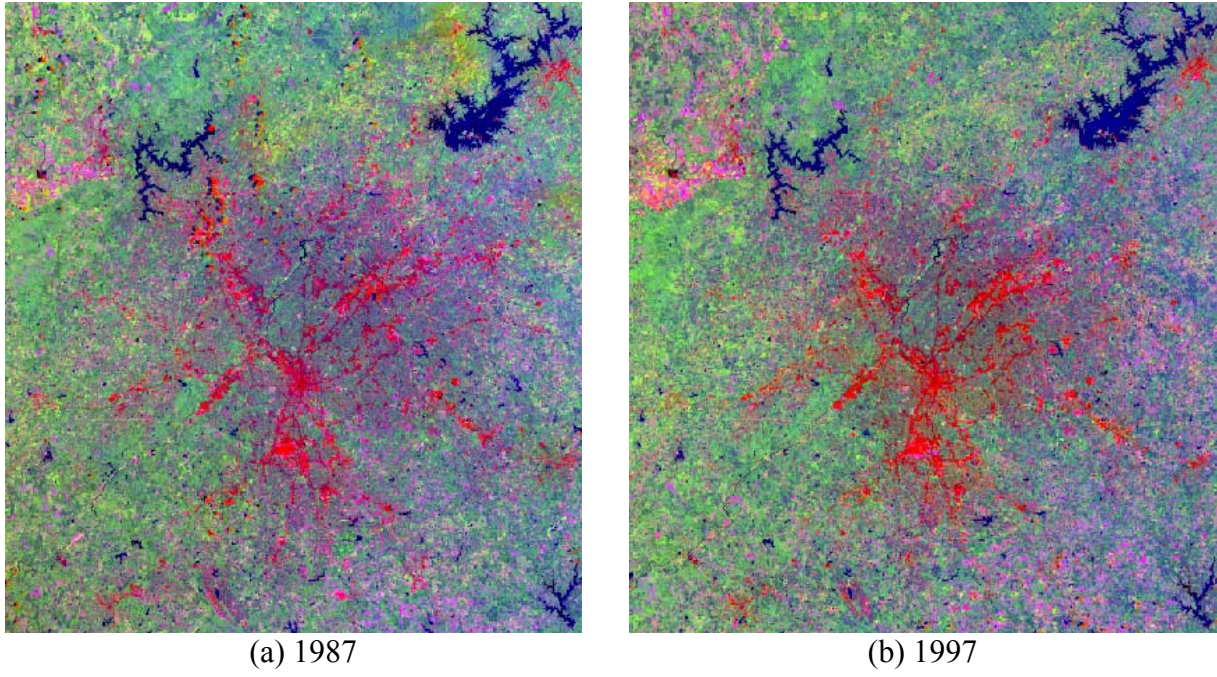


Figure 3.7 Principal components 1, 2,3 composite image displayed in red, green, and blue color combination.

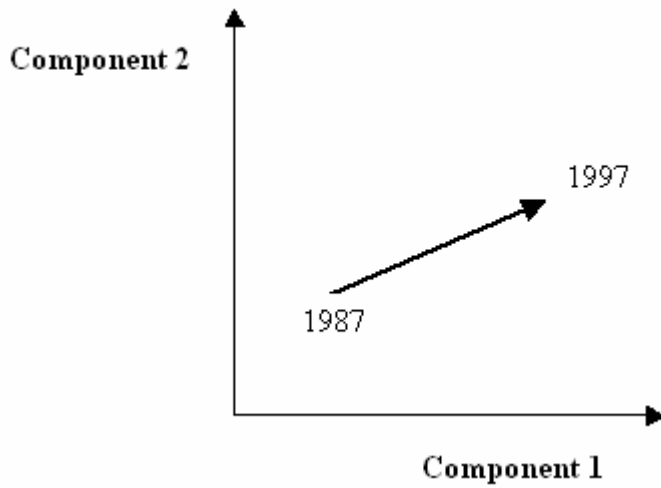
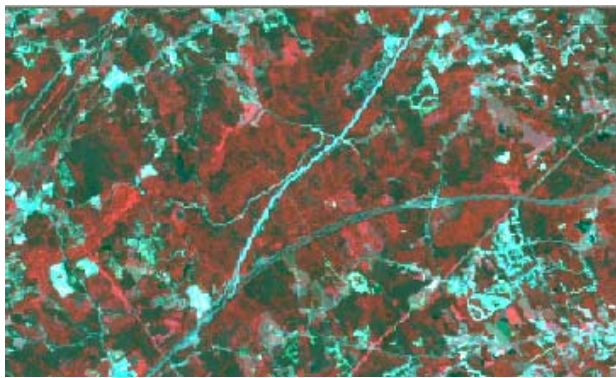
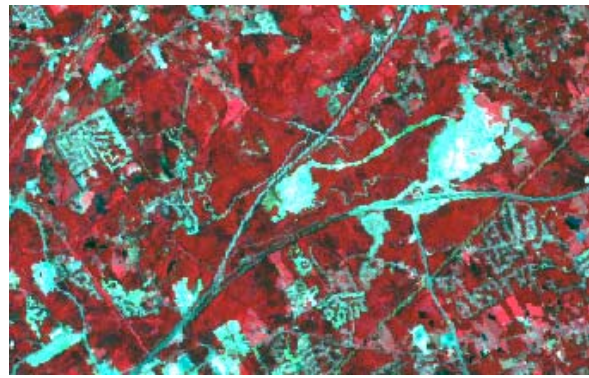


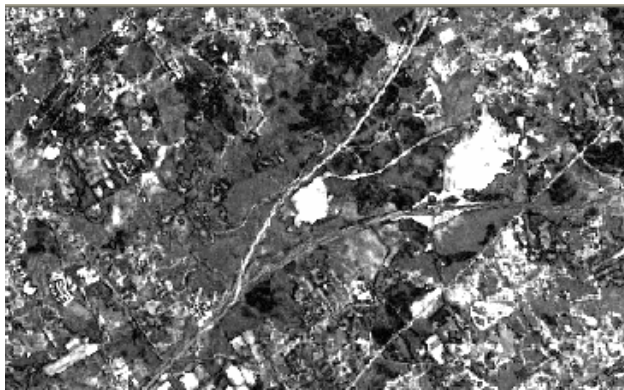
Figure 3.8 Change vector defined on the principal components 1 and 2 measurement space.



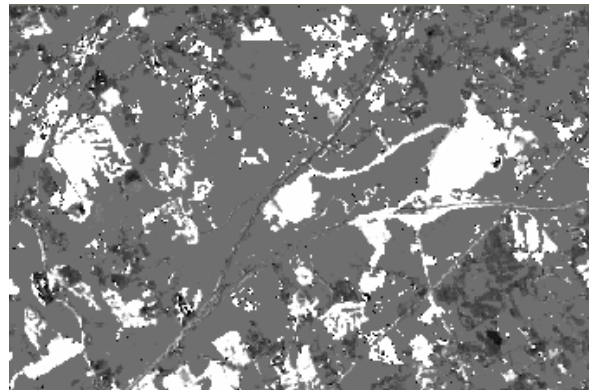
(a) TM 1987



(b) TM 1997



(c) Magnitude



(d) Direction

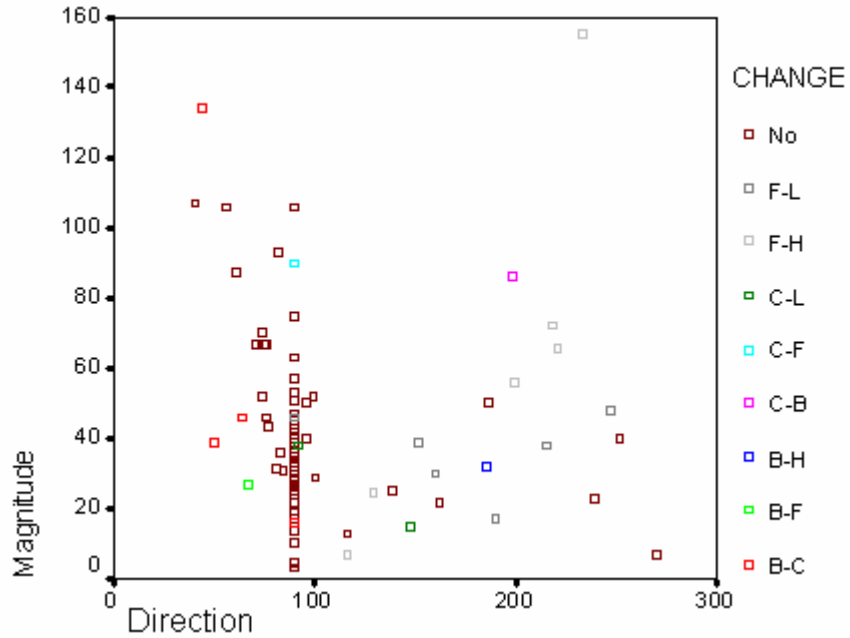
Figure 3.9 Land use/cover change magnitude and direction from change vector analysis. White tone represents change, and grey tone represents no-change.

By visual comparison of the magnitude and direction images with the original Landsat TM images it was found that in the whole study area, similar tones on the magnitude or direction images could indicate different types of land use/cover change, and similar land use/cover transformations can have very different spectral changes. A sample of 100 points was generated using the stratified random sampling technique. For each point, the magnitude, direction values

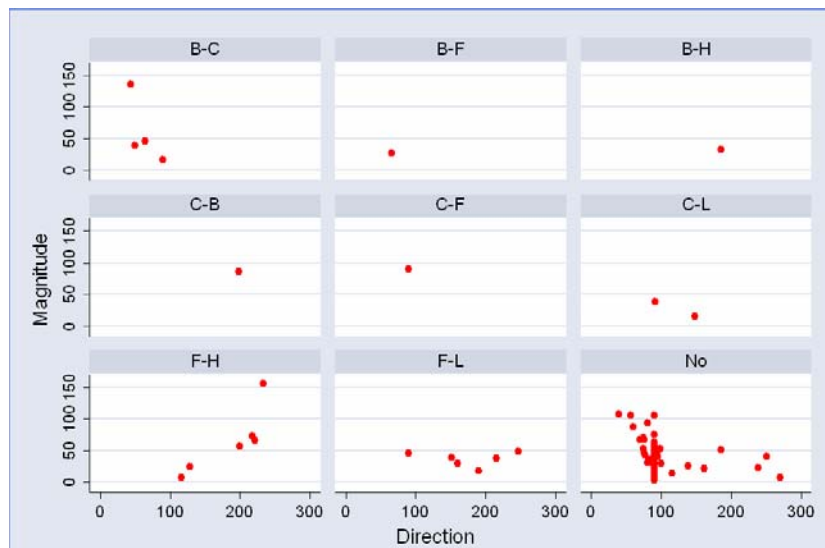
and the nature of land use/cover change was recorded and portrayed in Figure 3.10. In Figure 3.10(a), points for different types of land use/cover change are intermingled and a distinct cluster cannot be discerned for a kind of change. It is hard to define a box with upper and lower limits of values for each kind of land use/cover change. Therefore in complex landscapes such as the study area, where similar land use/cover conversions can have vastly different spectral changes and different types of land use/cover transformations can have very similar spectral changes on both direction and magnitude, change vector analysis is not an effective way to detect the specific nature of the land use/cover change. Although the change vector analysis conducted here cannot be used to differentiate the nature of land use/cover change, general land use/cover change dynamics can be monitored from Figure 3.10. Of the 100 data points, 22 points represent land use/cover change. The percentage value of 22% can be an indicator of land use/cover dynamics in the study area. During the 10 years from 1987 to 1997, the study area had experienced dramatic land use/cover change. From Figure 3.10(b), it is seen that the major land use/cover change is urban development at the cost of deforestation.

3.5 Errors in computer-assisted land use/cover classification from Landsat TM images

In a previous study of land use/cover changes in Atlanta, Yang (2000) classified Landsat TM images by using the unsupervised image clustering method ISODATA followed by manual editing with the support of on-screen digitizing, multiple zooming, AOI functionality and other GIS tools such as recoding. For the 1997 land use/cover map classified from the 1997 Landsat TM image, a total of 488 pixels were selected by a stratified random sampling design and were checked against color infrared aerial photos. The overall classification accuracy is 90.10% and the overall kappa index of agreement is 87.80% (Table 3.4). Forest and water classification



(a) Composite plot



B = bare land C = cropland/grassland F = forest
H = high-density urban L = low-density urban No = no change

(b) Plots separated by the type of land use/cover change/no-change

Figure 3.10 Change vector magnitude vs. direction and the type of land use/cover change.

Table 3.4 Accuracy assessment of the 1997 land use/cover map produced from Landsat TM image (Yang 2000)

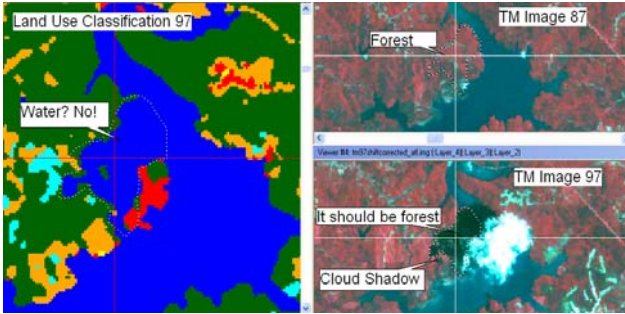
Classified Image	Reference Image						Row Total	User's Accuracy (%)
	1	2	3	4	5	6		
1	54	3	3	5	0	0	65	83.31
2	2	57	2	6	6	0	73	78.08
3	0	1	41	8	0	0	50	82.00
4	0	0	1	96	3	0	100	96.00
5	0	0	0	3	147	0	150	98.00
6	0	0	1	0	0	49	50	98.00
Column Total	56	61	48	118	156	49	488	
Producer's Accuracy (%)	96.43	93.44	85.42	81.36	94.23	100		
Number of pixels correctly classified = 444								
Overall classification accuracy = 90.10%								
Class code	Kappa		1 = high-density urban 2 = low-density urban 3 = bare land 4 = cropland or grassland 5 = forest 6 = water					
1	0.809							
2	0.750							
3	0.800							
4	0.951							
5	0.976							
6	0.978							
Overall Kappa Index of Agreement =								
0.878								

accuracies are higher than those for high-density urban, low-density urban and bare land.

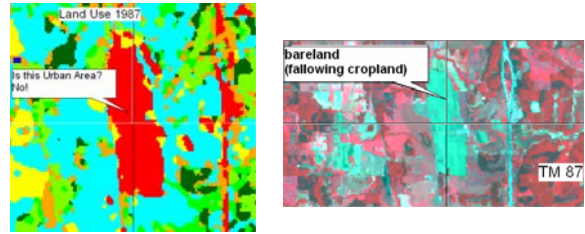
Classification of cropland or grassland achieved intermediate accuracy.

By examining the land use/cover maps and referring to the original satellite images and other ancillary air photos, it was found that there are four major types of errors (Figure 3.11). The first kind of error is cloud shadows being misclassified as water. The second kind of error is that fallow fields were misclassified as high-density urban. The third kind of error is forest clear-cuts being misclassified as high-density urban or low-density urban. The last type of error is forest clear-cuts being misclassified as cropland. These errors are the result of spectral confusions among land use/cover classes. The spectral confusions can be seen from the signature curves of different land use/cover types in the 1987 TM image in Figure 3.12. Only in bands 4 (NIR) and band 5 (MIR) is there some obvious spectral separability. In other bands, the spectral curves overlap. Figure 3.13 shows histogram plots that reveal the overlaps in pixel values of the 1987 Landsat TM image blue band between bare land (band 1) (fallow field or forest clear-cut) and high-density urban, low-density urban, or cropland/grassland.

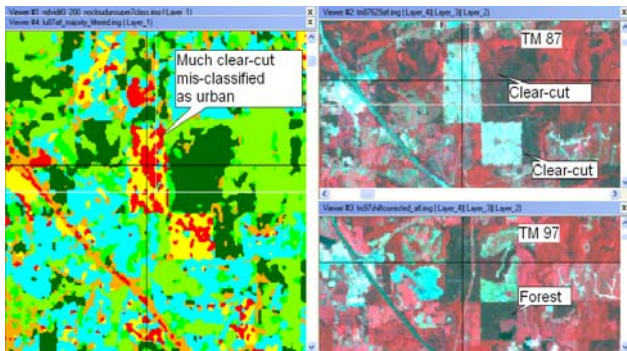
Although human intelligence can be employed in interpreting images by shape, size, pattern, shadow, tone or color, texture, association, and site in developing the land use/cover map, very limited spectral confusions could be resolved. A simple calculation will show that visual editing can only resolve limited amount of spectral confusion. Suppose two 4-inch by 4-inch image viewers are opened and arranged side by side on a desktop computer screen, one for displaying a land use/cover classification map to be visually inspected and edited, the other for displaying a reference image. From my experience, to effectively find classification errors and make on-screen corrections, we need to zoom into the images at least at the scale of 1:10,000.



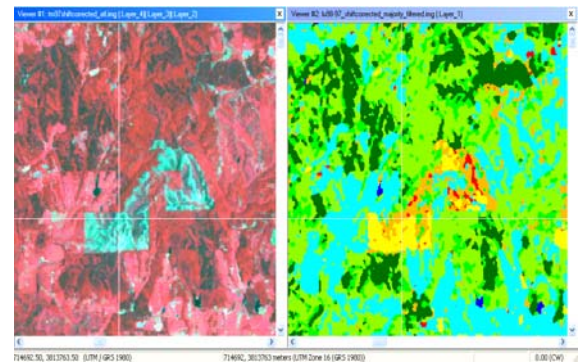
(a) Cloud shadow misclassified as water.



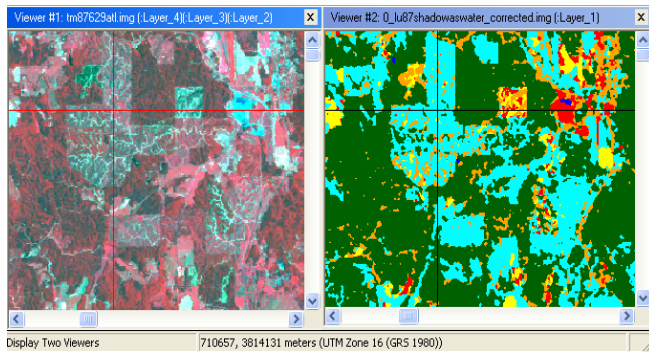
(b) Fallowing cropland misclassified as high-density urban (3 → 1).



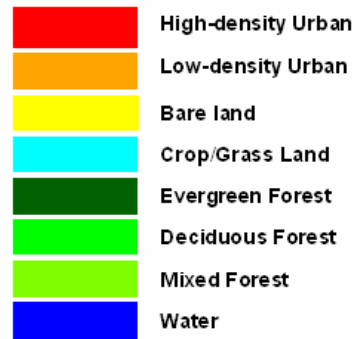
(c) Forest clear-cut misclassified as high-density urban (3 → 1).



(d) Forest clear-cut misclassified as high- or low-density urban (3 → 1 or 2)



(e) Forest clear-cut misclassified as cropland (3 → 4).



Legend

Figure 3.11 Major classification errors in the initial land use/cover classifications.

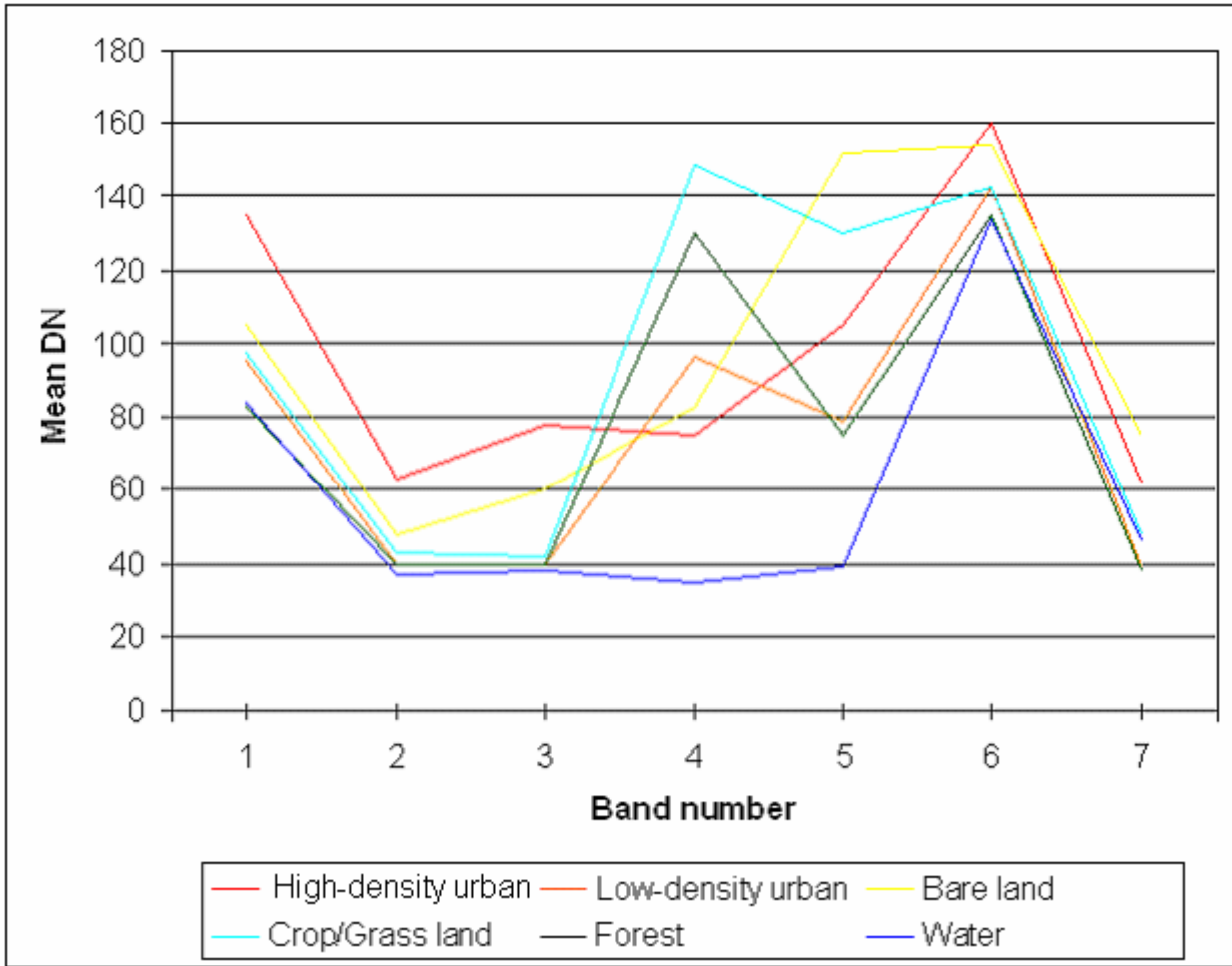
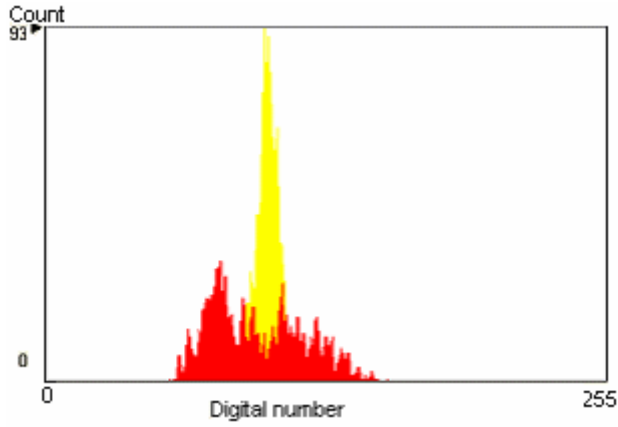
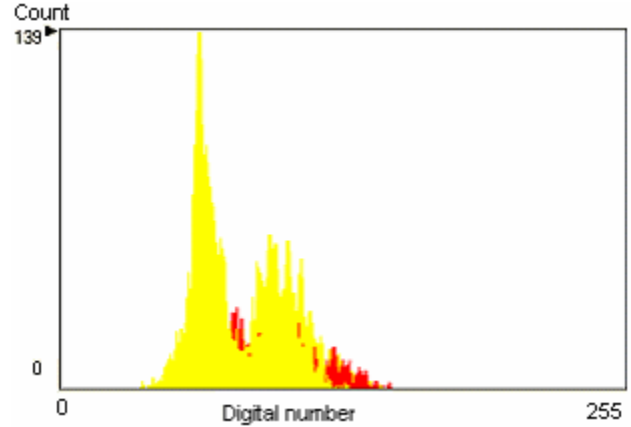


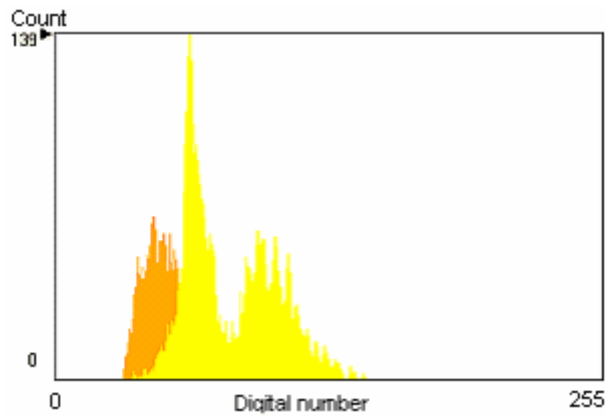
Figure 3.12 Spectral signature curves developed from some AOIs on the 1987 Landsat TM Image.



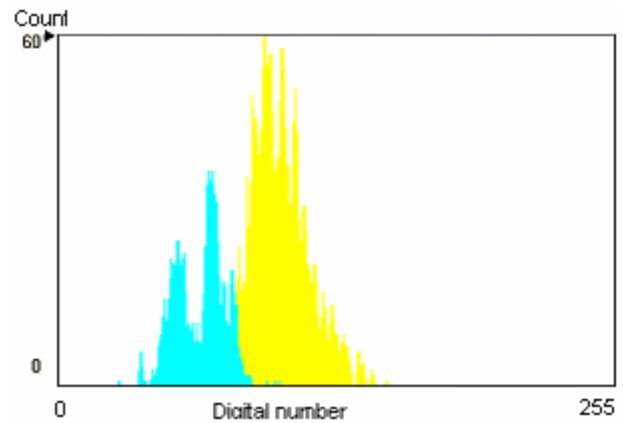
(a) Bare land (fallowed land) vs. high-density urban.



(b) Bare land (forest clear-cut) vs. high-density urban.



(c) Bare land (forest clear-cut) vs. low-density urban.



(d) Cropland/grassland vs. bare land.



Figure 3.13 Spectral confusions between land use/cover classes indicated by the overlaps in digital numbers (pixel values) of band 1, 1987 Landsat TM.

The study area dimension is 120 km by 140 km. Then the number of image frames we need to examine would be 2,025, thus the labor is intensive. Also frequent zooming in and zooming out are needed to get detailed local information and background contexture information for a land use/cover feature. Frequent zooming in and out can easily make image analysts lost. People probably would not be willing to do such a boring job. Therefore manual editing for relatively high-resolution satellite images with a large ground coverage should not be advocated. Computer automated approaches to improvement of land use/cover classification accuracy are a necessity. In Section 3.8, NDVI differencing and temporal logic will be used to enhance the initial land use/cover classification. Below, cloud shadow misclassified as water will be first corrected by a very simple but effective temporal logic.

3.6 Correction of classification errors caused by cloud shadows

To recover the true land use/cover under the cloud shadows, a simple temporal logic can be employed. It can be noticed from Figure 3.1 that clouds on the 1987 image are mostly distributed on the southeast and clouds on the 1997 image are mainly concentrated on the west. Chances of an area being shadowed by cloud on both dates are small. If an area with cloud was classified as water for one year, replacing the false water with the land use/cover classes of the other year will clear the spectral confusion between cloud shadow and water. To implement this temporal logic, first cloud and cloud shadow areas were identified visually on both Landsat TM images. Two binary images showing cloud and cloud shadow areas were created manually for both dates and combined together using raster GIS 'union' ('OR' logic) to form a single binary image with cloud or cloud shadow on either date being equal to 1 (Figure 3.14). Cloud and cloud shadow

coverage accounts for up to 2% of the area of the study area. The pseudo code for the logical expression is:

```
For  $Pixel_{i,j}$  {  
    If  $CLOUD == 1 \ \&\& \ LANDUSE_{t_1} == WATER$   
    Then  $LANDUSE_{t_1} = LANDUSE_{t_2}$   
} // '&&' means AND, "==" represents "is equal to", "=" is  
// assignment operation.
```

ERDAS Imagine Spatial Modeling Language (SML) was used to accomplish the above logic operation.

An example of how the temporal logic has cleared the confusion between cloud shadow and water is shown in Figures 3.15 and 3.16 for an area near Lake Lanier north of Atlanta. On the TM images shown in Figure 3.15, the 1987 image is cloud free, while on the 1997 image, there were cloud and cloud shadow. On the original 1997 land use/cover classification map produced using the ISODATA clustering method, cloud shadow area was assigned the class name of water, leaving a city island shown in red within the lake (see the left image on Figure 3.16). The same area was shown on the 1987 TM image to be mainly forest and some residential use. Chances of residential areas converting to water bodies are small. It is very likely that this area was still forest and residential. After all, the area of land use/cover change is much less than that of no-change area, noticing that the percentage of changed area is 22% from the change vector analysis in Section 3.4. This should justify the temporal logic operation that assigns land use/cover types of the past year to the area misclassified. The correction result was shown on the right image in Figure 3.16 on which the false water has been modified to forest and residential and the city island now becomes the waterfront.



Figure 3.14 Cloud and cloud shadow (shown in white) distribution in the 1987 image or the 1997 image.

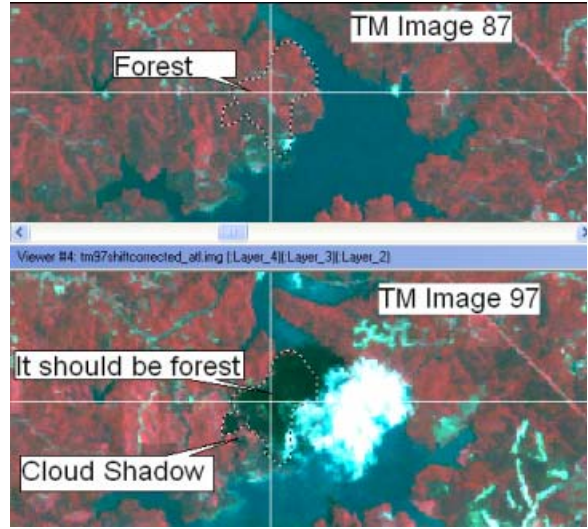


Figure 3.15 Landsat images for the both dates, Lake Lanier area.

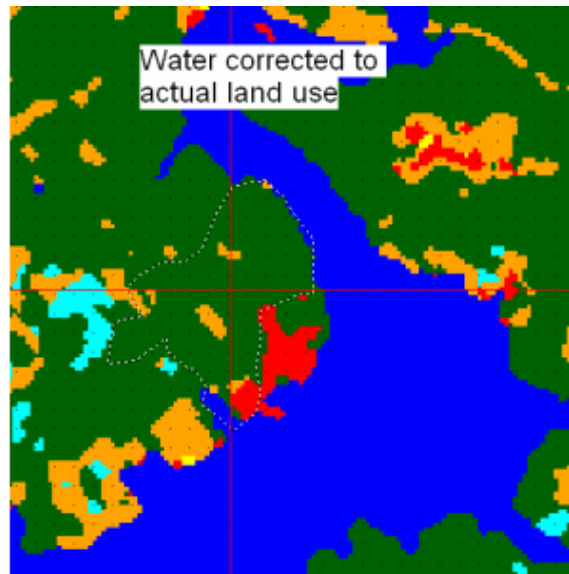
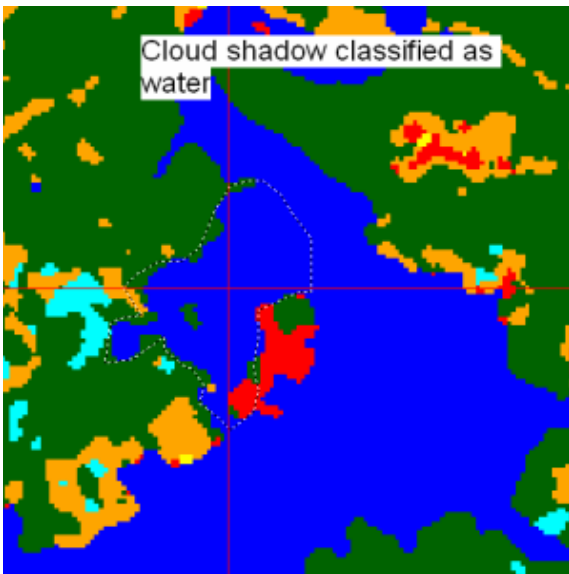


Figure 3.16 The initial classification of the 1997 image (left) and correct classification (right). Compare this figure with Figure 3.11(a). Cloud shadow misclassified as water has been corrected to the land use/cover types of the other year (1987) using temporal logic.

Since the white-purple tone of cloud is also similar to the tone of high-density urban, some clouds have been misclassified as high-density urban. This classification has caused overestimation of high-density urban area. To remove the error on the 1987 land use map, similar temporal logic can be used. For a pixel on the 1987 land use/cover map, if it had clouds and was labeled high-density urban, and if it was not high-density urban on the 1997 land use/cover map, then the pixel value is replaced with that for the year 1997. It is very unlikely that an area was not high-density urban in a more recent year but was high-density urban in an earlier year since concrete and asphalt cover is often irreversible. However, the temporal logic cannot be employed to correct the kind of error on the 1997 land use map by referring to an earlier land use map. If a pixel on a more recent image has cloud and is classified as high-density, the true land use/cover state cannot be derived from the earlier image since it is likely that this pixel was not urban in that past but is urban in the present. The cloud error on the 1997 land use/cover map has been corrected by Yang (2000) by referring to a 1998 TM cloud-free image.

3.7 Error propagation in post-classification comparison

This study uses post-classification comparison method to detect land use/cover change between two dates. Post-classification comparison compares land use/cover thematic raster maps created from image classification pixel by pixel. The advantages of this approach are that the nature of land use/cover change can be detected directly and that radiometric normalization of the multi-date images is not required since land use/cover classification is performed for each date based on its own spectral values independent of the values of different dates.

Basically, post-classification comparison change detection is a logical ‘AND’ operation. It produces a land use/cover change map with each pixel labeled as “This pixel was land

use/cover type A in date t_1 AND it is now land use/cover type B in date t_2 .” Newcomer and Szajgin (1984) developed a categorical data error model for the Boolean AND operator in which the accuracy of a given data layer i , $P[E_i]$, is defined as the proportion of the cells in the data layer that are correctly classified. So $P[E_i]$ is actually equivalent to the overall accuracy in Table 3.4. Given two data layers with accuracies of $P[E_1]$ and $P[E_2]$, the accuracy of the composite map resulting from the AND operation, $P[E_c]$, is given by

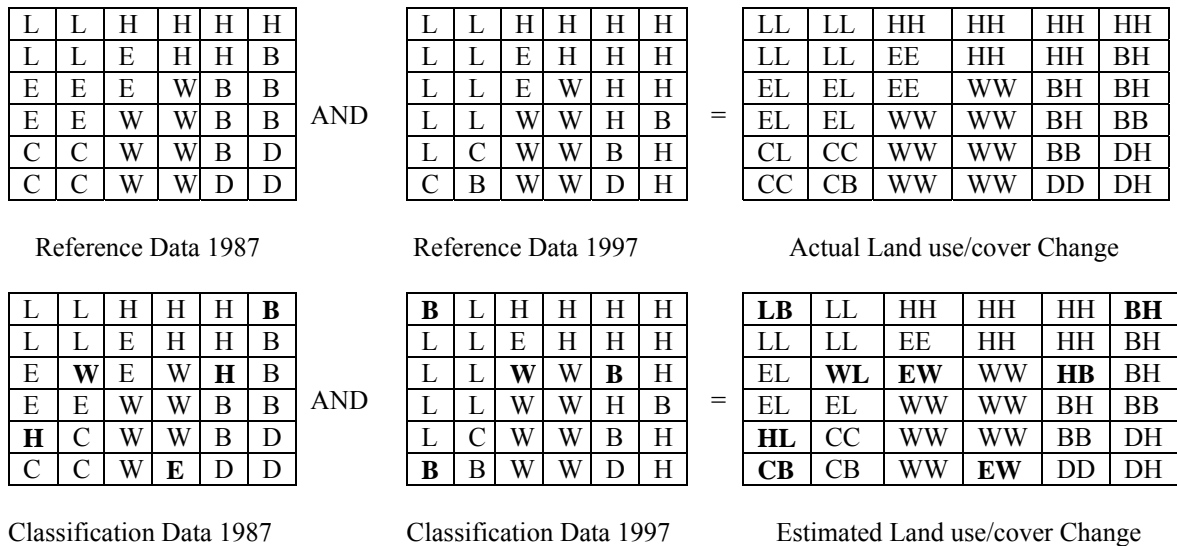
$$P[E_c] = P[E_1 \cap E_2] = P[E_1] \times P[E_2 | E_1] \quad (3-6)$$

where the conditional probability $P[E_2 | E_1]$ is the proportion of correctly classified cells in data layer 1 that are also correctly classified in data layer 2. This can be manifested in Figure 3.17 for a 6 by 6 neighborhood extracted from the land use/cover maps of the years 1987 and 1997.

Veregin (1989) derived from the above formula some general conclusions about composite map accuracy for the AND operator. Composite map accuracy will at best be equal to the accuracy of the least accurate data layer. The best accuracy can be achieved only when the misclassified cells on each layer coincide spatially with those on the least accurate data layer. The worst map accuracy will be equal to one minus the sum of the proportion of misclassified cells on each layer or to zero if the sum is greater one. This will occur when no misclassified cells on each layer coincide with each other. If errors on both layers are independent from each other, then the overlay AND operation will generate a composite map with an accuracy of

$$P[E_c] = P[E_1] * P[E_2] \quad (3-7)$$

The errors on multi-date satellite image classification maps should be independent from each other because the pixel clustering operation on one date image does not depend on the images of other dates.



Black body indicates misclassified pixels

L – Low-density urban H- High-density urban E- Evergreen forest
W-Water B- Bare land D- Deciduous forest

$$P[E_c] = P[E_1 \cap E_2] = P[E_1] P[E_2/E_1] = (31/36) * (28/31) = 28/36$$

Figure 3.17 Error propagation in the boolean AND operation in land use/cover change detection.

Thus, post-classification comparison for land use/cover change detection will compound the errors from multi-date land use/cover map layers. The accuracy of this change detection technique is only as good as the result of the multiplication of the accuracies of each individual classification (Singh 1989). For two conjugate pixels under comparison, only when they are correctly classified on both images would change/no-change be correctly detected. The overall accuracy is 90.10% for the 1997 land use/cover classification. Assuming that the accuracy of the

1987 land use/cover classification is the same as that of the 1997, then the land use/cover change map accuracy would be the product of the two maps' overall accuracies, which is equal to 81.18%. To improve the accuracy of land use/cover change, land use/cover classification accuracy must be improved first. The next section will use NDVI differencing and temporal logic to achieve this objective.

3.8 Using NDVI differencing and temporal logic to improve land use/cover classification accuracy

3.8.1 Normalized Difference Vegetation Index (NDVI)

The reflectance of vegetation varies across the electromagnetic spectrum. We see healthy vegetation as predominantly green with our naked eyes because the chlorophyll present in the leaf tissue of plants is absorbing blue and red radiation to carry on photosynthesis. Actively growing plants are highly reflective in the near-infrared portion of the spectrum (Figure 3.12) because of the multiple scattering that takes place between the spongy-mesophyll cells of the plant (Lillesand and Kiefer 1999). This contrast of reflectance and absorption by vegetation cover allows us to evaluate the amount of vegetation present on the surface. A popular index used to characterize the contrast of vegetation's higher reflectance in the near-infrared (NIR) band with lower reflectance in the red band is Normalized Difference Vegetation Index (NDVI). NDVI is the ratio of the difference in reflectance between the NIR band and the red band to the sum of the reflectance of the two bands. For Landsat 5 TM images, NDVI is measured on band 4 (ρ_4) (NIR band with wavelength range of 0.76-0.90 μm) and band 3 (ρ_3) (red band with wavelength range of 0.63-0.69 μm):

$$\text{NDVI} = \frac{\rho_4 - \rho_3}{\rho_4 + \rho_3} \quad (3-8)$$

NDVI takes values between -1 and 1, with values near 1 indicating dense vegetation and values less than zero indicating no vegetation. Vegetated areas will generally yield high values for NDVI because of their relatively high near-infrared reflectance and low visible reflectance. In contrast, cloud and water have larger reflectance in visible spectral bands than in near-infrared band. Bare soil and rock areas have similar reflectance in the two bands and thus have vegetation index near zero (Lillesand and Kiefer 1999).

The Landsat 5 TM images for the year 1987 and 1997 of the study area were obtained in summer when vegetation was actively growing. NDVI images should be able to distinguish between vegetated area and non-vegetated area. Commercial and industrial high intensity urban areas covered with asphalt must be distinctive from forest and cultivated cropland or grassland in an NDVI image. Multi-date NDVI difference maps could be indicative of urban sprawl at the expense of green space in a rapidly suburbanizing region.

3.8.2 NDVI calculation

By NDVI's definition in Formula (3-8), the calculation of NDVI values should be based on spectral reflectance, not on digital numbers in the Landsat TM near-infrared and red image bands (Lillesand and Kiefer 1999). The 8-bit digital numbers for individual pixels in Landsat 5 TM images are quantized and calibrated values (QCAL) obtained through radiometric calibration of the TM scanners. The radiometric calibration is accomplished by rescaling the raw digital data transmitted from the satellite to calibrated digital data. To calculate NDVI, the digital numbers should be converted to spectral radiance, then to exo-atmospheric reflectance. These conversions provide a basis for more normalized comparison of data in single scenes, or between images

taken on different dates and/or by different sensors (Markham and Barker 1986), which is important in land use/cover change detection from multi-date satellite images.

Conversion QCAL to spectral radiance L_λ is accomplished with the following equation by knowing the lower and upper limits of the post-calibrated dynamic range for a specific band, namely $LMIN_\lambda$ and $LMAX_\lambda$:

$$L_\lambda = LMIN_\lambda + \frac{LMAX_\lambda - LMIN_\lambda}{QCALMAX} \times QCAL \quad (3-9)$$

where

- L_λ = Spectral radiance, in $mW \cdot cm^{-2} \cdot ster^{-1} \cdot \mu m^{-1}$
- QCAL = Calibrated and quantized scaled radiance in units of DN (digital numbers)
- $LMIN_\lambda$ = Spectral radiance at QCAL = 0, in $mW \cdot cm^{-2} \cdot ster^{-1} \cdot \mu m^{-1}$
- $LMAX_\lambda$ = Spectral radiance at QCAL = QCALMAX, in $mW \cdot cm^{-2} \cdot ster^{-1} \cdot \mu m^{-1}$
- QCALMAX = Range of rescaled radiance in DN ,
- λ = Subscript to indicate the spectral band.

The parameters used to calculate the spectral radiance from Landsat TM 1987 and 1997 images are (Markham and Barker 1986):

$$LMIN_3 = -0.12, \quad LMAX_3 = 20.43;$$

$$LMIN_4 = -0.15, \quad LMAX_4 = 20.62;$$

$$QCALMAX = 255.$$

The Landsat TM images for 1987 and 1997 were captured on June 29 and July 29 respectively. Therefore, they are not anniversary data. Variation in such factors as scene illumination and surface moisture content causes the multi-date images to be incompatible. It is

necessary to apply a sun elevation correction to correct for variation in solar illumination angles and normalize the angles to the zenith, and an earth-sun distance correction to normalize for the seasonal changes in the distances between the earth and the sun (Lillesand and Kiefer 1999). For the TM image of June 29, 1987, the sun elevation is 61.84°, and the distance between the sun and the earth is 1.01665 astronomical units (USGS document, URL: http://landcover.usgs.gov/pdf/image_preprocessing.pdf). For the TM image of July 29, 1997, the sun elevation is 61.00°, and the distance from the sun to the earth is 1.01485 astronomical units. Mean solar exoatmospheric irradiance of Landsat 5 TM is $155.7mW \cdot cm^{-2} \cdot \mu m^{-1}$ for red band, and $104.77mW \cdot cm^{-2} \cdot \mu m^{-1}$ for near-infrared band. Given those parameters, the at-satellite reflectance, which is the combined surface and atmospheric reflectance, is given by (Markham & Barker 1986):

$$\rho_p = \frac{\pi L_\lambda d^2}{ESUN_\lambda \cos \theta_s} \quad (3-10)$$

where

ρ_p = unit-less effective at-satellite reflectance

L_λ = Spectral radiance

d = Earth-Sun distance in astronomical units

$ESUN$ = Mean solar exoatmospheric irradiances

θ_s = Solar zenith angle in degrees

The conversion of digital number to at-satellite spectral reflectance has achieved a reduction in between-scene variability through normalization for solar irradiance. The parameters for the computation of at-satellite spectral reflectance are summarized in Table 3.5. Based on formula (3-8), NDVI images were calculated using at-satellite spectral reflectance from formula (3-10).

Table 3.5 Parameters for the calculation of at-satellite spectral reflectance

Parameters		Landsat 5 TM images	
Date		29 June 1987	29 July 1997
Julian day		180	211
Earth-sun distance in astronomical unit ^a		1.01665	1.01485
Solar zenith angle θ_s (Solar elevation angle)		28.16° (61.84°)	29.00° (61.00°)
Dynamic range for spectral radiances ($mW \cdot cm^{-2} \cdot ster^{-1} \cdot \mu m^{-1}$) ^b	LMIN ₃	-0.12	
	LMAX ₃	20.43	
	LMIN ₄	-0.15	
	LMAX ₄	20.62	
QCALMAX		255 (=2 ⁸)	
ESUN ₃ ($mW \cdot cm^{-2} \cdot \mu m^{-1}$) ^b		155.7	
ESUN ₄ ($mW \cdot cm^{-2} \cdot \mu m^{-1}$) ^b		104.7	
^a USGS document, URL: http://landcover.usgs.gov/pdf/image_preprocessing.pdf			
^b Markham and Barker (1986)			

Absolute NDVI values tend to vary temporally in a non-systematic manner, subject to many controlling factors, including illumination condition which has been corrected for above, and surface moisture. When multi-temporal NDVI images are compared, moisture variation between dates degrades the comparability. Scaling of NDVI is necessary when the NDVI images for the two years are to be compared. This was accomplished by using the following equation (Gillies *et al.* 1997):

$$N^* = \frac{NDVI - NDVI_o}{NDVI_s - NDVI_o} \quad (3-11)$$

Where N^* is rescaled NDVI, which normalizes exo-rescaling vegetation index obtained from equation (3-8) by the NDVI values that are for 0% vegetation cover ($NDVI_o$) and 100% vegetation cover ($NDVI_s$). N^* is also called fractional vegetation cover, which can effectively act

as a surrogate for percent vegetation cover. The two Landsat TM images for the study area contain a complete spectrum of vegetation amount. $NDVI_o$ values were taken from a completely non-vegetated patch on Lake Lanier, and $NDVI_s$ values were extracted from several dense forest areas, which were used to calculate N^* :

$$N^*_{87} = \frac{NDVI_{87} - (-0.578352)}{1.0 - (-0.578352)} \quad (3-12)$$

$$N^*_{97} = \frac{NDVI_{97} - (-0.64776)}{0.93087 - (-0.64776)} \quad (3-13)$$

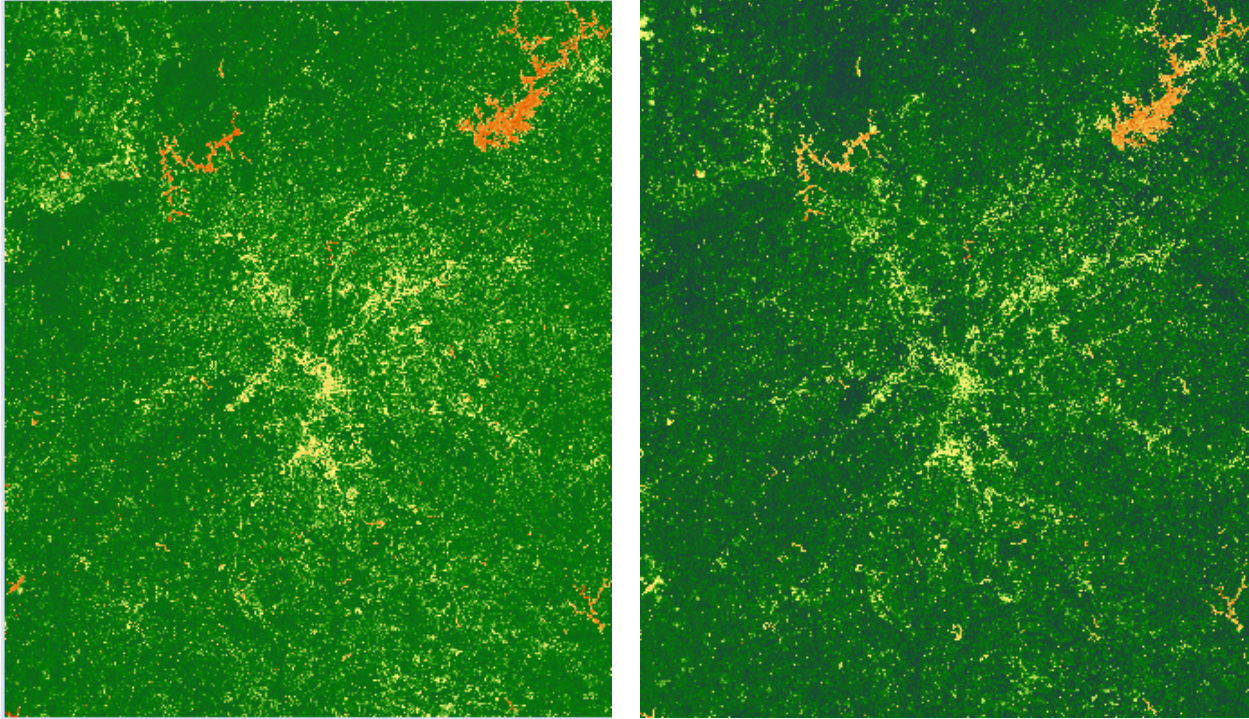
The rescaled NDVI values, N^* , are in the range of [0,1], which are too small to take full advantage of the display capacity of common GIS and remote sensing software. To facilitate the interpretation of NDVI images, N^* was further rescaled to the range of [0, 100] through equation:

$$NDVI = N^* \times 100 \quad (3-14)$$

The rescaled NDVI images for the years 1987 and 1997 are shown in Figure 3.18. Vegetations look green. The more vegetation cover, the darker the green color is. Water bodies do not have vegetation cover, having the lowest NDVI values. Lake Allatooha and Lake Lanier take on a tan color. The spatial patterns of high-density urban areas characteristic of asphalt and concrete are easy to perceive by brown tone. It is hard to see low-density residential settlements stand out from forests because low-density residential buildings and local streets and drives are hidden in the forests.

3.8.3 NDVI differencing, classification and interpretation

To improve the land use/cover classification accuracy using temporal information, an NDVI difference image was generated by subtracting the 1987 NDVI image from the 1997



(a) 1987

(b) 1997



Figure 3.18 NDVI Images for the year 1987 and 1997.

NDVI image (Figure 3.18). The result is shown in Figure 3.19. White tone represents NDVI increase, while dark tone represents NDVI decrease. White tone areas are mostly forest re-growth or replanting of fallowed cropland. On the southeast corner, large patches with white tone do not actually represent vegetation cover change. Clouds hovered over those areas on the first date where it was sunny on the second date, resulting in significant NDVI increase. The dark areas on the northwest corner do not indicate true NDVI change. Those areas were covered with forest, cropland or grassland on the first date but were covered with clouds on the second date. In the whole study area, most of the dark areas are urban development replacing forest or agriculture land. Those areas are concentrated in the north-northeast of the study area, particularly Gwinnett, north Fulton, south Forsyth, north Cobb, and south Cherokee counties. Taking a closer look at an area within Gwinnett county around the intersection of I-85 and I-985 by enlarging the image, the urban growth patterns manifested by the dark areas where NDVI values have dramatically decreased are obvious (Figure 3.20).

Different land use/cover change types may lead to different magnitude and direction of NDVI change. In order to detect the nature of land use/cover change, the NDVI difference image should be classified into a certain number of classes. It is expected that each class of NDVI change should be indicative of a certain kind of land use/cover change.

The NDVI difference image was classified using the ISODATA unsupervised classification method. The initial number of clusters was 20. The classified NDVI difference image was compared with the original Landsat TM images for the two years and ancillary air photos. Visual interpretation was conducted and each cluster was labeled with the specific nature of land use/cover change. Clusters with the same kind of land use/cover change were combined to form a single class. Some clusters represent different types of land use/cover change because

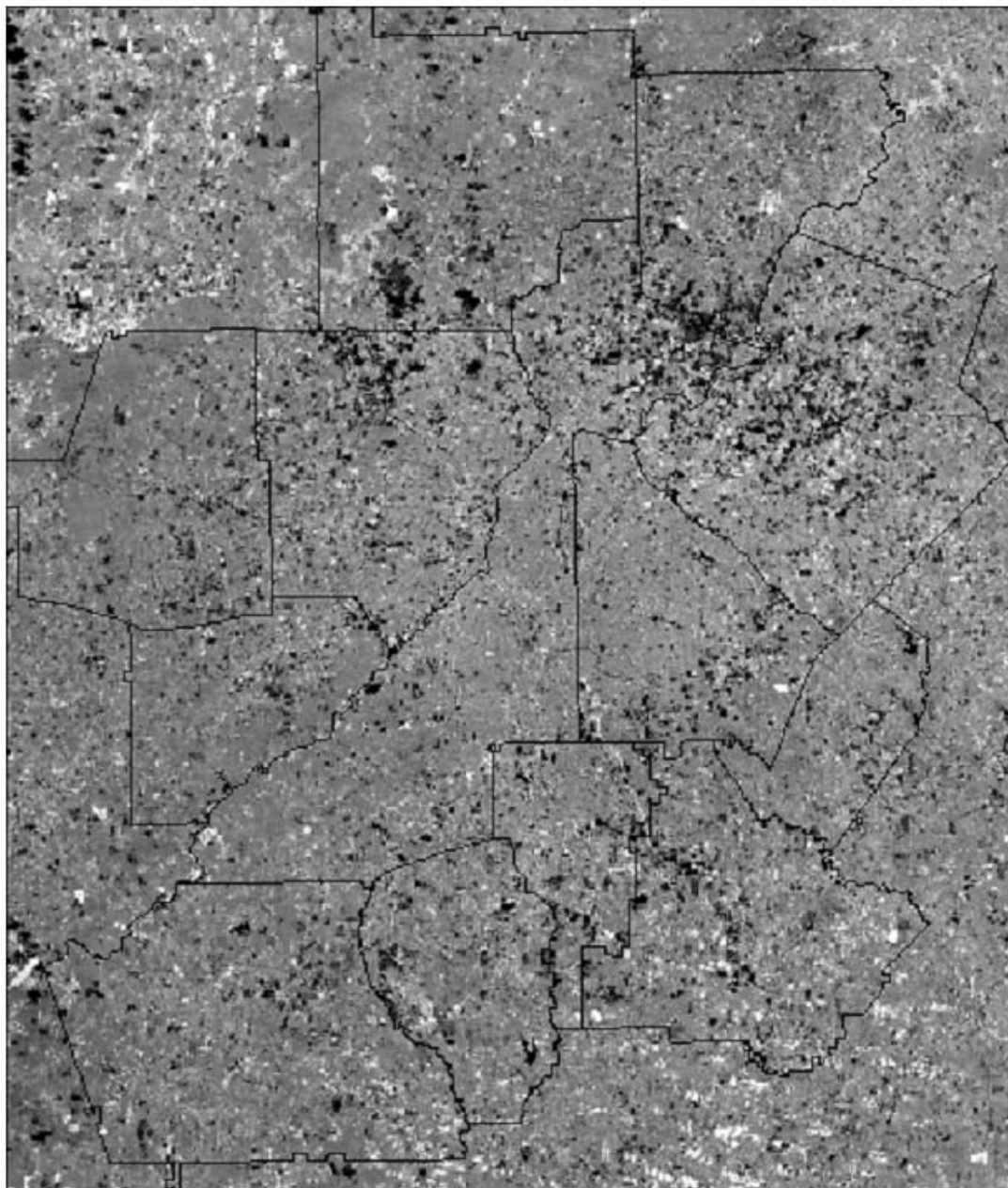


Figure 3.19 NDVI difference image for the whole study area. White tone represents NDVI increase, while dark tone represents NDVI decrease.

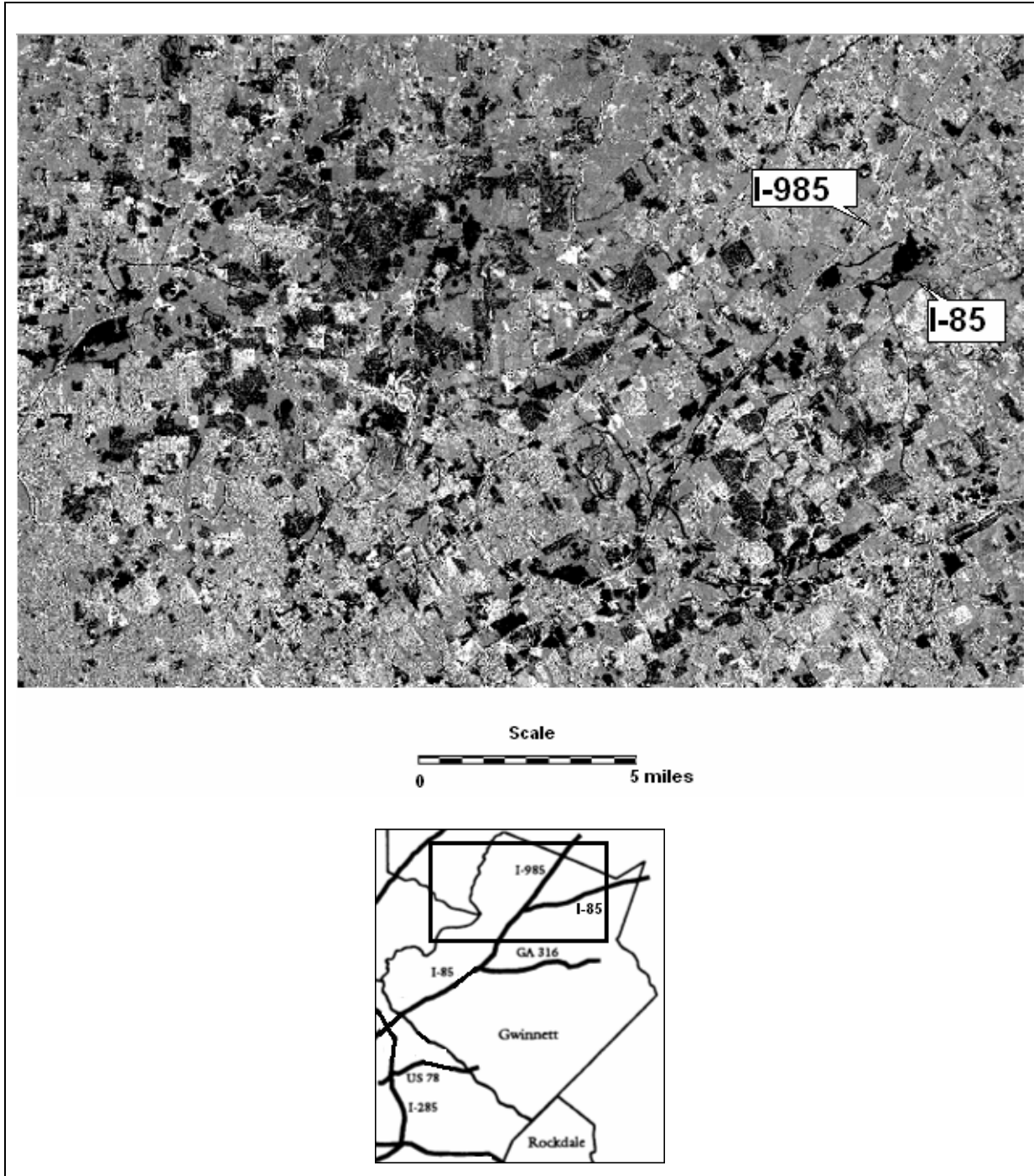


Figure 3.20 NDVI difference image, northeast of Atlanta. Urban growth patterns are manifested by the dark areas where NDVI values have dramatically decreased.

those types of land use/cover change cause equal amount of NDVI change. In this case, all types of land use/cover change were recorded for those clusters. Finally, the 20-cluster classification was recoded and combined to form a five-class NDVI difference map. The five classes are ‘dramatic decrease’, ‘moderate decrease’, ‘no change or subtle change’, ‘moderate increase’, and ‘dramatic increase’ of NDVI values. Figure 3.21 demonstrates the 5-class NDVI classification for the same area as in Figure 3.20. This map demonstrates that this area had experienced rapid urbanization from 1987 to 1997. Urban growth causing dramatic loss of green space is shown in brown color on the map. Many residential settlements had been developed to accommodate “white-flights” who moved from the central city to the suburb and new immigrants from other states to pursue new high-tech, white-collar and high-income job opportunities in this area. In the meantime, large shopping malls and other commercial facilities were constructed to meet the living demands of the new residents.

A table recording the different types of land use/cover change for each class of NDVI change was generated through the interpretation of the NDVI map (Table 3.6). Urban development on the forest and cropland/grassland has caused dramatic decrease of NDVI values. Forest change into water has also made NDVI dramatically decrease. Moderate decrease of NDVI has been accompanied with forest clear-cut and cropland being put into fallow. There are still shrubs or grass left with forest clear-cut and fallow cropland, thus the vegetation index does not decrease so dramatically as replacing forest and agriculture land with asphalt and concrete. No change or subtle change of NDVI represents either areas without land use/cover change or areas with land use/cover changes that do not cause much NDVI change. Conversions between forest and cropland/grassland cause subtle changes of NDVI. Transitions of bare land into urban

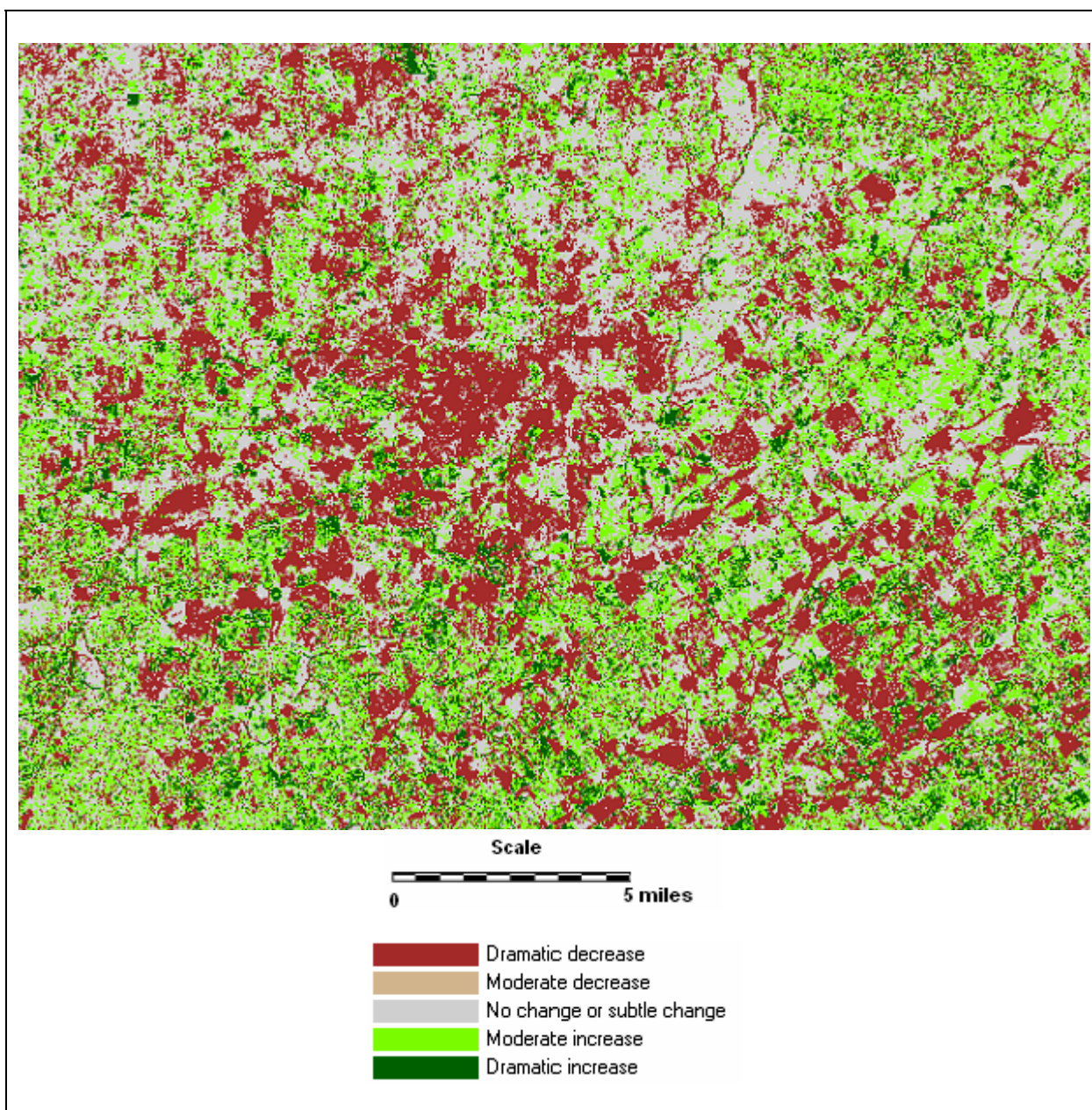


Figure 3.21 NDVI 1987-1997 difference classification map. Notice the conversion of forest and agriculture land for urban development in brown color (dramatic NDVI decrease).

Table 3.6 Interpretation of NDVI difference classes

Code	$\Delta NDVI$	Nature of land use/cover change (“ from -to”)
1	Dramatic decrease	4-1 4-2 5-1 5-2 5-6
2	Moderate decrease	5-3 4-3
3	No change or subtle change	No land use/cover change 4-5 5-4 3-1 3-2 Crop rotation Moisture variation Other changes
4	Moderate increase	3-5 3-4
5	Dramatic increase	6-5
<p>Land use/cover coding:</p> <ul style="list-style-type: none"> 1- High-density urban 2- Low-density urban 3- Bare land 4- Cropland or grassland 5- Forest 6- Water 		

use and practice of crop rotation (planting different crops in different years) do not bring about obvious vegetation index variations. Moisture variations cause subtle NDVI change. For example, the sky over Lake Lanier was foggy and wet on the first date while it was clear on the second date, resulting in minor variation of the vegetation index values. But the subtle change does not indicate any actual land use/cover conversions. Forest re-growth from clear-cut and crop plantation on the fallow land have led to moderate increase of NDVI. When small water bodies, such as ponds, become dry and are covered with grass, shrub or forest, the vegetation index values increase dramatically.

3.8.4 Using NDVI differencing and temporal logic to enhance land use/cover classification

The temporal logic revealed in Table 3.6 can help improve the accuracy of land use/cover classification. In Table 3.6, the second class of NDVI change (“moderate decrease”) indicates that if the land use/cover was forest or cropland/grassland in 1987, then the land use/cover type in 1997 must be bare land. This would recover bare land from high-density urban, low-density urban or cropland misclassified from bare land on the 1997 land use/cover map. The fourth class of NDVI change (“moderate increase”) suggests that if land use/cover types in 1997 were forest or cropland/grassland, then the land use/cover type in 1987 must be bare land. This would recover bare land from urban or cropland/grassland misclassified from bare land on the 1987 land use/cover map. This “If...then...” logic was implemented using ERDAS Imagine Spatial Modeling Language (SML). The original land use/cover classification images from Yang (2000) and the NDVI image difference classification image are the inputs to the spatial model. The cloud image (Figure 3.14) was used as a mask to exclude clouded areas from analysis since the

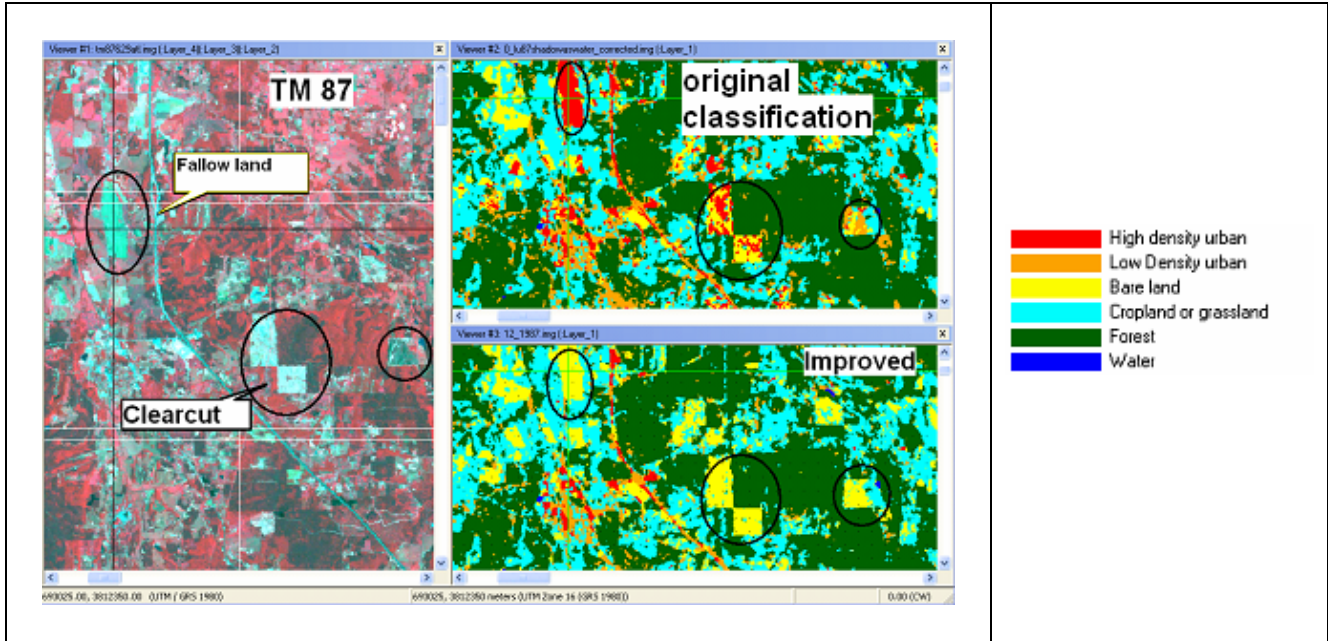
NDVI change in the clouded areas may not reflect the true vegetation change. The pseudo codes of the spatial model are shown in Table 3.7.

One should note that the classification accuracy of the land use/cover types in the IF portion of the logic rule must be higher than that of the land use/cover types in the THEN portion, otherwise the employment of the temporal logic would lower the land use/cover classification, rather than improve it. The reason is that much uncertainty in the classification of the land use/cover types in the IF portion would cause the assertion that “the land use/cover type in the other year must be ...” unreliable in the THEN portion. Take the first rule in Table 3.7 as an example. Since the overall classification accuracies of forest and cropland/grassland are 97.6% and 95.1% respectively, much higher than that of bare land which is 80.00% (Table 3.4), this logic rule does not have any problems. If the classification accuracies of forest or cropland/grassland were much lower than the accuracy of bare land, then for a pixel, though its cell value is 5 (forest) or 4 (cropland/grassland) in the 1987 land use/cover classification image, we are still not very sure if the cell values of 5 or 4 represent the true land use/cover types. If the actual land use/cover type is not forest or cropland/grassland, then the IF condition itself is not correct, thus the assignment of cell value 3 to the pixel on the 1997 land use/cover classification image will not be correct.

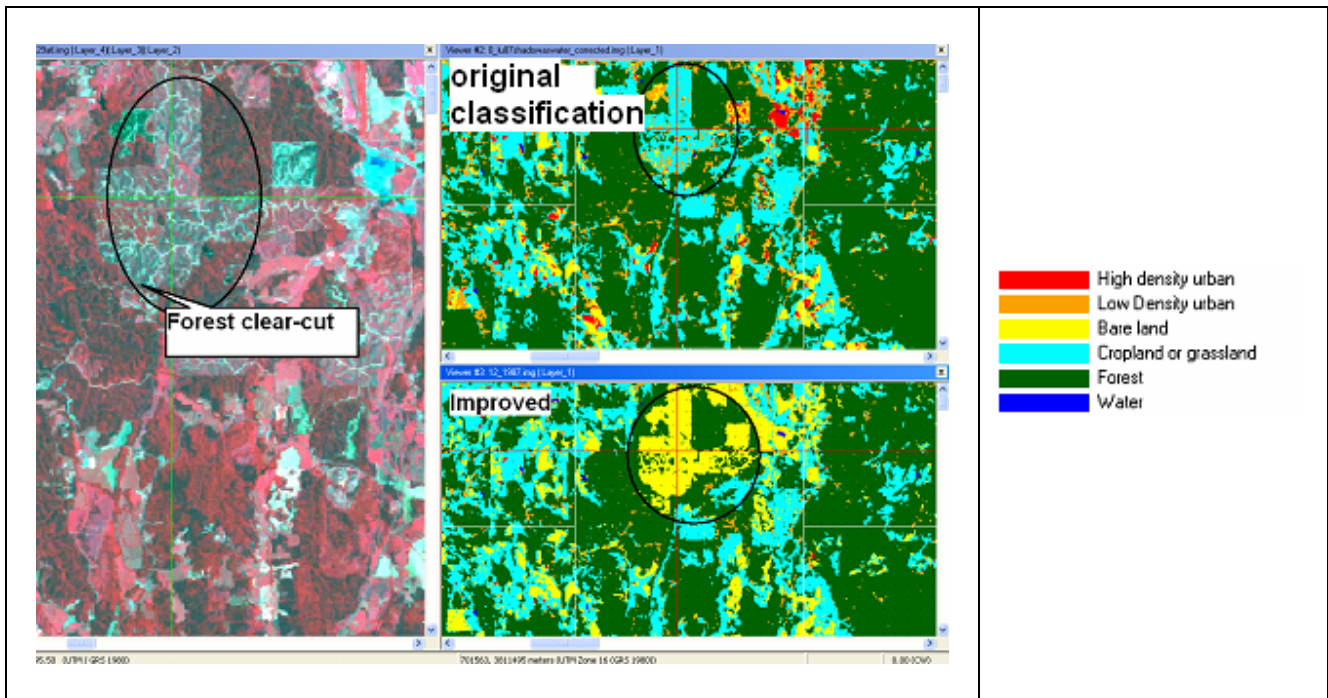
After the use of the two logic rules in Table 3.7 on the original land use/cover classification images, the misclassification of bare land as high-density urban, low-density urban, or cropland was corrected. Figure 3.22 gives two snapshots of how the temporal logic and NDVI differencing method has improved the land use/cover classification. In Figure 3.22(a), on the original 1987 land use/cover classification, a large patch of fallow land was misclassified as high-density urban. This piece of land was replanted in 1997. The vegetation index had increased

Table 3.7 Using NDVI differencing and temporal logic to enhance land use/cover classifications

If...Then logic	Description
<pre> For a pixel { If { CLOUD == 0 AND ΔNDVI == 2 AND (LANDUSE₈₇ == 5 OR LANDUSE₈₇ == 4) } THEN LANDUSE₉₇ = 3 } </pre>	<p>No cloud ΔNDVI is equal to ‘moderate decrease’ Land use/cover in 1987 was forest or cropland/grassland</p> <p>Assign code 3 (bare land) to the pixel in the 1997 land use/cover classification image</p>
<pre> For a pixel { If { CLOUD == 0 AND ΔNDVI == 4 AND (LANDUSE₉₇ == 5 OR LANDUSE₉₇ == 4) } THEN LANDUSE₈₇ = 3 } </pre>	<p>No cloud ΔNDVI is equal to ‘moderate increase’ Land use/cover in 1997 was forest or cropland/grassland</p> <p>Assign code 3 (bare land) to the pixel in the 1987 land use/cover classification image</p>



(a) Misclassified high/low-density urban corrected to bare land (forest clear-cut and fallow land).



(b) Misclassified cropland corrected to forest clear-cut.

Figure 3.22 Results of the use of temporal logic and NDVI differencing approach to improve the accuracy of land use/cover classification.

moderately. Therefore the second rule in Table 3.7 has taken effect and corrected the high-density urban to bare land. The same operation was performed on the three regular-shaped forest clear-cuts. Those three patches were forest in 1997. It was impossible for them to be high-density urban in 1987. In Figure 3.22(b), the patch of forest clear-cut was misclassified as cropland on the 1997 land use/cover classification map. It was forest in 1987. NDVI had decreased moderately ($\Delta NDVI = 2$). The first rule in Table 3.7 has taken effect on this piece of land and changed it from cropland to bare land.

The use of the NDVI differencing and temporal logic on the original land use/cover classification images, and the clearance of the confusion between cloud-shadows and water in Section 3.6 followed by 3 by 3 majority filtering have led to the final improved land use/cover classification maps shown in Figure 3.23. These two maps will serve as inputs to the Markov chain model in Chapter 4 and the logistic regression model in Chapter 5. Detection of land use/cover change, especially urban growth between 1987 and 1997 will be conducted based on these two images in the following section.

3.9 Post-classification comparison for land use/cover change detection

Pixel-by-pixel comparison of the 1987 and 1997 land use/cover maps (Figure 3.23) in support of raster GIS was performed to detect the land use/cover change during the 10 years. The quantitative information of land use/cover changes is shown in Table 3.8 and Figure 3.24. In terms of the absolute value of area of change, the four major land use/cover changes are high-density urban growth, low-density urban growth, decline of forest, and decline of cropland or forest land. The most intense land use/cover change is the growth of low-density urban area. Low-density urban area was 2468.62 square kilometers in 1987 and 3519.56 square kilometers in

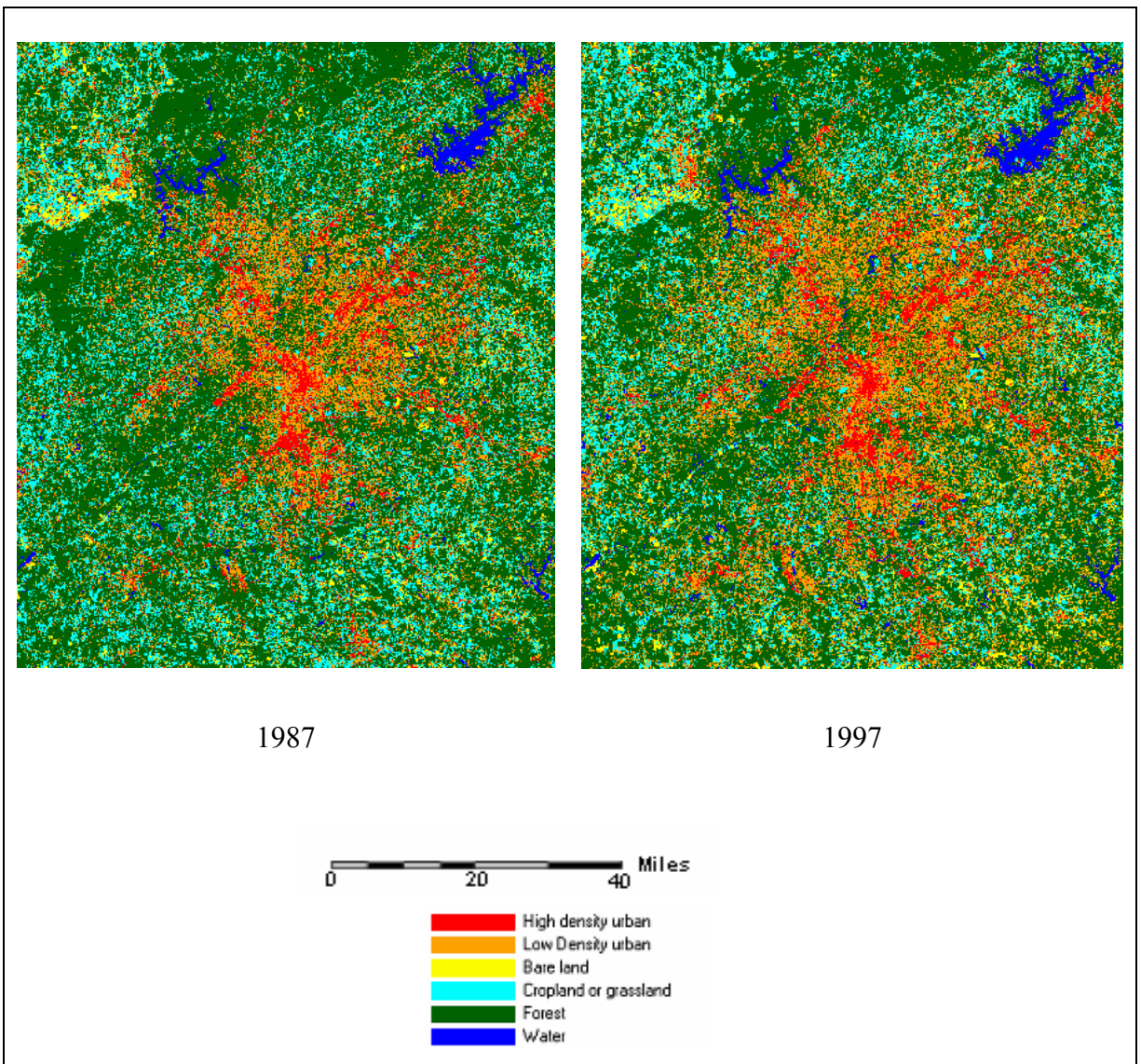


Figure 3.23 Final improved land use/cover maps for years 1987 and 1997.

Table 3.8 Quantitative information of land use/cover change

Land use/cover Type	Area 1987 (km ²)	Area 1997 (km ²)	Change area (Km ²)	Proportion 1987(%)	Proportion 1997(%)	%Change*
High-density urban	876.78	990.27	113.49	5.49	6.20	12.94
Low-density urban	2468.62	3519.56	1050.94	15.45	22.02	42.57
Bare land	397.37	474.11	76.75	2.49	2.97	19.31
Cropland or grassland	2702.52	2358.03	-344.49	16.91	14.75	-12.75
Forest	9217.04	8238.28	-978.76	57.67	51.54	-10.62
Water	320.87	402.96	82.09	2.01	2.52	25.58

* %change = (Area 1997 – Area 1987)/Area 1987 *100

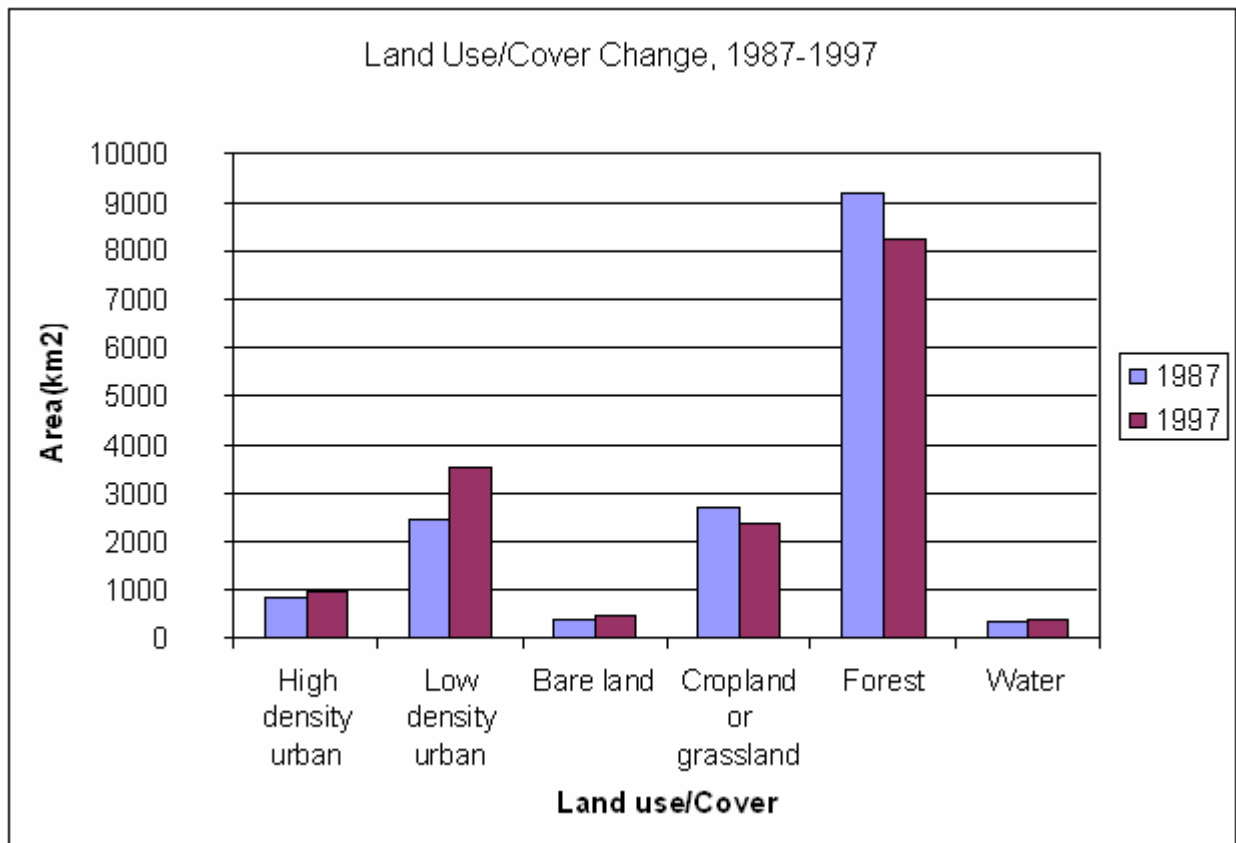


Figure 3.24 Land use/cover changes from 1987 to 1997.

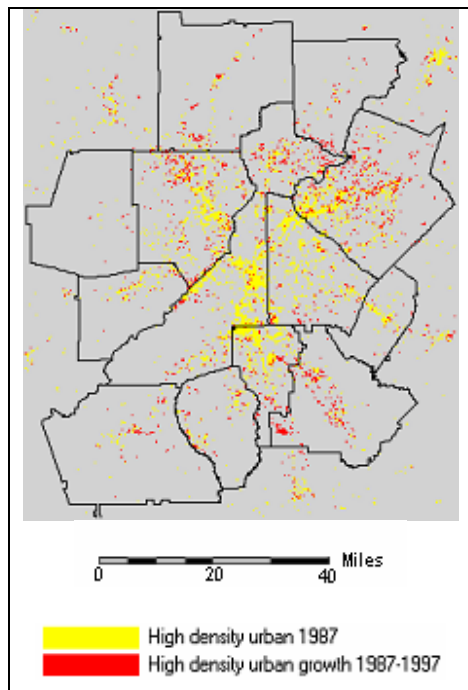
1997, representing an increase of 42.57% in ten years (Table 3.8). High-density urban area increased by 12.94% from 876.78 square kilometers in 1987 to 990.27 square kilometers in 1997, with a net increase of 113.49 square kilometers (Table 3.8). Urban was developed mainly at the expense of forest and cropland or grassland. The ten years had seen the loss of 978.76 square kilometers of forest and 344.49 square kilometers of cropland or grassland (Table 3.8).

To look at where those land use/cover changes had occurred, four change maps were created to portray the spatial patterns of the changes (Figure 3.25). These change maps can be easily produced using the 'CONDITIONAL' statement in ERDAS Imagine Spatial Modeling Language (SML). For example, Figure 3.25(a) was produced using the following statement:

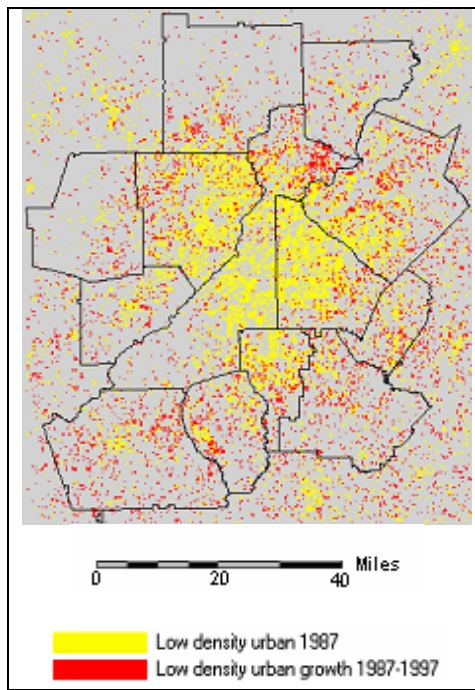
Output = CONDITIONAL { landuse87 == 1) 100 , landuse97 == 1 && landuse87 != 1) 200 }

where the first priority of pixel value assignment was given to the first condition '*landuse87 == 1*'. The statement can be deciphered as "If a pixel on the 1987 land use/cover map has a value of 1 (high-density urban), assign a value of 100 to the pixel on the output map; if the pixel value is 1 on the 1997 land use/cover map AND the pixel value is not 1 on the 1987 land use/cover map, assign a value of 200 to the pixel on the output map." The value of 100 on the output high-density urban growth map represents the 'base' high-density urban in 1987 shown in yellow color. The value of 200 indicates the net urban growth depicted in red (Figure 3.35(a)).

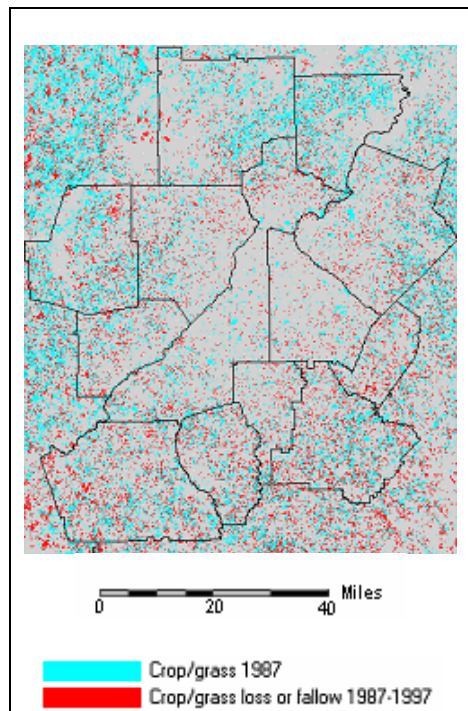
It can be seen that high-density urban growth had mainly occurred on the north and southeast and along the transportation arteries I-85, I-75, and GA-400. Contrary to the linear concentration of high-density urban along transportation corridors, the low-density urban growth has taken on both clustered and dispersed patterns. Clusters of new residential settlements can be seen on the northeast corner of Fulton County west of I-85, in the central part of Gwinnett County, south of Cherokee County, and along the dividing boundary line between Coweta



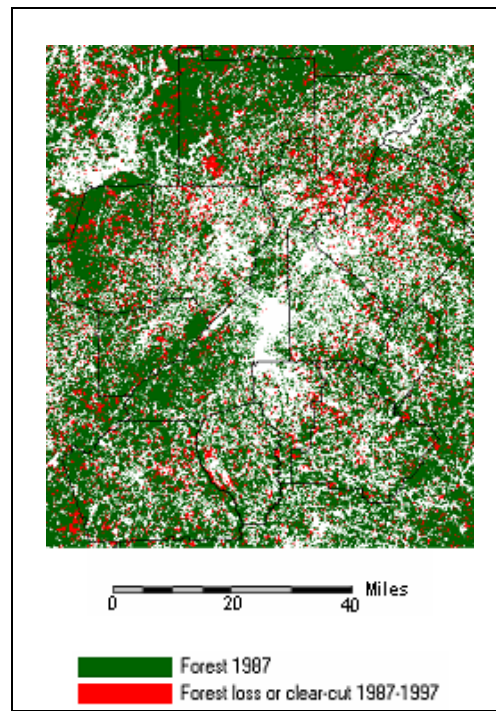
(a) High-density urban



(b) Low-density urban



(c) Cropland or grassland



(d) Forest

Figure 3.25 Land use/cover change from 1987 to 1997 for four major land use/cover types.

and Fayette Counties. Most newly constructed residential settlements were dispersed throughout the outer peripherals of the whole region. Comparing the cropland or grassland change map with the high-density and low-density urban growth maps, it was found that the patterns of the red areas indicating the cropland/grassland loss does not match well with the patterns of urban growth. This implies that only a small portion of the amount of 344.49 square kilometers of cropland/grassland was converted to urban use. Most of the decline was the result of cropland fallow as seen in the northwest, southeast and southwest corners. Within the 13-county areas, the locations of forest loss match well with the locations of urban growth, which means that urban development, especially low-density urban development, took place mainly in forested areas.

In Chapters 4 and 5, spatial modeling of urban growth does not differentiate high-density urban and low-density urban. Thus another urban growth map combining high-density urban and low-density urban together was created (Figure 3.26). This map more clearly shows the rapid urban growth the Atlanta metropolitan area had experienced during the 1990s. One can see the occurrence of urban growth in the existing edge of the city, as well as filling-in within established urban clusters.

3.10 Discussions and conclusions

Only by knowing the past can we predict the future. The information on historical land use/cover change in a rapid suburbanization region not only helps people understand how human activities have modified the regional urban and rural landscape, but also assists decision making in the regional management and planning. Most people may feel the change in their local environment, but they may not be able to realize the regional impact of the landscape change. It is not until we study the metropolitan landscapes from a spatial perspective and the time scale of decades that

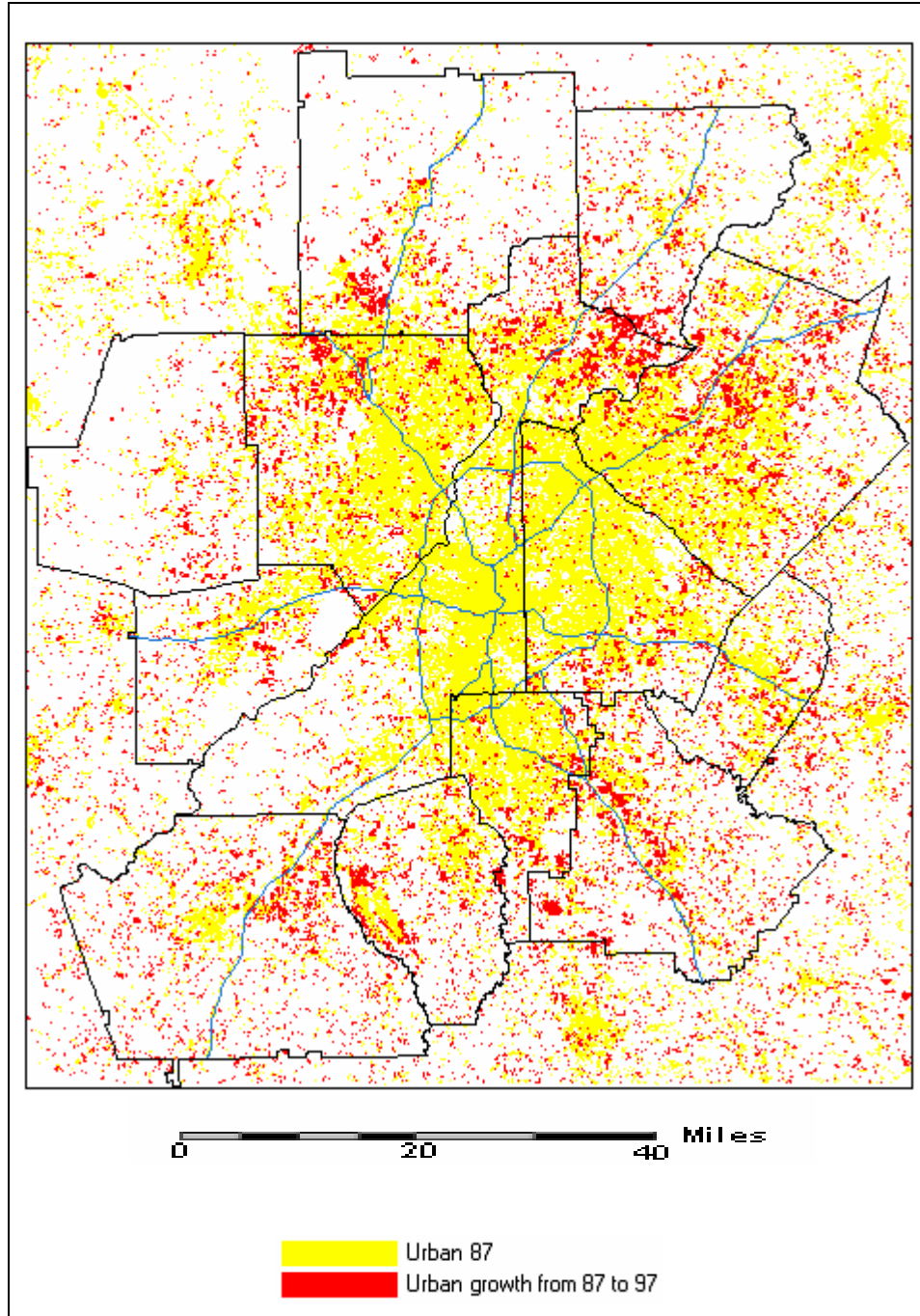


Figure 3.26 Urban growth from 1987 to 1997.

we can begin to measure the changes that have occurred and predict the changes and their impact to come. This study, using Atlanta metropolitan region as a case, has demonstrated that remote sensing, particularly Landsat TM images, integrated with image processing and GIS technology, is well suitable for providing this land use/cover change information.

To ensure accurate detection of land use/cover change, some preprocessing steps cannot be ignored, such as co-registration of multi-date satellite images. Analysis of change vectors defined on the first two principal components of the Landsat images has shown that the major changes that have occurred are deforestation for urban development. While the change vector analysis is able to reveal the general land use/cover dynamics in the complex landscape of a rapid suburbanization region, it cannot differentiate the specific nature of different types of land use/cover changes as some existing research asserts (Singh 1989; Lillesand and Kiefer 1999). Previous research on change vector analysis was conducted for study areas with only one kind of land use/cover change, such as deforestation. Post-classification comparison method can detect the nature of different land use/cover changes. However, errors can be compounded in the detection process, resulting in a land use/cover change map with low accuracy. Unsupervised classification based only on pixel spectral values cannot resolve the confusions between land use/cover types with similar spectral responses. Post-classification manual editing is time consuming and labor intensive. We need to take advantage of the automated computing ability of computer systems to correct for the misclassification errors.

This study makes use of temporal logic latent in the relationships between NDVI changes and land use/cover changes to improve the land use/cover classifications automatically by taking advantage of existing GIS functions. The use of NDVI differencing method in this study is not new, but it differs from and has advantages over the traditional NDVI differencing methods

(Masek *at al.* 2000; Mas 1999; Macleod and Congalton 1998; Singh 1989). Traditional studies on the NDVI differencing approach to detection of land use/cover change first make an NDVI difference image, then determine a threshold value and make a binary image. The binary images are created such that if the absolute value of NDVI difference of a pixel is greater than the threshold value, the pixel is labeled as change, otherwise, it is labeled as no-change. After that, the binary image is used as a mask to be applied on the second date original image, and land use/cover classification is performed again on those areas identified as change. The selection of threshold values is very subjective and needs a lot of trials and errors. The binary image contains only change/no-change information. This dichotomous delimitation may be appropriate for areas with simple land use/cover dynamics dominated by a single type of change, but may not be suitable for complex urban landscapes where various human-induced land use/cover changes have occurred. Also, the binary demarcation causes the loss of useful information within the vegetation index. Reclassification of changed areas on the second date image does not have its logical foundation.

In this study, the NDVI difference image was classified into 20 clusters first using the ISODATA method. By visual interpretation, these clusters were combined and recoded into five classes. The classification let data speak for itself without human subjectivity. The finer grouping of NDVI difference values contains more detailed information on the nature of different land use/cover changes. Temporal logic rules are developed from the interpretation of the NDVI classifications and applied to the original land use/cover maps produced from conventional clustering method to improve the classification. This temporal logic is easy to understand and implement in most raster GIS software packages. The study has shown that NDVI differencing classification combined with the temporal logic can effectively resolve the confusions between

bare land (forest clear-cuts or fallowed land) and cropland, as well as the confusions between bare land (forest clear-cuts or fallowed land) and high- or low-density urban.

The improved land use/cover change map has detected the vast amount of urban growth in the Atlanta region at the edge of the city and around urban clusters from 1987 to 1997 at the expense of forest, cropland, and open space. The area of high-density urban had increased by 12.94%, while low-density urban area had experienced more dramatic growth, increasing by 42.57%. The land use/cover change maps revealed that urban growth areas coincide spatially well with deforested areas. The depletion of green space has given rise to people's worries about the quality of the environment. What would the future environmental quality of Atlanta be like if the region continues its urban growth at the same speed as that in the 1990s? The Markov chain model and the logistic regression model in the following chapters will attempt to answer this and related questions.

CHAPTER FOUR

MARKOV CHAIN ANALYSIS OF LAND USE AND LAND COVER CHANGE

4.0 Introduction

Markov chains have been used to model plant succession (Usher 1992), to simulate sedimentary stratigraphic sequences in geology (Harbaugh and Bonham-Carter 1970), and to characterize land use/cover change dynamics (Turner 1987; Muller and John 1994; Wood *et al.* 1997; Petit *et al.* 2001; Weng 2002). Muller and John (1994) used small-scale (1:50,000) land use/cover maps, while Wood *et al.* (1997), Petit *et al.* (2001), and Weng (2002) used satellite remote sensing images. The research by Muller and John (1994) and Weng (2002) studied historical land use/cover change but did not predict the future. While Petit *et al.* (2001) quantified the processes of land use/cover change and generated short-term land-cover change projections, they did not predict the spatial patterns of land use/cover of the future. Turner (1987) compared three different types of spatial simulation using historical aerial photographs to simulate landscape changes in Georgia: a Markov chain random simulation based solely on transition probabilities, a spatial simulation in which the four nearest neighbors (adjacent cells only) influence transitions, and another spatial simulation in which the eight nearest neighbors (adjacent and diagonal cells) influence transitions. Turner found that the random Markov chain model simulated a highly fragmented landscape that were quite different from the actual landscape because the Markov chain model did not capture the contagion effects. The other two spatial models simulated the clustering of certain land uses reasonably well. All previous research on Markov chain modeling

of land use/cover change has employed first-order Markov chains based on the assumption of stationary transition probability. Few research examples have tested Markov properties and the assumption of stationary transition.

This chapter uses Markov chain model to characterize temporal and spatial changes in land use/land cover and to predict the quantities and spatial patterns of land use/cover in the future in the Atlanta metropolitan region. In this study, the 1987 and 1997 land use/cover maps derived from Landsat TM images as explained in Chapter 3 are used as inputs to the Markov chain model. The proportions of different land use/cover classes and the spatial patterns for the future years are generated from the model. To relate this chapter's study with the whole dissertation's objective of modeling urban growth, the spatial patterns of urban area simulated. The extent of urban growth will also be allocated to the urbanization probability map predicted from the logistic regression model to be explained in Chapter 5.

4.1 Markov chain model

Markov processes are named after the work of the Russian mathematician Andrei A. Markov (1856-1922) in the twentieth century to describe many natural processes that occur randomly and also exhibit an effect in which previous events influence, but not rigidly control, subsequent events (Collins 1975). A Markov process can be regarded as a process in which the probability of the system being in a given state at a particular time may be deduced from knowledge of the immediately preceding state. One form of a Markov process is a Markov chain. Markov chain is a sequence or chain of discrete states in time in which the probability of the transition from one state to a given state in the next step in the chain depends on the previous state, and not on how the process arrived in that state. Such a chain is called a first-order Markov chain. The definition of Markov chain can be extended to a higher order. If the probabilities associated with each

transition depend on events earlier than the immediately preceding event, the Markov chain is a higher-order chain. The Markov property refers to the dependence of probabilities associated with each transition on the immediately preceding state for a first-order Markov chain or several states for a higher-order Markov chain. The Markov property is one of the important aspects of Markov chains. Another important aspect of Markov chains is stationarity, which means, in a Markov chain, the probabilities associated with the transitions between states are constant throughout the predictive period (Collins 1975).

Implicit in the Markov property, there is a concept of conditional probability. By conditional probability, we mean that the probability of a particular event is conditional on other events. Thus, the Markov property of a first-order Markov chain can be expressed formally as:

$$P_{ij}^{\Delta t} = \Pr\{X_{t+1} = j \mid X_t = i\} \quad (4-1)$$

where X = discrete state variable

$P_{ij}^{\Delta t}$ = the probability of transition from state i to state j over the time interval Δt , and

$\Pr\{X_{t+1} = j \mid X_t = i\}$ = the probability of state being j at time $t+1$, given state i at time t .

Thus, this expression means that the probability of transition from state i at time t to state j at time $t+1$ is conditional on the state variable X 's value of i at time t .

Markov chains occupy an intermediate position in the spectrum of dynamic models, ranging from classical, deterministic models at one extreme to the purely random models at the other. A Markov-chain model is intermediate in that a random component is present, but that the state of the system at any point in time or space is not independent of the previous event or events (Harbaugh and Bonham-Carter 1970).

4.2 Formulation of a Markov chain model of land use/cover change

For the scope of this study, the process of land use/cover change in the study area is regarded as a Markov chain with discrete states in the form of land use/cover categorical classes. The basic assumptions are: (1) the land use/cover change is a stochastic process; (2) the land use/cover state at time t_2 is dependent only on the state at the immediately preceding time t_1 , i.e., the land use/cover change process has first-order dependence; and (3) the probabilities of land use/cover state transition are stationary, which means the transition probabilities do not change with time.

Although the Markov chain model of a land use/cover system has a stationarity assumption, actually it is implausible to expect the land use/cover system to change with a stationary transition probability due to complex and versatile social, economic, and biophysical factors. Non-stationarity of land use/cover transition probabilities has been observed in previous research (Wood *et al.* 1997; Weng 2002). Even if transitions are in reality non-stationary, stationarity can be assumed as a heuristic device to provide answers to ‘what if’ kinds of questions (Baker 1989). Thus, the non-stationarity does not compromise the Markov chain model’s prediction ability. In this study, the Markov chain model can answer the question “What will the future Atlanta be like if the land use/cover transition probabilities remain the same as those from 1987 to 1997?” Such projections contribute to an increased awareness of the ecological, environmental and societal consequences of the land use/cover change, particularly of the continuing urban growth.

Historical land use/cover maps at the resolution of 25 meters were derived from Landsat TM images for the years 1987 and 1997 as described in Chapter 3. The original six classes of land use/cover were recoded into five major classes after combining ‘high-density urban’ and ‘low-density urban’ into a single class ‘urban’. The five classes are urban, bare land,

cropland/grassland, forest, and water. The combination of high-density urban and low-density urban into a single class pertains to the major objective of this dissertation research — modeling urban growth, and facilitates the comparison of the Markov chain model with the logistical regression model in Chapter 5, which does not differentiate between high-density urban and low-density urban. It should be noticed that the definitions of land use/cover classes and the number of classes to be modeled are essentially subjective. The output from such a statistical model is bound to be dependent on the choice of states to be modeled. It is known from Chapter 3 that the major land use/cover change is the clearing of forest for urban use in the study area. Thus, a typical segment of the Markov chain for a particular land lot (actually a cell in remotely sensed images) would look like Figure 4.1 where the arrows represent first order dependence.

The behavior of a Markov chain can be depicted succinctly by a transition matrix. Each element in the matrix is the probability of the transition from a particular state pertaining to the particular row in the matrix to the next state pertaining to the particular column. The number of the rows equals the number of columns, corresponding to the number of states. For this study, the number of states is five, the number of land use/cover classes. A transition matrix P of the Markov chain of land use/cover change with five states may be written as follows:

$$P = \begin{matrix} & \begin{matrix} c_1 & c_2 & c_3 & c_4 & c_5 \end{matrix} \\ \begin{matrix} c_1 \\ c_2 \\ c_3 \\ c_4 \\ c_5 \end{matrix} & \begin{bmatrix} P_{11} & P_{12} & P_{13} & P_{14} & P_{15} \\ P_{21} & P_{22} & P_{23} & P_{24} & P_{25} \\ P_{31} & P_{32} & P_{33} & P_{34} & P_{35} \\ P_{41} & P_{42} & P_{43} & P_{44} & P_{45} \\ P_{51} & P_{52} & P_{53} & P_{54} & P_{55} \end{bmatrix} \end{matrix} \quad (4-2)$$

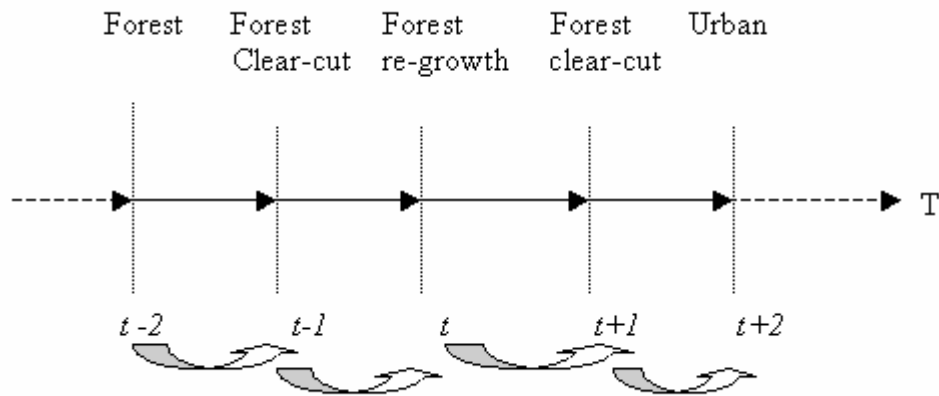


Figure 4.1 A segment of Markov chain representing land use/cover change in the study area.

where the p_{ij} ($i=1,2,\dots,5; j=1,2,\dots,5$) signifies the probabilities of transition from land use/cover category c_i to c_j . The transition matrix is subject to:

$$\sum_{j=1}^5 p_{ij} = 1 \quad (i, j=1,2,\dots,5) \quad (4-3)$$

which implies in effect that there is absolute certainty of transition from each land use/cover class to some class at the next time point in the Markov chain.

Transition probabilities are calculated based on the frequency distribution of the empirical observations. A frequency distribution of transitions is simply a tabulation of the number of transitions from each state to each other state, which forms a tally matrix (denoted as N) with the same form of the transition probability matrix P shown in Equation 4-2. It is easy to generate such a tally matrix by comparison of multi-temporal land use/cover raster thematic maps derived from satellite remote sensing images due to the regular grid data structure. Each element n_{ij} in the tally matrix represents the number of cells that have changed from class i to

class j . The marginal distribution of the row i calculated based on the grand total number of cells summarizes the percentage of area for land use/cover class i at time t . The marginal distribution of the column j calculated based on the grand total number of cells summarizes the percentage of area for land use/cover class j at time $t+1$. Dividing the count of transition n_{ij} by the row total would yield estimated transition probability value p_{ij} :

$$p_{ij} = \frac{n_{ij}}{\sum_{j=1}^m n_{ij}} \quad (4-4)$$

The diagonal elements of the transition matrix represent the self-replacement probabilities whereas the off-diagonal values indicate the probability of change occurring from one land use/cover class to another class.

The transition matrix P has two important uses. First, it can be used to predict the proportions of different land use/cover classes in the future. Post-multiplication of the proportion vector at time t by the matrix of transition probabilities yields the state vector at time $t+1$:

$$V_{t+1} = V_t \times P \quad (4-5)$$

where $V = [v_1, v_2, \dots, v_m]$, and

v_i = proportion of land use/cover class i .

The second use of P is to investigate when the process of change will stop, or when the Markov chain process will converge to a stable equilibrium endpoint. As the Markov chain advances in time, the transition matrix is successively powered:

$$P^{(n)} = P^{(n-1)} P \quad (4-6)$$

where $P^{(n)}$ = the n^{th} step transition matrix. Ultimately the P -matrix will have identical rows, which means that the probabilities of passing to a state are independent of the starting state. If

this occurs, the Markov chain process is said to culminate in the equilibrium distribution of the different land use/cover classes.

4.3 Testing for the Markov property

Calibration of the Markov chain model over the time period from 1987 to 1997 led to the land use/cover transition probability matrix shown in Table 4.1.

Table 4.1 Land use/cover transition probability matrix, 1987-1997

From \ To	1	2	3	4	5
1	0.8660	0.0203	0.0812	0.0211	0.0114
2	0.2586	0.2611	0.3294	0.1461	0.0049
3	0.2505	0.0597	0.4633	0.2243	0.0021
4	0.1569	0.0152	0.0760	0.7451	0.0067
5	0.0350	0.0023	0.0077	0.0337	0.9213
1- Urban 2- Bare land 3- Cropland/grassland 4- Forest 5- Water					

A statistical test for the Markov property distinguishes between two alternative hypotheses that either the successive land use/cover states are independent of each other (the null hypothesis) or the land use/cover states are dependent on the immediately preceding states. The test uses the tally matrix of land use/cover transitions observed from remote sensing and the transition probability matrix calculated from the tally matrix. The test statistic is

$$-2 \ln \lambda = 2 \sum_{i=1}^m \sum_{j=1}^m n_{ij} \ln \frac{p_{ij}}{p_j} \quad (4-7)$$

where p_{ij} = probability in cell i,j of the transition probability matrix

$$p_j = \text{marginal probabilities for the } j^{\text{th}} \text{ column of the tally matrix } \left(p_j = \frac{\sum_{i=1}^m n_{ij}}{\sum_{i=1}^m \sum_{j=1}^m n_{ij}} \right),$$

n_{ij} = transition frequency total in cell i,j of the original tally matrix of observed land use/cover transitions from 1987 to 1997, and

m = total number of land use/cover classes.

Anderson and Goodman (1957) showed that $-2 \ln \lambda$ is distributed asymptotically as χ^2 with $(m-1)^2$ degrees of freedom. The calculation of this statistic using the data from Table 4.1 and the corresponding tally matrix results in the value for $-2 \ln \lambda$ being equal to 14022986. The number of degrees of freedom is 16. At the level of significance $\alpha = 0.05$, the χ^2 value from the χ^2 distribution table is 26.30. The calculated value of $-2 \ln \lambda = 14022986$ is much greater. Therefore the null hypothesis that these land use/cover transitions are from an independent events process is rejected and the alternative hypothesis that the land use/cover transitions have the Markov property is accepted.

4.4 Prediction of land use/cover proportions

Short-term predictions for years after 1997, starting from 2000, at an interval of 5 years, ending at 2020, were made using the transition probability matrix P in Table 4.1 and the 1997 land use/cover proportion vector. First the transition rate matrix q_{ij} was derived by algebraic transformation of the p_{ij} matrix. The following equations relate transition probabilities to transition rates (Harbaugh and Bonham-Carter 1970):

$$p_{ii} = e^{-M_i \Delta t} \quad (4-8)$$

$$M_i = \frac{-\ln p_{ii}}{\Delta t} \quad (4-9)$$

$$p_{ij} = \frac{q_{ij}}{M_i} p_i \quad (i \neq j) \quad (4-10)$$

$$q_{ij} = \frac{p_{ij}}{p_i} M_i \quad (i \neq j) \quad (4-11)$$

where M_i = sum of the off-diagonal elements in the i^{th} row of the q^{ij} matrix ($\sum_{j=1, j \neq i}^k q_{ij}$), where k is the number of states,

p_i = sum of the off-diagonal elements in the i^{th} row of the p^{ij} matrix ($\sum_{j=1, j \neq i}^k p_{ij}$), or $[1 - p_{ii}]$, where p_{ii} is the diagonal element, and

Δt = unit time interval pertaining to the rate of transition.

The probability values associated with multiple-step transitions can be calculated readily by powering the transition rate matrix. The Markov chain transition probability matrix P (Table 4.1) was obtained by comparison of the land use/cover maps in the years 1987(t_1) and 1997(t_2). Annual transition rate matrix q_{ij} ($\Delta t = 1$ year) can be calculated using equations 4-8 through 4-11. After n steps (years) of transition from t_2 , the transition probability matrix $p_{ij}^{(n)}$ describing the probability of passing from state i at t_2 to state j at $t_2 + n \times \Delta t$ would be

$$p_{ij}^{(n)} = q_{ij}^n \quad (4-12)$$

The proportion vector at time $t_2 + n \times \Delta t$ thus can be calculated using equation:

$$V^{(n)} = V^{t_2} \times P^{(n)} \quad (4-13)$$

where $V^{(n)} = [c_1^{(n)}, c_2^{(n)}, \dots, c_m^{(n)}]$,

$$V^{t_2} = [c_1^{t_2}, c_2^{t_2}, \dots, c_m^{t_2}]$$

c_i = the proportion of class i ($i=1, 2, \dots, m$), and

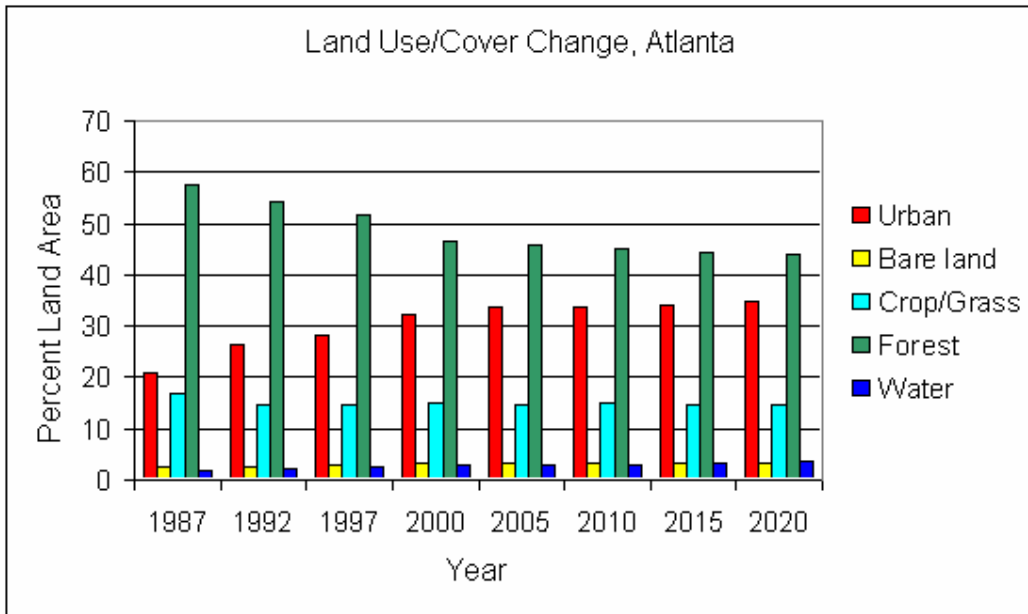
$P^{(n)}$ = transition probability matrix with elements calculated from Equation 4-12.

The historical and predicted land use/cover proportions are shown in Table 4.2 and visualized in Figure 4.2. From Table 4.2 and Figure 4.2, intuitively one can see the general trend of land use/cover change. Urban continues to grow at the cost of forest depletion. The proportion of urban area was 20.93% in 1987 and will increase to 35.45% in 2020, while forest will decrease from 57.67% in 1987 to 43.64% in 2030.

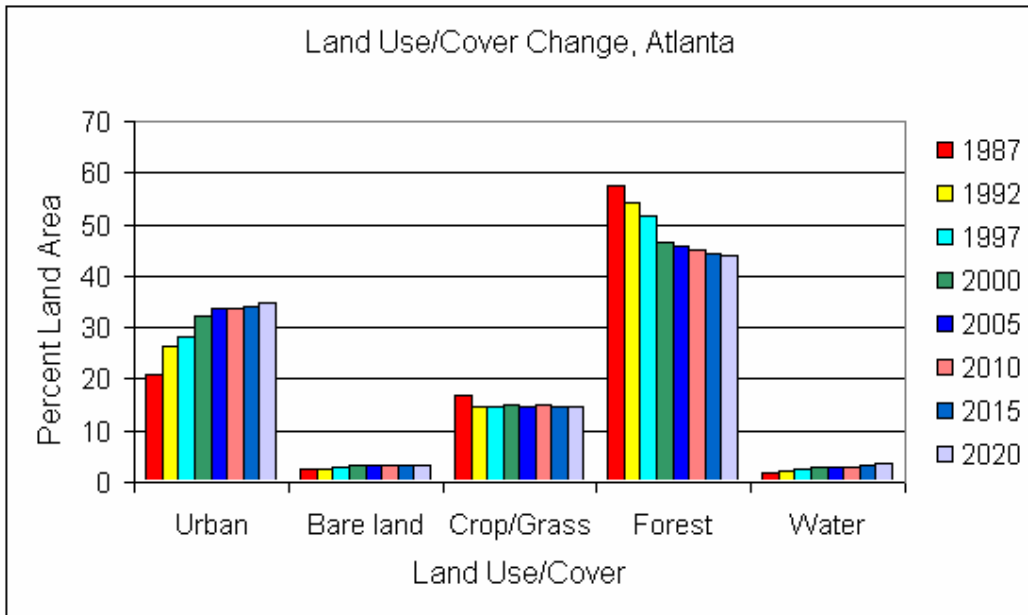
Table 4.2 Land use/cover proportions (%) from 1987 to 2020

Year	Land use/cover types				
	Urban	Bare land	Crop/Grass	Forest	Water
1987	20.93	2.49	16.91	57.67	2.01
1992	26.22	2.64	14.69	54.32	2.13
1997	28.22	2.97	14.75	51.54	2.52
2000	32.26	3.35	14.87	46.41	3.11
2005	33.54	3.19	14.77	45.64	2.87
2010	33.64	3.25	14.87	45.13	3.11
2015	34.14	3.30	14.68	44.50	3.38
2020	35.45	3.17	14.22	43.64	3.52

The trend of convergence of urban and forest can also be seen from Figure 4.2(a), which means the Markov chain will be approaching equilibrium distribution soon after 2020. This can also be judged from Table 4.3 which shows the transition probability matrix for the period from 1997 to 2020. Compare this table with Table 4.2 which shows the transition probabilities over the first five years (1987-1992). It is found that while row vectors in Table 4.2 are very different from each other, in Table 4.3 all the row vectors except those in the last row are almost identical, indicating the independence of transition probabilities on the starting land use/cover states and the Markov chain is becoming to advance to a stable endpoint at which different land use/cover classes will distribute in a balance.



(a) Series in years, grouped by land use/cover types



(b) Series in land use/cover types, grouped by years

Figure 4.2 Quantitative land use/cover change trends.

Table 4.3 Simulated transition probability matrix, 1997-2020

From \ To	1	2	3	4	5
1	0.3775	0.0321	0.1416	0.4182	0.0307
2	0.3790	0.0397	0.1888	0.3743	0.0183
3	0.3757	0.0396	0.1601	0.4085	0.0161
4	0.3424	0.0307	0.1419	0.4617	0.0233
5	0.1269	0.0093	0.0379	0.1374	0.6884
1- Urban 2- Bare land 3- Cropland/grassland 4- Forest 5- Water					

4.5 Prediction of future urban spatial patterns

An effective land use/cover change model should not only be able to answer the question of how much change has occurred and will occur, but also be able to supply the information on where the change has taken place and will take place. Based on the transition probability matrix ($P^{(n)}$) obtained after n steps of Markov chain process and the land use/cover image map at time t_2 (1997), the conditional probability image for the time n years after t_2 for class j can be obtained such that if a pixel is in state i at time t_2 , then the conditional probability value of the pixel for the time is $p_{ij}^{(n)}$. The conditional probability images report the probability that each land cover type would be found at each pixel after the specified number of time units. These images are calculated as projections from the later of the two input land cover images used to calibrate the Markov chain.

To generate the spatial patterns of land use/cover class j at time $t_2 + n \times \Delta t$, first the number of cells of class j is calculated according to the proportion values in the state vector $V^{(n)}$. The conditional probability image for class j is ranked with each cell having a unique rank value. Last the ranked image is re-classed to allocate the predicted number of cells for class j to the

cells with higher ranks of conditional probabilities. Water bodies and conservation areas are excluded from the allocation procedure. All these were carried out using ERDAS Imagine 8.6. The simulated urban spatial distribution patterns for each year are shown in Figure 4.3. This figure indicates that the successive urban growth will occur in rural and urban-fringe area, manifesting itself in scattered and disperse patterns. The spatial patterns are characterized by leapfrog development separated from continuous urban development by vacant, low-density, and rural land. The result coincides Turner (1987)'s finding that the random simulations based only on transition probabilities simulated a highly fragmented landscape.

4.6 Discussions and conclusions

This chapter has demonstrated that the Markov chains have provided a mathematically simple and compact approach by which a dynamic land use/cover system could be modeled. The model is easy to implement with empirical historical data obtained from remote sensing. The model lends itself well to characterization of past land use/cover change, prediction of future land proportions, and simulation of spatial patterns.

The Markov chain analysis has shown that, in the study area, land use/cover states at a time point depend on the immediately preceding states, thus the land use/cover change process is a Markov process. For the study area, the primary concern is the rapid suburbanization which has consumed a large extent of green space. The Markov chain analysis has found that in the short-term future, the predominant land use/cover change will lead to the depletion of forest for urban development. Urban growth will demonstrate dispersed spatial patterns. Soon after 2020, the dynamic land use/cover system will be in a state of balanced distribution of different land use/cover categories. The Markov chain model has simulated a highly dispersed urban landscape.

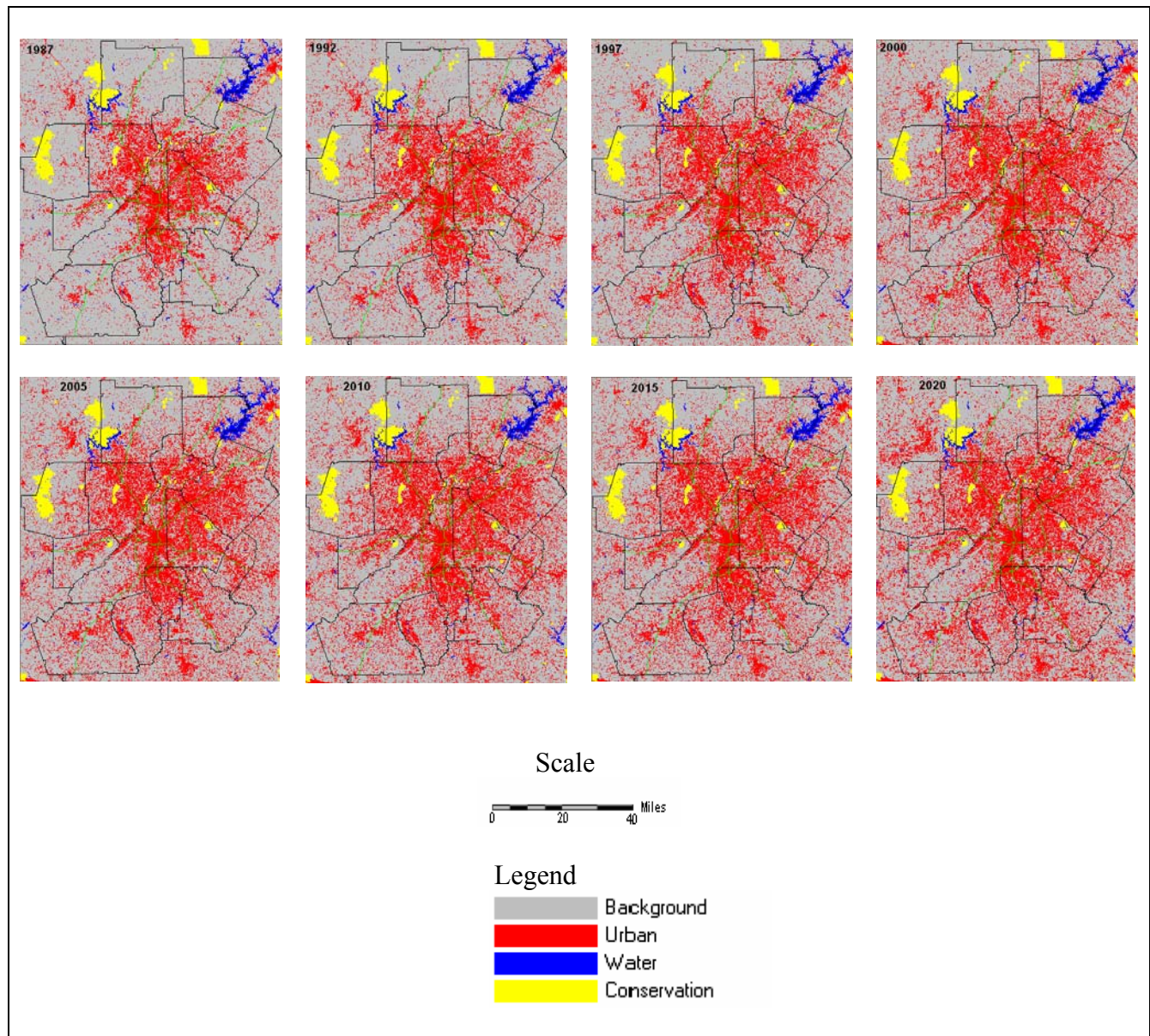


Figure 4.3 Historical and Markov chain model predicted urban patterns, 1987-2020.

Markov chain models are not without weaknesses. The major limitations of the models are: (1) A Markov chain may not necessarily be a first-order process. A higher order Markov chain model is hard to implement, and as a result few land use/cover change models have dealt with higher order Markov chains. (2) It may not be appropriate for Markov chain models to use a single order of dependence and a single homogeneous transition probability matrix to characterize the heterogeneous landscape, since transitions of individual cells in a particular state may vary with the location of the cell. (3) Spatial context and neighborhood effects are not accommodated in the model. The land use/cover state of a land lot could be affected by the surrounding lots. Land use/cover changes are not strictly Markovian; the change of a cell state is not simply a function of its current state, but is influenced by surrounding cells (Turner 1987 and 1988). Wood *et al.* (1997) developed a spatial Markov model by tallying frequency of class-to-class transitions between the grid cells for each pair of adjacent cells using the rook sampling pattern (4 neighbors). The combination of cellular automata (CA) model and Markov chain may take advantage of the ability of CA models to incorporate neighborhood effects and this has been realized in commercial software packages, such as the CA-Markov module in Idrisi Kilimanjaro. (4) A Markov chain model is purely a mathematical game, without consideration of exogenous or endogenous variables representing social, economic, and biophysical drivers of land use/cover change. The use of empirical transition probabilities masks the causality of land use/cover change. (5) The results of Markov chain models using remote sensing data are very sensitive to land use/cover classifications accuracy. The transition probability matrix is computed from the tally matrix obtained by comparison of multi-date land use/cover maps. The errors are compounded through the logical “AND” operation in the process of post-classification comparison. In an urbanization area, this problem becomes worse. It is common to see large

amount of urban areas transforming to other land use/cover categories in the frequency tally matrix, leading to high probabilities of such transitions, although urban development is often an irreversible process. For Markov chain modeling of land use/cover changes, a high degree of accuracy of land use/cover classification is necessary in order to avoid transition probability errors.

CHAPTER FIVE

LOGISTIC REGRESSION MODELING OF URBANIZATION PROBABILITY

5.0 Introduction

A logistic regression model was used to establish the relationship between the probability of urban development and its driving forces. The model was first built using 18 predictors and multi-resolution modeling was conducted. Fractal analysis assisted the choice of the optimal resolution of analysis. Later refined modeling was performed only on the best resolution. Spatial autocorrelation analysis was tested and corrected by including two extra spatial coordinates in the refined model. After model fitting, significance was tested against the coefficients and a reduced model was obtained with only the significant variables. Then goodness-of-fit of the model was assessed. The model was used to explain the urbanization dynamics. An urbanization probability prediction map was generated using the model and the spatial patterns were analyzed. The probability map was validated using the relative operating characteristic (ROC) index to determine if the model approximates the reality. The extent of urban growth predicted from the Markov Chain model in Chapter 4 was entered into the probability image to generate the spatial patterns of urban distribution of the future years.

5.1 Spatial data handling and integration

This chapter uses socioeconomic, biophysical, and remotely sensed data to conduct logistic regression modeling. These data are heterogeneous in terms of data sources, scales, projections,

data quality, and data formats. The original data used for this study are listed and described in Table 5.1. The Atlanta transportation network in 1990 and the map of the 1990 census block groups are shown in Figures 5.1 and 5.2 respectively. The map of major economy centers is shown in Figures 1.6, and the 1987 and 1997 land use/cover maps are shown in Figure 3.23.

Proper handling and integration of heterogeneous spatial data are necessary for implementing a GIS-based spatial analysis and modeling. The first step is to georeference the original data layers to a common coordinate system. In this study, the common georeferencing framework is the UTM coordinate system (Zone 16 North), NAD 1983 horizontal datum, and GRS 1980 ellipsoid. The land use/cover maps have already been georeferenced to this coordinate system. Geographic to UTM projection transformation was undertaken for the census map, the transportation map, and the conservation map (see Figure 5.6). The scanned image of major economic centers was imported to a raster GIS and registered to the transportation map in the UTM system using an image-to-map rectification procedure with the intersections of interstate highways used as ground control points. Points for the major economic centers were digitized on screen.

After georeferencing, raster data layers needed in the logistic regression model were derived. Initially all the raster layers were created at a spatial resolution of 25 meters. Raster data aggregation for multi-resolution modeling will be described in Section 5.3. A binary raster layer showing urban growth from 1987 to 1997 was generated by comparison of the two land use/cover maps. Distances to the nearest Department of Transportation (DOT) type one (interstate highway and state highway) roads were calculated. Raster maps of distances to the CBD, and to the major economic centers were generated. To create a map of distances to the nearest urban cluster, urban cells on the 1987 land use/cover map were clumped. Clusters

Table 5.1 Original data for logistic regression modeling

Data content	Source	Data format	Geo-reference system
Land use/cover maps 1987, 1997 derived from Landsat TM images in Chapter 3	Landsat TM images are for the project ATLANTA (Atlanta Land-use Analysis: Temperature and Air-quality) by C.P. Lo. Originator: 1987: USGS EROS Data Center; 1997: Space Imaging EOSAT	ERDAS Imagine(.img)	UTM coordinate system (Zone 16 North), NAD 1983 horizontal datum, and GRS 1980 ellipsoid; resampled to 25m resolution
Census data at the level of block groups, 1990	GeoLytics	ESRI shapefile	Geographic/Decimal degrees (Latitude/Longitude)
Map of conservation area	Georgia GIS Clearinghouse (http://www.gis.state.ga.us/), Originator: Georgia Department of Natural Resources	ESRI shapefile	Geographic/Decimal degrees (Latitude/Longitude)
Atlanta transportation map, 1990	Georgia GIS Clearinghouse (http://www.gis.state.ga.us/), Originator: Georgia Department of Transportation	ESRI shapefile	Geographic/Decimal degrees (Latitude/Longitude)
Map of major economic centers, 1995	Atlanta Region Outlook, Atlanta Regional Commission, 1995	JPEG, scanned from paper document	None
Digital Elevation Model	Georgia GIS Clearinghouse (http://www.gis.state.ga.us/); Originator: USGS	USGS DEM	Lambert Conic Conformal

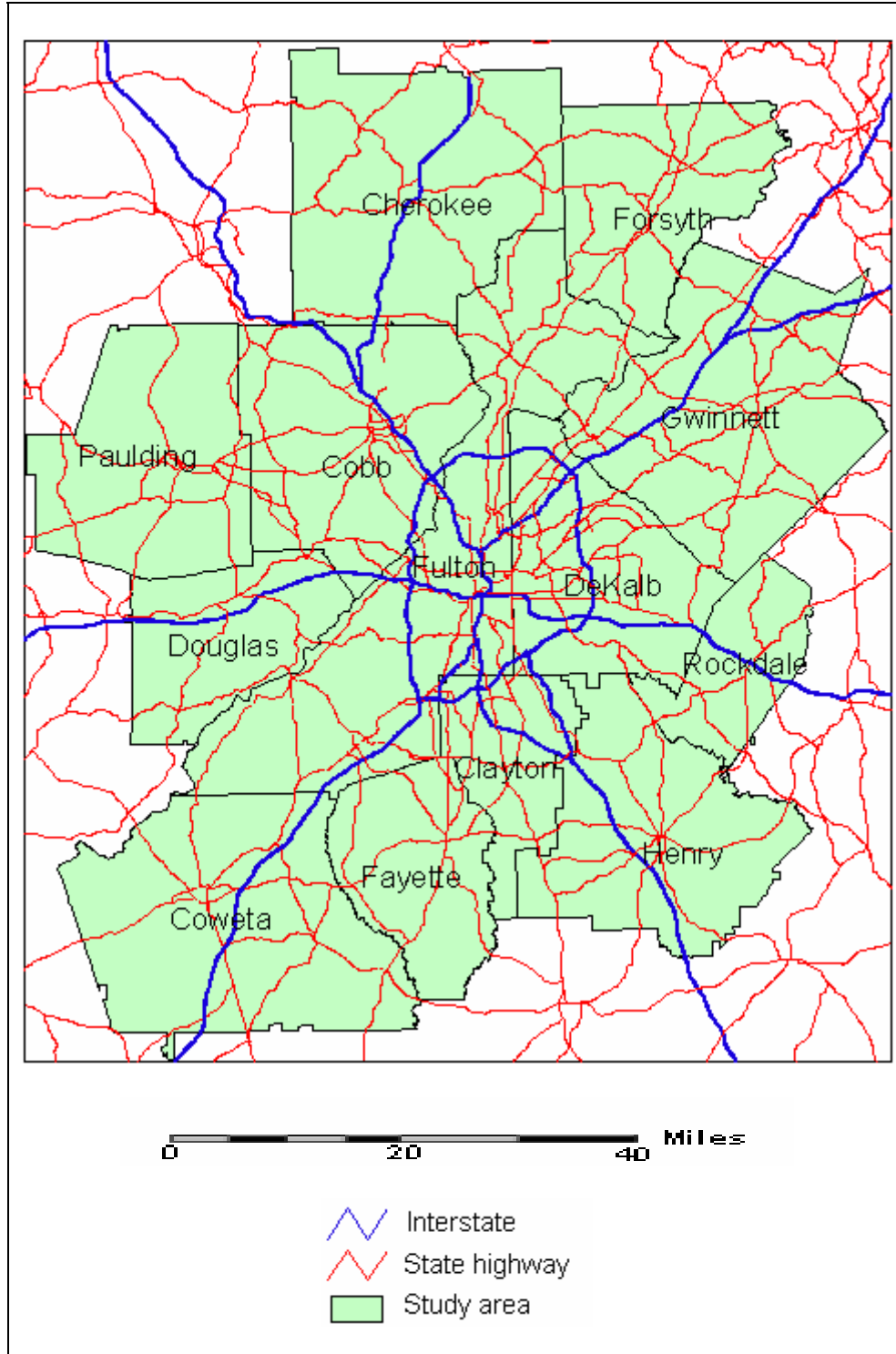


Figure 5.1 Atlanta metropolitan transportation network showing DOT road type 1 (interstate and state highways), 1990.

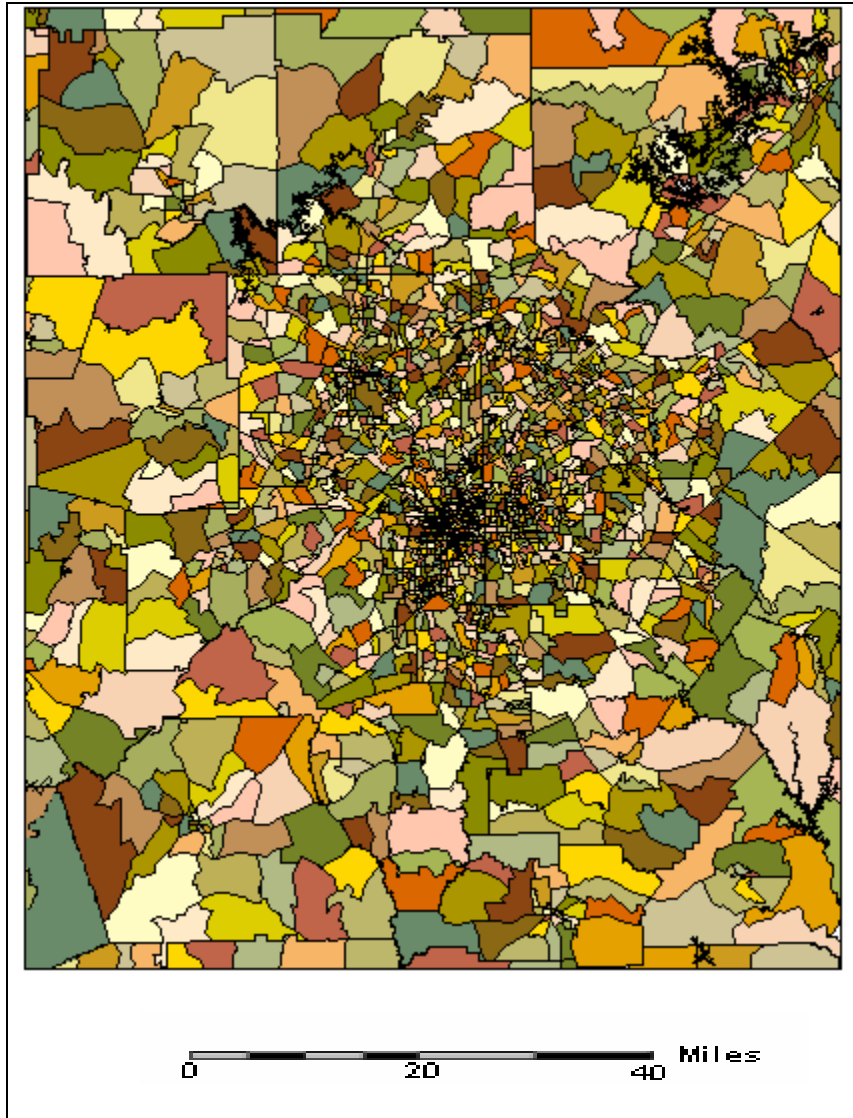


Figure 5.2 Census block groups, 1990, Atlanta metropolitan area.

smaller than 25 cells were filtered out and clusters larger than or equal to 25 cells were used to calculate the distances. An interaction term, the number of urban cells with a 7 by 7 cell neighborhood, was included in the logistic model. To derive a raster layer for this interaction variable, first, a binary image showing the 1987 urban distribution, with 1 indicating urban and 0 non-urban, was generated. Then a focal neighborhood analysis function in Erdas Imagine, DENSITY, was applied to the binary image to return the number of occurrences of the center pixel value in the focal window around each pixel of the binary image. After this, a logical operation was conducted such that if the cell is not urban, then the number of urban cells is set to 49 minus the density value (49 is the total number of the cells within the 7 by 7 cell neighborhood); otherwise the number of urban cells is set to the density value. The DEM raster layer was resampled to 25m and the slope (in percent) was calculated from the DEM.

The process of integrating the census data with the remotely sensed data is essentially a process of linking people with pixels. This linkage is bidirectional. On the one hand, the pixel values in the remotely sensed images, which are simply records of the spectral reflectance of the earth surface, are implanted social meanings by clustering the pixels and labeling the clusters with land use/cover class names. On the other hand, the census data, collected at the units defined by humans, are tessellated to form a raster grid so that raster-based spatial analysis and modeling can be conducted on a common data structure. Six socioeconomic information items were extracted from the 1990 census: population count, per capita income, poverty rate, median housing rent, percent of white people, and employment rate. Selection of these variables was guided by the historical review of urban growth in Atlanta (Section 1.1) and based on the hypothesis that changes in socioeconomic conditions affect urban growth. To rasterize the social

phenomena, a separate raster layer was created for each of the items using a GIS vector-to-raster conversion operation.

Data completeness is important to GIS applications. Spatial completeness means that the data cover the entire area of interest (Lo and Yeung 2002). It was found that the census data are not spatially complete. There exist sliver polygons in the original census vector file (Figure 5.3). When the census vector file is converted to a raster layer, these sliver polygons can result in cells with “No-Data” values if the width or height of the polygons exceed the cell size. “No-Data” values can bring a lot of trouble to the spatial modeling. Idrisi Kilimanjaro does not accept “No-Data” values when it performs the logistic regression model. Manual on-screen fixing of the holes is impractical since those polygons are too small to inspect and there are large numbers of them between the 1910 polygons of census block groups. Fortunately, image processing techniques can handle this problem. The objective is to replace the “No-Data” values with their neighboring values. First the raster layers generated from the vector census file were recoded such that the “No-Data” values were replaced with any one number between zero and the maximum value of the information item. Then the raster layers were smoothed using a 9 by 9 averaging filter to create a separate layer. The size of the filter was determined by trial and error to make sure the largest sliver polygon can be filtered out. Last, a logical operation was conducted such that if the original cell value was “No-Data”, the output cell value was set to the value in the smoothed raster layer, otherwise, the original value was kept.

The population density raster layer was derived using the pycnophylactic interpolation method. Pycnophylactic (or mass-preserving, or volume-preserving) interpolation was developed by Tobler (1979) to derive a continuous population density surface map from population count

collected on enumeration units. The assumption is that there exists a density function, $Z(x,y)$, which is nonnegative and has a finite value for every location x,y in the domain of concern.

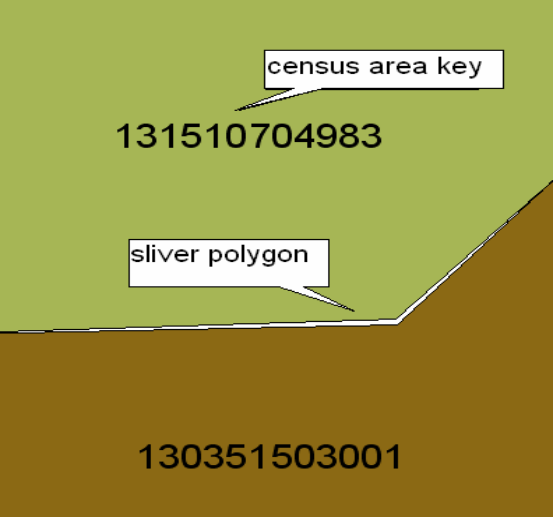


Figure 5.3 Sliver polygons in the census shape file.

The objective of pycnophylactic interpolation is to find the density function, $Z(x,y)$, such that it must have the pycnophylactic (mass-preserving) property defined by

$$\iint_{R_i} Z(x, y) dx dy = H_i \quad (5-1)$$

where R_i is the i^{th} region or enumeration unit, H_i is the population count in the i^{th} enumeration unit.

Lam (1983) developed a numerical algorithm to generate a population surface meeting the volume preserving requirement in Equation (5-1). This algorithm is illustrated in Figure 5.4. It has five steps. (1) A set of square cells (in this study, the cell size is equal to the modeling resolution) is overlaid on top of the enumeration units (Figure 5.4B), and point-in-polygon test is

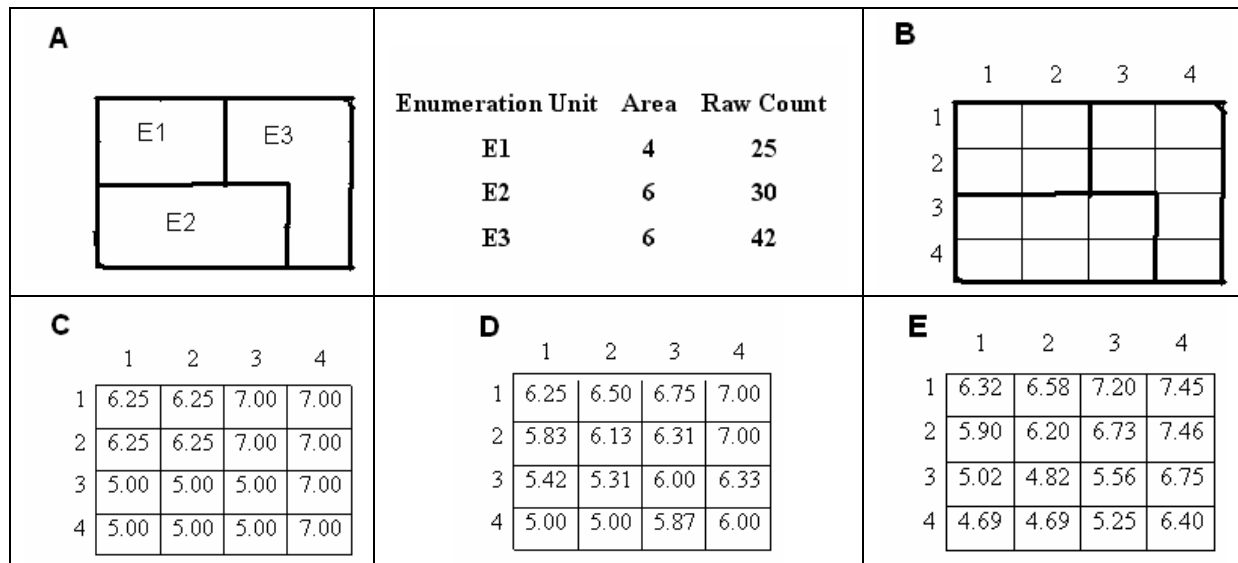


Figure 5.4 Basic steps of pycnophylactic interpolation: (A) three hypothetical enumeration units; (B) square grid overlaid on the enumeration units; (C) initial density values for each cell (computed by dividing the raw count for each enumeration unit by the number of cells in that unit); (D) smoothed cell values (computed by averaging the four non-diagonal neighbors); (E) smoothed values adjusted so that the sum within an enumeration unit is equal to the original total sum for that enumeration unit (the mass is preserved). (Lam 1983, pp 148-149).

used to determine which cells fall in each enumeration unit. (2) A raw count for each cell is determined by dividing the raw count for each enumeration unit by the number of cells in that unit (Figure 5.4C). (3) Each cell is computed as the average of its non-diagonal neighbors (Figure 5.4D). (4) The cell counts within each enumeration unit at the end of step 3 are added to obtain a total smoothed count value. (5) All cells values within each enumeration unit are multiplied by the ratio of the total raw count to the total smoothed count, leading to the result shown in Figure 5.4E. Steps 3 to 5 of the algorithm are executed in an iterative fashion. The iteration continues until there is no significant difference between the raw and smooth counts for

each enumeration unit or there is no significant change in the cell values compared with the last iteration.

For this study, an ArcView Avenue program obtained from the Environmental System Research Institute (ESRI) website (URL: <http://www.esri.com>) was used to implement Lam's pycnophylactic interpolation algorithm. The maximum number of iterations was set to 50, and the convergence limit is set to 1%. At the resolution of 25 m, it took 40 minutes for the interpolation process to generate the population density surface of the Atlanta metropolitan region in 1990 as shown in Figure 5.5.

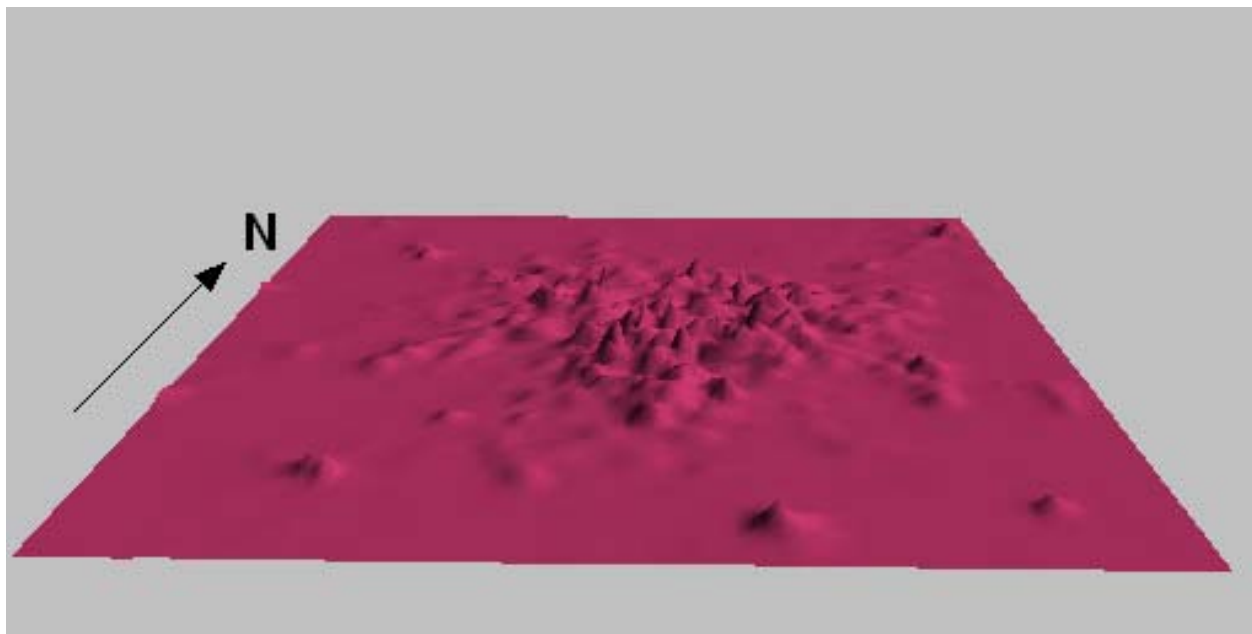


Figure 5.5 Surface of population density ($person/km^2$), Atlanta, Georgia based on the 1990 census data at the level of census block groups obtained using pycnophylactic interpolation method.

5.2 Statement of model

A logistic regression model was used to associate the urban growth with demographic, econometric and biophysical driving forces and to generate an urban growth probability (or suitability) map. In a raster GIS modeling environment, the data layers are tessellated to form a grid of cells. The nature of the land use/cover change of a cell is dichotomous: either the presence of urban growth or absence of urban growth. If binary values 1 and 0 are used to represent urban growth and no urban growth respectively and if it is assumed that the probability of a cell changing to urban use follows the logistic curve as described by the logistic function (Kleinbaum 1994):

$$f(z) = \frac{1}{1 + e^{-z}} \quad (5-2)$$

then the probability of a cell being urbanized can be estimated with the following logistic regression model:

$$P(Y = 1 | X_1, X_2, \dots, X_k) = \frac{1}{1 + e^{-\left(\alpha + \sum_{i=1}^k \beta_i X_i\right)}} \quad (5-3)$$

where: $P(Y = 1 | X_1, X_2, \dots, X_k)$ is the probability of the dependent variable Y being 1 given (X_1, X_2, \dots, X_k) , i.e. the probability of a cell being urbanized, where

X_i is an independent variable (or covariate) representing a driving force of urbanization, which can be of interval, ordinal or categorical nature; and

β_i is the coefficient for variable X_i .

For notational convenience, the probability statement $P(Y = 1 | X_1, X_2, \dots, X_k)$ is denoted as simply $P(\mathbf{X})$, where \mathbf{X} is a shortcut notation for the collection of variables X_1 through X_k .

The complete list of variables is shown in Table 5.2. These variables have been selected to reflect the socioeconomic characteristics of the population and the spatial influences of major highways and economic activity centers, all of which could have influenced the land use/cover changes. The images for those variables are shown in Figure 5.6. Assuming that the initial land use/cover status has effect on the probability of a cell being urbanized, then polynomial land use/cover categories should be included in the logistic model. Design variables were generated and used to distinguish the different categories of land use/cover. There are six categories of land use/cover: high-density urban, low-density urban, bare land, crop or grassland, forest, and water. Five design variables denoted as X_{14} through X_{18} representing the first five land use/cover classes respectively are generated to distinguish among the six categories by recoding the 1987 land use/cover map into a binary map for each land use/cover category. Table 5-3 gives the coding of the design variables for land use/cover. If all the five dummy variables take the value of zero, then a cell value in the “water” layer must be one; if any one of the five land use/cover classes takes the value of 1, a cell value in “water” layer must be zero. Including a “water” variable in the model would be redundant and violate the assumption of no linear relationship between independent variables. The initial model uses only the first 18 variables. The last two variables will be incorporated into the model in the model refining stage to correct for spatial autocorrelation that may exist.

Since $P(X)$ takes the form of a logistic function, its values fall within the range of $[0,1]$. The logistic regression model above is a nonlinear model. To linearize the above model, and to remove the 0/1 boundaries for the original dependent variable Y , logit transformation, denoted as $\text{logit}P(X)$, is given by the natural log (i.e., to the base e) of the quantity $P(X)$ divided by one minus $P(X)$, where $P(X)$ denotes the logistic model as equation (5-3) defines (Kleinbaum 1994):

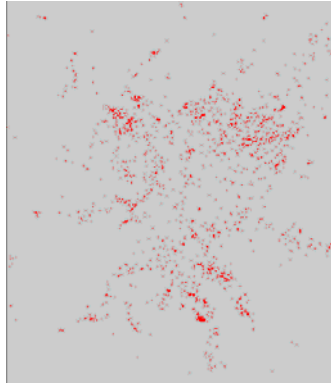
Table 5.2 List of variables in the logistic regression model

Variable		Meaning	Nature of variable
Dependent	Y	0- no urban growth; 1- urban growth	Dichotomous categorical
Independent	X ₁	Population density (person/km ²)	Continuous
	X ₂	Per capital income (\$)	Continuous
	X ₃	Poverty rate	Continuous
	X ₄	Median housing rent (\$)	Continuous
	X ₅	Percentage of white people	Continuous
	X ₆	Employment rate	Continuous
	X ₇	Slope (%)	Continuous
	X ₈	Distance to the nearest urban cluster (m)	Continuous
	X ₉	Distance to CBD(m)	Continuous
	X ₁₀	Distance to active economy centers (m)	Continuous
	X ₁₁	Distance to the nearest major road (m)	Continuous
	X ₁₂	Number of urban cells within a 7×7 cell window	Continuous
	X ₁₃	1-Conservation area; 0-Not conservation area	Design
	X ₁₄	1-high-density urban;0-not high-density urban	Design
	X ₁₅	1-low-density urban;0-not low-density urban	Design
	X ₁₆	1-bare land;0-not bare land	Design
	X ₁₇	1-cropland/grassland;0-not cropland/grassland	Design
	X ₁₈	1-forest;0-not forest	Design
E*	easing coordinate (m)	Continuous	
N*	northing coordinate (m)	Continuous	

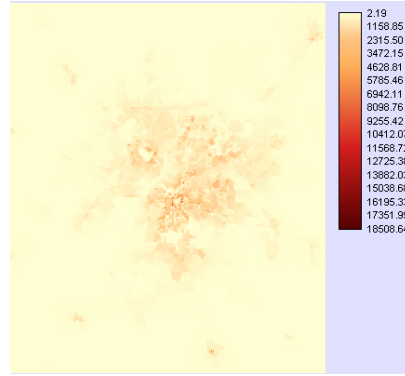
* E and N are used to correct for spatial autocorrelation. See section 5.5 and 5.6.

Table 5.3 The coding of the design variables for land use/cover, coded at Six Levels

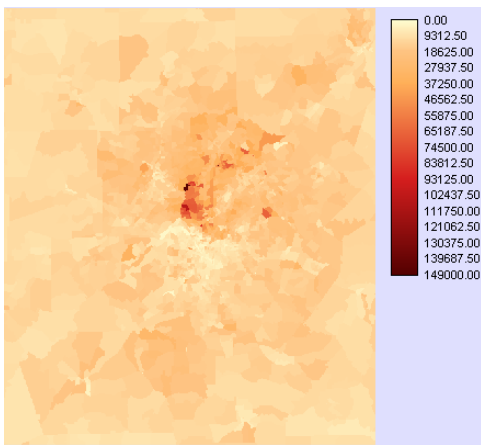
Land use/cover	Design variable				
	X ₁₄	X ₁₅	X ₁₆	X ₁₇	X ₁₈
High-density urban	1	0	0	0	0
Low-density urban	0	1	0	0	0
Bare land	0	0	1	0	0
Cropland/grassland	0	0	0	1	0
Forest	0	0	0	0	1
Water	0	0	0	0	0



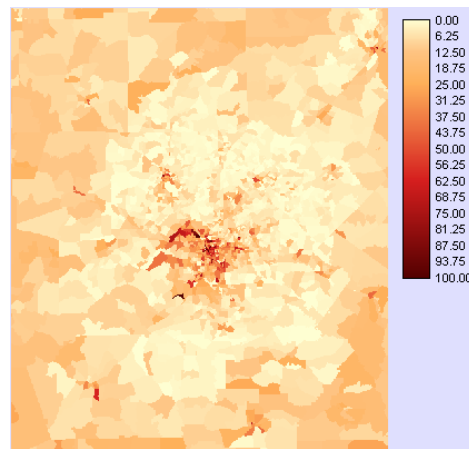
Y – Urban growth 1987-1997



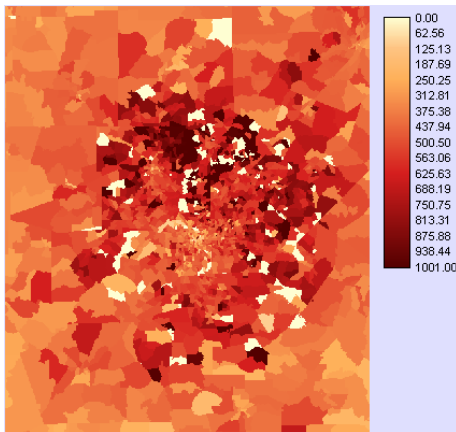
X₁-Population density 1990 (person/km²)



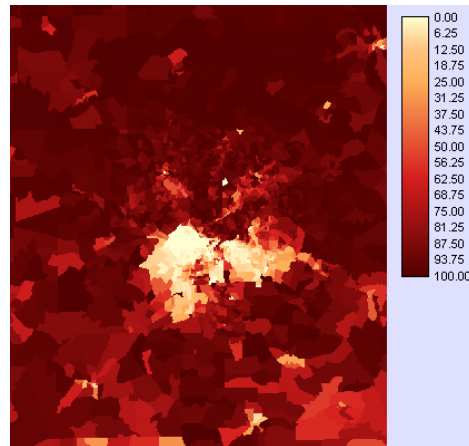
X₂ – Per capita income 1990 (\$)



X₃ - Poverty rate 1990 (%)



X₄ – Median housing rent 1990 (\$)

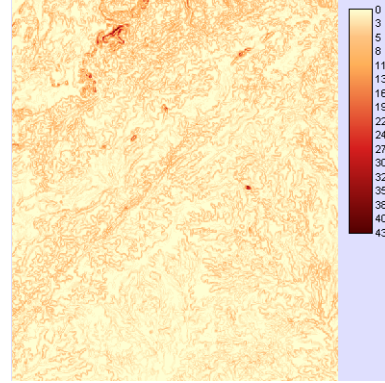


X₅ – Percentage of white people 1990 (%)

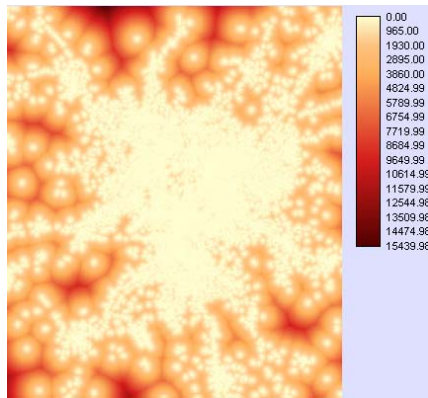
Figure 5.6 Variables in the logistic regression model, represented by raster layers.



X₆ – Employment rate 1990 (%)



X₇ – Slope (%)



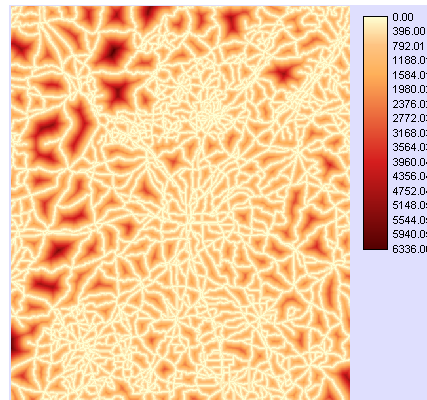
X₈ – Distance to the nearest urban cluster (m)



X₉ – Distance to CBD (m)

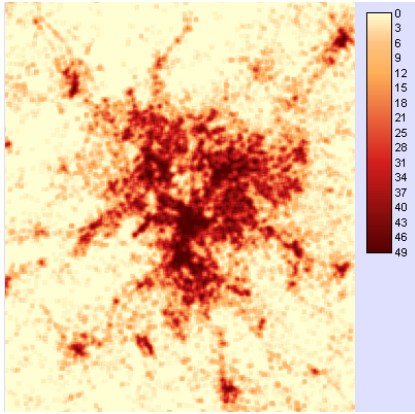


X₁₀ – Distance to active economy center (m)



X₁₁ – Distance to nearest major road (m)

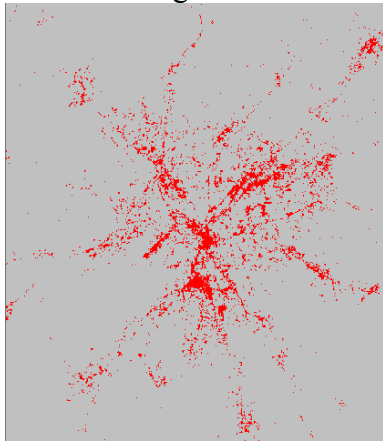
Figure 5.6 (continued) Variables in the logistic regression model, represented by raster layers.



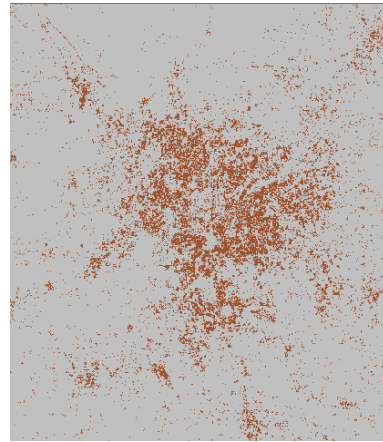
X₁₂ – Number of urban cells within a 7 by 7 cell neighborhood



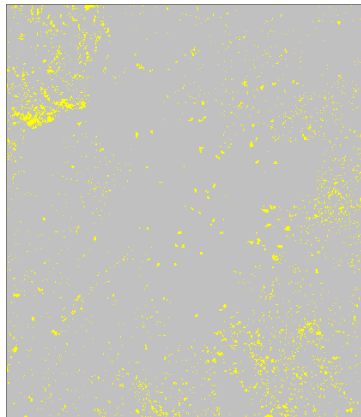
X₁₃ – Conservation area



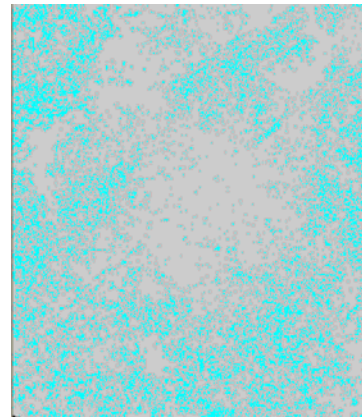
X₁₄ – High-density urban 1987



X₁₅ – Low-density urban 1987

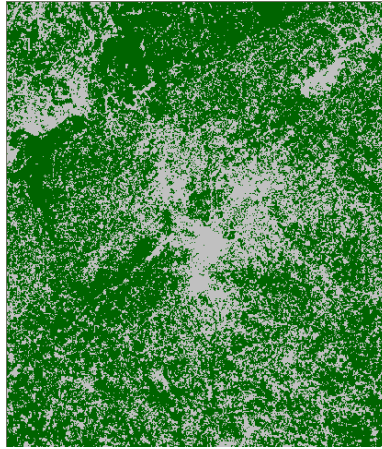


X₁₆ – Bare land 1987



X₁₇ – Cropland or grassland 1987

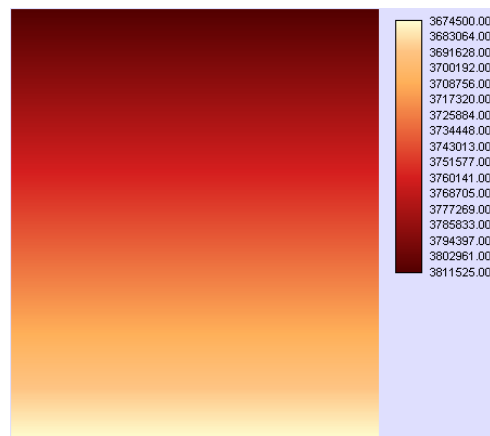
Figure 5.6 (continued) Variables in the logistic regression model, represented by raster layers.



X₁₈ - Forest 1987



X₁₉ (E) – UTM easting coordinate (m)



X₂₀ (N) – UTM northing coordinate (m)

Figure 5.6 (continued) Variables in the logistic regression model, represented by raster Layers.

$$\text{logit } P(X) = \ln \frac{P(X)}{1 - P(X)} \quad (5-4)$$

After the logit transformation, the logistic regression model becomes a linear regression model with logit P(X) being the dependent variable:

$$\text{logit } P(X) = \alpha + \sum_{i=1}^k \beta_i X_i \quad (5-5)$$

where α is a constant, and β_i is the coefficient for variable X_i .

In the above model, logit P(X) can theoretically take any continuous values between minus infinity and plus infinity without boundaries while ensuring that the predicted probability will be continuous within the range from zero to one.

By looking closely at the expression for the logit function in equation (5-4), it is found that the quantity P(X) divided by 1-P(X), whose value gives the logit, describes the odds of urban development for a cell with independent variables specified by X. In its simplest form, an odds, denoted as ψ , is the probability that urban development will occur over the probability that urban development will not occur. Thus the logit form of the logistic regression model shown in equation (5-5) gives an expression for the log odds of urban development for an individual cell with a specific set of X's. Suppose coefficients estimates of $\hat{\alpha}$ and $\hat{\beta}_i$ are obtained from model fitting, then given a set of X's, the estimated odds of urban development is:

$$\hat{\psi} = e^{\hat{\alpha} + \sum_{i=1}^k \hat{\beta}_i X_i} \quad (5-6)$$

So the logistic regression model can also be represented as:

$$\ln \psi = \alpha + \sum_{i=1}^k \beta_i X_i \quad (5-7)$$

The parameter α can be interpreted as the logarithm of the background odds. By background odds, we mean the odds that would result for the logistic model without any X's at all. The parameter β_i represents the change in the log odds that would result from one unit change in the variable X_i when other variables are fixed. For a continuous variable, controlling for other variables, increase 1 unit of the variable value, and the change in log odds will be:

$$\ln \psi_{X_i+1} - \ln \psi_{X_i} = \beta_i \quad (5-8)$$

or

$$\ln \frac{\psi_{X_i+1}}{\psi_{X_i}} = \beta_i \quad (5-9)$$

So β_i can be interpreted as log odds ratio for an increase of "1" unit in X_i . In this study, "1" unit change of a continuous variable may not be meaningful. For example, the effects of an increase of 1 meter in distance to highway (X_{11}) or an increase of 1 person per square meter (X_1) on the ratio of odds of urban development may be too small to be considered important. It may be more appropriate to specify a change of "c" units, such as an increase of 1000 meters or 1000 persons. Then the relationship between odds ratio and β_i becomes:

$$\ln \frac{\psi'}{\psi} = c\beta_i \quad (5-10)$$

For dichotomous variables ($X_{13}, X_{14}, \dots, X_{18}$), there are only two values: either 0 or 1. The relationship between the odds ratio and the coefficient conforms to equation (5-9). Controlling for other variables, a change of cell value from 0 to 1, for example, non-forest to forest, the odds ratio will be:

$$\frac{\psi_1}{\psi_0} = e^{\beta_i} \quad (5-11)$$

For continuous variable, the odds ratio is given by:

$$\frac{\psi'}{\psi} = e^{c\beta_i} \quad (5-12)$$

The odds ratio will be used to interpret the association between the probability of urbanization and its driving forces in section 5-8.

The assumptions of the logistic regression model are: (1) the dependent random variable, Y, is binary, taking only two values, with 0 representing no urban growth and 1 indicating urban growth; (2) Y depends on k observable variables X_1, X_2, \dots, X_k , and the relationship is nonlinear and follows the logistic curve; (3) the data are generated from a random sample; (4) no important variables are omitted; (4) no extraneous variables are included; (5) the independent variables are not linear combinations of each other; and (6) the error term of each observation is independent of the error term of all other observations.

In this study, the logistic regression model will be fitted using spatial data. Attention must be paid to possible spatial autocorrelation within spatial data, which may violate the last assumption. This is to be discussed and dealt with in Sections 5.4 and 5.5.

5.3 Multi-scale modeling and fractal analysis

Geographical phenomena and processes are scale dependent. Thus, spatial data depicting the phenomena and models representing the process are of multiple scale nature. Research on scale effects on spatial data handling, spatial analysis and modeling have been under way in geography (Meentemeyer 1989), remote sensing (Quattrochi and Goodchild 1997), cartography (Buttenfield and McMaster 1991; Lam and Quattrochi 1992), and spatial statistics (Wong and Amrhein 1996). Lam and Quattrochi (1992) summarized four connotations of scale as: cartographic scale, geographic scale, resolution, and operational scale.

The effect of resolution on logistic regression modeling is investigated using series of logistic regression models which are calibrated from the resolution of 50 m, then progressively scaled down to 250 m at an interval of 25 m. Techniques of GIS have provided the potential to generate multi-resolution data sets for scale up modeling. The simple and uniform geometry of raster data is convenient for aggregation.

Logistic regression models with 18 independent variables (X_1 — X_{18}) are calibrated in the support of Idrisi Kilimanjaro raster GIS program using full data points within the mask of the thirteen counties. The reason why the mask is applied is that data on distribution of active economic centers used to generate distance to activity centers (X_{10}) are not available for the area outside the 13 counties, which causes unreliable values of the variable in some areas outside the mask. For example, values of distance to active economic centers for cells close to Gainesville actually represent distances to an activity center within the mask since the points for the active economic centers for Gainesville were unavailable and thus were not used in distance calculation. Model calibration was tried at the resolution of 25 m, but Idrisi Kilimanjaro run on a DELL desktop computer failed to accomplish the model calibration due to the intensive computation — noting that there are 16,699,756 data points for each layer and 19 layers in total. The raster layers at the resolution of 25m are then aggregated to generate 50 m, 75 m, and so on down to 250 m data sets to accommodate the modeling at coarser scales.

Many existing scale studies rely heavily on the re-sampling methods to generate multi-scale raster data for analysis. Methods for aggregating regular grids include the average method, sampling every N^{th} cell, and dominant values (Bian 1997). In this study, for the dependent variable urban growth (Y), the conservation area (X_{13}), and design variables for land use/cover types (X_{14} — X_{18}), the method of selecting dominant values for re-sampling was used to generate

data with coarser resolution. Multi-resolution slope (X_7) data were created from DEM data of corresponding resolution. Raster layers for the number of urban cells within a 7×7 cell neighborhood (X_{12}) were calculated from urban distribution maps which are the union of high-density urban (X_{14}) and low-density urban (X_{15}) aggregated from a resolution of 25 meters using dominant value re-sampling method. The DEMs of coarser resolutions were generated using interpolation function for continuous data in the support of raster GIS. Existing scale studies show that variations of results from multi-scale analysis are not completely due to the 'real' scale effects, but rather they are artifacts attributable to the use of different resampling methods (Weigel 1996). To minimize and account for the effects of data aggregation on modeling, an explicit aggregation operation was not applied to raster layers of demographic data (X_1 — X_6), and distance variables (X_8 — X_{11}), rather multi-scale data for those variables were directly generated at each resolution.

Effects of multi-scale modeling are shown in Table 5.4 and Figures 5.7, 5.8, and 5.9. These results were obtained from the logistic regression model calibration using Idrisi Kilimanjaro. Figure 5.7 shows the general trend of decreasing area of urban growth from high resolution to low resolution. This observation coincides with Turner's research which has shown that reducing the resolution of a raster land use/cover map (to larger cells) can increase the dominance of the contiguous classes, but decrease the amount of small and scattered classes (like wetlands in some locations) in the representation (Turner *et al.* 1989). It also coincides with the findings of Meentemeyer and Box (1987) that heterogeneous landscapes lead to more rapid information loss as data are aggregated and analyzed at coarser scales. The relatively sparse distribution of heterogeneous patches of urban growth within the study area is very sensitive to the aggregation. This effect resulting from data aggregation should be considered and

Table 5.4 Effect of multi-resolution modeling

	50m	75m	100m	125m	150m	175m	200m	225m	250m
# of data points	4174939	1856514	1043857	668436	463952	341030	260982	206316	167042
# of 0s for Y	4054460	1797408	1015910	650851	453369	333593	255841	202493	164197
# of 1s for Y	120479	59106	27947	17585	10583	7437	5141	3823	2845
0s % for Y	97.11	96.82	97.32	97.37	97.72	97.82	98.03	98.15	98.30
1s % for Y	2.89	3.18	2.68	2.63	2.28	2.18	1.97	1.85	1.70
$-2\ln L_0$	1091734.8	523801.3	257495.9	162648.0	100941.5	71611.2	50559.5	38069.8	28814.8
$-2\ln(\text{likelihood})$	961744.9	463777.5	227781.7	143757.7	89016.2	62984.0	44227.1	33247.5	25122.4
Pseudo R^2	0.1191	0.1146	0.1154	0.1161	0.1181	0.1205	0.1252	0.1267	0.1281
Goodness-of-fit	10781924.0	3127842.3	1952394.5	1216031.1	845741.4	522747.5	429185.0	341499.3	181190.6
ROC	0.7788	0.7754	0.7808	0.7818	0.7873	0.7900	0.7974	0.7995	0.8027

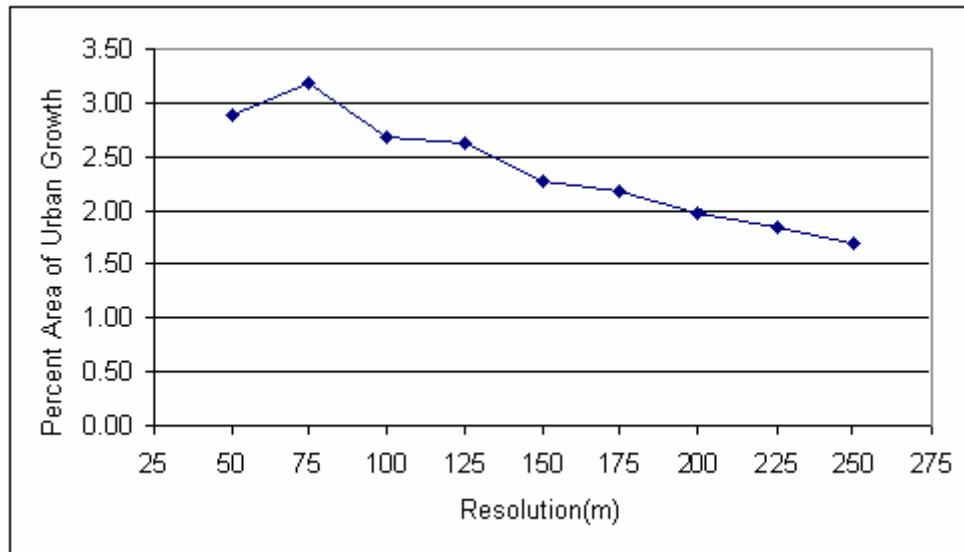


Figure 5.7 Effect of multi-resolution data aggregation on the percentage of urban growth area.

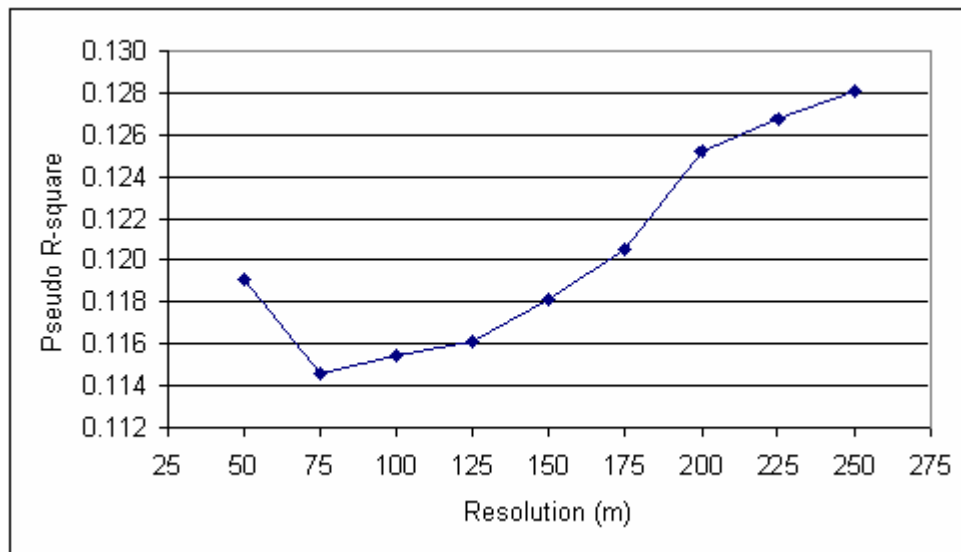


Figure 5.8 Effect of resolution on logistic regression model pseudo R square.

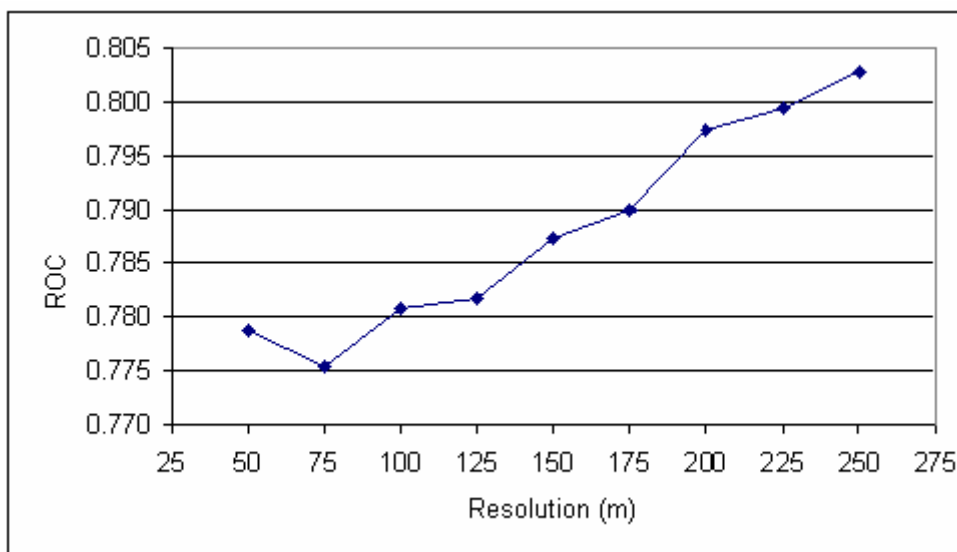


Figure 5.9 Effect of resolution on logistic regression model validation index relative operating characteristic (ROC).

differentiated from the true scale effect caused by the geographical process under the spatial patterns. Since urban growth serves as the dependent variable in the logistic regression model, the small amount of area of urban growth also tends to be under-sampled if only a portion of the data points are sampled for modeling, which will be discussed and handled in Sections 5.4 and 5.5.

From Figure 5.8, it can be seen that as the resolution of modeling becomes coarser, pseudo R square, which is an indicator of model fit, first decreases as the resolution changes from 50m to 75m, then continuously increases. A similar trend was observed for relative operating characteristic (ROC) index (Figure 5.9). The ROC index is used to validate the logistic regression model. It indicates the degree of spatial agreement between the actual urban growth map and the predicted probability map; a higher ROC value indicates higher validity of the model (for ROC, see Section 5.10.2). Another index indicating the model fit is called *goodness-*

of-fit. The smaller of a *goodness-of-fit* value, the better model fit it indicates. It shows a trend of decrease as the resolution becomes coarser (Table 5.4). The model fits better and approximates reality more closely at coarser resolutions. The probable reason is that at the finer resolutions, the model would suffer individualistic fallacy.

The process of urban growth is controlled by many demographic, socioeconomic, econometric and biophysical factors. Although the modeling is based on regular grid cells which serve as the framework for integration of heterogeneous data, not all the actual data describing the reality are observed at the unit of cells. Whereas land use/cover data are derived from Landsat TM images which collect average spectral reflectance over a pixel, and econometric distance data are obtained in the support of raster GIS, socioeconomic data are collected at census units and then disaggregated into regular raster grids. Certainly phenomena and processes represented by these explanatory variables operate at different scales. For a certain phenomenon or process, its scaling behavior may not be linear. This implies that in order to characterize the pattern or process at a scale other than the scale of observation, some knowledge of how the pattern or process changes with scale is needed so that the scaling process can be adjusted accordingly. In the multivariate model, trying to capture all the processes in a single unit (resolution) of analysis is impossible. The model behavior must be the compromised outcome of all the processes operating at various scales. Thus, there must exist an optimal scale at which the model best performs in its explanation and prediction functions. Fractals have long been thought to be an effective way to characterize multi-scale effects through mathematically relating complexity and scale (Lam and Quattrochi 1992; De Cola 1989; Goodchild and Mark 1987).

This study uses fractal analysis to determine the optimal scale of modeling. Fractal dimensions were calculated for the logistic regression model predicted probability surface maps

from the resolution of 50 m to 250 m. The triangular prism surface area method (Clarke 1986; Jaggie *et al.* 1993) was used to calculate the fractal dimensions. This method estimates lumped fractal dimension values from the predicted probability surface. The method takes the probability values at the corners of a square grid, interpolates a center value of the square by averaging, extends the cell values vertically, and divides the square into four triangles to form a triangular prism surface (Figure 5.10). The surface areas of the imaginary prisms resulting from raising the triangles to their given ‘elevations’ are calculated. This calculation is repeated for different square sizes, yielding the relationship between the total area of the surface and the spacing of the squares (resolution). The calculation will stop if the size of the square is too big to fit on the whole image. The computed surface area will decrease with increasing square size (decreasing resolution). A double log curve was then plotted to show the relationship between the log total surface area and the log of the step size. The fractal dimension is calculated by performing a regression on the pair of the variables, and fractal dimension D is equal to 2.0 minus the slope of regression. The fractal dimensions were calculated using the software package Image Characterization and Modeling System (ICAMS) (Quattrochi *et al.* 1997). Table 5.5 shows the number of steps used for calculation of fractional dimension for the predicted probability surface of each resolution. Figure 5.11 shows the R-square values obtained through regressing log surface areas on log spatial resolutions, which take values from 0.741 to 0.869, indicating a tight fit of calculation of fractal dimension for all the probability surfaces, with the maximum R-squared value for the predicted probability surface at the resolution of 225 m.

Figure 5.12 shows the change of fractional dimension with the resolution of modeling. Fractal dimension increases almost linearly with the change of resolution from 50 m to 225 m, then decreases at the turning point of 225 m. This suggests that the urbanization probability

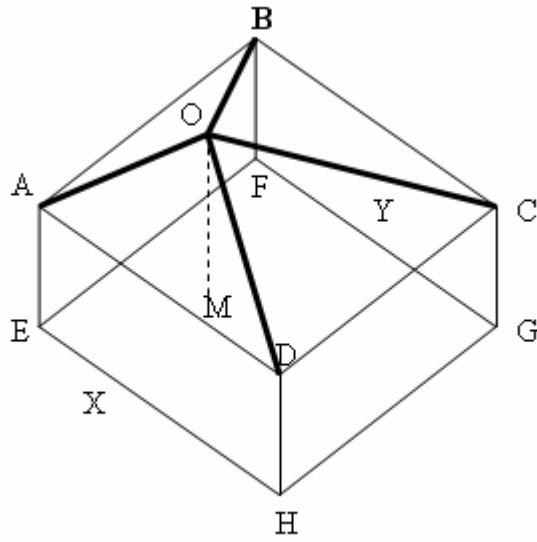


Figure 5.10 Coordinate structure for triangular prism method. (Source: Jaggie *et al.* 1993).

Table 5.5 Number of steps for calculation of fractal dimensions of predicted probability surfaces using triangular prism surface area method

Resolution (m)	No. of rows	No. of column	No. of steps
50	2744	$2332 < 2^{13}$	12
75	1830	$1555 < 2^{13}$	12
100	1372	$1166 < 2^{13}$	12
125	1098	$933 < 2^{12}$	11
150	915	$778 < 2^{12}$	11
175	784	$667 < 2^{12}$	11
200	686	$583 < 2^{12}$	11
225	610	$519 < 2^{12}$	11
250	549	$467 < 2^{11}$	10

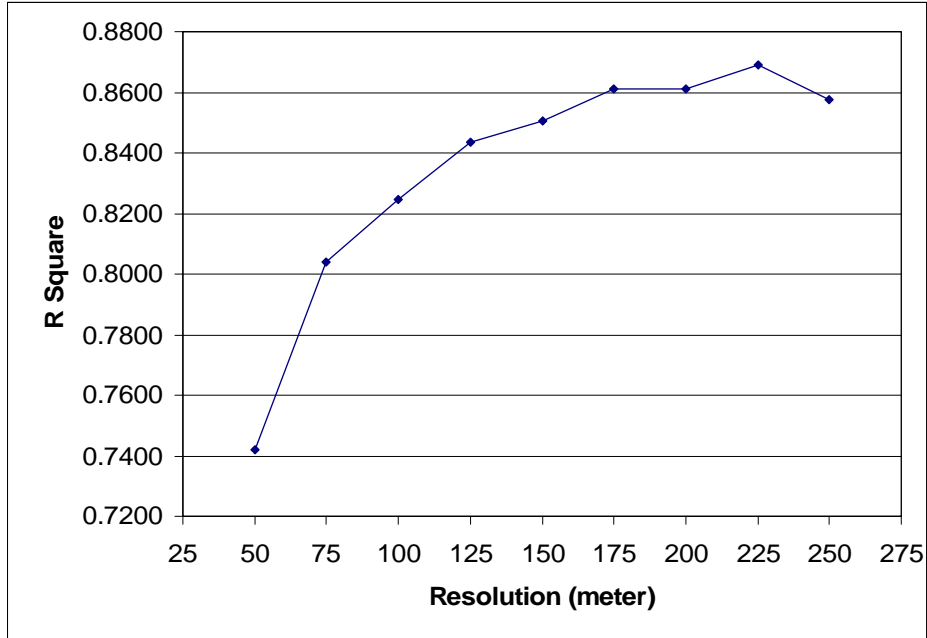


Figure 5.11 R-square values against resolutions. A R-square value is for the regression analysis at a resolution which regresses the log total surface area on the log of the step size. A fractal dimension D is equal to 2.0 minus the slope of this double log regression.

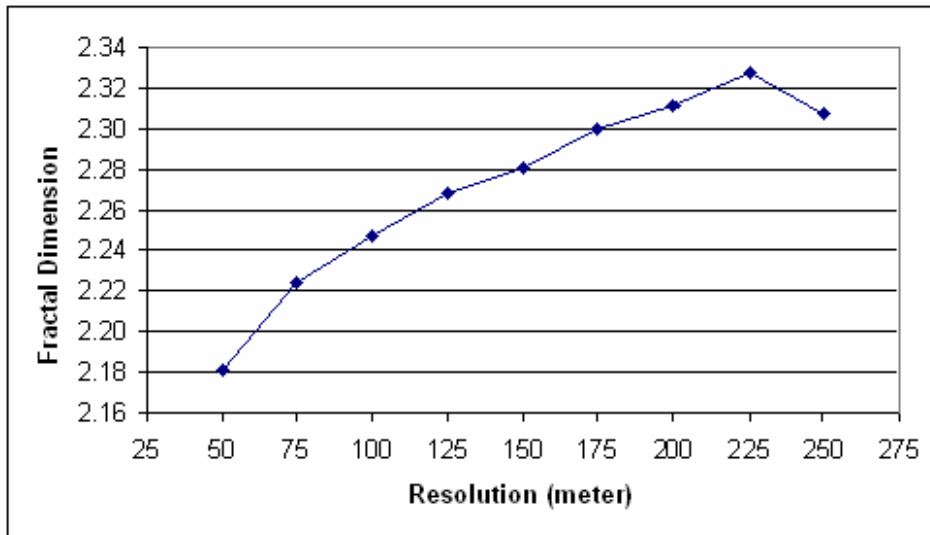


Figure 5.12 Lumped fractal dimension of logistic regression model predicted probability surface plotted against resolution.

surface does not demonstrate the property of self-similarity of real fractals since self-similar objects must have constant fractional dimension. Previous studies have demonstrated that true fractals with self-similarity at all scales are uncommon (Lam and Quattrochi 1992) and most real-world curves and surfaces are not pure fractals with a constant fractal dimension at all scales. The change of fractal dimension across scale, though controversial to the strict sense of fractal dimension as defined by Mandelbrot (1983), can be interpreted positively and used to summarize the scale changes of the spatial phenomena. The scale at which the highest fractal dimension is measured may be the scale at which most of the processes operate (Goodchild and Mark 1987; Lam and Quattrochi 1992; Cao and Lam 1996), and hence is the optimal scale of analysis. Thus the resolution of 225 m is selected as the optimal scale at which the logistic model best represents the dynamics of urbanization and the underlying controlling processes. The cell size of 225 m should be the best resolution for the study which avoids both individualistic fallacy and ecological fallacy. In the following sections, modeling and analysis will be based on the resolution of 225 m.

5.4 Testing logistic regression residual for spatial autocorrelation

In the previous sections, the logistic regression model was calibrated using the full data set comprising all cell values within the 13 county study area. The model calibration resulted in a predicted urbanization probability surface map and a residual map indicating the difference between the predicted and the observed probability.

The logistic regression model assumes that observations are independent of each other and the residuals are mutually independent. But this assumption may be violated due to the spatial autocorrelation. Spatial autocorrelation is the propensity for data values to be similar to

neighboring data values. The model has not taken spatial components into account, although the variable X_{12} (number of urban cells within a 7 by 7 cell neighborhood) has captured some spatial interaction effects. Spatial autocorrelation can occur in the residuals for several reasons: (1) a linear model has been used for a nonlinear relationship; (2) other causal variables have been excluded in the model; and (3) both the interactive and reactive processes have occurred (Goodchild 1987).

If present, spatial autocorrelation will violate the assumption of independence of residuals and call into question the validity of hypothesis testing. The main effect of such violation is the underestimation of the error sum of squares (ESS) which inflates the value of the test statistic. An inflated test statistic increases the chance of an incorrect rejection of a null hypothesis (Type I error in statistics terms). For example, spatial autocorrelation can lead to bias in the estimation of residual variance and therefore in pseudo R^2 and other measures of the success of the model, and hence the inefficiency in the estimation of the logistic regression coefficients—the β 's. Therefore it is necessary to examine and determine if spatial autocorrelation exists in the residuals which would violate the assumption of independent observations. If there is spatial autocorrelation, measures have to be taken to reduce it to achieve a more powerful model.

To test the logistic regression residual for spatial autocorrelation, Moran's I for the King's case was calculated under a normality assumption that the cell values represent independent drawings from a single normally distributed population, hence a null hypothesis that there is no spatial autocorrelation. The King's case (Figure 5.13) examines the cells diagonally connected to each cell as well as those cells to the left, right, above and below each image cell. The calculation of Moran's I was only limited to the cells within the 13-county study area by

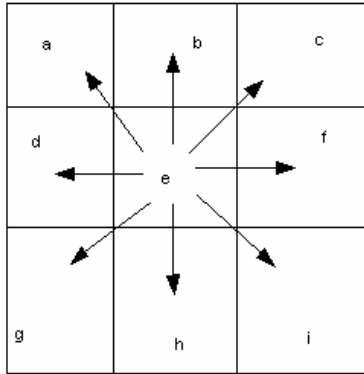


Figure 5.13 King's case in determining spatial autocorrelation.

specifying a Boolean mask image. The Boolean mask image contains 1's in all cells that should be considered and 0's for those to be ignored.

Assume that there are n observations of the residuals, with each residual value represented by z_i , and the mean residual values being \bar{z} . Moran's I was calculated by the following equation (Goodchild 1987):

$$I = \frac{\sum_i \sum_j w_{ij} c_{ij}}{s^2 \sum_i \sum_j w_{ij}} \quad (5-13)$$

where I is Moran's I index. Its values range from -1 to $+1$, with positive values indicating nearby areas being similar in attributes, negative values suggesting dissimilar attributes in nearby areas, and zero value for randomly and independently arranged attribute values. The c_{ij} term is the residual similarity measure:

$$c_{ij} = (z_i - \bar{z})(z_j - \bar{z}) \quad (5-14)$$

s^2 denotes the sample variance:

$$s^2 = \sum_i (z_i - \bar{z})^2 / n \quad (5-15)$$

The term w_{ij} is the spatial proximity between cell i and j . In this study, diagonal cells are given a weight of only 0.707 equal to $\sqrt{2}/2$ relative to a weight of 1.0 for those vertically or horizontally adjacent because diagonal distance between the centers of two diagonally neighbored cells is equal to the distance between the immediately neighboring cells times $\sqrt{2}$. Table 5.8 shows the spatial proximity matrix for the cells shown in Figure 5.13.

Table 5.8. Spatial Proximity matrix for King's case in Moran's I calculation

	a	b	c	d	e	f	g	h	i
a	0	1	0	1	0.707	0	0	0	0
b	1	0	1	0.707	1	0.707	0	0	0
c	0	1	0	0	0.707	1	0	0	0
d	1	0.707	0	0	1	0	1	0.707	0
e	0.707	1	0.707	1	0	1	0.707	1	0.707
f	0	0.707	1	0	1	0	0	0.707	1
g	0	0	0	1	0.707	0	0	1	0
h	0	0	0	0.707	1	0.707	1	0	1
i	0	0	0	0	0.707	1	0	1	0

To test the statistical significance of Moran's I obtained under the normality assumption, first the variance of I ($Var_N(I)$) is given as (Goodchild 1987):

$$Var_N = \left(\frac{1}{S_0^2(n^2 - 1)} (n^2 S_1 - n S_2 + 3 S_0^2) \right) - E_N(I)^2 \quad (5-16)$$

where subscript N denotes normality assumption;

N = number of observations,

$$E_N(I) = \frac{-1}{n-1}, \text{ expected value of Moran's } I,$$

$$S_0 = \sum_{i=1}^{i=n} \sum_{j=1}^{j=n} w_{ij}, \text{ the sum of the spatial proximity weight matrix elements,}$$

$$S_1 = \frac{\sum_{i=1}^{i=n} \sum_{j=1}^{j=n} (w_{ij} + w_{ji})^2}{2},$$

$$S_2 = \sum_{i=1}^{i=n} (w_{i\bullet} + w_{\bullet i})^2 \text{ the sum of the } (i^{\text{th}} \text{ row} + i^{\text{th}} \text{ column})^2 \text{ of the spatial proximity matrix.}$$

The standard deviation of Moran's I was then calculated as:

$$SD_N(I) = \sqrt{Var_N(I)} \quad (5-17)$$

Last, the z -score was computed as:

$$z = \frac{I - E_N(I)}{SD_N(I)} \quad (5-18)$$

From the z -score, we get p value, the probability that the null hypothesis is true given the observed sample. The smaller the p value, the less likely the null hypothesis, and the greater the confidence with which we can reject the null hypothesis, i.e., no spatial autocorrelation.

For the 13-county area within the residual image at the resolution of 225 meters, the King's case Moran's I and its statistics are calculated using Idrisi Kilimanjaro and are shown in Table 5.9.

Table 5.9 Spatial autocorrelation statistic

Statistics	Value
Number of cells included	206316
Mean of cells included	0.0000
Standard Deviation of cell values	0.0003
Spatial autocorrelation(Moran's I)	0.2826
Expected value of I if not autocorrelated	-0.0000
Variance of I (normality assumption)	0.0000
z test stat (normality assumption)	252.2894*

* $p = 2.22e-6$

The p value is much less than 5%, which leads to the conclusion that the null hypothesis of no spatial autocorrelation in the residuals can be rejected. In other words, spatial autocorrelation is present among the residual values.

Urban development is spatially autocorrelated. In the logistic regression model, the phenomena represented by the response variable (urban growth) and the explanatory variables could not occur independent of location. The closeness in attributes across space is related to spatial proximity. Urban growth has shown spatial autocorrelation due to the ‘push’ and ‘pull’ effects in the urban development process. For example, commercial development may be clustered around an existing commercial land lot to take advantage of scale economy, and may also be scattered to compete for customer sources. The status of the dichotomous variable of urban growth in a place is affected by the neighboring places. Cliff and Ord (1981) referred to this type of spatial dependence as interactive. Spatial autocorrelation may also be reactive in Cliff and Ord (1981)’s terms. The value of the response variable at a place may be determined by some other variable at the same place which is itself autocorrelated. Taking the causal variable population density for example, if it is spatially correlated, urban growth must show reactive spatial autocorrelation.

5.5 Correcting for spatial autocorrelation

The statistical methodology for considering spatial autocorrelation is not as well developed for logistic regression models as it is for the least squares regression models. Logistic regression models belong to the family of generalized linear models. Spatial forms of such models are not well developed. This study uses three steps to correct for the effects of space.

The first step is to use raster GIS data aggregation and pixel thinning functions, such as the DEGRADE function for continuous data and the AGGIE function for categorical data in ERDAS Imagine, and CONTRACT function for thematic pixel thinning and continuous value interpolation function in Idrisi Kilimanjaro. This was done in Section 5.3 where multi-scale data sets were created and multi-scale modeling was conducted. The multi-resolution modeling process from 25 m cell size to 250 m cell size is a process of alleviating the spatial effect by considering a series of spatial lags from the first order to the tenth order. The effect of spatial dependence at the resolution of 225 m must be weaker than that at 25 m since the attribute similarity becomes weaker as spatial lags progress from the first order to a higher order.

The second step is to include spatial coordinates of data points into the independent variable set. Spatial autocorrelation can be alleviated to some extent by attempting to introduce location into the link function to remove any such effects present (Bailey and Gatrell 1995). For example, spatial coordinates of observations might be introduced as additional covariates, or to classify regions in terms of their broad location and treat this classification as an extra categorical explanatory factor in the model. This assumes of course that one can “explain away” spatial dependence in terms of a first-order spatial trend, i.e., the first-lag autocorrelation. The following refined logistic regression model will include the UTM coordinates (eastings and northings) as two extra independent variables.

The last strategy is sampling. A stratified random sample image was generated and used as the feature definition file to extract cell values of dependent and independent variables on which the refined logistic regression model will be fitted. The spatial distances between sampling data points are larger than those between neighboring data points in the full data set, thus the spatial autocorrelation effects on modeling would be smaller than those by using the full data set.

5.6 Refining the model at the resolution of 225 m

5.6.1 Data preparation

Stratified random sampling was applied to the area covered by the rectangle (see Figure 3.2) bounding the 13-county study area to generate a vector point file in a GIS environment. There are two purposes for taking a sample of the full data set. The first purpose is to correct for spatial autocorrelation as explained in Section 5.5. The second purpose is to reserve non-sampled data points for model validation using the Relative Operating Characteristic (ROC) method that will be done in Section 5.10.2. The results of model validation using the full data sets on which model calibration is based would be biased and unreliable.

Stratified random sampling is thought to perform well when it is necessary to make sure that small, but important, areas are represented in the sample (Congalton 1988). The sampling percentage is around 10%. Since logistic regression model fitting will be performed within the 13-county study area, only those points within the study area were extracted using point-in-polygon GIS operation. At the resolution of 225 m, the number of cells within the study area is 206,316, of which 20,389 cells have been sampled. Within the study area, the number of cells that have changed from non-urban to urban, i.e, the number of 1s for variable Y (1= urban growth), is 20,631, accounting for 1.85% of the total number of cells. Of the 20,389 sample points, there are 370 points whose cell values are 1 in the Y variable layer. The percentage of 1s in the sample is 1.82%, matching very well with the percentage of 1.85% for the full data set, which demonstrates the accuracy of the stratified random sampling.

The UTM coordinates (eastings, denoted as E, and northings, denoted as N) for the sample points were retrieved using raster GIS and were used as two additional independent variables. Raster cell values of the sampled cells for the 18 independent variable layers were

extracted and exported to form an integrated text file together with (E, N) coordinates, which then were imported into the STATA software, a statistical software package (STATA 2003). The beginning and ending parts of data values are shown in Table 5.10. Model fitting was conducted with STATA.

5.6.2 Model fitting: maximum likelihood estimation

Fitting the logistic regression model requires that estimates of the parameters

$(\alpha, \beta_1, \beta_2, \dots, \beta_{19}, \beta_{20})$ be obtained. A maximum likelihood estimator is used to fit the model. The method of maximum likelihood yields values for the unknown parameters which maximize the probability of obtaining the observed set of data — the urban growth from 1987 to 1997 detected from remote sensing. In order to apply this method, a likelihood function was first constructed (modified from Hosmer *et al.* 1989):

$$L = \prod_{i=1}^n \mu_i^{y_i} * (1 - \mu_i)^{1-y_i} \quad (5-19)$$

where

L is the likelihood;

μ_i is the predicted value of the dependent variable for sample i :

$$\mu_i = \frac{1}{1 + e^{-\left(\hat{\alpha} + \sum_{j=1}^k \hat{\beta}_j X_j\right)}} \quad (5-20)$$

y_i is the observed value of the dependent variable for sample i , and

n is the number of observations, which equals to 20,389.

Table 5.10 Data Values for Logistic Regression Model

Id	Y	X1	X2	X3	X4	X5	X6	X7	X8	X9	X10	X11	X12	X13	X14	X15	X16	X17	X18	X19	E	H	
1	0	47.6	9426	15	300	76.9	91.3	3	225.0	75476.7	60675.8	225	5	0	0	0	0	0	1	0	700108.8	3674619.8	
2	0	19.1	10219	18	239	82.5	96.0	0	1922.4	75723.8	60135.2	675	0	0	0	0	0	0	1	0	698672.9	3675325.5	
3	0	50.0	9426	15	300	76.9	91.3	0	1272.8	75057.3	59830.1	225	0	0	0	0	0	0	1	0	699636.4	3675612.0	
4	0	52.1	9426	15	300	76.9	91.3	1	1935.5	75223.1	59665.7	450	0	0	0	0	0	1	0	0	698781.9	3675832.5	
5	0	49.0	9426	15	300	76.9	91.3	1	1575.0	74483.5	59157.5	225	0	0	0	0	0	1	0	0	699531.9	3676321.3	
6	0	47.2	9426	15	300	76.9	91.3	1	1125.0	74320.9	59329.2	900	0	0	0	0	0	1	0	0	700138.8	3675985.5	
7	0	48.2	9426	15	300	76.9	91.3	1	1125.0	74101.9	58709.1	225	0	0	0	0	0	0	1	0	0	699481.1	3676794.0
8	0	46.4	9426	15	300	76.9	91.3	0	225.0	73341.0	57812.3	0	2	0	0	0	0	0	1	0	0	699465.5	3677601.5
9	0	18.1	8306	15	316	94.6	94.5	3	1125.0	77043.4	58254.6	0	2	0	0	0	0	1	0	0	692130.9	3678217.0	
10	0	10.9	12537	5.9	413	93.7	100.0	1	2134.5	76365.2	58026.0	225	1	0	0	0	0	1	0	0	693259.8	3678420.5	
11	0	10.9	12537	5.9	413	93.7	100.0	0	2846.1	75782.3	57677.7	225	0	0	0	0	0	0	1	0	0	693964.3	3678583.8
12	0	11.1	12537	5.9	413	93.7	100.0	0	3276.1	75515.9	57596.9	0	0	0	0	0	0	0	1	0	0	694284.3	3678453.0
13	0	11.4	12537	5.9	413	93.7	100.0	1	3884.1	74727.5	57375.0	225	1	0	0	0	0	0	1	0	0	695721.2	3678555.5
14	0	11.8	12537	5.9	413	93.7	100.0	1	3404.9	74652.6	57530.5	225	1	0	0	0	0	0	1	0	0	696220.0	3678397.5
15	0	11.5	12537	5.9	413	93.7	100.0	1	2565.4	73955.2	57184.1	0	1	0	0	0	0	0	1	0	0	697146.3	3678631.3
16	0	11.6	12537	5.9	413	93.7	100.0	0	1638.0	73636.6	57297.7	225	1	0	0	0	0	0	1	0	0	697855.6	3678300.8
17	0	11.5	12537	5.9	413	93.7	100.0	2	1211.7	73387.3	57248.2	0	1	0	0	0	0	0	1	0	0	698471.1	3678253.8
18	0	45.3	9426	15	300	76.9	91.3	3	225.0	72961.8	57364.0	0	3	0	0	0	0	0	1	0	0	699567.0	3678033.0
.....																							
20374	0	34.3	11068	15	249	97.0	95.1	0	1591.0	64507.2	34996.7	2025	0	0	0	0	0	0	1	0	0	743397.0	3803907.5
20375	0	32.6	11068	15	249	97.0	95.1	7	1713.6	64800.4	35068.3	2700	0	0	0	0	0	0	1	0	0	744283.4	3804194.5
20376	0	31.6	11068	15	249	97.0	95.1	4	1935.5	64839.4	35001.8	2624	0	0	0	0	0	0	1	0	0	744663.4	3804177.8
20377	0	29.6	11068	15	249	97.0	95.1	0	2709.4	64703.1	34662.4	1757	0	0	0	0	0	0	1	0	0	745737.3	3803956.5
20378	0	11.1	9954	19	0	100.0	96.0	3	2925.0	65447.6	35261.9	1814	0	0	0	0	0	0	1	0	0	746226.6	3804513.0
20379	0	10.7	9954	19	0	100.0	96.0	2	3427.1	65276.8	34997.5	1312	0	0	0	0	0	0	1	0	0	746794.0	3804357.0
20380	0	10.1	9954	19	0	100.0	96.0	3	4269.1	65391.4	34933.7	636	0	1	0	0	0	0	1	0	0	747618.3	3804347.0
20381	0	9.7	9954	19	0	100.0	96.0	2	4980.6	65262.8	34676.3	0	0	0	0	0	0	0	1	0	0	748338.9	3804040.0
20383	0	9.2	9954	19	0	100.0	96.0	5	6443.0	65731.2	34875.7	225	0	0	0	0	0	0	1	0	0	749812.6	3804399.8
20384	0	9.2	9954	19	0	100.0	96.0	4	6883.7	65808.2	34881.5	503	0	0	0	0	0	0	1	0	0	750416.7	3804215.0
20385	0	9.3	9954	19	0	100.0	96.0	1	7546.7	65929.2	34901.1	225	0	0	0	0	0	0	1	0	0	750993.6	3804399.0
20386	0	9.7	9954	19	0	100.0	96.0	0	8297.6	65615.6	34484.5	225	0	0	0	0	0	0	1	0	0	751793.4	3803916.3
20387	0	13.4	11249	8.9	358	97.5	96.5	4	9861.6	69094.1	36227.8	1575	0	0	0	0	0	0	1	0	0	716102.9	3804844.0
20388	0	13.3	11249	8.9	358	97.5	96.5	4	9559.2	68807.7	35964.1	1350	0	0	0	0	0	0	1	0	0	716409.6	3804599.3
20389	0	13.8	11249	8.9	358	97.5	96.5	5	9301.5	69230.2	36509.0	2135	0	0	0	0	0	0	1	0	0	717063.2	3805288.0

The likelihood function expresses the probability of the observed data as a function of the unknown parameters. The maximum likelihood estimators of these parameters are chosen to be those values which maximize the function. Thus the resulting estimators are those which agree most closely with the observed data. To maximize the likelihood function requires the solution for the following simultaneous nonlinear equations (Hosmer *et al.* 1989):

$$\sum_{i=1}^n (y_i - \mu_i) * X_{ij} = 0 \quad (5-21)$$

where X_{ij} is the observed value of the independent variable j ($j=1,2,\dots,20$) for sample i ($i=1,2,\dots,20389$).

The results of fitting the logistic regression model to the data shown in Table 5-9 are given in Table 5.11. The estimated logit is given by the following expression:

$$\begin{aligned} \text{logit}(\hat{P}) = & 13.52805 - 0.0006117X_1 - 0.0000132X_2 + 0.0039253X_3 + 0.0001885X_4 \\ & - 0.0003437X_5 + 0.0101019X_6 - 0.0178212X_7 - 0.0009621X_8 + 0.0000177X_9 \\ & - 0.0000834X_{10} - 0.0007265X_{11} + 0.0172993X_{12} - 0.1838858X_{13} - 2.529919X_{14} \\ & - 1.513311X_{15} + 0.922617X_{16} + 0.7312305X_{17} + 0.3742606X_{18} \\ & + 0.000000258E - 0.00000454N \end{aligned} \quad (5-22)$$

The fitted values, \hat{P} , representing the probability of urban growth, were then obtained using the estimated logit — $\text{logit}(\hat{P})$, based on equation (5-4).

5.7 Testing for the significance of the Model

The assessment of the significance of the variables in the model fitted above involves formulation and testing of a statistical hypothesis to determine whether the independent variables

Table 5.11 Estimated Coefficients and Odds Ratio for the Logistic Regression Model
Using the 20 Independent Variable (M₂₀)

Y	Coefficient	Standard error	Odds Ratio	Standard error	Z	P> Z
X ₁	-0.000611	0.000216	0.9993884	0.0002156	-2.84	*0.005
X ₂	-1.3E-05	8.87E-06	0.9999868	8.87E-06	-1.49	0.135
X ₃	0.003925	0.008132	1.003933	0.0081635	0.48	0.629
X ₄	0.000189	0.000263	1.000188	0.0002626	0.72	0.473
X ₅	-0.00034	0.00298	0.9996563	0.0029785	-0.12	0.908
X ₆	0.010102	0.015917	1.010153	0.0160788	0.63	0.526
X ₇	-0.01782	0.031064	0.9823367	0.0305149	-0.57	0.566
X ₈	-0.00096	0.000129	0.9990383	0.0001293	-7.44	*0.000
X ₉	1.77E-05	8.92E-06	1.000018	8.92E-06	1.98	*0.047
X ₁₀	-8.3E-05	1.13E-05	0.9999166	0.0000113	-7.36	*0.000
X ₁₁	-0.00073	0.000119	0.9992738	0.0001191	-6.1	*0.000
X ₁₂	0.017299	0.007073	1.01745	0.0071968	2.45	*0.014
X ₁₃	-0.18389	0.522982	0.8320308	0.4351372	-0.35	0.725
X ₁₄	-2.52992	0.812327	0.0796655	0.0647144	-3.11	*0.002
X ₁₅	-1.51331	0.747177	0.2201799	0.1645132	-2.03	*0.043
X ₁₆	0.922617	0.76884	2.515866	1.934298	1.2	0.230
X ₁₇	0.731231	0.733594	2.077636	1.524141	1	0.319
X ₁₈	0.374261	0.722887	1.453916	1.051016	0.52	0.605
E	2.58E-07	2.65E-06	1	2.65E-06	0.1	0.922
N	-4.54E-06	2.72E-06	0.9999955	2.72E-06	-1.67	*0.095
_const	13.52805	10.68137	N/A	N/A	1.27	0.205

Y= Urban growth

X₁= *Population density (person/km²)

X₂= Per capital income (\$)

X₃= Poverty rate(%)

X₄= Median housing rent (\$)

X₅= Percentage of white people(%)

X₆= Employment rate(%)

X₇= Slope (%)

X₈= *Distance to the nearest urban cluster(m)

X₉= *Distance to CBD(m)

X₁₀= *Distance to active economy centers(m)

X₁₁= *Distance to the nearest major road

X₁₂= * # of urban cells within a 7×7 cell window

X₁₃= Conservation area

X₁₄= *High-density urban

X₁₅= *Low-density urban

X₁₆= Bare land

X₁₇= Cropland/grassland

X₁₈= Forest

E = Easing coordinate (m)

N= *Northing coordinate (m)

* These variables are significant at the $\alpha = 0.10$ level

in the model are significantly related to the outcome variable Y. The significance test is performed by comparing the observed values of the response variable to those predicted by the full (or saturated) model denoted as M_{20} (the subscript represents the number of independent variables) and a reduced model (M_0) without the variables in question.

5.7.1 Likelihood ratio test

A likelihood ratio (LR) test is used to assess the overall significance of variables in the full model with 20 independent variables. The likelihood ratio test is based on log likelihood statistic $-2 \ln \hat{L}$, where \hat{L} is the maximized likelihood value obtained from equation (5-19) by plugging the estimated parameters into the equation. The higher the \hat{L} value, the better the fit of the model. The log likelihood statistic is used for the calculation of likelihood ratio statistic (LR) (Kleinbaum 1994):

$$LR = (-2 \ln \hat{L}_1) - (-2 \ln \hat{L}_2) \quad (5-23)$$

Its equivalent equation is:

$$LR = -2 \ln \frac{\hat{L}_1}{\hat{L}_2} = -2 \ln(\text{likelihood_ratio}) \quad (5-24)$$

where

\hat{L}_1 is estimated likelihood for the full model, and

\hat{L}_2 is estimated likelihood for the reduced model.

The likelihood ratio statistic yields a value that lies between 0, when extreme non-significance occurs, and $+\infty$, when there is extreme significance of the contribution of variables to response. Provided that the number of observations n in the study is large and under the null

hypothesis: $H_0: \beta_1 = \beta_2 = \dots = \beta_k = 0$, LR follows the chi-square (χ^2) distribution with k degrees of freedom (k= number of parameters).

In this study, $-2 \ln L_f$ for the full model is equal to 3111.839, and $-2 \ln L_0$ is 2523.589 (L_0 is the likelihood value for the model in which coefficients for all the 20 independent variables are hypothesized to be zero). The LR is thus obtained using equation (5-24) and is equal to 588.25. The observation number is 20,389, which is large and justifies the χ^2 distribution of LR with 20 degrees of freedom. The p-value for the test is $p[\chi^2(20)] \approx 0$ which is significant at the $\alpha = 0.05$ level. The null hypothesis should be rejected. It may be concluded that at least one, and perhaps all the 20 coefficients are different from zero. We are confident that at least one variable, and perhaps all 20 variables, are significantly associated with the probability of urbanization.

5.7.2 Univariate Wald test

To test the significance of an individual variable, the Wald test statistic is computed by dividing the estimated coefficient of interest by its standard error (Kleinbaum 1994):

$$Z_j = \frac{\hat{\beta}_i}{s_{\beta_i}} \quad (5-25)$$

The Z values calculated are shown in Table 5.11. Under the hypothesis that an individual coefficient is zero, these statistics will follow the standard normal distribution in large samples ($n=20,389$). Thus, the values of these statistics may indicate which of the variables in the model may be significant. At the $\alpha = 0.05$ level, population density (X_1), distance to the nearest urban cluster (X_8), distance to CBD (X_9), distance to active economy centers (X_{10}), distance to major roads (X_{11}), number of urban cells with a neighborhood defined by a window of 7 by 7 cells

(X_{12}), design variables high-density urban area (X_{14}) and low-density urban area (X_{15}) are significant. At the $\alpha = 0.10$ level, the variable UTM coordinate N (X_{20}) is significant.

Following the significance test, it is logical to construct a reduced model which excludes those variables thought to be insignificant. Of the five design variables for land use/cover, only two (X_{14} and X_{15}) are significant. The other three (X_{16} , X_{17} and X_{18}) are insignificant. Thus confusion arises since we are not sure about the contribution of land use/cover as a single variable to the model when only part of the design variables are significant. Statisticians suggest that we must be careful in our use of the Wald statistics to assess the significance of the coefficients and that whenever a categorically scaled independent variable is included (or excluded) from a model, all of its design variables should be included (or excluded) (Hosmer and Lemeshow 1989). Strict adherence to the $\alpha = 0.05$ level of significance would justify excluding land use/cover from the model. However, the probability of urbanization of a land lot should be influenced by its initial land use/cover status and initial land use/cover should be considered important in land use/cover change dynamics in a biophysical and cultural sense. Thus all the five design variables for land use/cover are kept in the reduced model. The reduced model has 12 independent variables, denoted as M_{12} . The results of fitting the reduced logistic regression model M_{12} is shown in Table 5.12.

To ensure meaningful interpretation of odds ratios for population density (X_1), distance to the nearest urban cluster (X_8), distance to CBD (X_9), distance to active economy centers (X_{10}), and distance to the nearest major road (X_{11}), odds ratios were re-calculated for 1000 units of change of these variables using equation (5-12). The odds ratio values are shown in Table 5.13.

Table 5.12 Estimated Coefficients and Odds Ratio for the Logistic Regression Model Using the 12 Independent Variable (M_{12})

Y	Coefficient	Standard error	Odds Ratio	Standard error	Z	P> Z
X1	-0.0005622	0.0002110	0.9994380	0.00021090	-2.66	0.008
X8	-0.0009631	0.0001289	0.9990374	0.00012880	-7.47	0.000
X9	0.0000216	0.0000691	1.0000220	0.00000690	3.12	0.002
X10	-0.0000842	0.0000105	0.9999158	0.00001050	-8.03	0.000
X11	-0.0007321	0.0001188	0.9992682	0.00011870	-6.16	0.000
X12	0.0187475	0.0069979	1.0189240	0.00713040	2.68	0.007
X14	-2.0443720	0.8098608	0.0868372	0.07032600	-3.02	0.003
X15	-1.4689880	0.7457362	0.2301583	0.17163730	-1.97	0.049
X16	0.9592659	0.7679655	2.6097800	2.00422100	1.25	0.212
X17	0.7909088	0.7322479	2.2054000	1.61490300	1.08	0.280
X18	0.4215078	0.7216335	1.5242580	1.09995600	0.58	0.559
N	-0.0000574	0.0000026	0.9999943	0.00000259	-2.22	0.027
Const	18.804220	9.6770990			1.94	0.052

Y= Urban growth

X₁= Population density (person/km²)

X₈= Distance to the nearest urban cluster(m)

X₉= Distance to CBD(m)

X₁₀= Distance to active economy centers(m)

X₁₁= Distance to the nearest major road

X₁₂= # of urban cells within a 7×7 cell window

X₁₄= High-density urban

X₁₅= Low-density urban

X₁₆= Bare land

X₁₇= Cropland/grassland

X₁₈= Forest

N= Northing coordinate (m)

Table 5.13 Odds ratios provided that variable values increase by 1000 units

Variable	Meaning	Odds ratio
X ₁	Population density (person/km ²)	0.56995
X ₈	Distance to nearest urban cluster (m)	0.38171
X ₉	Distance to CBD (m)	1.02183
X ₁₀	Distance to active economy centers (m)	0.91924
X ₁₁	Distance to major roads (m)	0.48090

The fitted model in the logit form is expressed as:

$$\begin{aligned} \text{logit}(\hat{P}) = & 18.804220 - 0.0005622 X_1 - 0.0009631 X_8 + 0.0000216 X_9 - 0.0000842 X_{10} \\ & - 0.0007321 X_{11} + 0.0187475 X_{12} - 2.0443720 X_{14} - 1.4689880 X_{15} \\ & + 0.9592659 X_{16} + 0.7909088 X_{17} + 0.4215078 X_{18} - 0.0000574 X_{19} \end{aligned} \quad (5-26)$$

The difference between the full model M_{20} and the reduced model M_{12} is the exclusion of the eight variables $X_2, X_3, X_4, X_5, X_6, X_7, X_{13},$ and X_{19} . The likelihood ratio test comparing the two models is obtained using the definition of LR given in equation (5-24). It will have a chi-square distribution with 8 degrees of freedom under the hypothesis that the coefficients for the eight excluded variables are equal to zero:

$$H_0 : \beta_2 = \beta_3 = \beta_4 = \beta_5 = \beta_6 = \beta_7 = \beta_{13} = \beta_{19} = 0$$

The value of the log likelihood statistic $-2 \ln L_{12}$ is 3116.584, and $-2 \ln L_{20}$ is 3111.839, yielding a likelihood ratio test value equal to 4.7446, which, with 8 degrees of freedom, has a p -value of $p[\chi^2(8) > 4.7446] = 0.7845$. Since the p -value is large, far exceeding 0.05, the null hypothesis is accepted, which leads to the conclusion that the reduced model is as good as the full model. Thus there is no advantage to including the eight variables in the model. Later predictions of urbanization probability and spatial pattern of urban areas as well as model validation will be based on the reduced model. However, we must not base the assessment of the model entirely on the test of statistical significance and ignore the explanatory power of those variables thought to be insignificant and excluded from the full model. It will be seen in section 5-8 that interpretation of these variables will also render meaningful pictures of the association between them and urban growth.

5.8 Assessment of goodness of fit

The purpose of assessing goodness of fit of the model is to examine whether the predicted urbanization probability values are an accurate representation of the observed values in an

absolute sense. The model fits if (1) summary measures of the distance between the observed sample values of the outcome y ($y' = (y_1, y_2, y_3, \dots, y_n)$) and predicted values \hat{y} ($\hat{y}' = (\hat{y}_1, \hat{y}_2, \hat{y}_3, \dots, \hat{y}_n)$) are small and (2) the contribution of each pair (y_i, \hat{y}_i) , $i = 1, 2, 3, \dots, n$ to these summary measures is unsystematic and is small relative to the error structure of the model (Hosmer and Lemeshow 1989). The Pearson Chi-Square statistic and the Hosmer-Lemeshow statistic were used to assess the model fit in this study. Goodness of fit was assessed over fitted values of covariate patterns, not the total collection of covariates. The observations with the same set of data values for the covariates form a covariate pattern. So each covariate pattern has a unique set of data values. Let J denotes the number of covariate patterns and m_j represents the number of observations with $X=X_j$, it follows that the sum of m_j ($j=1, 2, \dots, J$) is equal to the total number of observation n .

5.8.1 Pearson chi-square statistic

The Pearson chi-square statistic is based on Pearson residuals. For the j^{th} covariate pattern, the Pearson residual is defined as follows (Hosmer and Lemeshow 1989):

$$r(y_j, \hat{\mu}_j) = \frac{y_j - m_j \hat{\mu}_j}{\sqrt{m_j \hat{\mu}_j (1 - \hat{\mu}_j)}} \quad (5-27)$$

The summary Pearson chi-square statistic is:

$$X^2 = \sum_{j=1}^J r(y_j, \hat{\mu}_j)^2 \quad (5-28)$$

The statistics X^2 under the assumption that the fitted model is correct in all aspects follows chi-square distribution with degrees of freedom equal to $J - (p + 1)$, where p is the number of independent variables (covariates).

For the reduced model M_{12} , the Pearson χ^2 goodness of fit test shows that the number of covariate patterns is equal to the number of observations, which means that each observation has a unique set of values for the variables and no observations share the same set of variable values. This may be due to the inclusion of the continuous distance (X_8, X_9, X_{10} , and X_{11}), coordinate(N), and population density(X_1) variables in the model. Pearson chi-square is 31864.39 with 20376 degrees of freedom, yielding a p value $p[\chi^2(20,376)]$ of zero. This would lead to the conclusion that the model does not fit at all. However, this conclusion is not reliable because the number of covariate patterns J is equal to the number of observations n . When $J \approx n$, p -values calculated for Pearson chi-square statistic using $\chi^2(J - p - 1)$ distribution are incorrect (Hosmer and Lemeshow 1989). In this case, the Hosmer-Lemeshow test (see the following section) is preferred.

5.8.2 Hosmer-Lemeshow test

In the Hosmer-Lemeshow (1989) test, the observations are first sorted in increasing order of their estimated event probability. The observations are then divided into g groups based on the percentiles of the estimated probabilities. This results in the first group containing the $n_1' = n/g$ observations having the smallest estimated probabilities, and the last group containing the $n_g' = n/g$ observations having the largest estimated probabilities. Then the Hosmer-Lemeshow goodness-of-fit statistic, \hat{C} , is obtained by calculating the Pearson chi-square from a summary table of observed and estimated expected frequencies of the presence and absence of an event:

$$\hat{C} = \sum_{k=1}^g \frac{(o_k - n_k' \bar{\mu}_k)^2}{n_k' \bar{\mu}_k (1 - \bar{\mu}_k)} \quad (5-29)$$

where

n_k' is the total number of observations in the k^{th} group,

$O_k = \sum_{j=1}^{c_k} y_j$ is the number of responses among the c_k covariate patterns,

$\bar{\mu}_k = \sum_{j=1}^{c_k} \frac{m_j \hat{\mu}_j}{n_k}$ is the average estimated probability, and c_k is the number of covariate patterns

in the k^{th} group.

When $J=n$ and the fitted logistic regression model is correct, the distribution of the statistic \hat{C} approximates the chi-square distribution with $g-2$ degrees of freedom, $\chi^2(g-2)$. \hat{C} 's value range is $[0,1]$. The bigger the p value, the better the model fits.

Table 5.14 shows the observed (*Obs*) and the expected (*Exp*) frequencies with each decile ($g=10$) for each outcome $Y=1$ or $Y=0$ using the fitted reduced logistic regression model M_{12} as expressed in equation (5-25). The value of the Hosmer-Lemeshow goodness-of-fit statistic computed from the frequencies in Table 5.14 is $\hat{C}=10.47$, and the corresponding p -value computed from the chi-square distribution with 8 degrees of freedom is 0.2334. This indicates that the model seems to fit, but weakly.

5.8.3 Pseudo R-square test

Logistic regression does not have an equivalent to the R-square that is found in ordinary least square (OLS) regression; however, many people have tried to come up with one. There are a wide variety of pseudo R-square statistics. Because this statistic does not mean what R-square means in OLS regression (the proportion of variance explained by the predictors), it is suggested

Table 5.14 Hosmer-Lemeshow goodness-of-fit test for the reduced Model M₁₂

<i>Group</i>	<i>Prob</i>	<i>Obs_1</i>	<i>Exp_1</i>	<i>Obs_0</i>	<i>Exp_0</i>	<i>Total</i>
1	0.0002	1	0.1	2038	2038.9	2039
2	0.0008	1	0.9	2038	2038.1	2039
3	0.0024	2	3.1	2037	2035.9	2039
4	0.0049	9	7.3	2030	2031.7	2039
5	0.0079	9	12.9	2030	2026.1	2039
6	0.0118	16	19.8	2023	2019.2	2039
7	0.0180	29	29.7	2010	2009.3	2039
8	0.0297	52	47.3	1987	1991.7	2039
9	0.0526	86	81.6	1953	1957.4	2039
10	0.2494	165	167.4	1873	1870.6	2038
Number of observations: n=20389 Number of groups: g = 10 Hosmer-Lemeshow: $\hat{C} = 10.47$ Probability > $\chi^2(8)$: p[$\chi^2(8)$]=0.2334						

to interpret this statistic with great caution. Hosmer and Lemeshow (1989) do not advocate the use of pseudo R-square statistics.

This study used McFadden's pseudo R-square to test the goodness of fit of the model. This statistic measures adjusted $-2\ln(\text{likelihood})$ for sample size and is calculated using the following formula (McFadden 1973):

$$1 - \frac{\ln(\text{likelihood})}{\ln(L_0)} \quad (5-30)$$

where L_0 is the value of the likelihood function if all coefficients except the intercept are zero.

Pseudo R square greater than 0.2 is considered a good fit (Clark and Hosking 1986). The pseudo R^2 values for the full model M₂₀ and the reduced model M₁₂ are 0.159 and 0.158 respectively, thus again indicating that the model fit is weak.

5.9 Model interpretation

The purpose of the interpretation of the above logistic regression models M_{12} and M_{20} is to address the questions: (1) what do the estimated coefficients in the model tell us about the association between urbanization probability and the driving forces? and (2) what are the processes controlling the dynamics of urban growth? To answer these questions requires us to draw practical inferences from the estimated coefficients of the model.

The coefficients β_i 's for the predictor variables measure the change in the log odds of urban growth that would result from a one unit change in the predictor variables. Since the β_i coefficients are in log units, their meaning cannot be directly interpreted as a measure of change in the probability of urban growth. However, when the β_i coefficient is used as a power to which the natural log (2.71828) is raised, the result represents an odds ratio as shown in equation (5-11), or the ratio of the probabilities that urban growth will occur divided by the probability that urban growth will not occur with or without β_i . If a coefficient is positive, its transformed log value will be greater than one, meaning that the event is more likely to occur with one unit increase in the explanatory variable. If a coefficient is negative, its transformed log value will be less than one, and the odds of the event occurring decrease with one unit increase in the explanatory variable. A coefficient of zero (0) has a transformed log value of 1.0, meaning that this coefficient does not change the odds of the event one way or the other. Since the odds ratio is a measure of association, the following interpretation will be based on the odds ratios.

Interpretation will be first given to significant variables as shown in the model M_{12} .

Urban development tends to occur in area of lower population density (X_1). The estimated odds ratio is 0.999438, or $1/1.000562$, which is less than one, which indicates that the probability of urban growth in area of higher population density is less than the probability of

urban growth in area of lower population density. In particular, with an increase of one person per square kilometer, the odds of urban growth is estimated to decrease by 0.000562. An increase of one person may not make any sense. For more practical interpretation, it would be more appropriate to specify the change of population density in 1,000 units. If the population increases by 1000 persons per square kilometer, according to equation (5-12), the odds ratio will be $e^{1000 \times (-0.0005622)}$, or 0.56995, or 1/1.7542 (see Table 5.13), which means that the odds of urban development would decrease by 0.7542 if population density increases by 1000 persons per square kilometer. Like most other American cities, urban sprawl and sub-urbanization in the study area are characteristic of low-density urban development, which replaces farmland, forest and open space with single-family homes on large lots. In developing countries, this may not be the case. For example, in Chinese cities that are experiencing rapid urbanization, new commercial and industrial facilities and residential subdivisions housing middle-class people often replace slums and villages populated with large number of the poor and lower-class workers living in peripheral areas, old towns, or city centers.

Urban areas tend to grow close to the nearest urban cluster. Distance to the nearest urban cluster (X_8) has a coefficient of -0.0009631 . The odds ratio is equal to 0.3817, or 1/2.6198 if a land lot is 1000 meters further away from an existing urban area. In particular, the probability of urban development in an area is estimated as 2.6198 times as large as the probability of urban development in an area 1000 meters further away from the nearest urban area. This demonstrates that pulling force has taken effect in the scale economy where commercial facilities tend to cluster together in a localized area. The influence of distance to the nearest urban cluster corresponds to Clarke's 'edge growth' rule in his cellular automata model of urban growth (Clarke and Hoppen 1997).

The decentralized, polycentric sub-urbanization trend in the metropolitan Atlanta area is evidenced by the interpretation of the odds ratios for the two predictors: distance to CBD (X_9) and distance to active economy centers (X_{10}). The odds of urban development in an area 1000 meters further away from the CBD is estimated as 1.000562 as large as that in area closer to CBD. The odds ratio for a 1000-unit increase of distance to active economic centers is 0.91924, or 1/1.0878, which means that the odds of urban development in area close to active economy centers is estimated as 1.0878 times as large as that in area 1000 meter further away from active economic centers. Like other American metropolises, the massive suburbanization of economic activities since the 1960s contributed significantly to the spatial restructuring of the business landscape of the Metropolitan Atlanta, resulting in the clustering of high-order activities in new metropolitan-level urban centers — ‘suburban downtowns’ (Hartshorn and Muller 1989). The emergence of these large multifunctional complexes in the outer suburban cities rendered obsolete the three classic models of urban structure — the concentric zone, sector, and multiple nuclei models, but conformed to the urban realms model, in which the closer it is to major activity centers, rather than to CBD, the more probable a land lot will be developed for urban use (Hartshorn and Muller 1989).

The model also demonstrates that urban development has been controlled by road accessibility. The odds ratio resulting from an increase of 1000 meters in distance to major roads (X_{11}) is 0.48090, or 1/2.079443. The odds of urban development in an area closer to major roads is estimated as 2.079443 times as large as the odds of urban development in an area 1000 meters further away from major roads. The road influence contributes to the spatial patterns of ribbon and strip development as can be discerned in the urban growth map obtained from land use/cover change detection from remote sensing in Chapter 3 (Figure 3.26). Similar observations can be

found in other urban growth models. The road influence is also one of the growth rules in Clarke's cellular automata model.

A land lot with more neighboring areas that are urban is more likely to be developed for urban use. The variable number of urban cells within a neighborhood of 7×7 cell size (X_{12}) has an odds ratio equal to 1.018924. With an increase of 1 urban cell within the neighborhood, the odds of development will increase 0.018924. The use of a land lot is often influenced by the land use/cover status of the adjacent area. Land managers and real estate developers have some propensity of imitating the land use/cover behaviors in the neighborhood. This neighborhood effect, along with the 'edge growth' rule captured by the distance to the nearest urban cluster, have acted to create a clustered pattern of urban development.

Of the five land use/cover types, only high-density urban (X_{14}) and low-density urban (X_{15}) areas have negative coefficients, resulting in odds ratio of less than 1. The odds of urban development in the existing urban area is estimated only as 0.08684 times for high-density urban use and 0.23016 times for low-density urban use respectively as large as the odds of urban development in non-developed area. Urban development has shown irreversibility. The irreversibility of high-density urban area is more obvious than that of low-density urban use as evidenced by the much lower odds ratio value of high-density urban use. Certainly the cost of redeveloping commercial and industrial areas is much higher than that in redeveloping residential areas. New urban development has occurred mainly in undeveloped peripheral urban-rural fringe areas or open space within established urban areas.

The probability of urban development in bare land area is larger than the probability of urban development in areas covered with cropland or grassland. The probability of transition from cropland or grassland to urban use is larger than that of deforestation for urban use. This

can be seen from the odds ratio values of 2.61, 2.21 and 1.52 in a decreasing order for bare land, cropland or grassland, and forest, respectively. All values are greater than one, indicating a higher probability of urban development in those areas. It should be noted that in the study area much bare land is forest clear-cut area. So it can be said that urban development has taken place mainly at the expense of the depletion of green space.

It is interesting to notice that the UTM coordinate northing (N) is a significant predictor while the UTM coordinate easting (E) is not significant and has an odds ratio value of 1. The variable N is originally intended to correct for spatial autocorrelation. The interpretation of its odds ratio has shown that it not only acts as a spatial autocorrelation corrector, but also indicates an unbalanced growth along the north-south direction, since its odds ratio is not equal to 1. There has been an unbalanced and polarizing growth in Atlanta: a dividing line exists between the north and the south, strongly corresponding with the long-standing residential racial segregation patterns. This unbalanced growth has many dimensions: separation by class and race, poverty, job and housing growth, and transportation patterns (BICUMP 2000).

5.10 Prediction and validation

5.10.1 Prediction

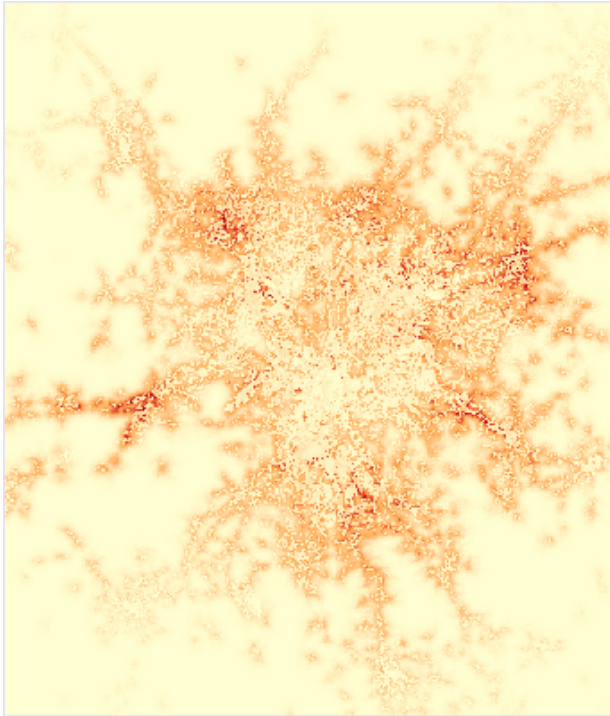
Prediction of the spatial patterns of the future urban area is the main objective of this study. The probability of urbanization was predicted by plugging the coefficients obtained from the logistic regression model containing the 12 significant predictors (M_{12}) and the cell values in the raster layers representing these predictors into equation (5-3). This was done using map algebra functions within raster GIS package Idrisi Kilimanjaro. The original predicted probability of urbanization is shown in Figure 5.14(a). To better perceive the spatial patterns of the probable

sites of urbanization, the original probability image was classified into ten classes based on equal intervals of the probability values (Figure 5.14(b)). The darker red areas indicate higher probabilities of urban growth. Some new clusters far from existing urban areas can be discerned from this map. Most probable areas for urban development are closer to major highways and existing urban clusters.

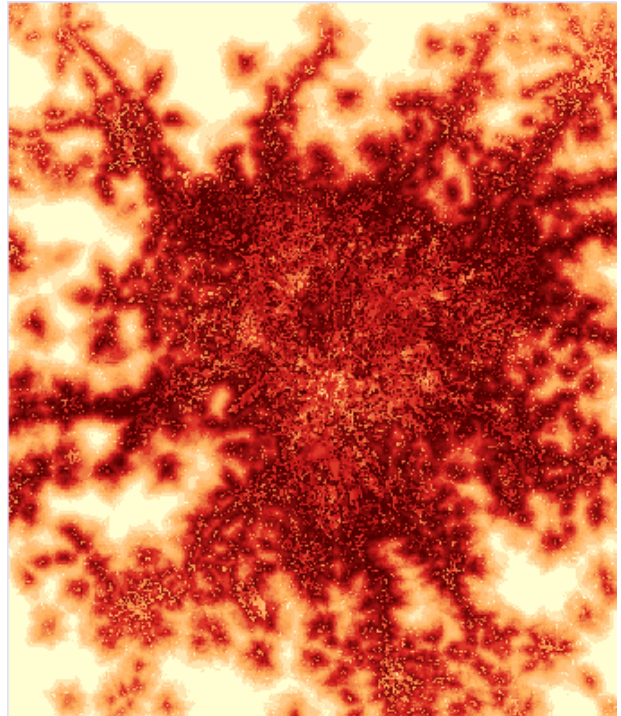
5.10.2 Model validation – ROC method

This study uses ROC method to validate the logistic regression model. ROC curves were developed in the 1950's as a by-product of research into making sense of radio signals contaminated by noise. ROC is widely used in engineering, meteorology, psychology, and medical science to measure the relationship between a signal and reality (Egan 1975; Swets 1988; Swets 1996). Recently the ROC method was brought to the field of land use/cover change modeling to measure the relationship between simulated change and real change (Pontius 2000). Pontius and Schneider (2001) explained how to use the ROC technique to examine how well a suitability map portrays the likely locations of a category of new development. Schneider and Pontius (2001) applied the ROC method to compare several modeling techniques. ROC method is an excellent method to evaluate the validity of a model that predicts the occurrence of an event by comparing a suitability image depicting the probability of that event occurring and a binary image showing where that class actually exists.

In this study, ROC was used to compare the image of probability of urban development (Figure 5.14) predicted from the logistic regression model against the image of actual urban growth (reference image) (Y variable in Figure 5.6). The ROC method offers a statistical



(a) Original probability



(b) Classified probability (10 classes, equal interval)

Figure 5.14 Urbanization probability maps of Atlanta, Georgia. Darker red areas indicate higher probabilities of urban growth.

analysis that answers one important question: “ How well is urban growth concentrated at the locations of relatively high suitability for urban growth?” Basically, ROC assesses how well the pair of maps agrees in terms of the location of cells being urbanized. Model validation using ROC reports a summary ROC value, a ROC curve as well as the coordinates of the points on the curve that are used to calculate the ROC value. A ROC value of 1 indicates that there is a perfect spatial agreement between the actual urban growth map and the predicted probability map. A ROC value of 0.5 is the agreement that would be expected due to chance, i.e., the cells values on the predicted probability image were assigned to random locations.

To conduct the model validation, first the ranked image of probability of urbanization was sliced at a series of threshold levels. A threshold refers to the percentage of cells in the probability image to be reclassified as 1 in preparation for comparison with the reference image. In this study, the series of thresholds are specified at an equal interval of 5%. The threshold values are cumulative, therefore setting the equal interval thresholds 5, 10, 15, ..., 95 would yield 20 threshold intervals 0-5%, 0-10%, 0-15%, ... and 95-100%. ROC will begin with the cell ranked the highest for probability, reclassify it as 1 and continue down through the ranked cells until 5% of the cells have been reclassified as 1. The remaining 95% will be classified as 0. This slice image was then compared with the reference image. Then ROC continues for the successive threshold. For each slice generated from each threshold, a two-by-two contingency table was created based on the comparison of the predicted probability image with the reference image (Table 5.15). In the table, A represents the number of true positive cells which are predicted as urban growth and are actually urban growth in the reference image. B is the number of false positive cells. C is the number of false negative cells. D is the number of true negative cells.

From each contingency table for each threshold, one data point (x,y) was generated where x is the rate of false positives (false positive %) and y is the rate of true positives (true positive %):

$$\text{true positive \%} = \frac{A}{A + C} \quad (5-31)$$

$$\text{false positive \%} = \frac{B}{B + D} \quad (5-32)$$

Table 5.15 Contingency table showing the comparison of predicted probability image with the reference image

		Reference Image	
		Urban growth (1)	No urban growth (0)
Predicted Image	Urban growth (1)	A (true positive)	B (false positive)
	No urban growth (0)	C (false negative)	D (true negative)

These data points were connected to create a ROC curve from which the ROC value is calculated. The ROC statistic is the area under the curve that connects the plotted points. The area was calculated using the trapezoidal rule:

$$\text{AreaUnderCurve} = \sum_{i=1}^n [x_{i+1} - x_i] \times [y_i + (y_{i+1} - y_i) / 2] \quad (5-33)$$

where x_i is rate of false positives for threshold i , y_i is the rate of true positives for threshold i , and $n + 1$ is the number of thresholds.

Table 5.16 gives the number of true positive cells A, true positive %, the number of false positive cells B, and false positive % for each threshold. The ROC curve is shown in Figure 5.15. The ROC value is 0.85. This indicates the model matches the reality quite well and is valid enough to predict the probability of urbanization.

Table 5.16 True positive % and false positive % for each threshold for validation of the logistic regression model using ROC method

No.	Thresholds(%)	A	True positive(%)	B	False positive(%)
1	0	0	0.000	0	0.000
2	5	1414	33.699	14417	4.615
3	10	2197	52.359	29463	9.431
4	15	2689	64.085	44800	14.341
5	20	3019	71.949	60300	19.303
6	25	3263	77.765	75886	24.292
7	30	3434	81.840	91544	29.304
8	35	3519	83.866	107288	34.344
9	40	3590	85.558	123047	39.388
10	45	3626	86.416	138841	44.444
11	50	3659	87.202	154637	49.501
12	55	3676	87.607	170449	54.562
13	60	3682	87.750	186273	59.628
14	65	3693	88.012	202092	64.691
15	70	3694	88.036	217920	69.758
16	75	3697	88.108	233746	74.824
17	80	3701	88.203	249572	79.890
18	85	3772	89.895	265331	84.935
19	90	3960	94.376	280972	89.942
20	95	4100	97.712	296661	94.964
21	100	4196	100.000	312394	100.000

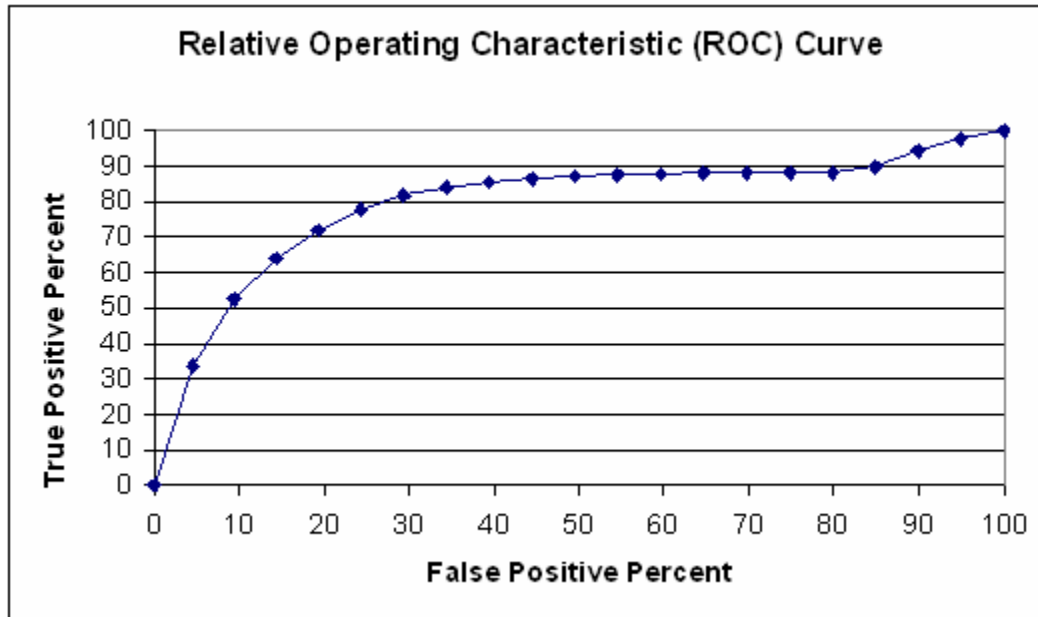


Figure 5.15 ROC curve.

5.11 Prediction of spatial patterns of urban distribution

The logistic regression model can only generate a probability map (Figure 5.14). It cannot predict the proportions of land use/cover classes. However, any quantitative data on the future total areas of urban distribution, including land use planning data or information output from other land use/cover change models, can be allocated to the suitability map. In this study, the proportions of urban area in the future were predicted using the Markov chain model in Chapter 4. These are allocated to the probability map and urban spatial patterns from 1987 to 2020 are generated and shown in Figure 5.16. The series of maps do not obviously show the urban growth because the amount of urban growth predicted from the Markov chain model is not large enough to reveal itself from the small scale map series and most newly urbanized cells are located in urban peripheries or fills in un-urbanized cells within existing urban areas.

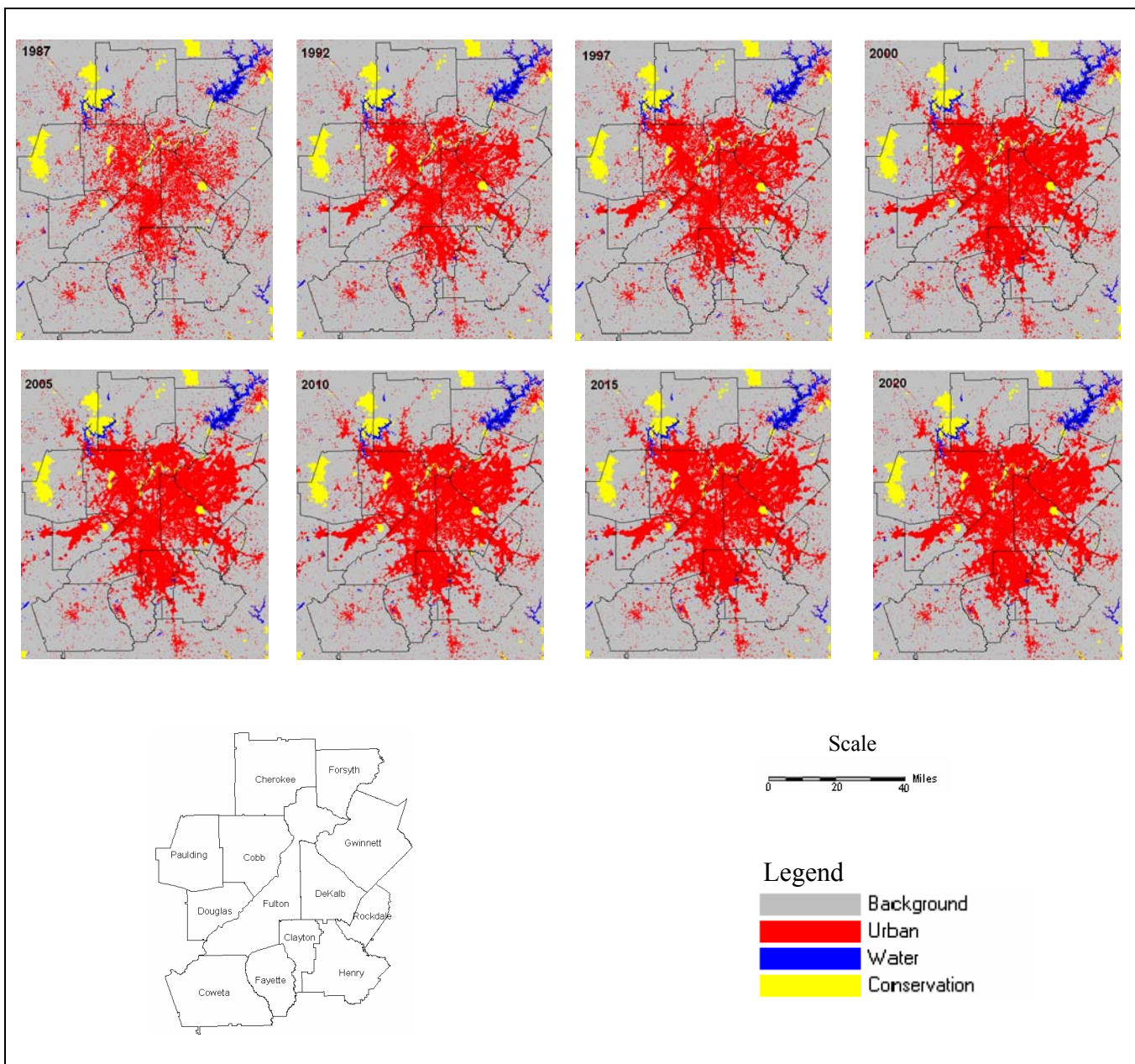


Figure 5.16 Spatial patterns of urban area in the Atlanta region, 1987-2020.

Unlike the Markov chain model which is temporally dynamic, the logistic regression model is not dynamic in terms of time. The probability map from the logistic regression model can only tell where urbanization will occur, it cannot tell when it will happen. In other words, from the probability map alone, one cannot generate the temporal series (or order) of urban growth. However, from the probability map the spatial order of urbanization can be presented by creating a series of maps showing the location order of urban growth. To this end, the classified probability map was reclassified in an accumulative way such that the number of cells to be urbanized are accumulated from the class of the highest probability to the class of the lowest. Outcomes were a series of urban growth maps. These growth maps were combined with the 1987 urban base map and masked with water bodies and conservation areas. Figure 5.17 shows only seven maps of the series. The tenth map should indicate that the whole area is urban. From Figure 5.17, it can be seen that urban growth will occur around existing or newly formed urban clusters or along the major roads.

5.12 Conclusions

This chapter first examined the multi-scale effects of the logistic regression modeling of urbanization probability using fractal analysis. It was found that the resolution of 225 m is the optimal scale at which the model performs best. Later spatial autocorrelation was corrected by using data aggregation, and sampling, as well as inclusion of spatial coordinates into the model. by a fractal analysis. Spatial autocorrelation was corrected by data aggregation, sampling, and the inclusion of spatial coordinates into the model.

The model results have demonstrated that, in the Atlanta metropolitan region: (1) Urban development tends to take place in areas with lower population density, indicating low-density

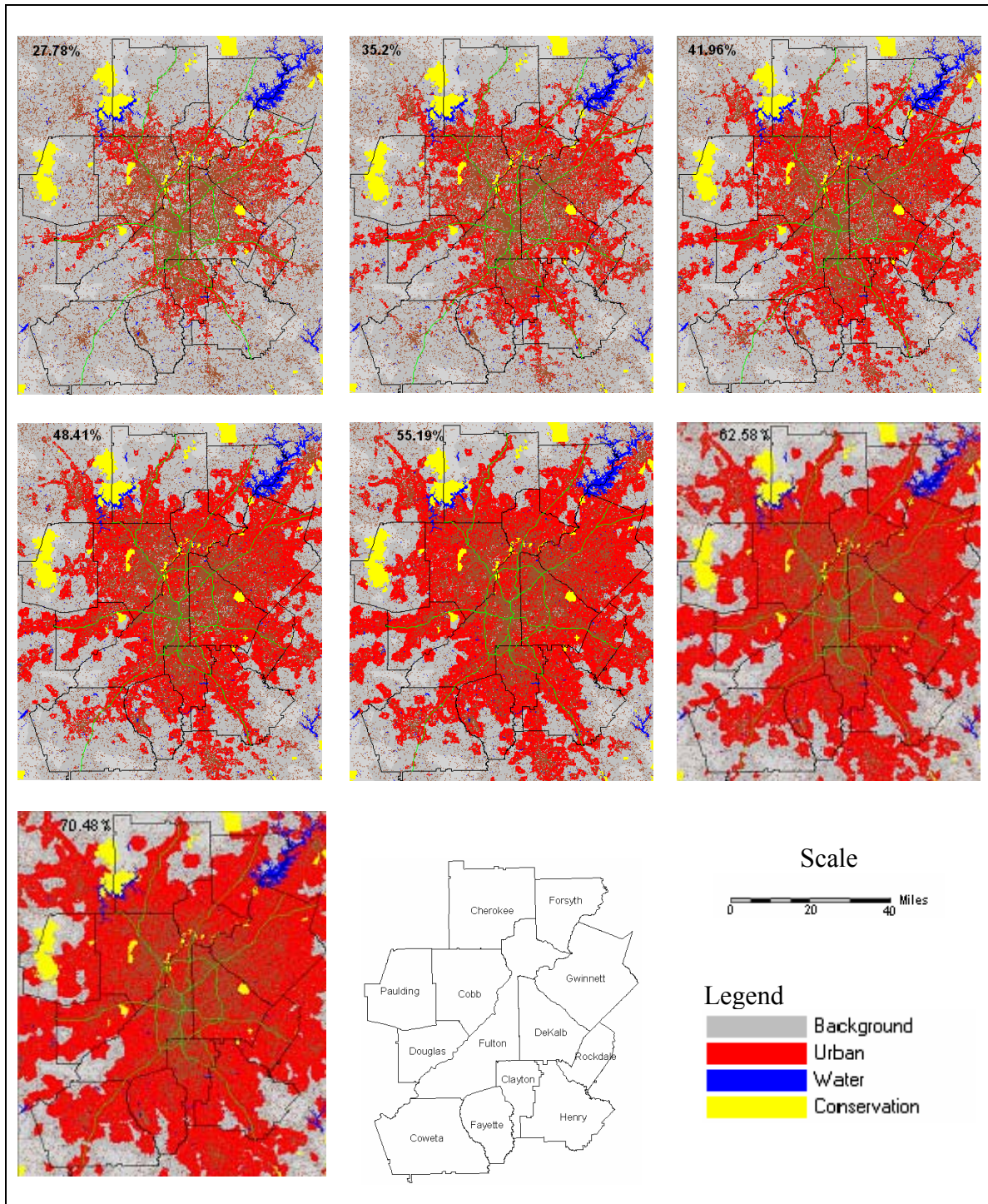


Figure 5.17 Spatial order of urban growth. The percentage values represent the percent of urban area.

development at urban peripheries or rural areas, leading to a scattered pattern; (2) New urban areas tend to be close to the nearest existing urban cluster, leading to the edge growth or filling-in, and hence, a compact pattern; (3) Urban development tends to occur farther from the CBD, but closer to the active economy centers, manifesting the decentralized, polycentric suburbanization trend of Atlanta; (4) Roads have gravity effects on urban development, contributing to the ribbon and strip patterns of urban growth along the transportation arteries; (5) It is more probable for a land lot to be converted to urban use if its neighbors are in urban use, thus contributing to the edge growth or filling-in of undeveloped areas within the urban areas; (6) Existing urban areas, especially high-density urban, resist redevelopment; (7) Urban development tends to occur on bare land, cropland/grassland, or forest; and (8) Urban development had taken place predominantly along the north-south direction, rather than east-west. The predicted spatial patterns of the future urban areas are the compromised outcomes of the above driving forces. Urban growth areas are found mainly around existing urban areas and close to major roads, while some new clusters located at a distance from the existing urban areas can also form.

CHAPTER SIX

SUMMARY AND CONCLUSIONS

The primary objective of this dissertation study is to characterize and model the human-induced land use/cover changes, especially urban growth, in Atlanta, Georgia metropolitan region that has been experiencing rapid suburbanization. The objective has been achieved through measuring quantitatively and spatially the historical land use/cover changes observed from remote sensing and linking the changes with the biophysical and socioeconomic driving forces using image processing, spatial analysis and modeling integrated in the framework of a GIS. The collection of geospatial techniques, as well as spatial analysis and modeling are loosely integrated . The study has demonstrated that the strategy of loose integration can effectively accomplish a study aiming to explore a complex human-land interaction system. This strategy can take full advantage of various proprietary data handling, analysis and modeling functions supplied by different software packages.

The specific objectives have been addressed by using different combinations of the geospatial techniques, analysis and modeling methods in three phases. The first phase is mapping land use/cover change from Landsat TM data using a new approach. Principal components analysis and change vector analysis are used to reveal the general land use/cover change dynamics. The analyses have found that during the ten years from 1987 to 1997, Atlanta had experienced rapid modifications of its landscape and that the most intense land use/cover change is deforestation for urban development. Next, an NDVI difference map was created, classified

and interpreted. The NDVI difference map has shown that rapid urbanization had caused a massive loss of green space. Then temporal logic was applied on the NDVI difference classification map and the land use/cover maps produced from unsupervised ISODATA classification. The temporal logical operation successfully improved the land use/cover mapping by resolving the confusions between urban areas and bare land or cropland/grassland. It was found from the land use/cover change detection by comparison of the accuracy-enhanced land use/cover maps that a large extent of forest had been converted to urban use. It was also found that low-density urban areas had grown much faster than high-density urban areas. While high-density urban growth had mainly taken place linearly along the transportation corridors on the north and southeast of the study area, low-density urban had taken on both clustered and dispersed patterns.

In the second phase, the accuracy-enhanced land use/cover maps provided land use/cover transition probabilities as input to a Markov chain model to predict the quantities and spatial patterns of land use/cover in the future. A statistical test has shown that, in the study area, successive land use/cover states are dependent on the immediate past. Assuming that the land use/cover transition probabilities are constant over time, the simulation of the Markov chain model revealed that urban use will continue to grow at the expense of forest. The proportions of urban use and forest show the trend of convergence after 2020, indicating that the Markov chain will approach an equilibrium distribution. The successive phases of urban growth will occur in the rural and urban-fringe areas, taking on a dispersed pattern. In this study, the Markov chain model is dynamic in the temporal dimension, but not in the spatial dimension. Spatial context and neighborhood effects were not accommodated in the Markov chain model. It did not deal with the human dimensions at all, and thus, did not incorporate exogenous variables. In the

Markov chain model, it was assumed that urban growth has not been controlled by demographic variables and econometric variables that are the outcomes of economic and social processes. Without the incorporation of those variables, the predicted patterns from the Markov chain model are dispersed and fragmented, an outcome caused by the stochastic nature of the Markov chain model.

In the third phase, a different land use/cover change model, a logistic regression model, is used to identify and improve our understanding of the socioeconomic and biophysical forces that have driven the urban growth and to find the most probable sites of urban growth in Atlanta. The scalar dynamics was examined by multi-resolution modeling. The optimal scale of modeling is found by a fractal analysis. Spatial autocorrelation was corrected by data aggregation, sampling, and the inclusion of spatial coordinates into the model. Findings from the model results for the Atlanta region are: (1) Urban development tends to take place in areas with lower population density, indicating low-density development at urban peripheries or rural areas, leading to a scattered pattern; (2) New urban areas tend to be close to the nearest existing urban cluster, leading to the edge growth or filling-in, and hence, a compact pattern; (3) Urban development tends to occur farther from the CBD, but closer to the active economy centers, manifesting the decentralized, polycentric suburbanization trend of Atlanta; (4) Roads have gravity effects on urban development, contributing to the ribbon and strip patterns of urban growth along the transportation arteries; (5) It is more probable for a land lot to be converted to urban use if its neighbors are in urban use, thus contributing to the edge growth or filling-in of undeveloped areas within the urban areas; (6) Existing urban areas, especially high-density urban, resist redevelopment; (7) Urban development tends to occur on bare land, cropland/grassland, or forest; and (8) Urban development had taken place predominantly along the north-south

direction, rather than east-west. The predicted spatial patterns of the future urban areas are the compromised outcomes of the above driving forces. Urban growth areas are found mainly around existing urban areas and close to major roads, while some new clusters located at a distance from the existing urban areas can also form. The logistic regression model is made spatially explicit partially by the incorporation of a neighborhood effect variable. The model is good at dealing with the human dimensions by including socioeconomic, biophysical, and econometric variables. However, the logistic regression model is not temporally explicit. Its output probability map can only answer where urban development will occur, but cannot answer when it will take place. The model uses only one set of explanatory variables for all the predictions, hence a lack of temporal dynamics. Further research should include more recent data on the predictors in the model or seek a self-modifying approach so that the model variables can update themselves automatically after each model run.

In terms of methodologies, this dissertation research has found that:

(1) Remote sensing and GIS can be used to model land use/cover changes in general and urban growth in particular, in a complex urban landscape. In particular, the integration of remote sensing and GIS with Markov chain and logistic regression provides a deeper understanding of the driving forces and the spatio-temporal dynamics of land use/cover changes, which stimulates the interests of the social scientists to pursue the “spatial turn” in their research (Goodchild 2004).

(2) Temporal information behind the changes of NDVI combined with logic rules can be a valuable approach to improving the land use/cover classification accuracy, and hence, the land use/cover change detection accuracy.

(3) Different land use/cover change modeling methods deal with spatial-temporal dynamics and human dimensions behind the land use/cover patterns in different ways. A single model usually cannot handle space-time-being simultaneously. This dissertation has demonstrated that it is useful to employ different modeling approaches to reveal the land use/cover change processes.

This study has also revealed some limitations of the Markov chain modeling. First, it was based only on first-order dependence and did not take into account the spatial context and neighborhood effects. Second, it did not accommodate any exogenous variables in the simulation. Although the logistic regression model has incorporated spatial econometric variables (distances), neighborhood effects, as well as biophysical and socioeconomic driving forces, it adopted a single set of static values of the predictors without dynamic updates. While the optimum resolution was determined by the fractal dimensions analysis for the logistic regression, the modeling based on the single scale could not capture the multi-scale dynamics behind the land use/cover change drivers.

Future research will have to overcome these modeling limitations by creating a more realistic land use/cover change model that can deal with space, time, and people simultaneously. To achieve this goal, one has to adopt the following approaches: First, develop a spatial Markov chain model with higher-order dependence. Second, to overcome the shortcoming of the lack of temporal dynamics in the empirical logistic model, explore a hybrid model that combines an empirical model with a dynamic simulation model, so that the probabilities of land use/cover changes predicted from the empirical model can be used as one of the rules in the simulation model and the probabilities can be updated dynamically to reflect the changes in spatial contexts as simulated from the dynamic model. Third, address the multi-scale characteristics of land

use/cover systems by using multi-level statistics or a hierarchical modeling structure so that the scalar dynamics of the land use/cover change driving forces operating from bottom-up (micro-behavior) and top-down (such as regional planning policies) can be handled. Fourth, develop a holistic model that tightly couples different sub-modules, so that the whole model contains a feedback or cycling mechanism, which means that the model can not only simulate land use/cover changes, but also evaluate the societal and environmental impacts of the changes, and assess the feedback of the impacts on the land use/cover systems.

REFERENCES

- Agarwal, C., Green G. M., Grove J. M., Evans T. P., and Schweik C. M. 2001. A review and assessment of land-use change models: Dynamics of space, time, and human choice. *USDA Forest Service, Northeastern Research Station, General Technical Report NE-297.*
- Allen, P. M. 1997. *Cities and Regions as Self-Organizing Systems: Models of Complexity.* Amsterdam: Gordon and Breach Science Publishers.
- Alonso, W. 1964. *Location and Land Use: Toward a General Theory of Land rent.* Cambridge: Harvard University Press.
- Anderson, J. R., Hardy, E. E., Roach, J. T., and Witmer, R. E. 1976. A land use and land cover classification system for use with remote sensor data. USGS Professional Paper 964, Sioux Falls, SD, USA.
- Anderson, T. W. and Goodman, L. A. 1957. "Statistical Inference about Markov Chains," *Annals of Mathematical Statistics*, 28:89-110.
- Aplin, P. and Atkinson, P. M. 2004. Predicting missing field boundaries to increase per-field classification accuracy. *Photogrammetric Engineering & Remote Sensing* 70(1):141-149.
- ARC (Atlanta Regional Commission) 1994, 1995, 1996, 1997, and 2001. Atlanta Region Outlook. Atlanta, GA: Atlanta Regional Commission.
- Arthur, W.B. 1989. Competing technologies, increasing returns, and lock-in by historical small events. *The Economic Journal* 99:116-131.
- Aspinall, R.J., and Hill, M.J. 1997. Land cover change: a method for assessing the reliability of land cover changes measured from remotely sensed data. *Proceedings of the*

- international Geoscience and Remote Sensing Symposium, GARSS'97, Singapore, 4-8 August 1997. Piscataway, NJ: IEEE, pp. 269-271.*
- Bailey, T. C., and Gatrell, A. C. 1995. *Interactive Spatial Data Analysis*. Harlow Essex, England :Longman Scientific & Technical; New York, NY: J. Wiley, 1995.p.313.
- Baker, W. L. 1989. A review of models of landscape change. *Landscape Ecology* 2(2):111-133.
- Banks, J., Carson II, J. S., Nelson, B.L. and Nicol, D.M. 2000. *Discrete System Simulation*, Third edition, Prentice Hall, pp 374-375.
- Battern, D. F. 2001. Complex landscapes of spatial interaction. *Annals of Regional Science* 35:81-111.
- Batty, M. and Longley, P. 1994. *Fractal Cities*. London: Academic Press.
- Bian,Ling. 1997. Multiscale Nature of spatial data in scaling up environmental models. In *Scaling in Remote Sensing and GIS*. Edited by Quattrochi, D. A., and M. F. Goodchild. Boca Raton, FL: CRC/Lewis Publishers, Inc. pp.13-25.
- BICUMP (The Brookings Institution Center on Urban & Metropolitan Policy). 2000. *Moving beyond sprawl: The Challenge for Metropolitan Atlanta*. Washington, D.C.: Brookings Institution Center on Urban & Metropolitan Policy.
- Bockstael, N., and Goetz, S.J. 2002. Spatial predictive modeling and remote sensing of land use change in the Chesapeake Bay Watershed, NASA LCLUC program progress report. URL:http://lcluc.gsfc.nasa.gov/products/pdfs/2002AnPrgRp/AnPrgRp_Bockstael_Goetz2002.pdf
- Burgess, E.1925. The growth of the city. In *The City*. Edited by Park, R. E., Burgess, E. W. and McKenzie, R. D. Chicago: The University of Chicago Press, pp.47-62.

- Burnham, B.O. 1973. Markov inter-temporal land use simulation model. *Southern Journal of Agricultural Economics*, July,1973, pp253-258.
- Buttenfield, B. P., and R. B. McMaster (editors). 1991. *Map Generalization: Making Rules for Knowledge Representation*. New York: Longman Scientific and Technical.
- Cao, C. and Lam, N. S. 1996. Understanding the scale and resolution effects in remote sensing and GIS. In *Scaling in Remote Sensing and GIS*. Edited by Quattrochi, D. A., and M. F. Goodchild. Boca Raton, FL: CRC/Lewis Publishers, Inc. pp.57-71.
- Casti, J. 1997. *Would-be Worlds*. John Willey & Sons: New York.
- Chauncy.H., and Ullman, E. 1945. The Nature of Cities. *Annals of the Academy of Political and Social Science* 242:7-17.
- Clark, W.A., and P.L. Hosking. 1986. *Statistical Methods for Geographers*. New York: John Wiley & Sons.
- Clarke, K. C., 1986. Computation of the fractal dimension of topographic surfaces using the triangular prism surface area method, *Computers & Geosciences*, 12(5):713-722.
- Clarke, K. C., and Gaydos, L. J. 1998. Loose-coupling a cellular automata model and GIS: long-term urban growth prediction for San Francisco and Washington/Baltimore. *International Journal of Geographical Information Science*, 12:699-714.
- Clarke, K.C., and Hoppen, S. 1997. A self-modifying cellular automaton model of historical urbanization in the San Francisco Bay area. *Environment and Planning B: Planning and Design* 24:247-261.
- Cliff, A. D., and Ord, J. K. 1973. *Spatial Autocorrelation*. London: Pion.
- Cochran, W. G. 1977. *Sampling Techniques*. New York, NY: John Wiley & Sons.
- Collins, L. 1975. An Introduction to Markov Chain Analysis. *CATMOG 1*. London: Headley

- Brothers Ltd., London.
- Congalton, R., and L. Plourde. 2002. Quality Assurance and Accuracy Assessment of Information Derived from Remotely Sensed Data. IN: *Manual of Geospatial Science and Technology*. John Bossler. (Editor). Taylor & Francis, London. pp. 349-361.
- Congalton, R., and MacLeod, R. 1994. Change detection accuracy assessment on the NOAA Chesapeake Bay Pilot Study. *Proceedings of the 1st International Symposium on the Spatial Accuracy of Natural Resource data Bases*, Williamsburg, Virginia (Bethesda, Maryland: American Society for Photogrammetry and Remote Sensing), pp.78-87.
- Congalton, R. G. 1996. Accuracy assessment: A critical component of land cover mapping. IN: *Gap Analysis: A Landscape Approach to Biodiversity Planning. A Peer-Reviewed Proceedings of the ASPRS/GAP Symposium*. Charlotte, NC. pp. 119-131
- Congalton, R.G. 1991. A review of assessing the accuracy of classifications of remotely sensed data. *Remote Sensing of Environment* 37:35-46.
- Congalton, Russell G. 1988. A comparison of sampling schemes used in generating error matrices for assessing the accuracy of maps generated from remotely sensed data. *Photogrammetric engineering and remote sensing* 54(5):593-600.
- Coppin, P. R., and BAUER, M.E. 1996. Digital change detection in forest ecosystems with remote sensing imagery. *Remote Sensing Reviews*, 13:207-234.
- Curry, M.R. 1996. On space and spatial practice in contemporary geography. In C. Earle, K. Mathewson, and M.S. Kenzer (eds.), *Concepts in Human Geography*. Lanham, MD: Rowman and Littlefield, pp. 3-32.
- de Blij, H. 1993. *Human Geography: Culture, society, and space*, 4th ed. John Willey & Sons, Inc., pp. 400-405.

- De Cola, L. 1989. Fractal analysis of a classified landscape scene. *Photogrammetric Engineering and Remote Sensing*, 55(5):601-10.
- Egan, J.P. 1975. *Signal Detection Theory and ROC analysis*. Academic Press, New York.
- Fischer, G., and Sun, L. X. 2001. Model based analysis of future land-use development in China. *Agriculture, Ecosystems and Environment* 85: 163-176.
- Fujü,T., and Hartshorn T.A. 1995. The changing metropolitan structure of Atlanta, Georgia: Locations of functions and regional structure in a multi-nucleated urban area. *Urban Geography* 16(8):680-707.
- Fulton, William, Rolf Pendall, Mai Nguyen, and Alicia, Harrison. 2001. Who sprawls most? How growth patterns differ across the U.S.? Survey series, The Brooking Institution, Washington, DC. URL: www.brookings.edu/dybdocroot/es/urban/publications/fulton.pdf
- Fung, T., and LeDrew, E. 1987. Application of principal component analysis to change detection. *Photogrammetric Engineering and Remote Sensing* 53(12):1649-1658.
- Gallo, K. P., Elvidge, C. D., Yang, L, and Reed B. C. 2004. Trends in night-time city lights and vegetation indices associated with urbanization within the conterminous USA. *International Journal of Remote Sensing*, 25(10):2003-2007.
- Geller, C., Ihlanfeldt, K., and Sjoquist, D.L. 1995. *Atlanta in black and white: racial attitudes and perspectives*. Research Atlanta, Inc. : Policy Research Center, Georgia State University.
- Geoghegan, J., Pritchard, L., Chowdhury, Y. O., Sanderson, S. and Turner, B. L. 1998. “Socializing the Pixel” and “Pixelizing the Social” in Land-use and Land-cover Change. In: Liverman, D., Moran, E. F., Rondfuss, R. R. and Stern, P.C. (Eds). *People and*

- Pixels: Linking Remote Sensing and Social Science*. National Academy Press, Washington, D.C. 1998.
- Geoghegan, J., Villar, S. C., Klepeis, P., Mendoza, P.M., Himmelberger, Y. O., Chowdhury, R. R., Turner II, B. L., and Vance, C. 2001. Modeling tropical deforestation in the southern Yucatan peninsular region: comparing survey and satellite data. *Agriculture, Ecosystems & Environment* 85: 25-46.
- Geoghegan, J., Wainger, L. A., and Bockstael, N. E. 1997. Spatial landscape indices in a hedonic framework: an ecological economics analysis using GIS. *Ecological Economics* 23:251-264.
- Gibson, C.C., Ostrom, E., and Anh, T. K. 2000. The concept of scale and the human dimensions of global change: a survey. *Ecological Economics* 32:217-239.
- Gillies, R. R., Carlson T. N., Cui, J., Kustas, W. P., and Humes, K. S. 1997. A verification of the 'triangle' method for obtaining surface soil water content and energy fluxes from remote measurements of Normalized Difference vegetation Index (NDVI) and surface radiant temperature, *International Journal of Remote Sensing*:18(15):3145-3166.
- Gimblett, R. 2002. *Integrating Geographic Information Systems and Agent-based Modeling Techniques for Simulating Social and Ecological Processes*, Edited by Gimblett, R. Oxford University Press, 2002.
- Goldenstein, H. 1995. *Multilevel statistical models*. New York, Halstaed.
- Goodchild, M. F. 2004. Social sciences: interest in GIS grows. *ArcNews* 26(1):1-3.
- Goodchild, M. F. 1987. *Spatial Autocorrelation*. Concepts and Techniques in Modern Geography 47, Geo Books, UK.

- Goodchild, M. F. and Mark, D.M.. 1987. The fractal nature of geographical phenomena, *Annals of the Association of American Geographers* 77(2):265-78.
- Gross, D. and Strand R. 2000. Can agent-based models assist decisions on large-scale practical problems? A philosophical analysis. *Complexity* 5(6): 26-33.
- Harbaugh, J. W., and Bonham-Carter, G. 1970. *Computer simulation in Geology*. John Wiley & Sons, New York.
- Harris, C. D., and Ullman, E. L. 1945. The nature of cities. *Annals of the American Academy of Political and Social Science* 242:7-17.
- Hartshorn, T. A., and Muller, P. O. 1989. Suburban downfalls and the transformation of metropolitan Atlanta's business landscape. *Urban Geography* 10(4): 375-395.
- Harvey, D. 1969. Temporal modes of explanation in geography. In D. Harvey, *Explanation in Geography*. New York: St Martin's Press, pp. 407-432.
- Hilts, V. L. 1973. Statistics and social science. In R.N. Giere and R.S. Westfall (eds.), *Foundations of Scientific Method: The Nineteenth Century*. Bloomington: Indiana University Press, pp. 206-233.
- Hosmer, D. W. and Lemeshow, S. 1989. *Applied Logistic Regression*. New York: Wiley.
- Howarth, J. P. and Wickware, G. M. 1981. Procedures of change detection using Landsat digital data. *International Journal of Remote Sensing* 2:277-191.
- Hoyt, Homer. 1939. *The structure and Growth of Residential Neighborhoods in American Cities*. Washington D.C.: Federal Housing Administration.
- Hudson, J. 1992. Scale in space and time. In R. F. Abler, M. G. Markus, and J. M. Olson (editors), *Geography's Inner Worlds: Pervasive Themes in Contemporary American Geography*. New Brunswick, NJ: Rutgers University Press, pp. 280-300.

- Irwin, E.G., and Bockstael, N.E. 2002. Interacting Agents, spatial externalities, and the endogenous evolution of land use patterns. *Journal of Economic Geography* 2(1):31-54.
- Irwin, E.G., and Geoghegan J. 2001. Theory, data, methods: developing spatially explicit economic models of land use change. *Agriculture, Ecosystems and Environment* 85:7-23.
- Jaggie, S., Quattrochi, A. and Lam, S. 1993. Implementation and operation of three fractal measurement algorithms for analysis of remote-sensing data, *Computers & Geosciences*, 19(6):745-767.
- Jensen, J.R. 1996. *Introductory digital Image Processing: A Remote Sensing Perspective*, 2nd ed., Prentice-Hall, Englewood Cliffs, NJ.
- Kleinbaum, David G. 1994. *Logistic regression : a self-learning text*. New York: Springer.
- Knox, Paul L. 1993. *The Restless Urban Landscape*. Englewood Cliffs: Prentice Hall.
- Koeln, G., and Bissonnette, J. 2000. Cross-correlation analysis: mapping land-cover change with a historic land-cover database and a recent, single date multi-spectral image. In: *Proceedings of 2000 ASPRS Annual Convention*, Washington, D.C. p. 8.
- Kok, K., and Veldcamp A. 2001. Evaluating impact of spatial scales on land use pattern analysis in Central America. *Agriculture, Ecosystems and Environment* 85:205-221.
- Kok, K., Farro, A., Veldcamp, A. and Verbug, P. H. 2001. A method and application of multi-scale validation in spatial land use models. *Agriculture, Ecosystems and Environment* 85:223-238.
- Kuhn, T. 1962. *The structure of scientific revolutions*. University of Chicago Press: Chicago.
- Lam, N. S., and Quattrochi, D.A. 1992. On the issues of scale, resolution, and fractal analysis in the mapping sciences, *Professional Geographers* 44: 88-98.

- Lam, N. S. 1983. Spatial interpolation methods: A review.” *Cartography and Geographical Information Systems* 10(2):129-149.
- Landis, J. and Zhang, M. 1998. The second generation of the California urban futures model. *Environment and Planning A* 25:795-824.
- Lillesand, Thomas M. and Kiefer Ralph W. 1999. *Remote sensing and image interpretation*. 4th Edition, John Wiley & Sons, Inc.
- Liverman, D., Moran, E.F., Rondfuss, R.R. and Stern, P.C.(Eds) 1998. *People and Pixels: Linking Remote Sensing and Social Science*. National Academy Press, Washington,D.C. 1998.
- Livingstone, D.N. 1992. Statistics don't bleed: Quantification and its detractors. In D.N. Livingstone, *The Geographical Tradition: Episodes in the History of a Contested Enterprise*. Cambridge, MA: Blackwell, pp. 304-346.
- Lo, C. P. 2002. Urban indicators of China from radiance-calibrated digital DMSP-OLS nighttime images. *Annals of the Association of American Geographers*, 92(2):225-240.
- Lo, C. P. 1998. Applications of imaging Radar to land use and land cover mapping. In *Principles and Applications of Imaging Radar (Manual of Remote Sensing, 3rd edition, volume 2)*. Edited by F.M. Henderson and A.J. Lewis. Published in cooperation with the American Society for Photogrammetry and Remote Sensing (ASPRS). New York: John Wiley & Sons, Inc. pp705-732.
- Lo, C.P. 1986. *Applied Remote Sensing*. New York: Longman.
- Lo, C. P. and Faber, B. J. 1997. Integration of Landsat Thematic Mapper and census data for quality of life assessment. *Remote Sensing of Environment* 62:143-157.

- Lo, C. P. and Shipman, R.L. 1990. A GIS approach to land-use change dynamics detection, *Photogrammetric Engineering and Remote Sensing* 56:1483-1491.
- Lo, C. P. and Yeung, Albert K.W. 2002. *Concepts and Techniques of Geographic Information Systems*. New Jersey: Prentice-Hall, Inc..
- Lo, C. P., Quattrochi, D.A. and Luvall, J.C. 1997. Application of high-resolution thermal infrared remote sensing and GIS to assess the urban heat island effect, *International Journal of Remote Sensing* 18:287-304.
- Lowell, K. 2001. An area-based accuracy assessment methodology for digital change maps. *Journal of Remote Sensing* 22(17): 3571-3596.
- MacLeod, R.D., and Congalton, R.G. 1998. A quantitative comparison of change-detection algorithm for monitoring eelgrass from remotely sensed data. *Photogrammetric Engineering and Remote Sensing* 64: 207-216.
- Malila, W. A. 1980. Change vector analysis: an approach for detection forest changes with Landsat. *Proceedings of the 6th Annual Symposium on Machine Processing of Remotely Sensed Data held at Purdue University in 1980 (Indiana: Purdue University)*,pp.326-335.
- Mandelbrot, B. B. 1983. *The Fractal Geometry of Nature*. San Francisco: Freeman.
- Markham, B.L., and Barker, J.L. 1986. Landsat MSS and TM post-calibration dynamic ranges, exoatmospheric reflectances and at-satellite temperatures: EOSAT Landsat Technical Notes, v.1, pp.3-8.
- Mas, J. F. 1999. Monitoring land-cover changes: a comparison of change detection techniques. *International Journal of Remote Sensing* 20-1:139-152.

- Masek, J.G., Lindsay, F.E., and Goward, S.N. 2000. Dynamics of urban growth in the Washington DC metropolitan area, 1973-1996, from Landsat observations, *International Journal of Remote Sensing* 21(18):3473-3486.
- McFadden, D. S. 1973. Conditional logit analysis of qualitative choice behavior. In *Frontiers in Econometrics*. Edited by Zarembka, P. Academic Press.
- McMillen, D.P., and McDonald, J.F. 1989. Selectivity Bias in Urban Land Value Functions, *Land Economics* 65(4):341-351.
- Meentemeyer, V. 1989. Geographical perspectives of space, time, and scale. *Landscape Ecology* 3: 163-173.
- Meentemeyer, V., and Box, E.O. 1987. Scale effects in landscape studies. *Ecological Studies*, 64-15.
- Mieskowski, P., and Mills, E. 1993. The causes of metropolitan suburbanization. *Journal of Economic Perspectives*, 7(3):135-147.
- Michalek, J., Wagner, T., Luczkovich, J., and Stoffle, R. 1993. Multispectral change vector analysis for monitoring coastal marine environments. *Photogrammetric Engineering and Remote Sensing* 59(3):381-384.
- Muller, Michael R., and Middleton, John. 1994. A Markov model of land-use change dynamics in the Niagara Region, Ontario, Canada. *Landscape Ecology* 9(2):151-157.
- NEWCOMER, J. A., and J. SZAJGIN. 1984. Accumulation of thematic map errors in digital overlay analysis. *American Cartographer* 11:58-62.
- Parker, D.C., Evans, T., and Meretsky, V. 2001. Measuring emergent properties of agent-based landcover/landuse models using spatial metrics. *Computing in Economics and Finance*, 261.

- Parks, P. J. 1990. Models of forested and agricultural landscapes: integrating economics. In: Turner M.G. and Gardner R.H.(eds), *Qualitative Methods in Landscape Ecology*. Springer-Verlag.
- Payne K., Samples, K., Epstein J., Ostrander, A., Lee, J. W., Schmidt, J. P., Mathes, S. Elliot, M, Nackone, J., Sand S., Hay, F., Merrill, M., Golbali, Higgs, M., Howell J., and Kramer L. 2003. Multi-source data integration for Georgia Land-cover mapping. *Southeastern Geographer* Vol. XXXXIII, No.1.,pp.1-27.
- Petit, C., Scudder, T., and Lambin, E. 2001. Quantifying processes of land-cover change by remote sensing: resettlement and rapid land-cover changes in south-eastern Zambia. *International Journal of Remote Sensing* 22(17):3435-3456.
- Polsky, C., and Easterling III, W.E. 2001. Ricardian climate sensitivities: accounting for adaptation across scales. *Agriculture, Ecosystems and Environment* 85, 133-144.
- Pontius, R. G. 2000. Quantification error versus location error in the comparison of categorical maps. *Photogrammetric Engineering & Remote Sensing*: 66 (8):1011-1016.
- Pontius, R. G. and Schneider L. 2001. Land use change model validation by a ROC method for the Ipswich watershed, Massachusetts, USA. *Agriculture, Ecosystems & Environment* 85(1-3): 239-248.
- Pontius, R. G., Cornell, J.D., and Hall, C.A.S. 2001. Modeling the spatial pattern of land-use change with GEOMOD2: application and validation for Costa Rica. *Agriculture, Ecosystems and Environment* 85:191-203.
- Popper, K. 1959. *The logic of Scientific Discovery*. Hutchinson, London.
- Portugali, J., Benenson, I. and Omer, I. 1997. Spatial cognitive dissonance and sociospatial emergence in a self-organizing city. *Environment and Planning B* 24:263-285.

- Quattrochi, D.A., and Luvall, J.C. 1999. Urban sprawl and urban pall: assessing the impacts of Atlanta's growth on meteorology and air quality using remote sensing and GIS. *Geo Info Systems* 9(5):26-33.
- Quattrochi, D. A., and M. F. Goodchild (editors). 1997. *Scaling in Remote Sensing and GIS*. Boca Raton, FL: CRC/Lewis Publishers, Inc.
- Quattrochi, D.A., Nina Siu-Ngan Lam, Hong-lie Qiu, and Wei Zhao. 1997. Image characterization and modeling system (ICAMS):A geographic information system for the characterization and modeling of multiscale remote sensing data. In *Scaling in Remote Sensing and GIS*. Boca Raton, FL: CRC/Lewis Publishers, Inc. pp.295-307.
- Rand, W., Brown, D.G., Page, S. E., Riolo, R., Fernandez, L.E. and Zellner, M. 2003. *Statistical validation of spatial patterns in agent-based models*. URL: <http://cscs.umich.edu/research/projects/slucel/> .
- Richardson, A.J., and Milne, A.K. 1983. Mapping fire burns and vegetation regeneration using principal components analysis. *Proceedings of IGARSS' 83 held in San Francisco in 1983*. New York: I.E.E.E. pp.51-56.
- Rosenfield, G. H., Fitzpatrick-Lins, K. and Ling, H. S. 1982. Sampling for thematic map accuracy testing. *Photogrammetric Engineering and Remote Sensing* 48:131-137.
- Sanders, L.,Pumain, D., Mathian, H., Guerin-Pace, F., and Bura, S. 1997. SIMPOP: a multiagent system for the study of urbanism. *Environment and Planning B* 24:287-305.
- Schneider, L. and Pontius, R.G. 2001. Modeling land use change in the Ipswich watershed, Massachusetts, USA. *Agriculture, Ecosystems & Environment* 85(1-3): 83-94.
- Serneels, S., and Lambin, E. F. 2001. Proximate causes of land-use change in Narok District, Kenya: a spatial statistical model. *Agriculture, Ecosystems and environment* 85:65-81.

- Serra, P., Pons, X. and Sauri, D. 2003. Post-classification change detection with data from different sensors: some accuracy considerations. *International Journal of Remote Sensing* 24 (16):3311-3340.
- Singh, A. 1986. Change detection in the tropical forest environment of northeastern India using Landsat. In *Remote Sensing and Land Management*, edited by M.J. Eden and J.T. Parry (New Zealand), pp. 237-253.
- Singh, A. 1989. Digital change detection techniques using remotely-sensed data. *International Journal of Remote Sensing* 10:989-1003.
- Soja, E. 1989. *Postmodern Geographies: The Reassertion of Space in Critical Social Theory*. London: Verso, pp. 1-9; 10-42; 43-75.
- Sommer, S., Hill, J., and Megier, J. 1998. The potential of remote sensing for monitoring rural land use changes and their effects on soil conditions. *Agriculture, Ecosystems and Environment*, 67:197-209.
- STATA 2003. *STATA Base Reference Manual*. Release 8. College Station, Texas: Stata Press.
- Swets, John A. 1996. *Signal detection theory and ROC analysis in psychology and diagnostics*. Mahwah, N.J.: L. Erlbaum Associates.
- Swets, John A. 1988. Measuring the accuracy of diagnostic systems. *Science, June*: 1285-93.
- Thünen, Johann Heinrich Von. 1966. *Isolated state*, an English edition of *Der isolierte Staat*. Translated by Carla M. Wartenberg. Edited with an introduction by Peter Hall. Oxford, New York: Pergamon Press.
- Tobler, W.R. 1979. Smooth pycnophylactic interpolation for geographical regions. *Journal of the American Statistical Association* 74-367:519-530.

- Torrens, P. M. 2001. Can geo-computation save urban simulation? Throw some agents into the mixture, simmer, and wait... Working paper series, Center for Advanced Spatial Analysis(CASA), UCL.
- Torres, A.O., Bullard, R.D., and Johnson, C.G. 2000. Closed doors: persistent barriers to fair housing, in: Bullard, R.D., Johnson, G.S. and Torres, A.O.(eds), *Sprawl City: Race, politics, and planning in Atlanta*. Washington D.C.: Island Press, pp. 89-109.
- Train, K.E. 2003. *Discrete choice methods with simulation*. New York : Cambridge University Press.
- Turner, M.G. 1988. A spatial simulation model of land use changes in a Piedmont county in Georgia. *Applied Mathematics and Computation* 27:39-51.
- Turner, M.G. 1987. Spatial simulation of landscape changes in Georgia: A comparison of 3 transition models. *Landscape Ecology* 1:29-36.
- Turner, M.G., Costanza, R., and Sklar, F. H. 1989. Methods to evaluate the performance of spatial simulation models. *Ecological Modeling* 48:1-18.
- Turner, M. G., O'Neill, R. V., Gardner, R. H. and Milne, B. T.. 1989. Effects of changing spatial scale on the analysis of landscape pattern. *Landscape Ecology* 3:153-162.
- Usher 1992. Statistical models of succession. In *Plant Succession: Theory and Prediction*. Edited by David C. Glenn-Lewin, Robert K. Peet and Thomas T. Veblen. London: Chapman & Hall. pp.215-247.
- Vance, J. E. 1964. *Geography and urban evolution in the San Francisco Bay Area*. Berkeley, CA: University of California, Institute of Governmental Studies.
- Veldcamp, A., and Fresco, L. O. 1996. CLUE: a conceptual model to study the conversion of land use and its effects. *Ecological Modelling*. 85(2):253-270.

- Veldkamp, A., and Lambin E.F. 2001. Predicting land-use change. *Agriculture, Ecosystems and Environment* 85:1-6.
- Verbyla, D.L., and Boles, S.H. 2000. Bias in land cover change estimates due to misregistration. *International Journal of Remote Sensing* 21(18):3553-3560.
- Veregin, H. 1989. Error modeling for the map overlay operation. Chapter in *Accuracy of Spatial Databases*, Edited by Goodchild M. and Gopal S., Taylor & Francis, pp. 3-17.
- Verburg, P. H., Schot, P., Dijst, M., and Velkamp, A. 2004. Land-Use Change Modeling: Current Practice and Research Priorities.
- URL:
[http://www.geo.ucl.ac.be/LUCC/MODLUC_Course/PDF/T.%20Veldkamp%20\(intro\).pdf](http://www.geo.ucl.ac.be/LUCC/MODLUC_Course/PDF/T.%20Veldkamp%20(intro).pdf).
- Walsh, S.J., Crawford, T.W., Crews-Meyer, K.A., and Welsh, W.F. 2001. A multi-scale analysis of land use land cover change and NDVI variation in Nang Rong District, Northeast Thailand. *Agriculture, Ecosystems and Environment* 85: 47-64.
- Ward, D.P., Murray A.T. and Phinn S.R. 2000. A stochastically constrained cellular model of urban growth. *Computers, Environment and Urban Systems* 24(6):539-558.
- Weigel, S. J. 1996. Scale, Resolution and Resampling: Representation and Analysis of Remotely Sensed Landscapes Across Scale in Geographic Information Systems. Ph.D. Dissertation, Louisiana State University.
- Weismiller, R. A., Kristof, S. J., Scholz, D. K., Anuta, P.E. and Momen, S. A. 1977. Change detection in coastal zone environments. *Photogrammetric Engineering and Remote Sensing* 43:1533-1539.

- Weng, Q. 2002. Land use change analysis in the Zhujiang Delta of China using satellite remote sensing, GIS and stochastic modeling. *Journal of Environmental Management* 64:273-284.
- Weng, Q. 2001, A remote sensing-GIS evaluation of urban expansion and its impact on surface temperature in the Zhujiang Delta, China. *International Journal of Remote Sensing*, 22(10):1999-2014.
- White, R., and Engelen, G. 2000. High-resolution integrated modeling of the spatial dynamics of urban and regional systems. *Computers, Environment and Urban Systems* 24(5): 383-400.
- Wong, D., and Amrhein C. (editors).1996. *The Modifiable Areal Unit Problem*. Special issue of *Geographical Systems* 3:2-3.
- Wood, E.C., Lewis, J.E., Tappan G.G., and Lietzow, R.W. 1997. "The Development of a Land Cover Change Model for Southern Senegal." Presented at Land Use Modeling Workshop, EROS Data Center, Sioux Falls, South Dakota, June 5-6, 1997.
- Wu, F. 2002. Calibration of stochastic cellular automata: the application to rural-urban land conversions. *International Journal of Geographical Information Science*16(8):795-818.
- Yang, X., and Lo, C. P. 2002. Using a time series of satellite imagery to detect land use and land cover changes in the Atlanta, Georgia metropolitan area. *International Journal of Remote Sensing* 23(9):1775-1798.
- Yang, Xiaojun. 2000. Integrating image analysis and dynamic spatial modeling with GIS in a rapidly suburbanizing environment. Ph.D. dissertation. The University of Georgia.